(2)

AD-A206 278

SOUTHWEST RESEARCH INSTITUTE
Post Office Drawer 28510, 6220 Culebra Road
San Antonio, Texas 78284

ANALYSIS OF VIBRATION TEST DATA FROM HARPOON GRADE-B CANISTER TESTING AT WYLE LABORATORIES

Prepared For:

PACIFIC MISSILE TEST CENTER
Point Mugu, California 93042

By:

SOUTHWEST RESEARCH INSTITUTE
6220 Culebra Road
San Antonio, Texas 78284

Daniel J. Pomerening

FINAL REPORT
SwRI Project 17-7958-815

Performed as a Special Task for the Nondestructive Testing Information Analysis Center Under Contract No. DLA900-84-C-0910 CLIN 0001AN

March 1989

Approved:

Robert L. Bass, Director
Department of Mechanical Sciences

TABLE OF CONTENTS

LIST OF FIGURES

LIST OF TABLES

1.0 PURPOSE

The purpose of the testing was to perform Nondestructive Evaluation (NDE) of the HARPOON weapons system. In particular, the intent was to investigate the effect of modified shock isolation pads on the dynamic response of the missile/ canister system under vibration excitation, and to determine the adequacy of the modified shock isolator design.

Two different designs of isolation pads between the clamp frame and the canister were compared. The testing was conducted with the production style isolation pads and a modified pad designed to reduce cost and installation complexity. The proposed isolation pads were prototypes, so the testing was exploratory in nature rather than aimed at qualification.

To accomplish this task, four HARPOON Grade-B canisters on a Launch Support Structure (LSS), Figure 1.1, were subjected to a modified portion of MIL-STD-167 [2.1][1] vibration testing. HARPOON dynamic simulators were placed inside two of the canisters, while the other two were trainers. MIL-STD-167 vibration levels were chosen since the HARPOON system was designed to this requirement. A test plan [2.2] was utilized to define the specific requirements of this program.

During the testing the acceleration response at a number of points on the structure was monitored. The location of these points was chosen to provide information on the influence of the pads, as well as the general response of the entire structure. Keywords: Surface to Surface Missiles.

The test program was initiated by Pacific Missile Test Center (PMTC) to satisfy a requirement to demonstrate the adequacy of the modified isolation pads. The actual testing was performed by Wyle Laboratories at their Norco facility under delivery order with China Lake. Southwest Research Institute (SwRI) was contracted to develop the test plan, provide technical advice during the testing, and perform data reduction on the acceleration data.

---

1 Numbers in brackets refer to references.

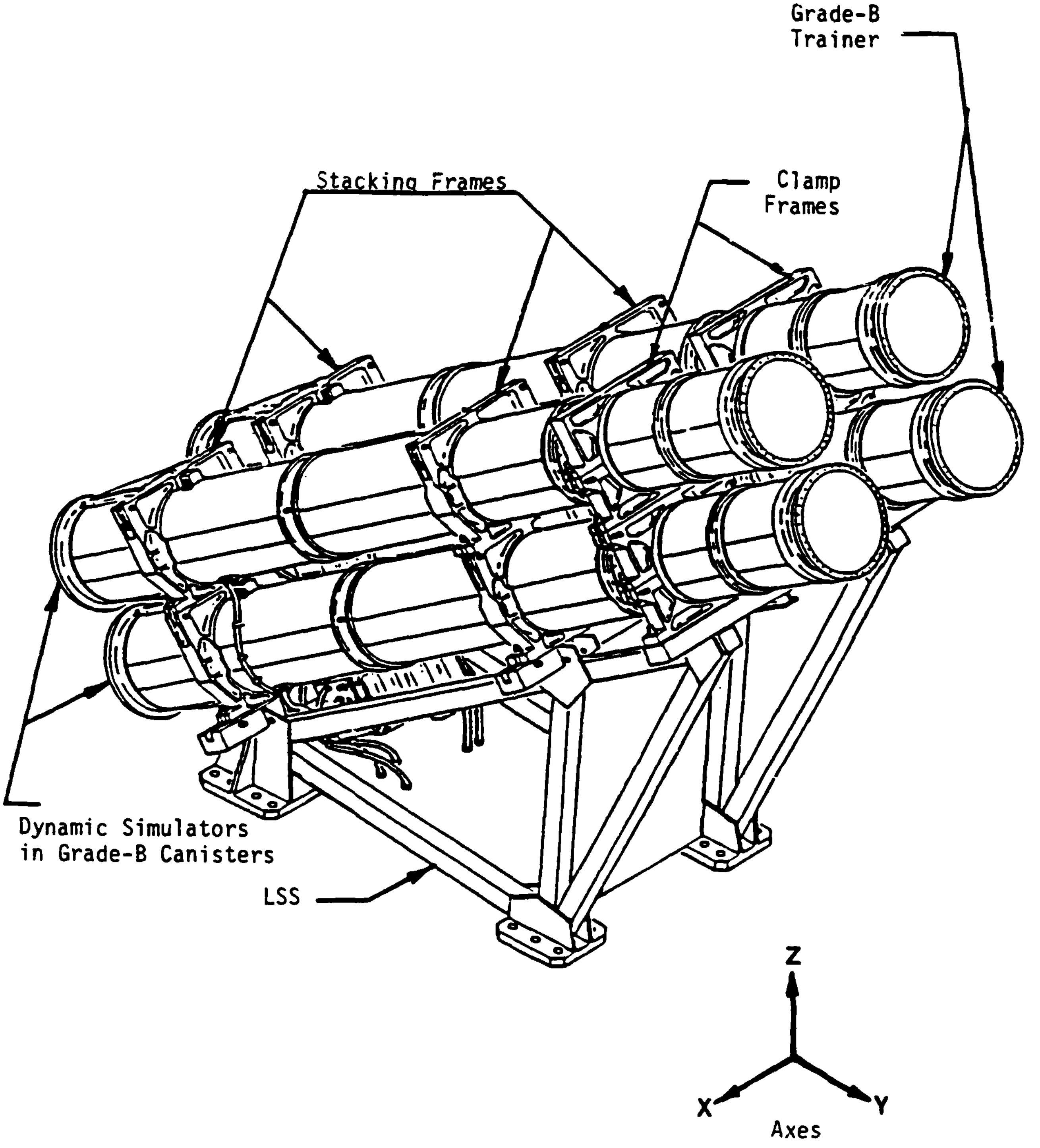

Figure 1.1 Test Configuration

2.0 REFERENCES

2.1 MIL-STD-167, Mechanical Vibrations of Shipboard Equipment (Type I - Environmental and Type II - Internally Excited), May 1974.

2.2 Test Plan for HARPOON Grade B Canisters Clamp Frame Isolation Pads, Revision 3, SwRI Project 17-7958-816, August 1987.

2.3 HARPOON Canister System Testing, Wyle Laboratories Test Report No. 14653, December 1988.

2.4 A Report on the USS Mississippi HARPOON Canister Launcher Shipboard Dynamic Environment Measurement Program, McDonnell Douglas Corporation, August 1985.

2.5 Status Report on CGN-40 HARPOON Canister Shipboard Test Data Analysis, SwRI Project 15-5607-826, June 1984.

2.6 Status Report on DD-995 HARPOON Shipboard Modal Analysis, SwRI Project 15-5607-826, February 1985.

2.7 Status Report on HARPOON Canister Laboratory Test Data Analysis, SwRI Report 15-5607-826, July 1985.

2.8 MIL-STD-810D, Military Standard, Environmental Test Methods and Engineering Guidelines, 19 July 1983.

3.0 TEST ITEM

The test set up consisted of a LSS bolted to 3 inch thick steel pads at each of the four feet. These pads were in turn welded to the shaker table at Wyle Laboratories, see photographs. Two dynamic simulators (DS) in Grade-B canisters were stacked on top of each other on one side of the LSS, the left side when looking from the front. Two Grade-B trainers were used on the other side of the LSS. Overall weight of the test item was approximately 13,870 lb; 9,570 lb for the dynamic simulators and canisters, and 4,300 lb for the LSS.

The LSS is designed to support four HARPOON canisters primarily for shipboard configurations. It consists of square tubing welded together to provide a launch platform. The four feet of the structure are attached to the deck of the ship. The canisters are supported at their stacking and clamp frames at a 35-degree angle from horizontal for firing.

Two HARPOON dynamic simulators, LO521 and LO55, in Grade-B canisters were utilized for the testing. The dynamic simulators are designed to represent the physical and dynamic characteristics of the production missiles. They are inert and therefore have no warhead or propellant. Other than that, the simulators are similar to production missiles. They are installed in the canisters in a manner similar to actual production missiles.

Three accelerometers were mounted on each missile at the seeker bulkhead. They were oriented such that motion along, transverse, and vertical to the missile axes could be measured. These accelerometers were calibrated and installed by PMTC personnel prior to shipment to Wyle Laboratories.

The two dynamic simulators were stacked one on top of each other for the testing. The initial series of tests was performed with the original isolation pads installed on the two dynamic simulator canisters. For the second series of tests, the modified isolation pads were installed on the two dynamic simulator canisters. The original isolation pads were kept on the two trainer canisters.

Two HARPOON Grade B trainers, RTM-84A-4B-1 and RTM-84A-4B-2, were utilized to simulate the other two missiles on the LSS. A trainer is designed to simulate the weight and cg of the actual missile configuration. This was accomplished by attaching weights to the canister walls in the appropriate locations.

It should be noted that although the overall physical dimensions and weight on the trainers are identical to the production missile/canister combination, there are a number of important differences. The canisters are attached to the clamp rings with fewer bolts. In addition the interaction between the canister and the missile supported on its studs and shoes is not simulated. Because of these differences, it can be assumed that the overall response of the LSS will be modeled correctly, but local responses due to missile action will not be simulated.

It was not possible to perform functional checks on the missile systems utilizing the dynamic simulators and trainers. Therefore, the program was exploratory in nature rather than aimed at qualification.

The original production of the isolation pads consisted of a metal and elastomeric laminate formed to the curvature of the canisters, Figure 3.1. On installation, these are shimmed to provide for proper alignment along the length of the canister. This configuration has been susceptible to corrosion in the field.

The modified pad was developed by PMTC, consisting of a single piece of elastomeric material which is noncorrosive and easier to manufacture and install, Figure 3.2. This design was developed with respect to function and ease of installation.

It should be noted that gaps were found between clamp frame and the canisters on the trainers during the testing. An additional rubber shim was placed in this gap when the failed bolts were replaced.

Instrumentation required for the testing consisted of accelerometers mounted at various locations on the test item. The locations of the accelerometers are given in Figure 3.3. In addition, the orientation for each of the accelerometers for a given axis of excitation is given in Table 3.1. A total of 25 accelerometers were utilized for this testing, including the control accelerometer which was located in the center of the vibration table.

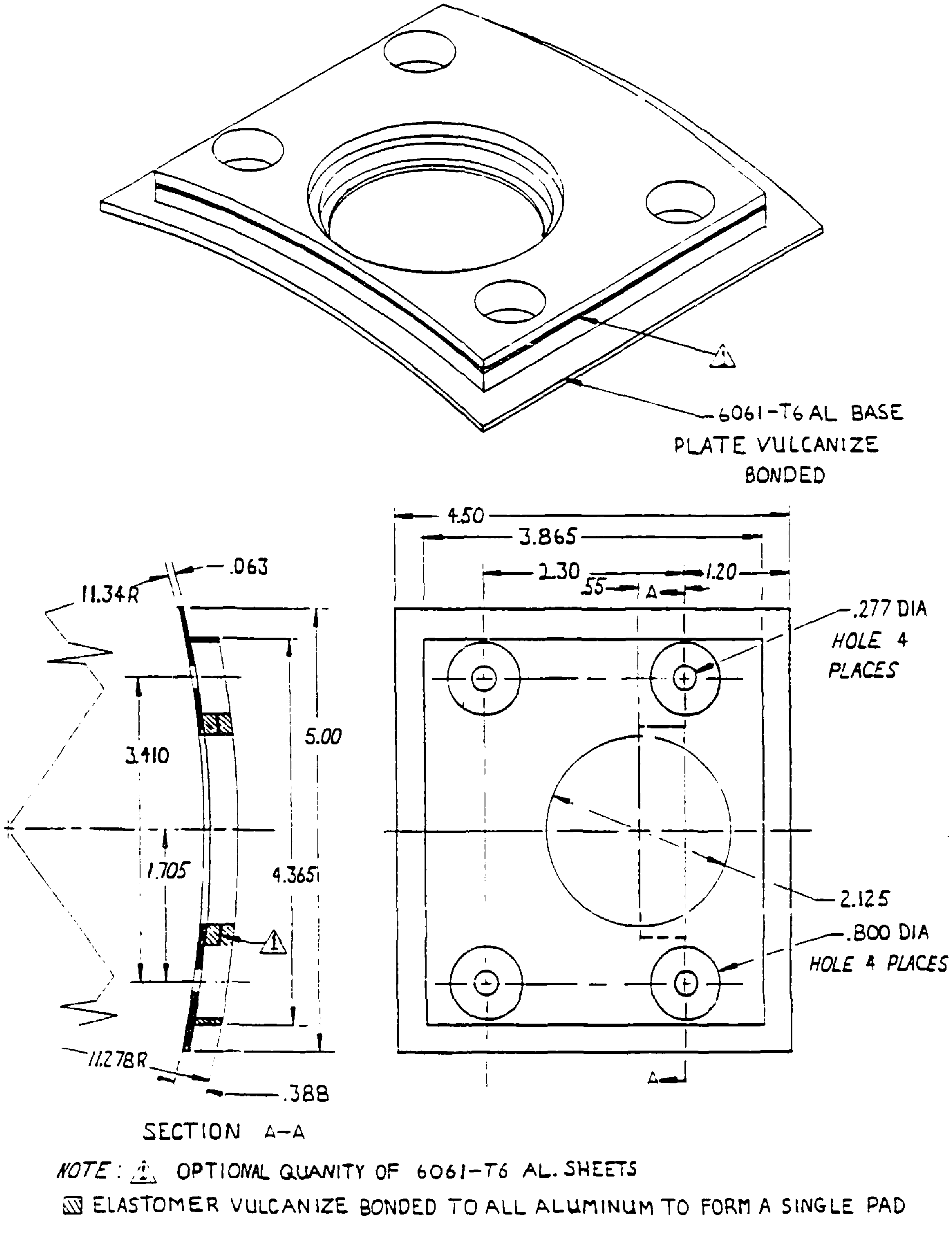

Figure 3.1 Production Isolation Pad Configuration

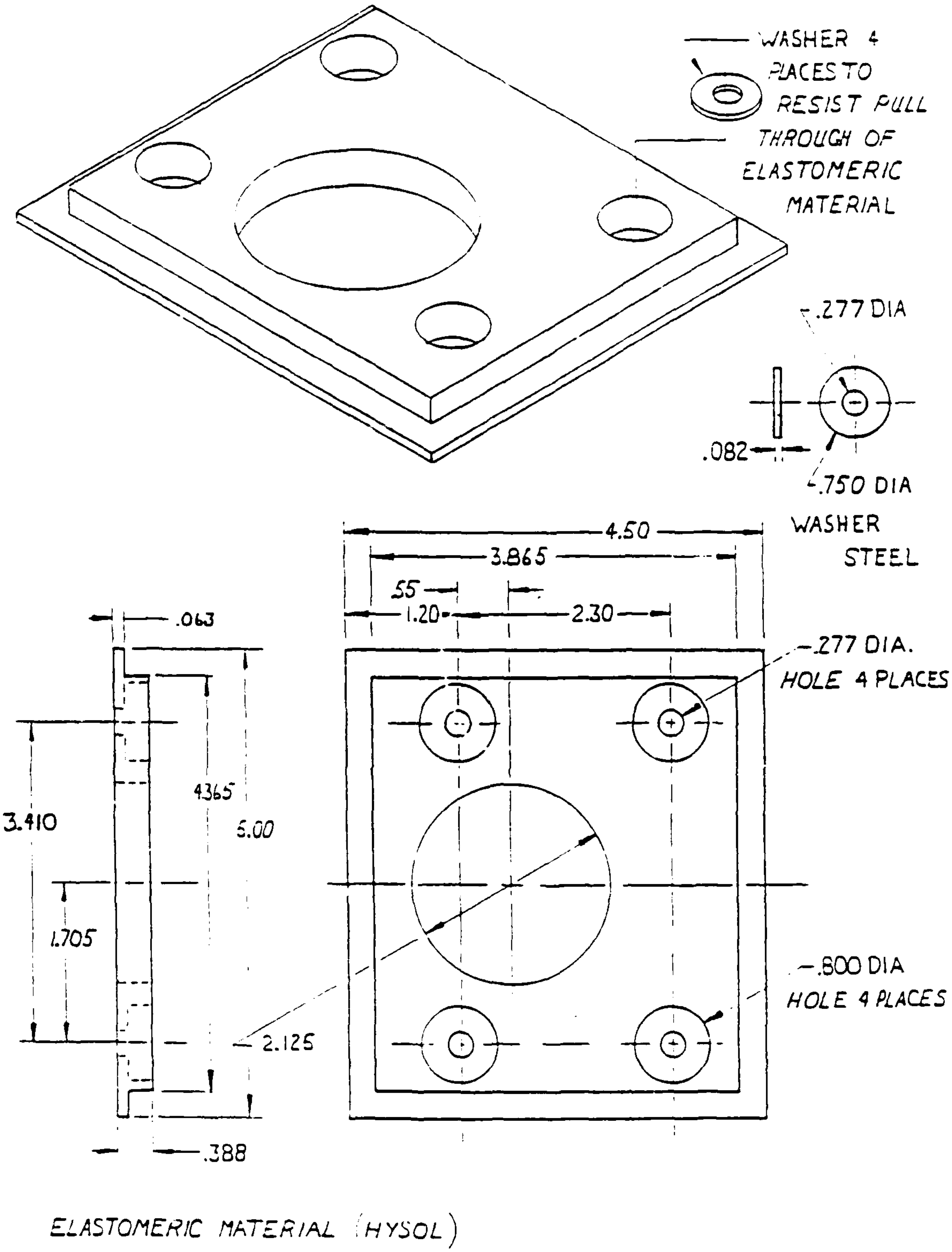

Figure 3.2 Modified Isolation Pad Configuration

Number	Location
1	Control
2-4	Lower Dynamic Simulator
5-7	Upper Dynamic Simulator
8-15	LSS Feet
16, 21, 23, 24	Clamp Frame
18, 19, 20, 22	Grade-B Canister @ Clamp Frame
17, 25	Grade-B Canister @ Nose

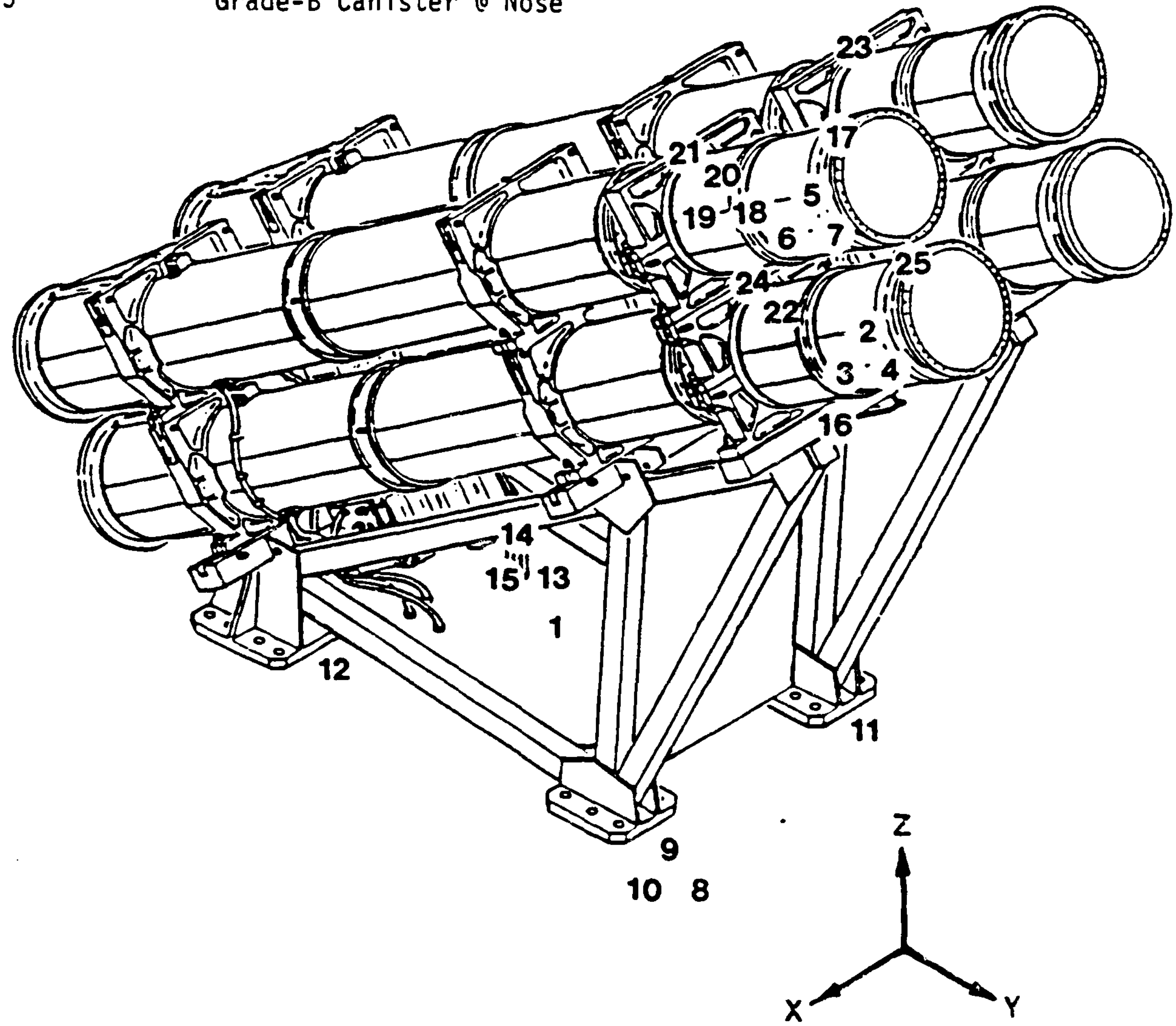

Figure 3.3 Accelerometer Locations

The dynamic simulator data, in dynamic simulator coordinates, was transformed to the global coordinate system during the analysis. In addition, sign corrections were applied to certain channels to insure proper phasing for the low frequency results.

Data from the accelerometers was recorded on a 14-channel tape deck for later analysis. In addition, certain channels were recorded on a strip-chart for information during the testing sequence.

Table 3.1 Accelerometer Location and Orientation

Number	Location	Response Direction		
		X-Axis Test	Y-Axis Test	Z-Axis Test
1	Table Center (Control)	X-Axis	Y-Axis	Z-Axis
2	Lower DS[2] Interior	DS Longitudinal		
3	Lower DS Interior	DS Transverse		
4	Lower DS Interior	DS Vertical		
5	Upper DS Interior	DS Longitudinal		
6	Upper DS Interior	DS Transverse		
7	Upper DS Interior	DS Vertical		
8	Forward Left Foot	Y-Axis		
9	Forward Left Foot	Z-Axis		
10	Forward Left Foot	X-Axis		
11	Forward Right Foot	X-Axis	Y-Axis	Z-Axis
12	Rear Left Foot	X-Axis	Y-Axis	Z-Axis
13	Rear Right Foot	Y-Axis		
14	Rear Right Foot	Z-Axis		
15	Rear Right Foot	X-Axis		
16	Left Clamp Frame Lower	X-Axis	Y-Axis	Z-Axis
17	Top DS at Nose	X-Axis	Y-Axis	Z-Axis
18	Top DS at Clamp Frame	Y-Axis		
19	Top DS at Clamp Frame	X-Axis		
20	Top DS at Clamp Frame	Z-Axis		
21	Left Clamp Frame Upper	X-Axis	Y-Axis	Z-Axis
22	Lower DS at Clamp Frame	X-Axis	Y-Axis	Z-Axis
23	Right Clamp Frame Upper	X-Axis	Y-Axis	Z-Axis
24	Left Clamp Frame Middle	X-Axis	Y-Axis	Z-Axis
25	Lower DS at Nose	X-Axis	Y-Axis	Z-Axis

2 DS = Dynamic Simulators

4.0 TESTING PERFORMED

Following the testing, Wyle Laboratories produced a test report [2.3] which gives the testing performed and the instrumentation utilized in the testing. Note tnat their definition of the axes are different than those in the test plan or those utilized in this report. Axes utilized for this report are:

X-Axis	Transverse (Perpendicular to length of dynamic simulator/ canister)
Y-Axis	Longitudinal (Along length of dynamic simulator/canister)
Z-Axis	Vertical

Table 4.1 summarizes the testing performed. The complete sequence of MIL-STD-167 testing was not performed due to the damage sustained by the trainers during the initial series of variable frequency tests. To eliminate the potential of damage to the test items, it was determined that only the exploratory vibration testing was to be performed for both configurations. In this way, the concept of NDE could be maintained.

Table 4.1 Summary of Testing Performed

Configuration	Axis	Test	Date
Original Pads	X	Modified Exploratory	8/25/88
		Variable Frequency to 12 Hz	8/25/88
		Damage to Trainers	
	X	Modified Exploratory	8/31/88
	Z	Modified Exploratory	9/1/88
	Y	Modified Exploratory	9/1/88
Modified Pads	Y	Modified Exploratory	9/7/88
	Z	Modified Exploratory	9/7/88
	X	Modified Exploratory	9/8/88

The first group of tests defined in MIL-STD-167 is the Exploratory Vibration tests, Figure 4.1. In MIL-STD-167 these are defined as stepped sine tests at 1 Hz intervals with defined displacement inputs. The frequency range is defined as 4 to 50 Hz. These tests are designed to define the dynamic characteristics of the system under test. For this series of tests the stepped sine tests were replaced with swept sine tests at a constant input acceleration of 0.2 g's. In addition, the frequency range was extended up to 100 Hz. These changes to the modified exploratory conditions, Figure 4.1, were made to facilitate subsequent data reduction and provide additional data.

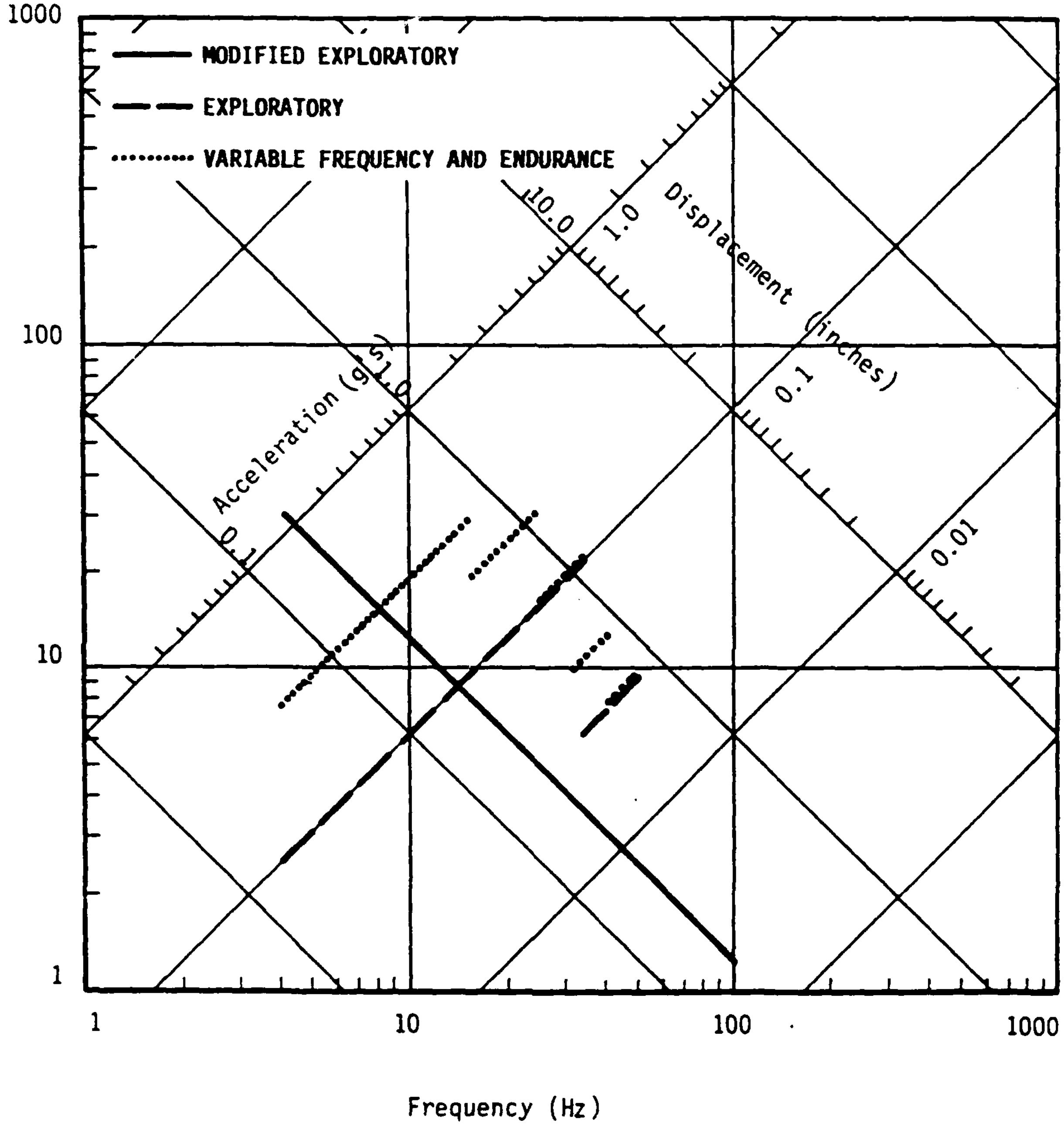

Figure 4.1 MIL-STD-167 Vibration Levels

The second group of tests defined in MIL-STD-167 is the Variable Frequency tests, Figure 4.1. For this testing, the item was to be tested at discrete frequency intervals of 1 Hz from 4 to 50 Hz. At each frequency, the duration of the testing was five minutes at a defined level, as given in Table 4.2. Due to the damage to the trainers during the initial series of variable frequency tests, this part of the requirement was dropped by consent of all concerned parties.

Table 4.2 Vibration Displacement Amplitudes

Frequency Range (Hz)	Table Amplitude Peak Displacement (Inches)
4 to 15	0.030 ± 0.006
16 to 25	0.020 ± 0.004
16 to 33	0.010 ± 0.002
34 to 40	0.005 ± 0.001
41 to 50	0.003 + 0.000, - 0.001

The final sequence of testing defined in MIL-STD-167 are endurance tests. These are long duration sine dwells at the resonances defined during the exploratory vibration tests. The levels of excitation at the defined resonances are again given by Table 4.2. This group of tests was also dropped with the consent of all groups concerned.

As the testing was finally completed, only the modified exploratory vibration tests were performed. Because of the fact that the modified isolation pads were only prototypes and it was not possible to perform functional checks on the missiles, this was acceptable. Sufficient information was obtained to satisfy the basic requirements of the program.

5.0 RESULTS

The results of the testing are broken down into two major groups. The first are those observations and conclusions drawn during the testing sequence. They deal primarily with subjective observations of the performance of the item during the testing. The second group is a result of the analysis of the recorded acceleration data.

5.1 Testing

The first major observation, which has been touched on already, is the fact that the trainers are not designed to withstand dynamic excitation. During the X-Axis Variable Frequency testing, there was significant damage to the attachment of the trainers to the stacking frames. The bolts utilized to make this connection broke in a number of locations. Damage occurred during the testing at 13 Hz and was accompanied by a popping noise. It was noted that the number of bolts on the trainers was significantly less than on the other Grade-B canisters, by a factor of four. To allow for subsequent testing, the bolts were replaced with 1/4-inch Grade 8 bolts.

In addition to the bolts, it was noted that there was a gap, 0.025 inches, between the clamp frame and the isolation pad on one of the trainers. An additional shim was added to fill this gap at the same time the bolts were replaced.

A crack was noted in the flange and web on the aft stacking frame of one of the trainers, see photographs. A pre-test inspection was not performed of this region, so it was not possible to determine if it was a result of the testing. To blunt the crack in the web, a hole was drilled at its tip. In addition, a steel channel section was laid across the bolts to provide support, see photographs. It was felt that these modifications would not significantly affect the overall dynamic response of the system.

Observations made during the testing indicated that the primary response for X-Axis input of the configuration with production isolation pads was motion of the canisters on the LSS. The LSS structure showed very little motion.

Motion in the first mode was dominated by rocking of the canisters and their frames on the LSS. At the higher frequencies, there was significant rattling of the dynamic simulator in the canisters.

For Y-Axis input, longitudinal, the first mode was a longitudinal bending mode. For this mode, the separation of LSS and canister motion was not as evident. Again, there was significant rattling of the dynamic simulator in the canister at the higher frequencies.

It was not possible to observe the vertical mode in any detail during the Z-Axis testing. It was evident that there was coupling between the vertical, input, and longitudinal response of the test item.

During the installation of the new isolation pads, several problems were encountered. The first was associated with the torque in the bolts utilized to hold the pads to the canister. The production pads are designed so that the torque on the mounting bolts should be between 25 and 40 in-lb. The bolts holding the modified isolation pads were initially torqued to 30 in-lb. At this level, the bolts pulled themselves through the elastomeric material and the edges of the pads rolled up. The internal metal parts in the production shims allowed for the higher level of bolt torque. It was decided to install the modified pads with bolt torques between 2.5 and 5 in-lb.

It was also determined that the modified isolation pads would require the same shims that were utilized in the production pads to bring the thickness up to that required. It is possible that thickness of the modified pads can be increased such that these shims are not required.

A final problem with the modified isolation pads was that two of the pads did not line up completely with the clamping frame. Approximately 1/4 inch of pad stuck out past the frame.

Observations made during the testing of the configuration with the modified isolation pads were similar to those made during the initial series of tests.

5.2 Data Analysis

All data analysis was performed using the taped acceleration data. The data was recorded on standard IRIG 14-channel tape such that it would be compatible with equipment at SwRI.

It was first necessary to develop scaling factors to convert the voltage levels to acceleration. This was accomplished by reading the calibration signals of the tape and developing the appropriate conversion factor, acceleration per volt, for each channel of data. These conversion factors were then utilized for all subsequent data analysis.

In addition, it was necessary to apply correction factors associated with the sign of the acceleration signal. During the testing, the sign of the accelerometers in relationship to the control was not noted. It was assumed that the signals should be in-phase at the low frequency limit. Sign correction factors were applied to the appropriate channels to accomplish this.

The data analysis required the development of power spectral densities (PSD's) and transfer function data from swept sine tests. Typically, swept sine data is analyzed utilizing tracking filters and plotting the amplitude of the filtered data as a function of frequency. In most cases, this assumes the input level is constant with respect to the excitation frequency, an appropriate assumption in most cases.

To expedite the data analysis for the large number of channels of acceleration data, 25 channels for 6 different test conditions, the analysis was performed utilizing a ZONIC 6088 8-channel fast Fourier transform (FFT) analyzer. This hardware was utilized to generate the PSD's and frequency response function data which was then transferred to a VAX lab/RT for subsequent analysis and display. The interface between these two systems had been developed at SwRI in a previous program.

The ZONIC is designed primarily for the analysis of random data. Because of this, it was necessary to perform some preliminary analysis to determine the expected results due to swept sine input. The first check was the calculation of a PSD for the constant amplitude swept sine data recorded on the tape. This PSD is given in Figure 5.1, where data are plotted for frequencies from 5 to 100 Hz.

It should be noted that the theoretical PSD for a sine wave is an impulse function of infinite amplitude at the sine wave frequency. Because of the

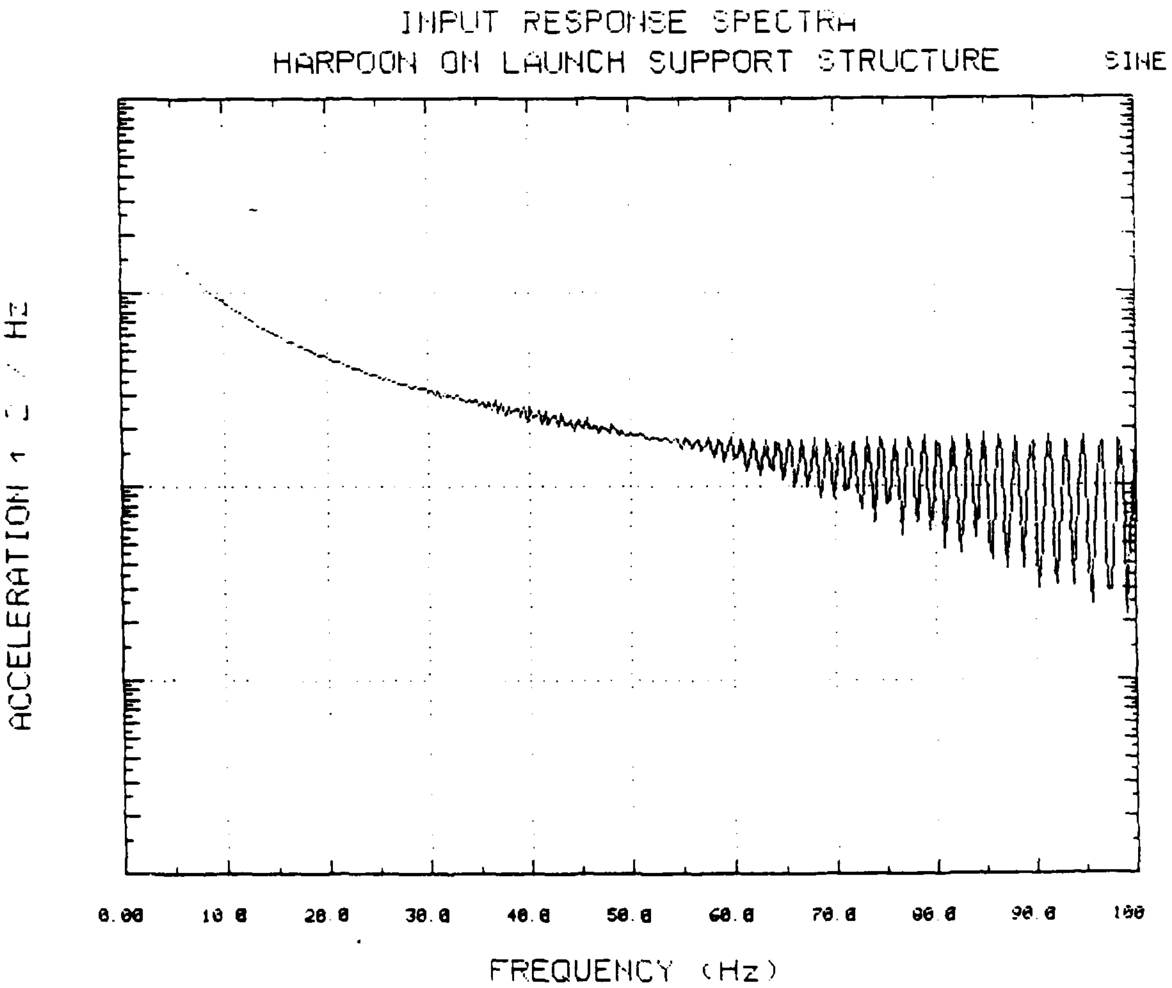

Figure 5.1 Data Analysis of a Constant Amplitude Sine Wave

finite bandwidth of the FFT analyzers, the calculated amplitude is finite. Therefore. it is possible to develop PSD for swept sine data that can be used for comparative purposes.

The important thing about this figure is the shape of the curve. For a logarithmic swept sine input at a constant level, the resulting curve is not flat with frequency. This is due to the averaging technique utilized during the analysis. To develop the composite PSD, the individual PSD's are summed together and then divided by the total number of averages. For a defined cutoff frequency of 125 Hz, the duration of each individual PSD is a constant, 3.2 seconds. For a logarithmic swept input, the amount of time spent in each frequency range is less with increasing frequencies. The result is that in the lower frequency ranges, there are more individual PSD's summed together resulting in a higher indicated level.

The second observation is associated with the oscillations evident in the higher frequency range. This oscillation is due in part to the fact that there are not a sufficient number of individual PSD's in this frequency range to get a good average. In addition, the time interval between samples in the analysis was too large.

5.2.1 Control Accelerometer PSD's

The PSD given in Figure 5.1 is the result of a constant level sine wave input. Actual PSD's from the control accelerometer are given in Section 9.0. Superimposed on these plots is a reference line representing the constant level sine wave data drawn at the appropriate amplitude. The general trend of all the control accelerometer data follows the theoretical line. The region where the test data drops significantly below the theoretical data is associated with resonances of the test item. In this region, it was not possible for the controller to maintain the appropriate input level due to dynamic compliance of the system.

Figures 9.1 to 9.3 are examples of the input PSD's for three successive runs for X-Axis input with the production isolation pads. The overall shape of each of these PSD's is similar, which indicates that successive runs had similar input. The drop-off in the high frequency region of Figure 9.2 is a result of the termination of data analysis at that frequency. The dip in the input PSD at 14 Hz indicates that this is the dominant mode for this axis.

Note that only representative samples of the data are presented in this report. Y-Axis input with the production isolation pads is given in Figure 9.4. The reduced level of the PSD at the dominant mode for this axis was not as evident as the X-Axis data. The controller was better able to control the input in this longitudinal direction.

The Z-Axis input with the production isolation pads are given in Figures 9.5 and 9.6. There is a significant difference between the two Z-Axis runs in the 35 to 42-Hz frequency range. The first run, Figure 9.5, had significantly more dropout in this region than the second, Figure 9.6. It is most likely that this dropout is due to the data acquisition mode utilized where data samples with overloads in any channel are rejected. Due to the resonance in this frequency range, overloads on some of the elevated locations are likely.

Data for the configuration with the modified isolation pads is given in Figures 9.7 to 9.10. The X-Axis data, Figure 9.7, is very similar to the original configuration with a significant reduction in level at approximately 14 Hz. This reduced level is also evident in the Y-Axis data, Figure 9.8, at approximately 16 Hz. The Z-Axis data, Figures 9.9 and 9.10, again show significant difference between runs. The difference is not evident for the input acceleration histories provided in the Wyle Test Report [2.3]. Again, this is probable because data obtained during overloads in a given channel are rejected. The overloads could have been the result of high frequency noise present at some response location at these frequencies.

5.2.2 Frequency Response Functions for the LSS Feet

The frequency response functions were obtained by relating the response acceleration data at a given location to the control acceleration data. Transfer functions were obtained in terms of both the amplitude and phase relationships between the two signals and the corresponding real and imaginary parts. In most cases, only the amplitude and phase data are given in this report since most readers will be more familiar with this presentation.

Data is plotted in the frequency range of 5 to 100 Hz. The amplitude term in the frequency response function is scaled to optimize data presentation. A value of 10^0, i.e., 1.0, would represent the case where the response is equal to the input level. Anything above this line represents an amplification, while data below is an indication of isolation. Phase data is plotted from -180 to +180 degrees, with 0 degrees in the center. Scales on the real and imaginary part are again optimized for data presentation.

Since both the input and response values were in terms of acceleration, the transfer functions can be used to indicate the expected acceleration at a point for a given input acceleration at any given frequency. As with most analysis of this type, the concept of linearity with input amplitude is assumed.

Data is given in order of accelerometer number.

The frequency response functions for the accelerometers located on the feet of the LSS for the configuration with the production isolation pads are given in Figures 10.1 to 10.24. Results for the modified isolation pads are similar with the exception of two conditions, Figures 10.25 and 10.26. Results at these two locations seem to be off by a scale factor. Since both of these are cross-axis response, it was not possible to determine if there was any error. As expected, the modified isolation pads had little effect on the response at the feet of the LSS.

For X-Axis input, Figures 10.1 to 10.8, there is significant motion in all three directions. This is evident at the first dominant mode of the system, approximately 14 Hz. At this frequency the transverse motion of the front, Figures 10.3 and 10.4, and rear, Figures 10.5 and 10.8, feet are out-of-phase. For the longitudinal direction, the motion at the front, Figure 10.1, and rear, Figure 10.6, are in-phase prior to the resonance and out-of-phase after the resonance. The magnitude of the longitudinal response at both the front and rear feet is comparable to the input levels with the front foot showing slightly higher response, amplifications of 3.4 and 1.0 respectively. Similar conclusions can be drawn for the vertical motion, Figures 10.2 and 10.7. The vertical response levels at the front and rear feet are lower than the longitudinal direction, amplifications of 1.3 and 0.13, respectively.

It can be concluded that for X-Axis input, transverse motion, there was significant cross-coupling of motion at the feet of the LSS during testing at the first dominant mode. Testing on a larger table with more restraint against out-of-plane motion would have helped this problem.

Cross-coupling for Y-Axis input, Figures 10.9 to 10.16, is not as dominant as that for X-Axis input. In the input axis, Figures 10.9, 10.12, 10.13, and 10.14, there are no major variations in level below 60 Hz. The transverse motion, Figures 10.11 and 10.16, shows an increased level, amplification of 0.6 of the input level at approximately 18 Hz. The vertical response, Figures 10.10 and 10.15, has a response at the same frequency at a level approximately equal to the input.

Z-Axis input, Figures 10.17 to 10.24, again shows significant cross-coupling. Above 30 Hz, magnitude of the vertical response at the four feet, Figures 10.18, 10.20, 10.21, and 10.23, varies significantly. The transverse response, Figures 10.19 and 10.24, shows significant motion at approximately 9 Hz, amplification of 0.6 at the front foot and 0.4 at the rear foot; and at 32.5 Hz, amplification of 7.7 at the front foot and 2.5 at the rear foot. Similar data is evident in the longitudinal direction, Figures 10.17 and 10.22. For this direction, the front foot shows amplification of 1.0 and 5.6 at the two frequencies, while the rear foot is 0.3 and 1.9, respectively. This means that at approximately 32.5 Hz for a 1 g vertical input at the table center, one could expect 7.7 g's in the transverse direction and 5.6 g's in the longitudinal direction.

It can be concluded that for Z-Axis input, vertical motion, there was significant cross-coupling of motion at the feet of the LSS during testing at two modes. Testing on a larger table with more restraint against out-of-plane motion would have helped this problem.

5.2.3 Frequency Response Functions for Elevated Positions

As with the previous data, the frequency response functions at the elevated positions were obtained by relating the response acceleration data at a given location to the control acceleration data. Transfer functions were displayed in terms of both the amplitude and phase relationships between the two signals and the corresponding real and imaginary parts.

The frequency response functions are used to define the resonance frequencies of the system and the corresponding mode shapes. Interpretation of the frequency response functions is based on the assumption of widely separated modes and a linear system. In this case, a resonance of the system can be defined in terms of the amplitude and phase response function or the real and imaginary response function. These two are mathematically related and are just different ways of viewing the same data.

For the amplitude and phase response function, a resonance is defined when the amplitude reaches a peak and the phase shows a shift through 90 degrees. This assumes that the accelerations are either in-phase or 180 degrees out-of-phase prior to the resonance. The corresponding resonance will show up as a peak in the imaginary part, with a transition through zero on the real part.

For the actual system under consideration, there are a number of frequencies where there are closely spaced modes. These represent modes on the cross axes as well as those in the same axis. An example of this is the response of the dynamic simulator and trainer sides, which have slightly different masses and stiffness resulting in slightly different frequencies. This makes interpretation of the data more difficult. Local as well as global peaks and transitions through zero represent resonances. Therefore, results must be based on engineering interpretation of the data.

Since both the input and response values were in terms of acceleration, the transfer functions can be used to indicate the expected acceleration at a point for a given input acceleration. As with most analysis of this type, the concept of linearity with input amplitude is assumed.

Table 5.1 summarizes the frequency response function data for elevated locations given in Section 10.0. A large amount of data is included so that the reader can make his own interpretation if he desires.

Table 5.1 Summary of Elevated Response Data

Input Axes	Pads	Figures
X	Production	10.27 to 10.45
X	Modified	10.46 to 10.55
Y	Production	10.56 to 10.68
Y	Modified	10.69 to 10.81
Z	Production	10.82 to 10.94
Z	Modified	10.95 to 10.107

remember is that there is significant cross-axis response for X, transverse, and Z, vertical, input. The level of the cross-axis response is dependent on the frequency and the foot in question, with the forward foot showing more response.

Accelerometers 16 to 25 represent elevated locations on the LSS and canisters (Figure 3.3). The final group of data, GB X, GB Y, GB Z, GT X, GT Y and GT Z, represents the response at the seeker bulkhead of the dynamic simulators. They are defined in terms of the global response direction, G, for the bottom, B, and top, T, dynamic simulators for each of three axes.

X-Axis input for the configuration with the production isolation pads, Table 5.2 (a), and the modified isolation pads, Table 5.2 (b), shows similar response at the clamp frame locations, accelerometers 16, 24 and 21 (bottom to top). This is true for the majority of frequencies indicated. It therefore can be assumed that the isolation pads have little effect on the acceleration levels on the clamp frame, i.e., input into the isolation pads is similar for both configurations. In the low frequency range, below 20 Hz, the level of response increases with increased height.

Based on the assumption that the response at the clamp frame is similar for both isolation pads, it is then necessary to look at the response of the Grade-B canister adjacent to the clamp frames, accelerometers 24 and 19. On the lower canister, the input levels are only slightly higher for the configuration with modified isolation pads. The top canister shows a significant increase in levels, in some cases a factor of two, for the modified isolation pads.

The interesting aspect of this is that the response of the dynamic simulators in the direction of excitation is lower for the configuration with the modified isolation pads. Therefore, even though the input levels into the canister are higher, the response of the dynamic simulators are lower. When considering cross-axis response, the bottom dynamic simulator shows a lower level, while the top dynamic simulator shows a higher level for the configuration with the modified isolation pads.

It is not apparent why the dynamic simulator results are as shown. It may be because the tests with the modified isolation pads were done subsequent to the production pads. Results from the laboratory testing performed

Table 5.2 (a)

HARPOON on LSS Wyle Testing

Amplification for X-Input Original Configuration

Accel No.	Node No.	Resonant Frequency (Hz)					
		13.75	15.31	21.25	25.94	34.38	41.56
8	1 *	3.44	1.70	0.43	0.65	3.86	1.14
9	*	1.33	0.84	0.21	0.26	0.41	0.29
10		0.63	1.71	1.21	1.27	1.16	1.04
11	2	0.78	1.62	1.15	1.22	1.09	1.01
12	3	2.40	0.36	0.87	0.70	1.06	1.08
13	4 *	0.96	0.44	0.11	0.10	0.40	0.83
14	*	0.13	0.05	0.69	0.29	0.23	0.54
15		2.17	0.34	0.86	0.67	0.98	1.07
16	5	2.49	0.41	1.97	0.16	1.13	1.74
17	5	11.23	7.49	2.16	2.44	1.99	1.51
18	7 *	3.48	3.10	4.02	1.14	0.47	0.56
19		7.06	4.49	1.35	1.51	0.91	0.79
20	*	1.28	0.88	1.13	1.20	0.89	1.88
21	8	11.17	7.10	1.95	2.28	1.79	1.29
22	9	5.87	3.23	1.52	0.89	0.10	0.67
23	10						
24	11	7.24	4.11	1.25	1.12	0.35	0.20
25	12	5.50	2.93	1.56	0.86	0.22	1.30
GB X	13	11.40	6.60	1.76	2.33	2.06	1.26
GB Y	*	4.79	3.34	5.00	1.13	0.78	1.13
GB Z	*	1.76	1.30	3.23	0.25	1.05	2.85
GT X	14	5.50	2.88	0.70	0.61	0.15	0.83
GT Y	*	0.46	1.71	5.26	0.61	1.67	5.19
GT Z	*	1.32	0.44	2.43	0.44	1.57	4.27

* Indicates Cross-Axes Responses

Table 5.2 (c)

HARPOON on LSS Wyle Testing

Amplification for Y-Input Original Configuration

Accel No.	Node No.	Resonant Frequency (Hz) 15.94	17.19	30.00	47.50	57.50
8	1	0.99	1.01	0.93	0.81	0.96
9	*	0.72	0.88	0.46	0.26	0.48
10	*	0.31	0.52	0.13	0.24	0.24
11	2	0.96	0.94	1.02	1.04	1.03
12	3	0.99	0.99	0.93	0.90	1.06
13	4	0.92	0.85	0.95	0.97	1.03
14	*	0.77	0.77	0.22	0.87	0.25
15	*	0.40	0.54	0.09	0.13	0.23
16	5	3.28	3.02	0.23	0.82	1.19
17	6	6.20	6.10	1.32	1.16	0.99
18	7	5.53	5.43	0.97	0.50	0.85
19	*	1.16	1.52	0.31	0.44	0.07
20	*	0.55	0.54	0.74	1.25	0.47
21	8	7.18	7.36	2.54	5.97	3.22
22	9	4.24	4.01	0.44	0.27	0.88
23	10	11.43	10.42	1.21	1.53	1.46
24	11	4.22	3.21	0.22	0.17	0.46
25	12	5.14	4.57	0.81	0.52	1.14
GB X	13 *	1.75	2.12	0.55	1.53	0.65
GB Y		5.08	5.80	0.90	1.19	0.21
GB Z	*	1.99	2.20	1.66	4.06	3.06
GT X	14 *	0.90	1.10	0.33	0.17	0.32
GT Y		5.70	6.13	1.40	2.17	1.96
GT Z	*	3.33	3.62	1.65	2.59	0.70

* Indicates Cross-Axes Responses

Table 5.2 (d)

HARPOON on LSS Wyle Testing

Amplification for Y-Input New Configuration

Accel No.	Node No.	Resonant Frequency (Hz) 16.25		30.00	49.38	57.19
8	1	0.88		0.99	0.77	0.91
9	*	1.78		0.42	0.94	0.55
10	*	0.12		0.07	0.37	0.18
11	2	1.02		0.95	1.02	0.97
12	3	0.92		0.95	0.83	1.01
13	4	1.02		0.94	1.05	0.99
14	*	0.96		0.21	1.04	0.81
15	*	0.18		0.04	0.14	0.25
16	5	6.00		0.07	0.97	1.43
17	6	12.23		1.37	1.38	1.37
18	7	10.73		0.94	0.19	1.09
19	*	0.31		0.34	0.63	0.18
20	*	1.66		0.68	1.93	0.55
21	8	15.09		1.28	2.98	0.77
22	9	8.21		0.36	0.60	1.41
23	10	14.90		1.17	2.08	1.33
24	11	8.97		0.45	0.86	1.24
25	12	8.66		0.70	1.09	1.70
GB X	13 *	0.85		0.77	2.22	0.78
GB Y		10.57		0.93	1.30	1.15
GB Z	*	4.28		1.49	5.28	1.87
GT X	14 *	1.92		0.23	0.18	1.46
GT Y		12.55		1.22	3.78	4.33
GT Z	*	8.18		1.51	2.65	2.36

* Indicates Cross-Axes Responses

at PMTC indicated that resetting of the stud torques was important in developing consistent results. The torques could have loosened during the original sequence of testing, resulting in the lower level of input in the low frequency range.

When considering Y-Axis input, Tables 5.2 (c) and 5.2 (d), the response of the frames for the lowest frequency, approximately 16 Hz, shows a significant increase, a factor of two, with the modified isolation pads. At the other frequencies, the levels are similar. For this configuration, there seems to be some feedback of energy from the canisters to the stacking frame at the first mode, assuming no other changes to the system.

When considering the transfer of energy from the clamp frame to the canister, with a normalized level at the clamp frame, there is no significant difference between the two configurations for Y-axis input. The actual levels at the canister for the new configuration are higher as a result of the higher levels at the clamp frame.

Similar results are also evident for the response of the dynamic simulators. The first frequency shows a significant increase, with higher frequencies similar in level. When considering cross-axes response, the levels are similar throughout the frequency range.

It is possible that the reason for this significant difference in the lower frequency range is that the two modes noted in the original configuration, 15.94 and 17.19 Hz, have collapsed into a signal frequency at 16.25 Hz. If one sums the levels for the first two frequencies in the original configuration, they are similar to that with the modified isolation pads. It is possible that the stiffness of the two isolation pads is different enough to cause this change. It may also be possible that the difference is a result of the installation procedures. With the information available, it is not possible to provide a concrete answer to the question.

Z-Axis input for the configuration with the production isolation pads, Table 5.2 (e), and the modified isolation pads, Table 5.2 (f), shows similar response at the clamp frame locations. This is true for the majority of frequencies indicated. The exception is the upper clamp frame around 30 Hz where the production configuration shows a higher level than the modified isolation pads. It therefore can be assume that the isolation pads have little effect on the acceleration levels on the clamp frame, i.e., input into the isolation pads is similar for both configurations.

Based on the assumption that the response at the clamp frame is similar for both isolation pads, it is then necessary to look at the response of the Grade-B canister adjacent to the clamp frames, accelerometers 24 and 19. On the lower canister, the input levels are only slightly higher for the configuration with modified isolation pads. The top canister shows an increase in levels for the modified isolation pads.

Both along-axis and cross-axes response of the dynamic simulators are similar for both configurations. In virtually all aspects, the response of both configurations to Z-axis input is similar.

From a review of the amplification at elevated location presented in Table 5.2, the response of both configurations is similar for the swept sinusoidal input at 0.2 g's input. The only differences noted were for the Y-Axis response, which may be a result of collapsing modes. It therefore can be assumed that a change in isolation pads to those designed by PMTC will not have a significant effect on the dynamic response of the system, within the frequency range up to 60 Hz. Above this frequency, it was not possible to define the response with enough detail to compare results. It was also not possible to compare the overall levels due to modal response and rattling.

Table 5.2 (e)

HARPOON on LSS Wyle Testing

Amplification for Z-Input Original Configuration

Accel No.	Node No.	Resonant Frequency (Hz)			
		20.00	32.50	36.88	41.56
8	1 *	0.22	5.55	0.58	1.99
9		1.01	1.39	1.17	0.80
10	*	0.33	7.63	2.73	1.21
11	2	1.11	2.01	0.90	0.41
12	3	0.93	2.52	1.80	2.57
13	4 *	0.07	1.89	0.45	0.40
14		0.98	0.72	1.11	1.55
15	*	0.11	2.49	1.40	0.39
16	5	1.07	2.00	2.32	0.96
17	6	1.52	4.73	5.93	3.88
18	7 *	0.44	0.79	2.26	1.28
19	*	0.29	0.84	1.89	1.19
20		1.49	3.68	5.47	3.28
21	8	2.05	25.07	18.79	8.64
22	9	1.20	2.54	3.91	2.09
23	10	1.66	11.22	6.76	4.28
24	11	1.30	3.07	2.78	2.07
25	12	1.21	2.93	4.34	3.19
GB X	13 *	0.60	5.66	2.32	3.54
GB Y	*	1.59	0.84	3.77	1.42
GB Z		1.94	5.55	5.16	7.13
GT X	14 *	0.38	1.25	0.39	0.38
GT Y	*	2.30	3.44	4.63	7.84
GT Z		1.37	4.11	4.03	7.37

* Indicates Cross-Axes Responses

Table 5.2 (f)

HARPOON on LSS Wyle Testing

Amplification for Z-Input New Configuration

Accel No.	Node No.	Resonant Frequency (Hz) 20.00	32.50	36.88	39.69
8	1 *	0.03	1.04	0.51	0.48
9		1.07	1.27	1.05	0.87
10	*	0.36	6.39	2.46	1.53
11	2	1.01	1.80	0.93	0.68
12	3	0.78	1.58	1.83	2.07
13	4 *	0.10	2.13	0.75	0.48
14		1.18	1.66	0.85	1.06
15	*	0.12	3.69	1.75	1.28
16	5	1.30	1.91	2.17	1.16
17	6	1.66	3.81	8.55	6.91
18	7 *	1.73	1.06	1.63	1.14
19	*	1.01	2.40	2.31	1.89
20		1.48	3.43	6.53	5.23
21	8	2.37	11.03	7.62	4.99
22	9	1.25	2.32	3.52	2.36
23	10	2.14	9.28	5.98	3.78
24	11	1.38	1.55	1.85	1.72
25	12	1.33	2.52	4.75	3.25
GB X	13 *	1.02	2.42	3.19	1.92
GB Y	*	1.52	1.34	2.72	2.02
GB Z		1.83	4.01	7.60	7.18
GT X	14 *	0.47	0.92	1.18	1.36
GT Y	*	2.47	2.47	7.41	7.14
GT Z		1.87	4.52	8.06	6.44

* Indicates Cross-Axes Responses

5.2.4 Mode Shapes

The final aspect of the data analysis procedure was the development of mode shape plots for the resonances defined in the previous section. As noted earlier, the mode shapes were obtained by extracting the value of the imaginary part of the frequency response function at the selected frequencies. These values were then input into a plot package to display the results.

For this analysis, only response in the direction of input was considered. Data for cross-axes response was not available for all locations, so it was not possible to generate a full model with response in three mutually perpendicular axes.

The configuration of the model in relation to the structure is given in Figure 5.2. The description of locations is identical to that given in Figure 3.3. In addition, the relationship between accelerometer number and node number on the modal model is given in Table 5.2. Figure 5.3 shows the undeformed model from the oblique view utilized through the analysis. The reader is referred to Figures 5.2 and 5.3 for a relationship between the modal model and the physical system.

Mode shape plots for all the configurations are given in Section 11.0. In all cases, the plots are static representations of animated plots of the results. For this analysis, a total of seven time frames is represented. The middle configuration can be considered the undeformed shape of the system.

Figures 11.1 to 11.6 represent the results with the original production pads for X-Axis input, transverse. The first mode, 13.75 Hz, represents side-to-side bending of the system with the majority of the response coming from motion of the clamp frames, Figure 11.1. All points on the elevated structure are in-phase for this first mode with peak response at the upper clamp frame and the nose of the top Grade-B canister amplification of 11.2.

Note that data for X-Axis input with the production isolation pads at the upper clamp frame on the trainers was lost. Data recorded on the tape consisted of noise, so there was an apparent loss of signal for this specific channel during the testing.

Number	Location
1 to 4	LSS Feet
5, 8, 10, 11	Clamp Frames
7, 9	Grade-B Canisters @ Clamp Frame
6, 12	Grade-B Canisteers @ Nose
13, 14	Dynamic Switches

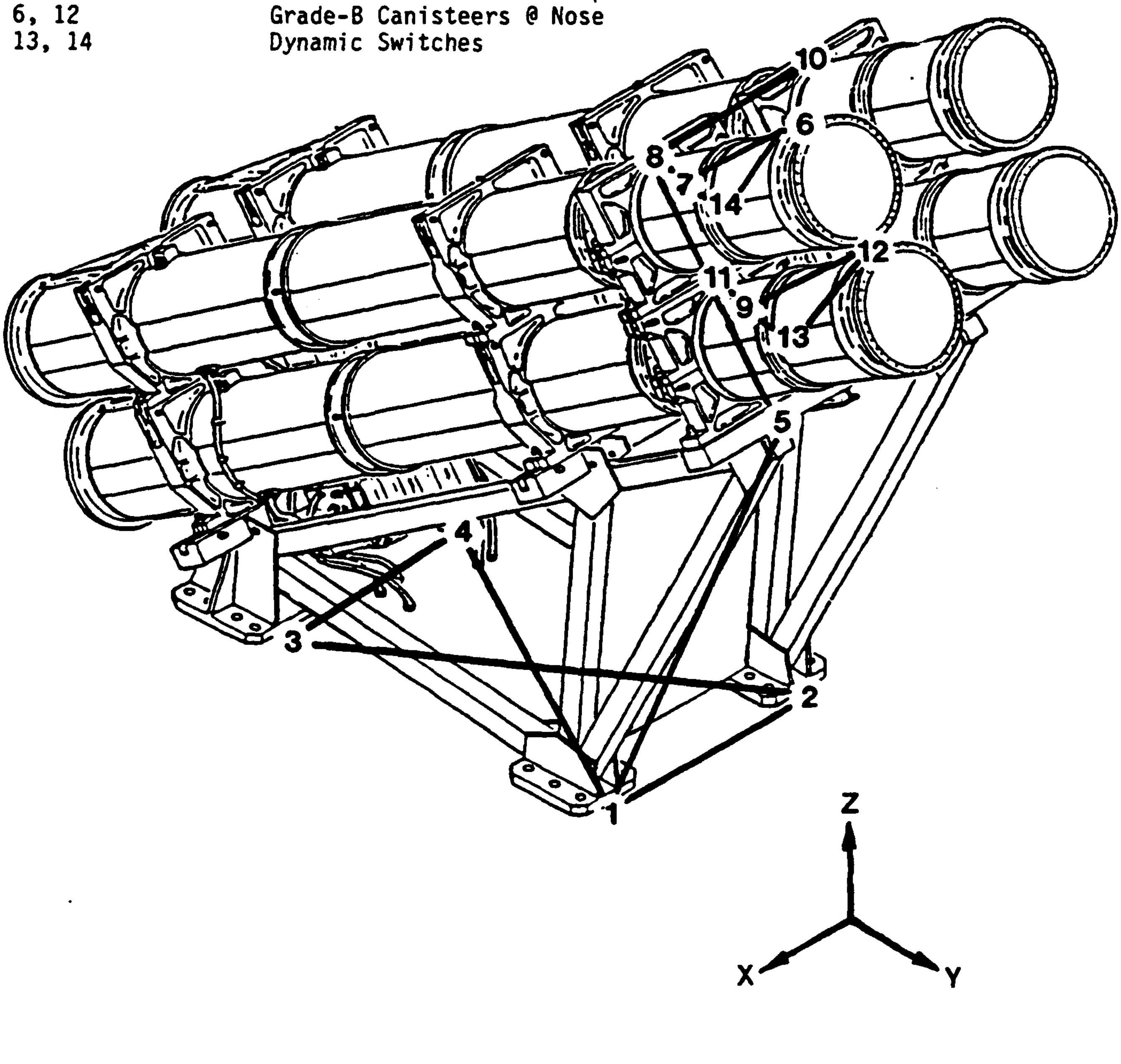

Figure 5.2 Modal Analysis Model

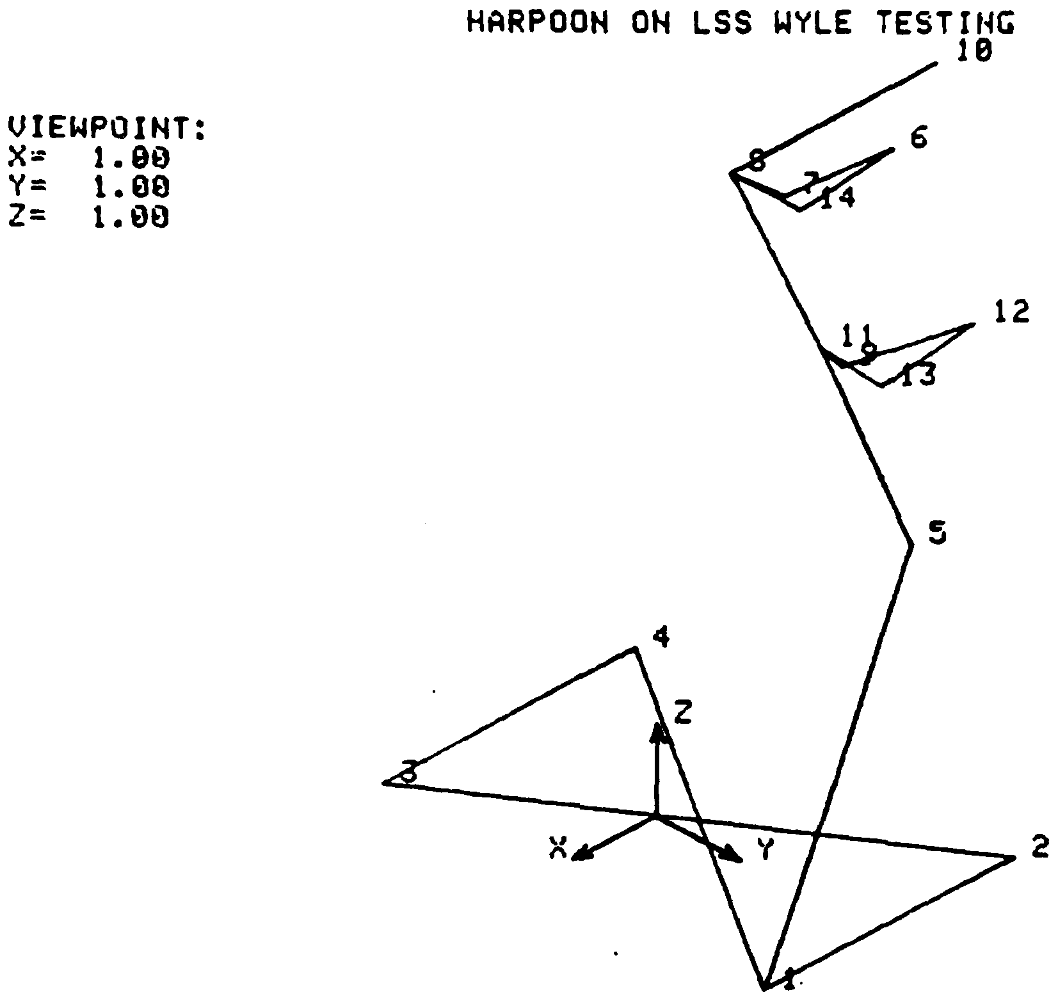

Figure 5.3 Undeformed Shape of Modal Analysis Model

The second mode, Figure 11.2, is 15.31 Hz and again represents a side-to-side bending. In this case, there is a definite node point at the attachment of the lower clamp frame to the LSS. Points above and below this location are out-of-phase with the exception of the dynamic simulator location. The dynamic simulator response is out-of-phase with the canister response, at a comparable level. The peak response is at the nose of the top canister with an amplification of 7.5.

All points on the model are again in-phase for the third mode, Figure 11.3, at 21.25 Hz. This seems to be some type of rigid body response of the system on the vibration table. It is possible that this is not a true mode of the system. For the along-axis response, amplification is greatest at the upper Grade-B canister near the clamp frame, 4.0. There is significant Y-axis response on both dynamic simulators, with amplifications of approximately 5.

The fourth mode, 25.94 Hz, is shown in Figure 11.4. This mode is very similar to the 15.31 Hz mode, with the exception that the dynamic simulators are in-phase with the canister for this mode. For this mode, the peak amplifications, 2.3 to 2.4, are on the upper clamp frame, the nose of the top Grade-B canister and the bottom dynamic simulator.

For the next mode, 34.38 Hz, the location of the node point has moved upward to approximately the center of the lower dynamic simulator. The lower dynamics simulator, upper clamp frame, and nose of the top canister all have amplifications of approximately 2.0. For this mode, there is significant response, an amplification of 3.8, in the Y-axis, longitudinal direction, at the front foot of the LSS.

The final mode defined for this configuration, Figure 11.6, again has the node point moving upward. In this case, it is located at the interface between the two clamp frames. In addition there is significant cross-axis response on both dynamic simulators. The upper missile shows the greatest response, with amplifications of 5.2 and 4.3 in the Y- and Z-axes, respectively.

Mode shape plots for the configuration with the modified isolation pads, Figures 11.7 to 11.11, show similar results to the original configuration. The first four modes at 13.44, 15.00, 20.94, and 23.75 Hz can be directly related to the 13.75, 15.31, 21.25, and 25.94 modes, with only slight variations in the amplitudes of the response. Note that the configuration with the modified isolation pads has slightly lower frequencies. Therefore, it can be assumed that this system is softer.

Data corresponding to the 34.38 Hz mode on the production configuration was not obtained for the modified isolation pads. The last mode, Figure 11.11, is similar to the 41.56 Hz mode of the production configuration. This correlation of mode shapes for X-Axis response again confirms that the modified isolation pads will not have a significant effect on the dynamic response of the system in the frequency range below 40 Hz. There could be some effect in the higher frequency range, but it was not possible to derive that information from the available data.

Mode shapes for Y-Axis input with the production isolation are given in Figures 11.12 to 11.16. In this case, we are looking at motion in the longitudinal direction only. The first two modes, at 15.94 and 17.19, are very similar, with only minor variations in amplifications at several locations. The maximum amplification on the dynamic simulator sides, located on the top of the upper clamp frame, was 7.2 and 7.4 for the two modes. For these modes, there was vertical response at both the front and rear feet of the LSS at an amplification of approximately 0.8. The vibration table was pitching under this longitudinal excitation.

The next mode, at 30.00 Hz, is complex in nature. Note that the upper clamp frame on the trainer side is out-of-phase with that on the dynamic simulator side. As can be seen, there are two nodes located at the mid-height of the LSS and the interface between the two clamp frames. For this mode, the dynamic simulators show significant motion in both the longitudinal and vertical direction. This is to be expected considering the geometry of the system. There is also significant motion of the LSS feet, indicating that the test item is driving the table. Maximum amplification for this mode is located at the upper clamp frame, at a level of 2.5.

The 47.5 Hz mode, Figure 11.15, appears to be primarily motion of the upper clamp frame with respect to the rest of the structure. The peak amplification, 6.0, is located at the upper clamp frame.

The final mode for this configuration, 57.5 Hz, again displays the out-of-phase relationship between motion on the trainer and dynamic simulators upper clamp frame. For this mode, the lower dynamic simulator has little motion in the longitudinal direction, 0.2, but significant motion in the vertical direction, 3.1. Conversely, the top missile is dominant by motion in the direction of excitation, an amplification of 2.0.

It is again possible to relate some of the mode shapes of the configuration with the modified isolation pads, Figures 11.17 to 11.20, to that with the production pads. The first mode for the modified isolation pads, 16.25 Hz, is similar in shape to the first two modes of the production configuration, 15.94 and 17.19 Hz. As indicated previously, it is possible that minor changes due to the installation of the pads caused these two modes to coalesce.

It is difficult to relate the three higher modes, at 30.00, 49.38, and 57.19 Hz, for the modified configuration with nose of the production pads. There are similarities, such as the motion of the feet of the LSS on the 30 00 Hz mode and response of the dynamic simulators on the 57.19 Hz mode. As the frequency increases, it becomes more difficult to pick out the resonances and resolve details of the motion.

Figures 11.21 to 11.24 represent the response of the system with the production isolation pads due to Z-axis, vertical, input. The first mode, at 20.00 Hz, represents a bounce mode of the system. The entire structure, including the feet of the LSS, is moving in the vertical direction. The dynamic simulators are the only locations which show significant cross-axis motion, Y-axis. The maximum amplification for this mode is 2.1, located at the upper clamp frame.

The second mode, 32.5 Hz, represents bending of the clamp frame in relation to the LSS. Although both clamp frames are moving, the top one shows significantly more relative motion between its top and bottom than the lower clamp frame. The trainer side is in-phase with the motion on the dynamic simulator side. The peak response is again on the top clamp frame with an amplification of 25.1.

The last two modes, Figures 11.23 and 11.24, show similar response, with the exception of the phasing of the trainer clamp frame motion with respect to the dynamic simulator clamp frame motion and the amplification, 18.8

and 8.6, respectively. In both cases, there is a node location at the junction of the upper and lower clamp frames. The top dynamic simulator in both cases shows comparable motion in both the Y- and Z-directions. On the bottom dynamic simulator, there is cross-axes response in both horizontal directions.

The rigid body bounce mode is also evident for the configuration with the modified isolation pads, Figure 11.25. There is one difference in the response in that the motion of the upper clamp frame is out-of-phase with the rest of the structure.

The bending mode of the clamp frame, 32.5 Hz, is similar to the production configuration. The primary difference is the reduction in amplification at the upper clamp frame for the modified isolation pad, 11.0 in relationship to 25.1. This reduction in amplification is also evident for the other two modes, Figures 11.27 and 11.28. The peak response is down by a factor of approximately two for the configuration with modified isolators. Although the response levels on the clamp frames are reduced, the levels on the dynamic simulators are comparable or greater for the modified configuration.

In summary, the mode shapes for both configurations tested, with production and modified isolation pads, are similar for all three axes of excitation. It can therefore be concluded that the modified isolation pads do not have a significant effect on the overall dynamic response of the HARPOON on the LSS.

6.0 COMPARISON TO PREVIOUS RESULTS

Results for the vibration testing of the HARPOON on the LSS has provided some useful information. One objective was to compare the response of the system with production and modified isolation pads. Results of this comparison are presented above. A second objective of the test program was to define the dynamic response of the system subjected to base input. Discussion of the mode shapes obtained from analysis of the data has already been presented.

Another objective of the analysis was to compare the results to previous information. Initial information on the dynamic response of the system was obtained from data during shipboard testing on the USS Mississippi [2.4 and 2.5]. From this data, it was apparent that there was some significant dynamic response under certain operating conditions.

To obtain a better understanding of the response, a modal analysis was performed aboard the USS Scott [2.6]. This series of tests verified the presence of dynamic compliance of the system. Modes of the system were defined for this specific installation.

Parallel to this study was a series of tests at PMTC to define the nature of the support of the missile inside a canister [2.7]. The laboratory tests consisted of excitation of a single dynamic simulator in a Grade-B canister on a test fixture. A number of tests were run with variations in the stud and shoes used to support the missile in the canister.

The results from each of these groups of tests will be briefly compared to the results of this series tests. In general, the results are favorable.

6.1 USS Mississippi Shipboard Testing

The shipboard testing on the USS Mississippi was performed to define the level of response on the HARPOON during normal shipboard operations. The testing consisted of measuring the acceleration response at a number of locations on the system during constant RPM tests, maneuvers, and gunfire conditions. The reader is referred to References 2.4 and 2.5 for detailed discussion of the results of this testing.

Both references indicated the presence of elevated response at specific frequencies. The dominant response was noted at 13 Hz under constant RPM testing. From the data, it was not possible to define the nature of the response, although McDonnell Douglas indicated that the highest response was in launcher lateral axes. Peaks were also noted at other frequencies, including 25, 37, 60, and 170 Hz. These frequencies were evident in both the vibration data and that produced during the gunfire.

The analysis of the data indicated a number of problems. These included clipping of the data during the gunfire and a variety of questions concerning accelerometer calibration, location, and orientation. In addition sea states occurring during the testing were benign, so their influence on the system was not observed. Because of these problems, additional tests were specified to clarify some of the results.

6.2 USS Scott Modal Testing

Among these tests was a modal analysis of the system performed on-board the USS Scott. Results of this testing are contained in Reference 2.6. These tests were performed by exciting the system in the transverse direction at the LSS near the clamp frame, and measuring the response at various locations on the structure. The results were then analyzed and displayed using a modal analysis system.

Table 6-1 summarizes the modes defined during the modal testing sequence. It is evident that the results compare favorably with those given in this report. The first mode at 13.13 corresponds directly to the 13.75 Hz X-axis input mode. There are slight differences in the frequency that are primarily due to difference in the compliance of the ship deck in relationship to the vibration table.

The second mode can be related to either the 15.94 or 17.19 Hz mode for Y-axis input, or the 20.0 Hz mode for Z-axis input.

The third mode, 25.94 Hz, obtained during the modal testing can be related to the 25.94 X-axis input mode. This is again transverse motion. Note that some modes indicated during the more recent testing were not analyzed during the initial modal testing on the USS Scott. During the USS Scott testing, all the analysis was performed on board ship. The selection of the specific frequencies at which modal data was recorded was made utilizing a limited number of locations. In the more recent data, the time history data was taped, and it was possible .o make the selection of the appropriate frequencies from a complete set of data.

Similar correspondence can be made for the fourth mode, 27.50 Hz, and either the Y-axis input mode at 30.0 Hz or the Z-axis mode at 32.5 Hz. The fifth mode at 31.25 Hz can be related to either the 32.5 of 36.88 Hz, Z-axis input modes. Finally the sixth mode can be related to the 47.5 Hz, Y-axis input mode.

Table 6.1 Summary of Modal Testing Results

Mode No.	Frequency Hz	Primary Response Direction	Region of Maximum Response
1	13.13	Transverse	Top of Forward Missile Support
2	18.44	Longitudinal and Vertical	Nose of Top Canister
3	25.95	Transverse	Rear of Top Canister
4	27.50	Longitudinal	Top of Forward Canister Support
5	31.25	Vertical	Forward Region of Top Canister
6	45.00	Longitudinal and Vertical	Top of Forward Canister Support
7	81.88	Transverse	Bottom of Forward Canister Support

In general, the frequencies obtained during each sequence of testing are similar. Each of the tests provides additional information of the shape of the various modes. One thing that the new series of tests did provide that was not previously available was the amplification at the various points.

6.3 PMTC Laboratory Testing

The final series of tests that will be compared to the current program is the laboratory tests performed at PMTC [2.7]. The comparison is more difficult in that the testing at PMTC was performed on a single dynamic simulator in a canister rather than a complete system.

For the condition with production hardware, the testing at PMTC indicated the presence of a resonance at the seeker bulkhead at approximately 74 Hz. This represents motion of the canister and dynamic simulator system on a fixture. Detailed modal analysis was not carried out in this frequency range during the current program.

It is interesting to note that there was significant rattling of the dynamic simulator inside the canister during both sequences of testing.

7.0 CONCLUSIONS AND RECOMMENDATIONS

Vibration testing was performed on the HARPOON on a LSS to determine the influence of two different designs of the isolation pads between the clamp frame and the Grade-B canisters. The major objective of the testing was to preform NDE of the two configurations. A secondary objective of the program was to define resonance frequencies of the system and the corresponding mode shapes. These two objectives have been satisfied.

The design of the isolation pads does not have a significant influence on the dynamic response of the overall system. At specific frequencies and locations on the system there are differences, but overall the levels seen by the dynamic simulators are similar. These results are based on the low-level excitation performed during the testing. It is always possible that nonlinearities in the system may play an important part in the functional performance of the missiles in service. In addition, the results are for base input sinusoidal motion, and the responses to other loads, such as blast waves, may be different.

It can therefore be concluded that use of the modified isolation pads will not significantly effect the overall performance of the HARPOON missile on the LSS. This conclusion is based on the assumption that all other failure modes, other than those produced by vibration, are similar for both configurations.

There are several problems that need to be resolved concerning the design of the isolation pads prior to going into production. The first is a determination of the proper thickness of the pads to insure that shims are not required for field installation.

It will also be necessary to determine the appropriate torques to insure that the bolts do not pull through. One solution would be the inclusion of a plastic insert near the bolt holes with sufficient strength to resist pull through. Another solution would be to provide a bolt with a large washer of sufficient size to prevent pull through.

A final concern in the design of the pads is the alignment problem noted during installation at PMTC. This alignment problem may have been the result of variations in manufacturing tolerances or installation procedures. To insure that the pads are effective, they must be designed to fully support the canister at the clamp frame.

Prior to insertion into service, it will be necessary to perform some form of qualification program on the isolation pads. Since one of the concerns is vibration, it will be necessary to develop a test procedure that will represent service conditions. The first approach is to do a complete set of MIL-STD-167 tests with four functioning missiles on a LSS structure. The problems associated with this approach are discussed in some detail later. In conjunction with this, it would also be necessary to perform 901 shock testing.

Another approach would be to install the pads on two canisters on two of a set of four missiles onboard a ship. A comparative study could be made of the performance of the missile during routine BIT tests for a defined test period. The duration of testing would have to be based on a statistical analysis of the testing.

It is also possible that a test of a single missile inside a canister could be performed. This testing would be similar to that performed at PMTC. It would first be necessary to develop a test level for the system. Utilization of the modal response defined in this program would be necessary to accomplish this task. In addition, it would be necessary to insure that compliance of the test fixture would not adversely affect the results. A true multi-axial test with control over input to each of the clamp frame and stacking frames would be most realistic. For this testing it would be necessary to use a functional missile.

One major fact that came out of this test program was that the trainers are not designed to withstand dynamic motion of a level in MIL-STD-167. Therefore, any testing performed to qualification levels will require the use of four Grade-B canisters with some form of simulated or actual missile in them.

It was possible to define the modal response of the system in some detail with the data obtained during this testing. These will be useful in interpretation of other dynamic data that may be produced. It was also possible to relate the data obtained during this program to previous results.

Due to the limited number of acceleration channels that were recorded within the budget of the program, it was not possible to obtain a complete model. If desired, a modal test program can be performed on the system for a rigid base configuration. This would consist of mounting an LSS on a rigid mass and placing the appropriate Grade-B canisters and missiles or simulators on the LSS. The structure could then be excited by means of an impact hammer and the response at a large number of points. This approach is more cost effective than testing on a shake table.

The final discussion is associated with MIL-STD-167 testing. A large amount of interaction between the test item and the vibration table occurred during this testing. It would not be possible to perform a full MIL-STD-167 test at this test facility for an item of this size and configuration. The major problem is restraint of the table motion to uniaxial excitation. Because of the geometry of the structure, there will be response in cross-axes directions. When this response drives the cross-axes motion at the feet of the LSS to levels comparable to the excitation, questions concerning the validity of the test arise. This was evident in the initial series of MIL-STD-167 tests performed on this system early in the HARPOON program. Functional anomalies of the missiles were noted as a result of the testing, but they were dismissed due to concerns about the quality of the testing.

The question arises: Is MIL-STD-167 an acceptable level of testing for items of this size and configuration? The levels defined in MIL-STD-167 have historically been shown to indicate the susceptibility of equipment to shipboard vibration. It is possible to develop small systems that will withstand the levels imposed in the standard. As the size and structural complexity of the item increases, it becomes more difficult to design an acceptable system within acceptable weight limitations.

The conservative levels of vibration imposed by the standard impose a severe burden on the design of large scale equipment. It then becomes necessary to tailor the testing to the specific item and platform in question. The concept of tailoring is slowly being adapted into the military since the adoption of Revision D of MIL-STD-810 [2.8]. By tailoring, a realistic test level can be developed that will provide confidence that the item will perform in the field.

One consideration when determining the appropriate actions to be taken is the age of this weapons system. The HARPOON is a mature system that has been in the fleet for a long time. Because of this, changes that would normally be acceptable in a development stage are no longer appropriate. Any corrective action needs to take into account the expected life of the system and any effect on functional and cost that they may have. It is appropriate that lessons learned in this program are applied to similar systems.

SECTION 8.0

PHOTOGRAPHS

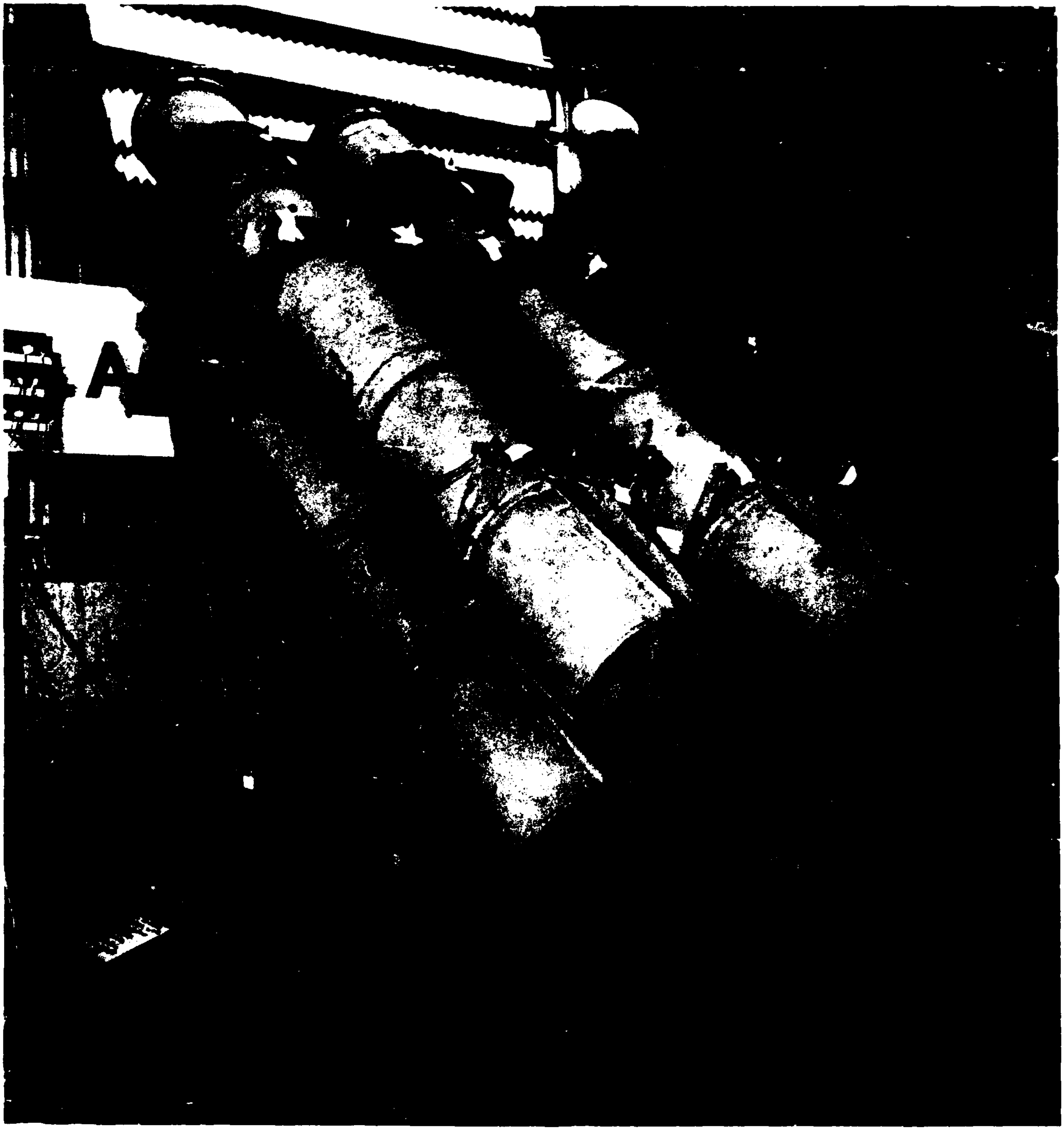

Figure 8.1 Test Set-up for X-Axis and Z-Axis Modified Exploratory Vibration

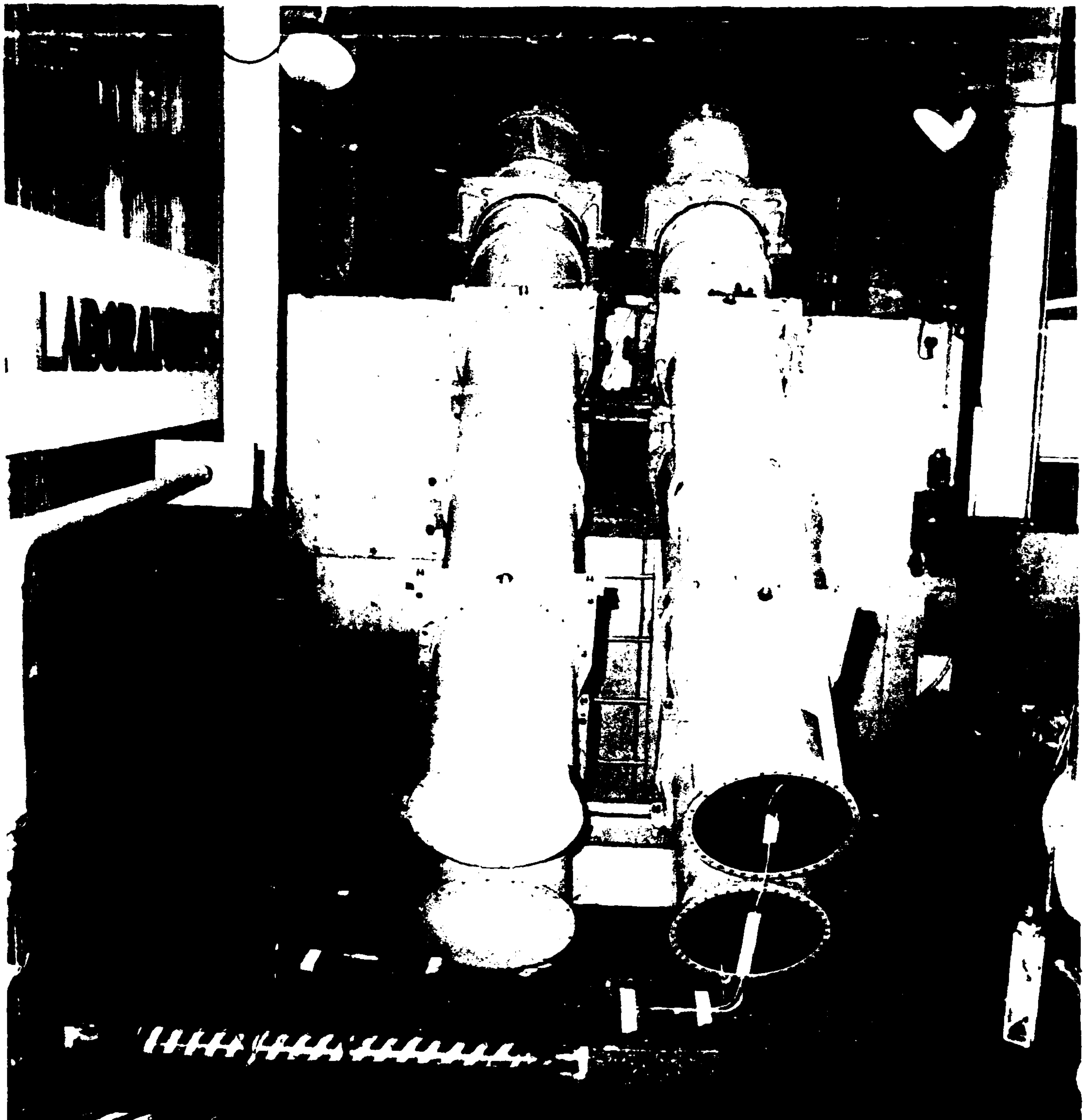

Figure 8.2 Test Set-up for Y-Axis Modified Exploratory Vibration

Figure 8.3 Crack and Failed Bolts in Trainer Stacking Frame

Figure 8.4 Trainer Clamp Frame Brace and Blunted Crack Tip

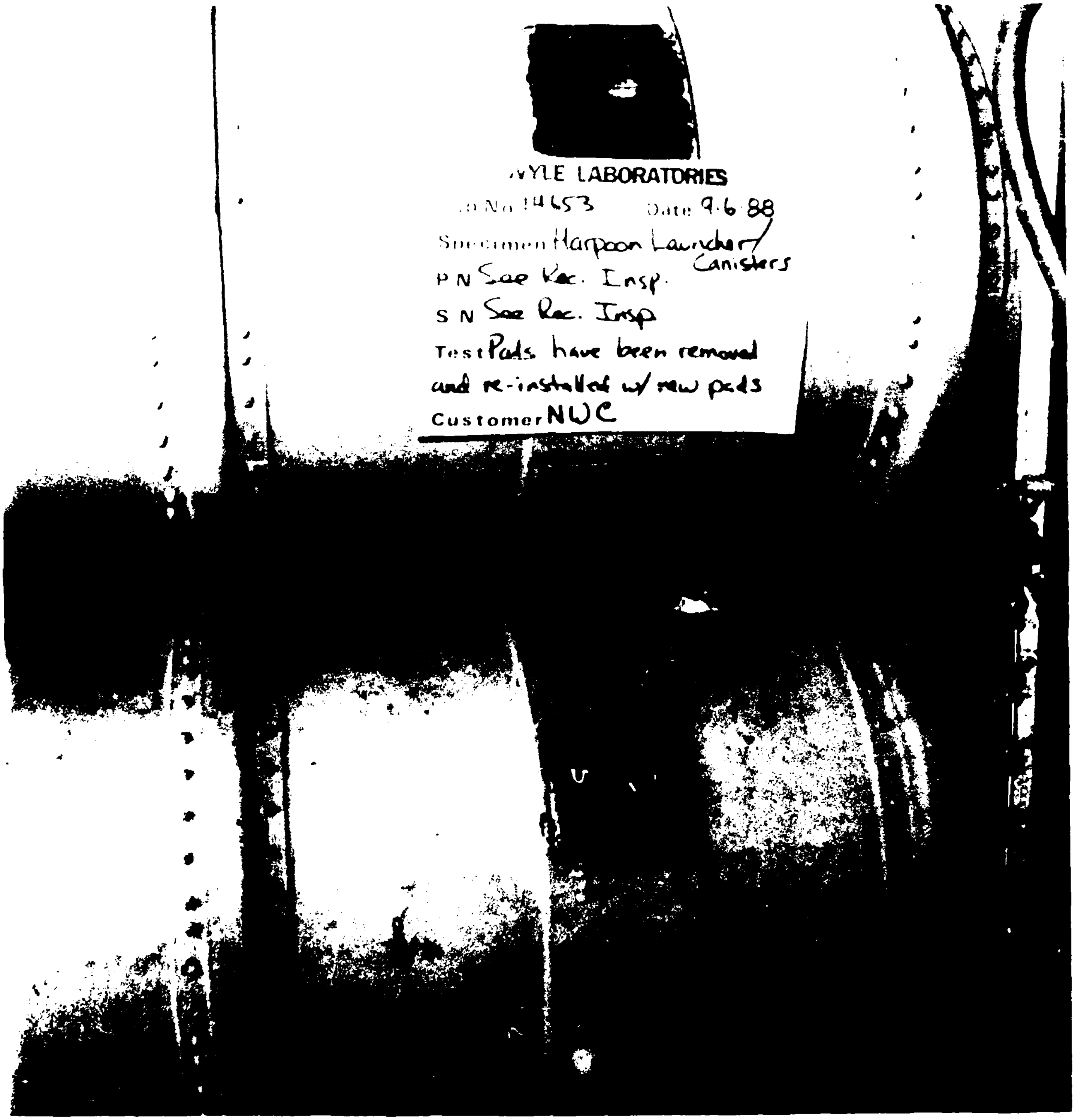

Figure 8.5 Modified Isolation Pads Installed on Grade B Canisters

SECTION 9.0

PSD'S

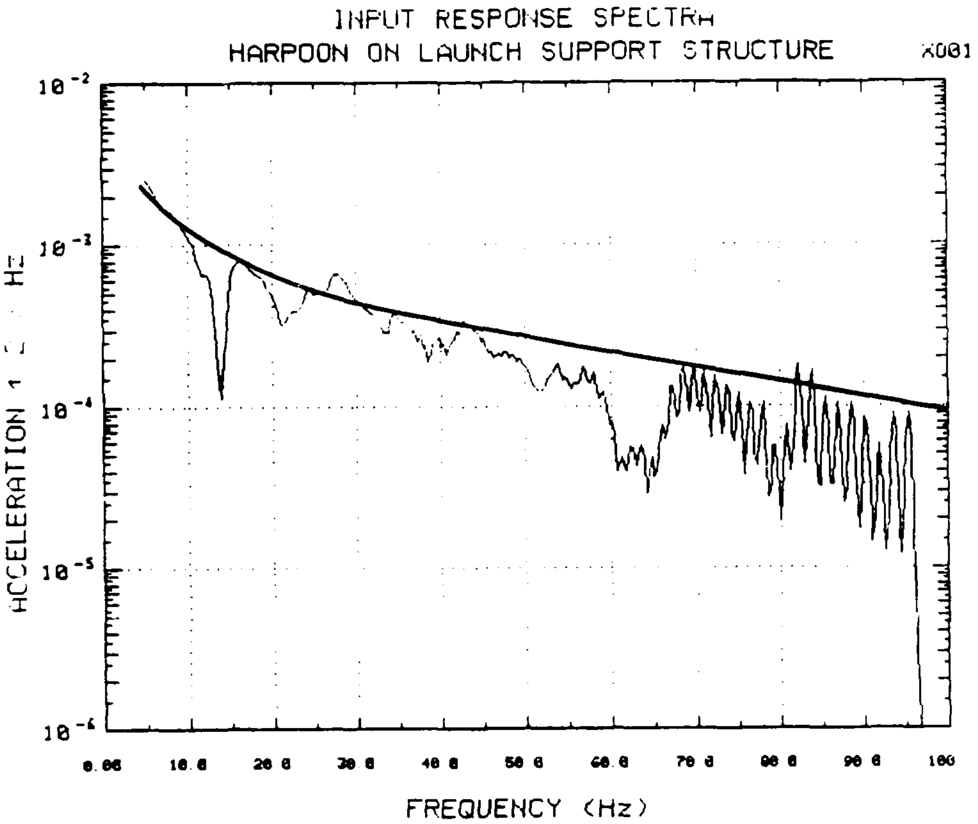

Figure 9.1 X-Axis Input PSD with Production Pads, Run No. 1

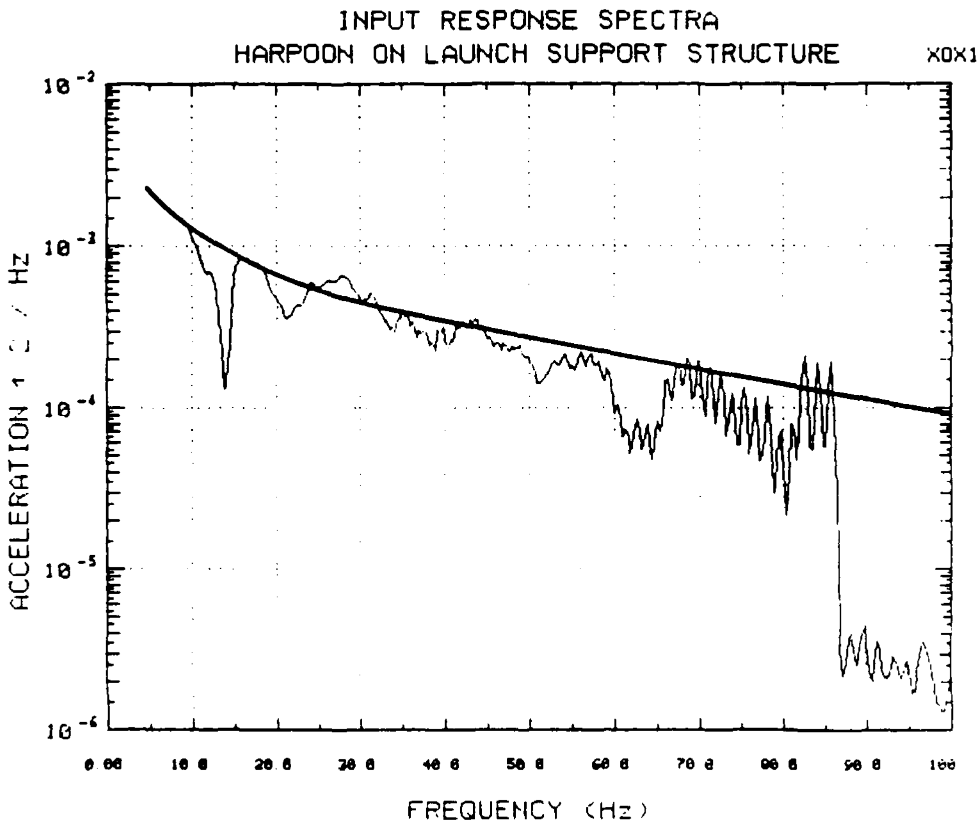

Figure 9.2 X-Axis Input PSD with Production Pads, Run No. 2

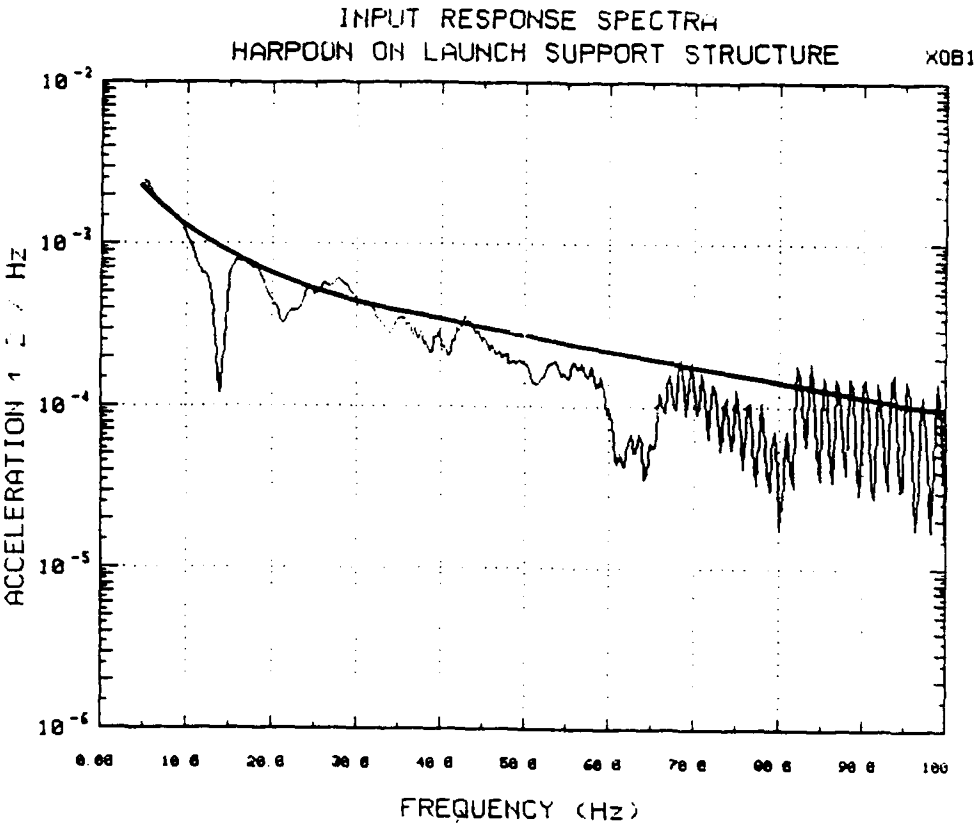

Figure 9.3 X-Axis Input PSD with Production Pads, Run No. 3

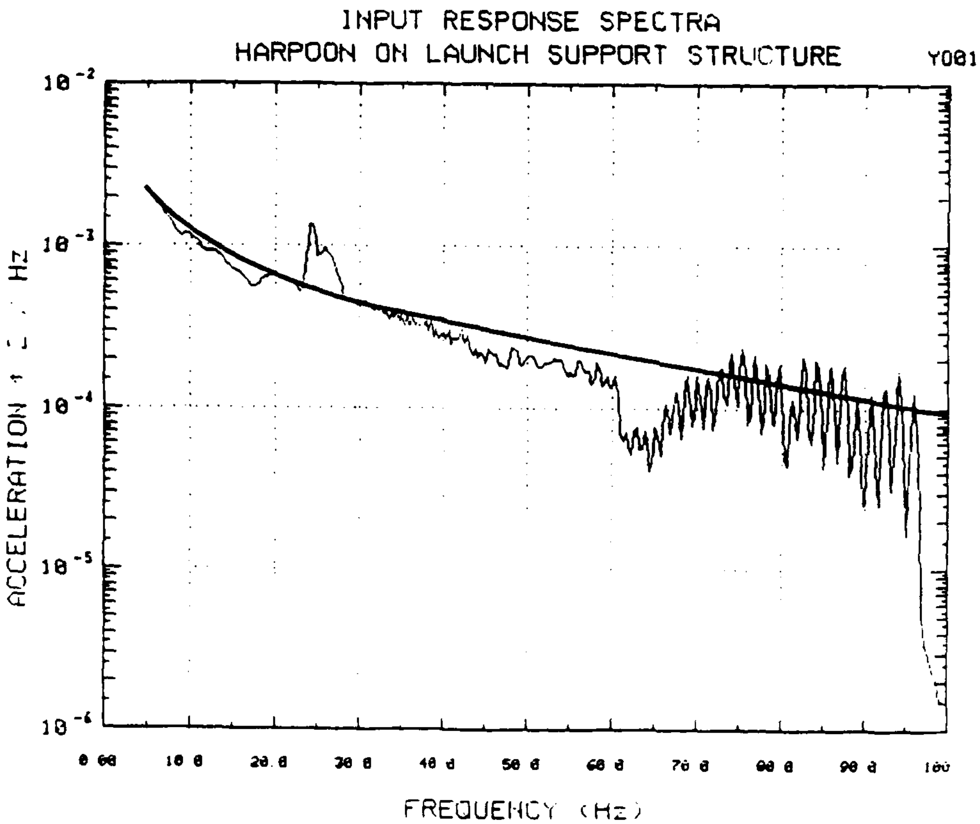

Figure 9.4 Y-Axis Input PSD with Production Pads, Run No. 1

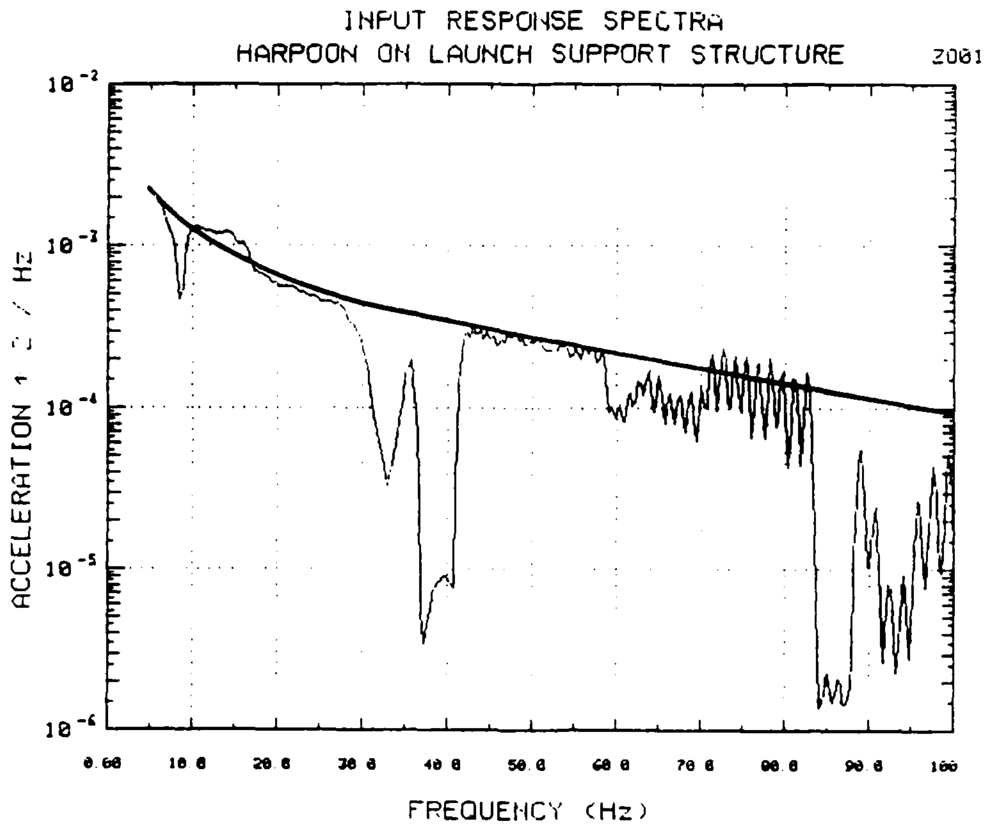

Figure 9.5 Z-Axis Input PSD with Production Pads, Run No. 1

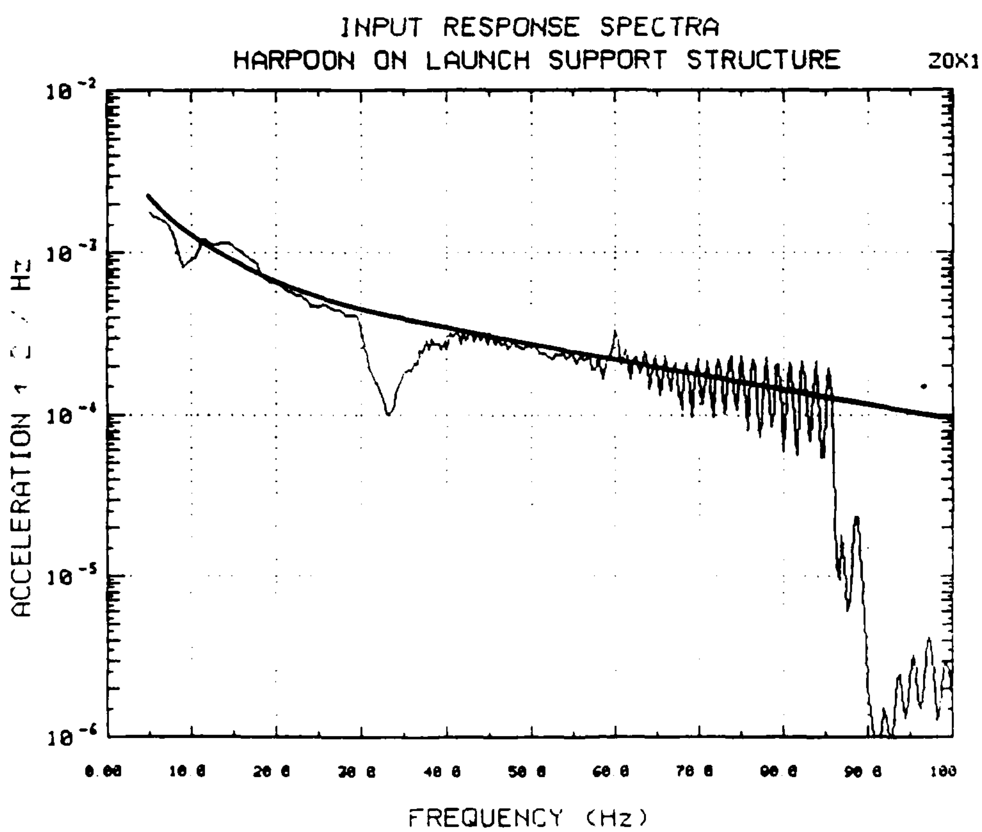

Figure 9.6 Z-Axis Input PSD with Production Pads, Run No. 3

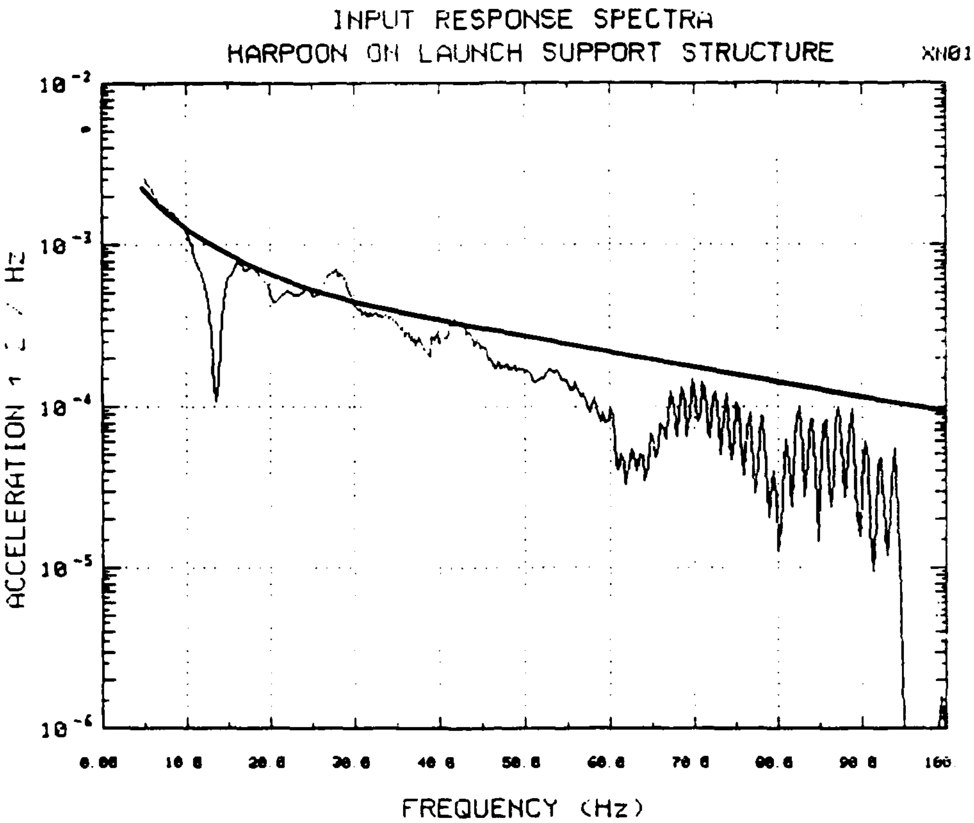

Figure 9.7 X-Axis Input PSD with Modified Pads, Run No. 1

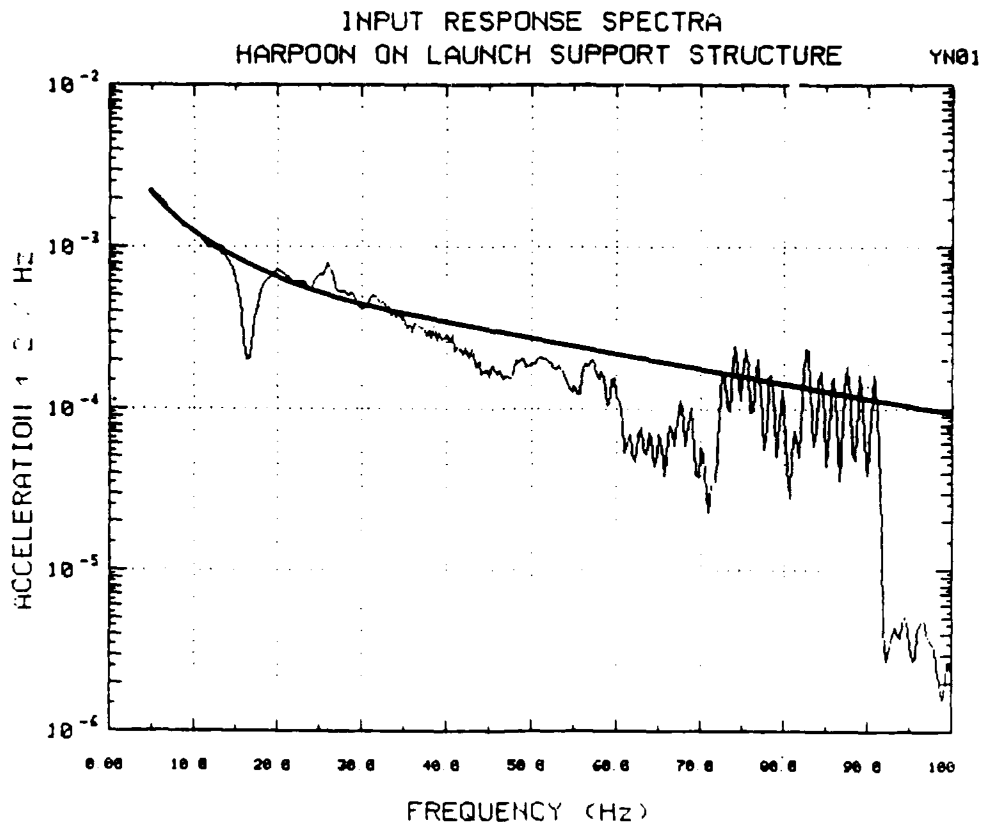

Figure 9.8 Y-Axis Input PSD with Modified Pads, Run No. 1

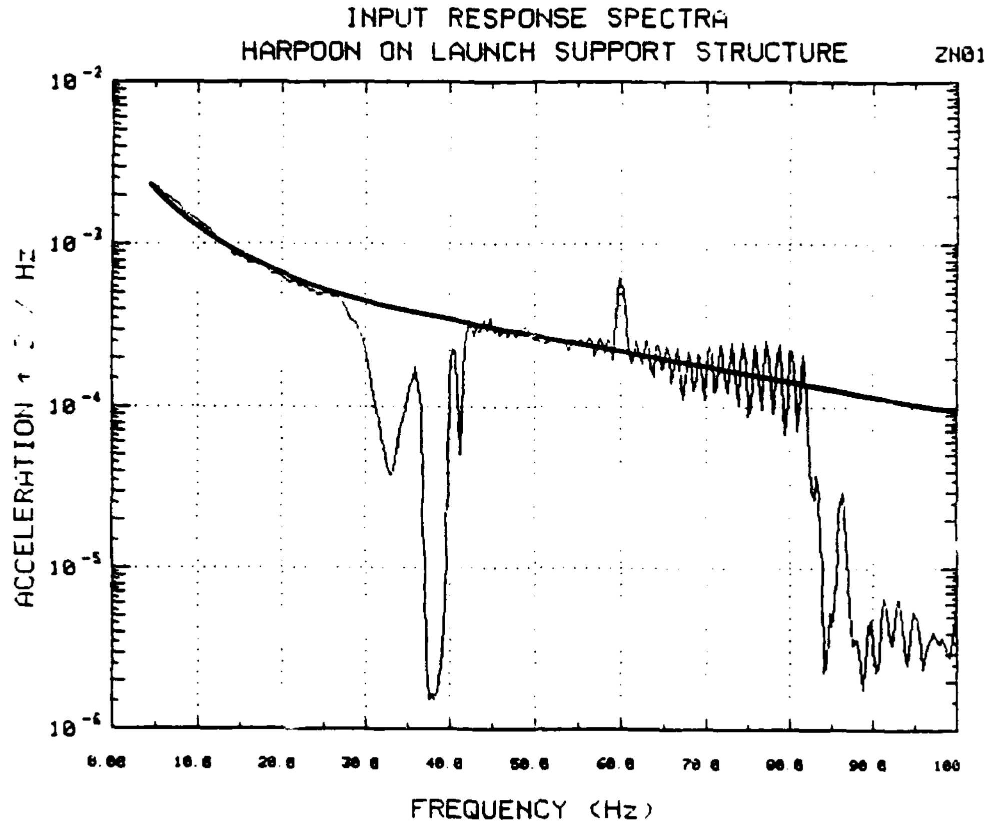

Figure 9.9 Z-Axis Input PSD with Modified Pads, Run No. 1

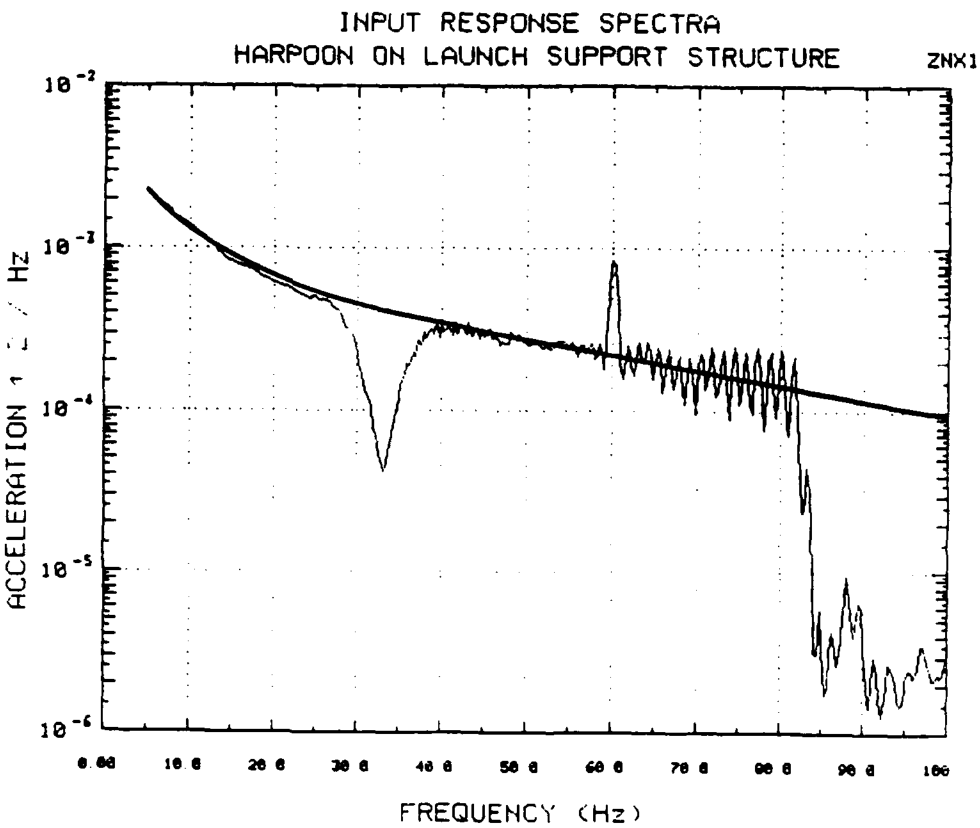

Figure 9.10 Z-Axis Input PSD with Modified Pads, Run No. 3

SECTION 10.0

FREQUENCY RESPONSE FUNCTIONS

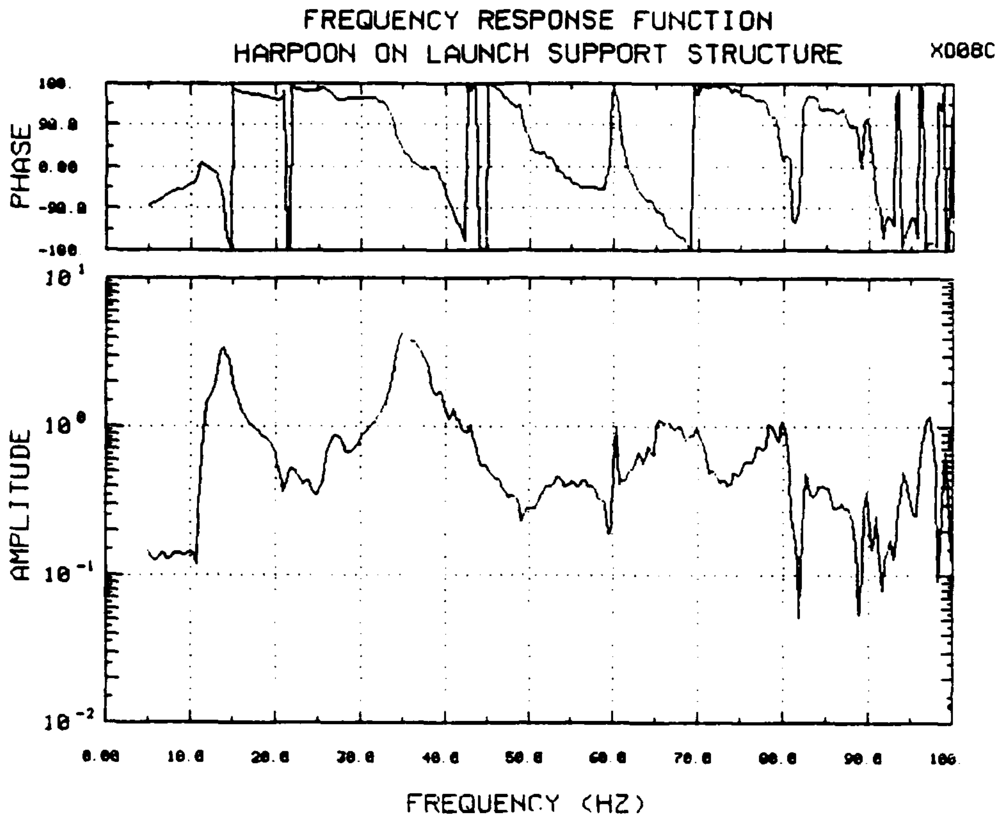

Figure 10.1 Y-Axis Response at Forward Left Foot Due to X-Axis Input, Production Pads

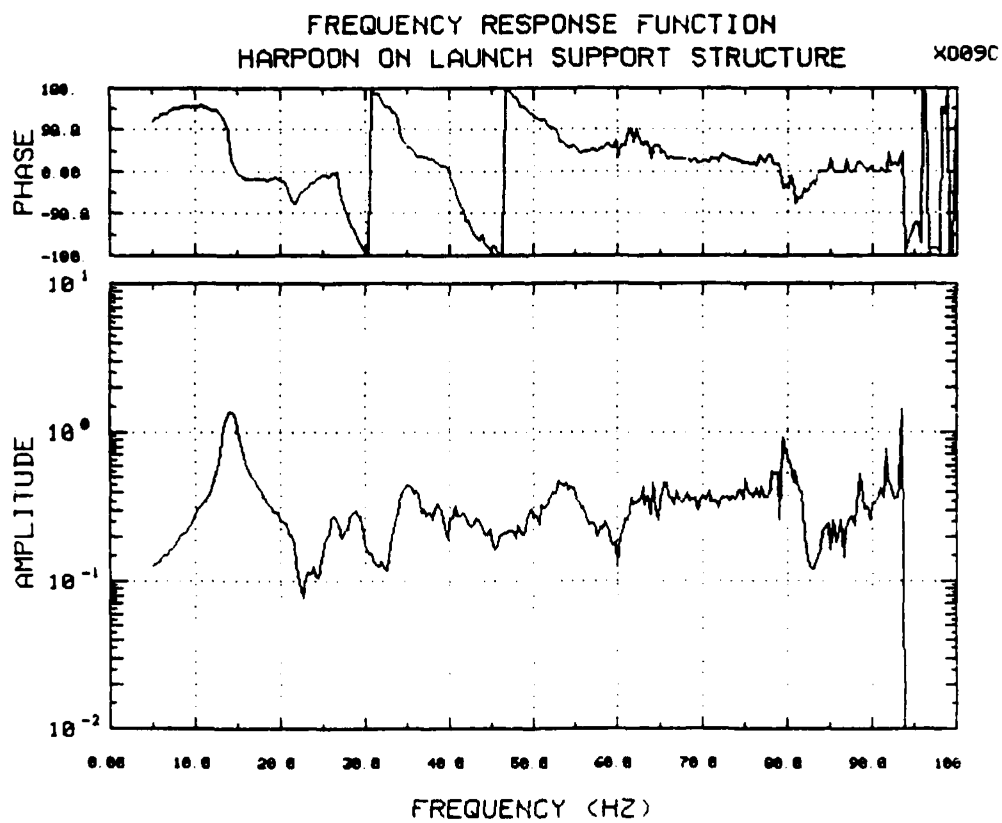

Figure 10.2 Z-Axis Response at Forward Left Foot Due to X-Axis Input, Production Pads

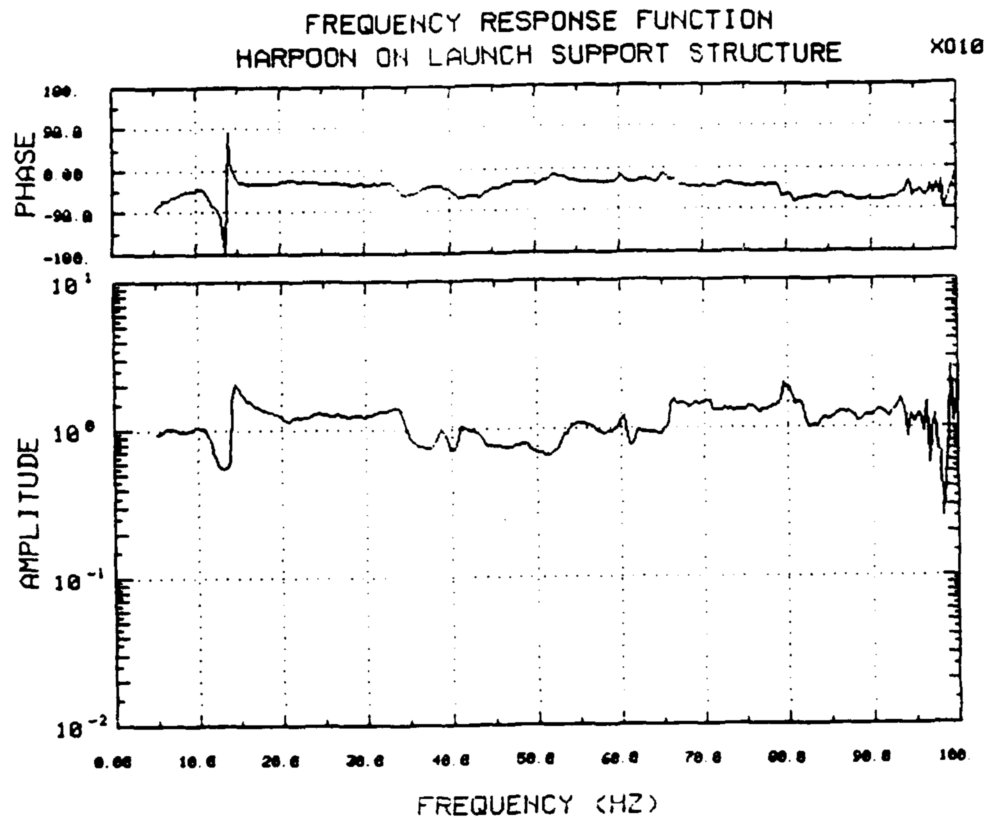

Figure 10.3 X-Axis Response at Forward Left Foot Due to X-Axis Input, Production Pads

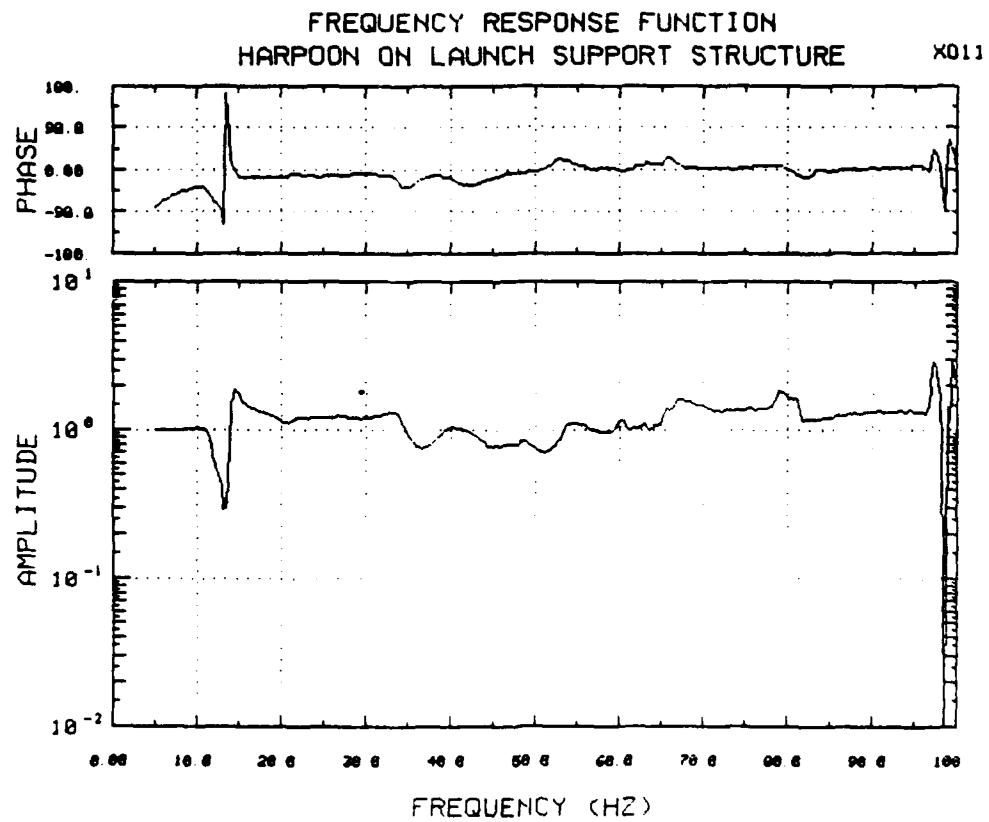

Figure 10.4 X-Axis Response at Forward Right Foot Due to X-Axis Input, Production Pads

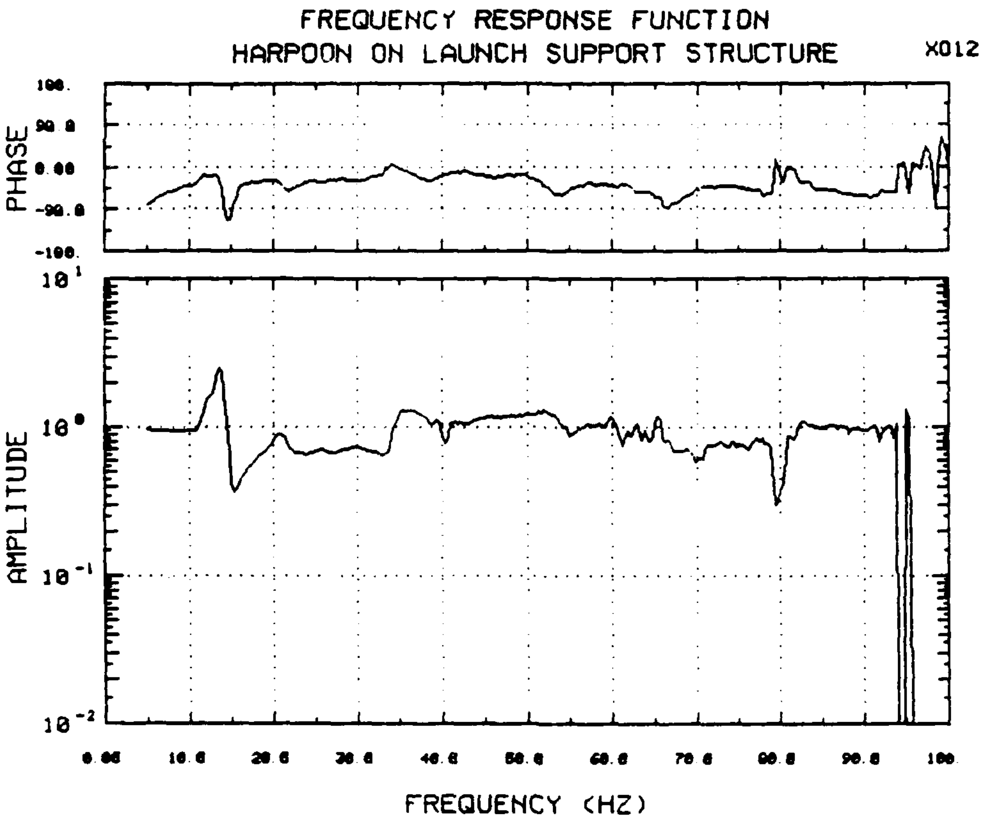

Figure 10.5 X-Axis Response at Rear Left Foot Due to X-Axis Input, Production Pads

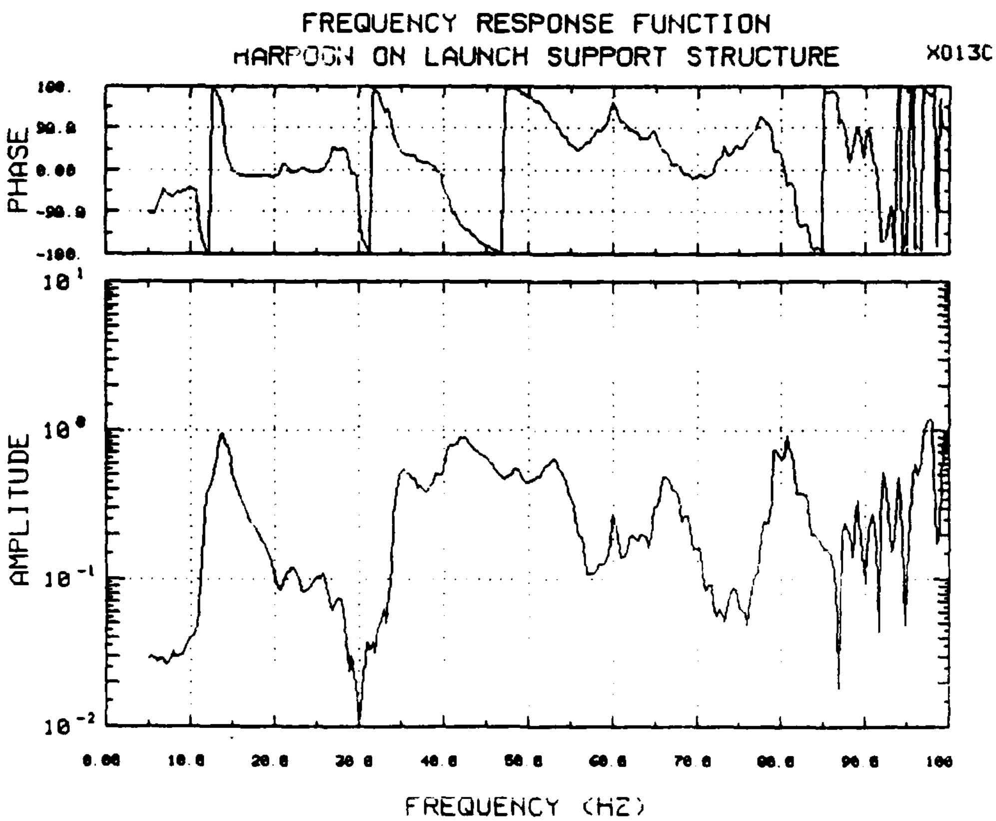

Figure 10.6 Y-Axis Response at Rear Right Foot Due to X-Axis Input, Production Pads

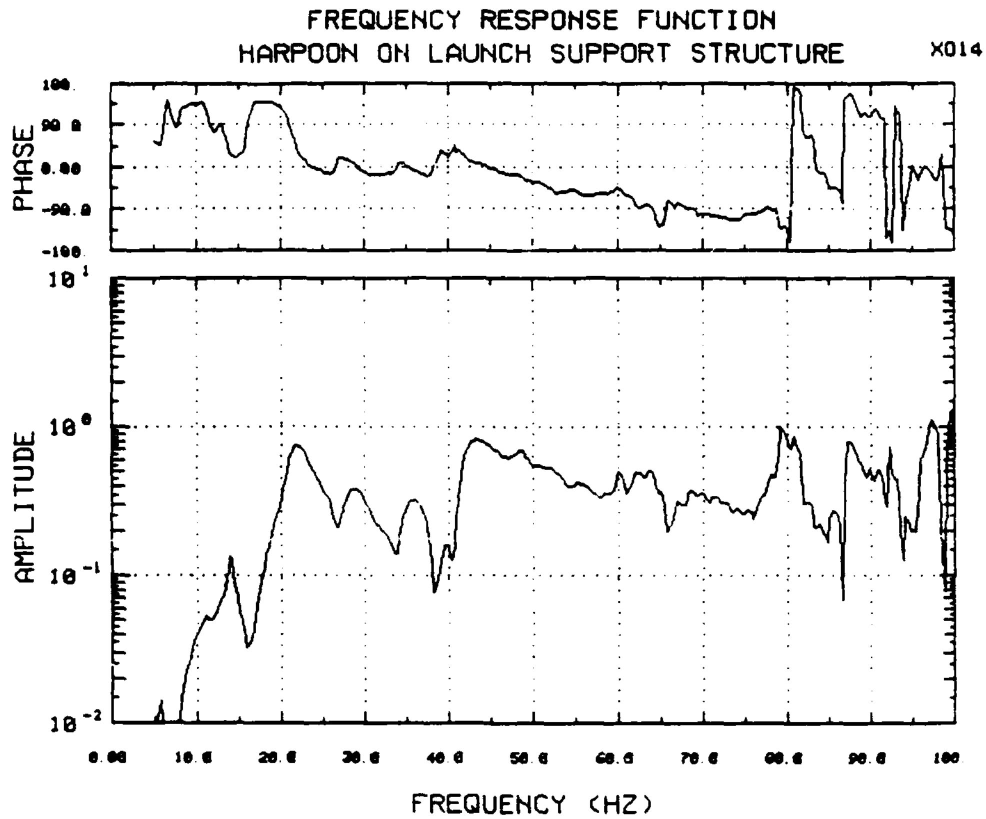

Figure 10.7 Z-Axis Response at Rear Right Foot Due to X-Axis Input, Production Pads

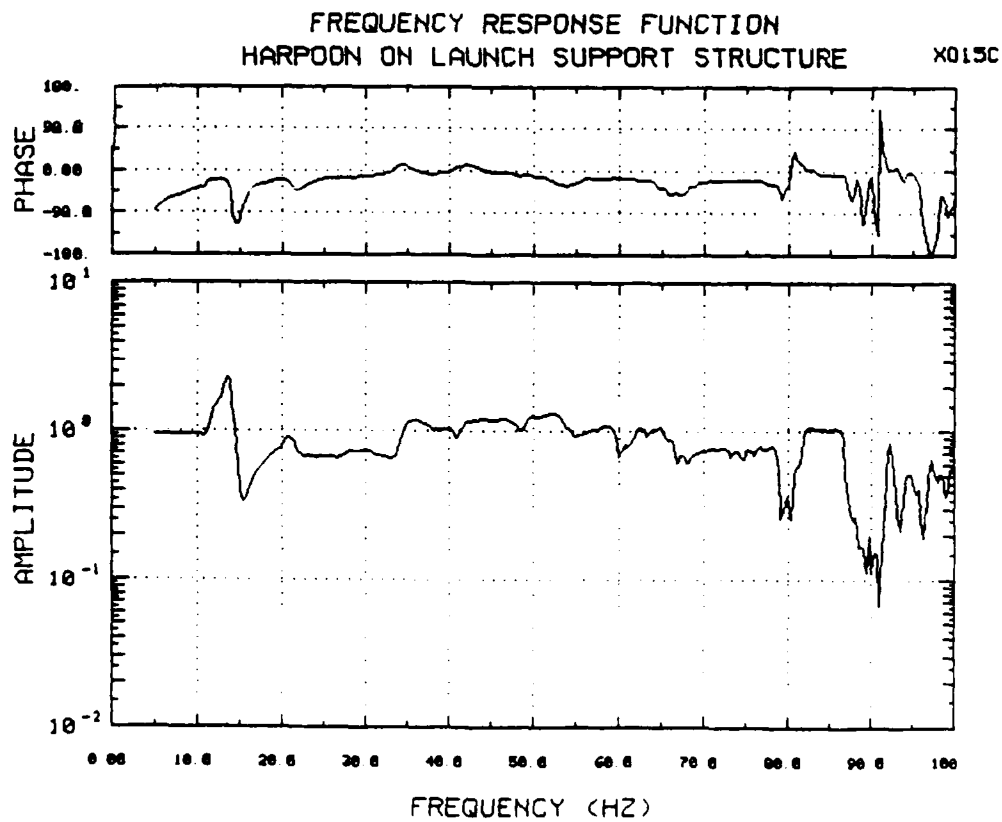

Figure 10.8 X-Axis Response at Rear Right Foot Due to X-Axis Input, Production Pads

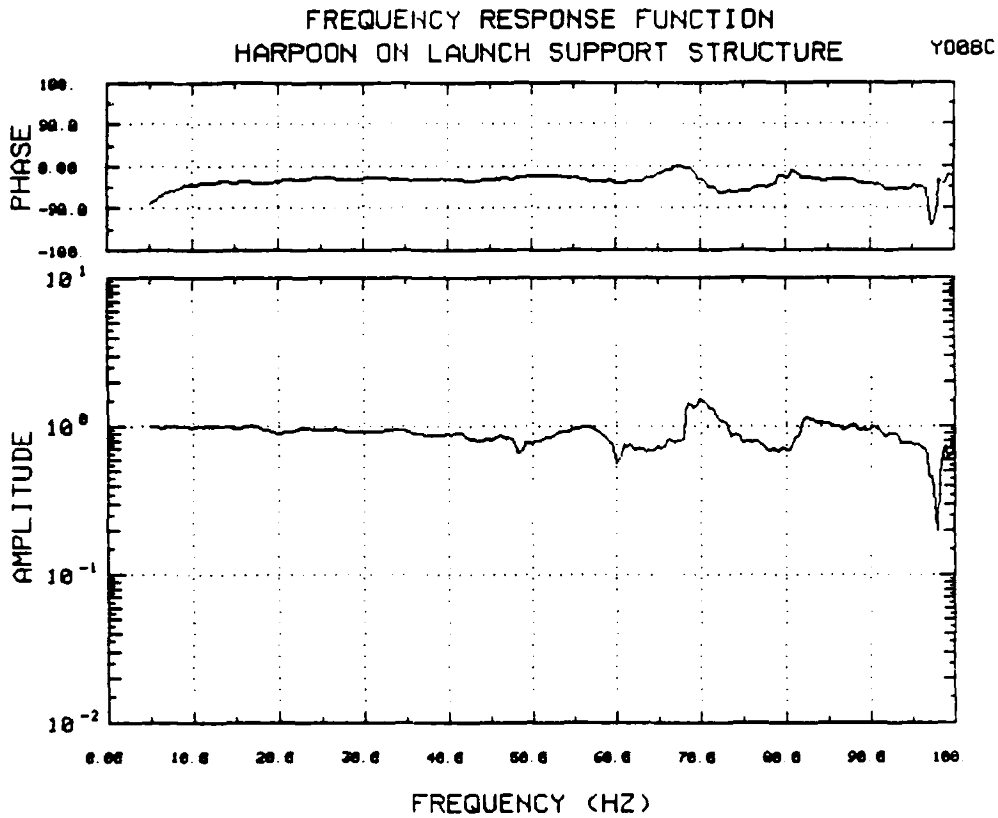

Figure 10.9 Y-Axis Response at Forward Left Foot Due to Y-Axis Input, Production Pads

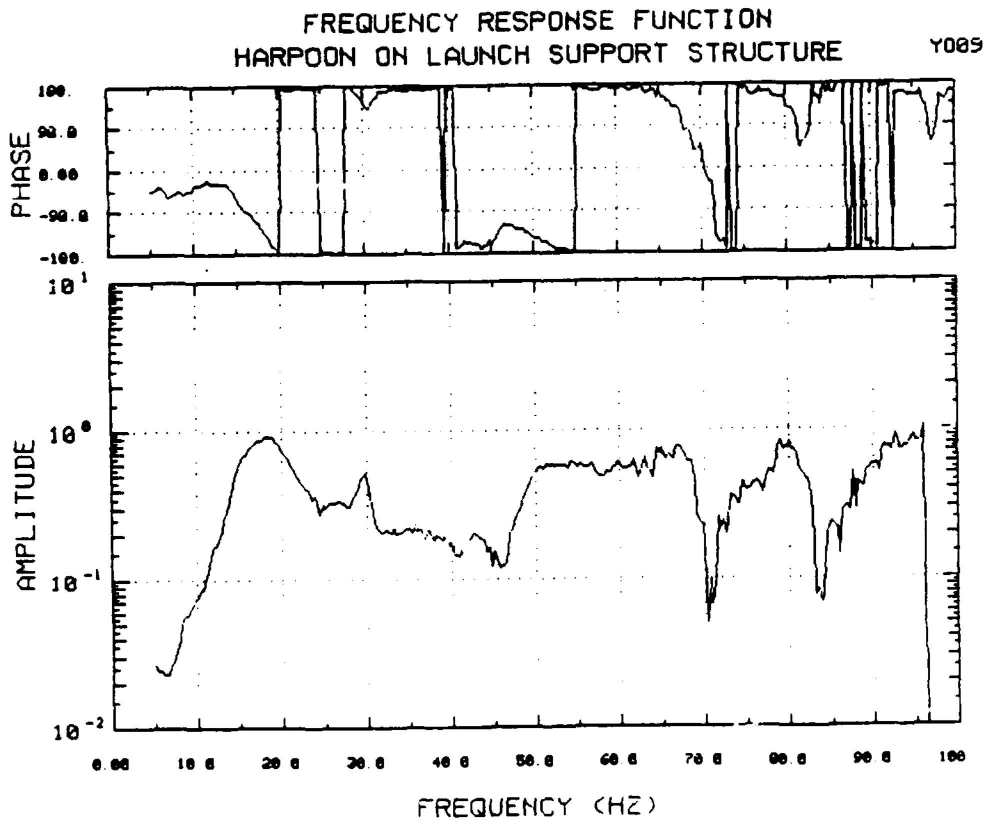

Figure 10.10 Z-Axis Response at Forward Left Foot Due to Y-Axis Input, Production Pads

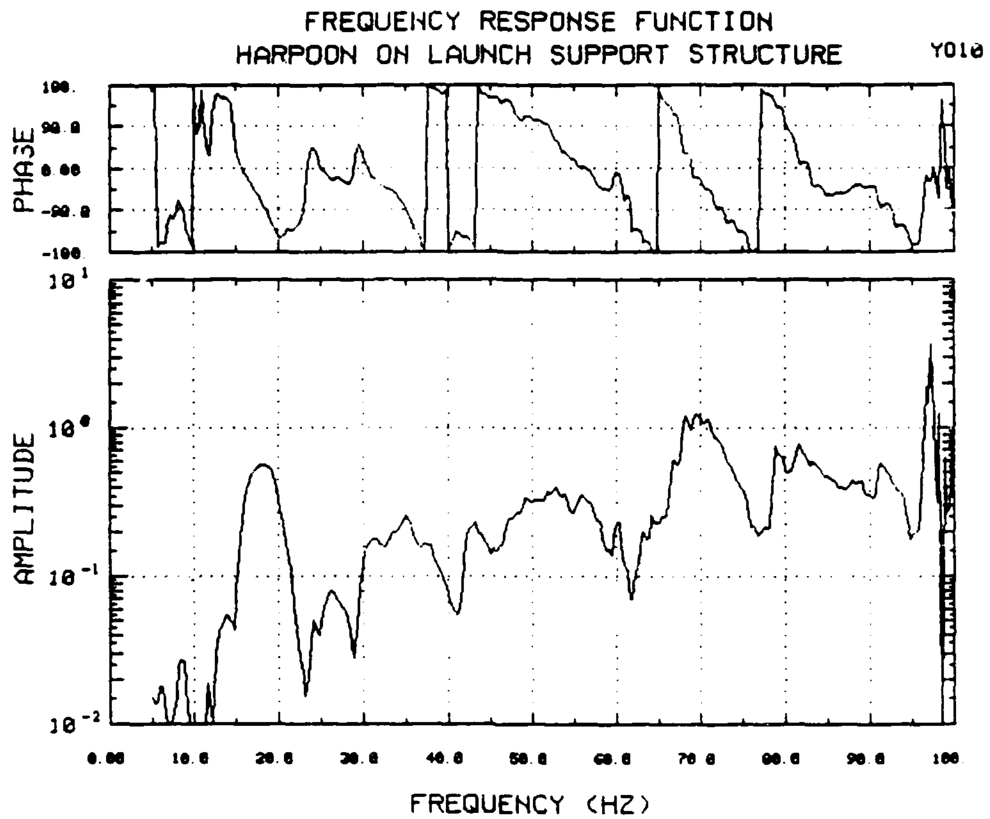

Figure 10.11 X-Axis Response at Forward Left Foot Due to Y-Axis Input, Production Pads

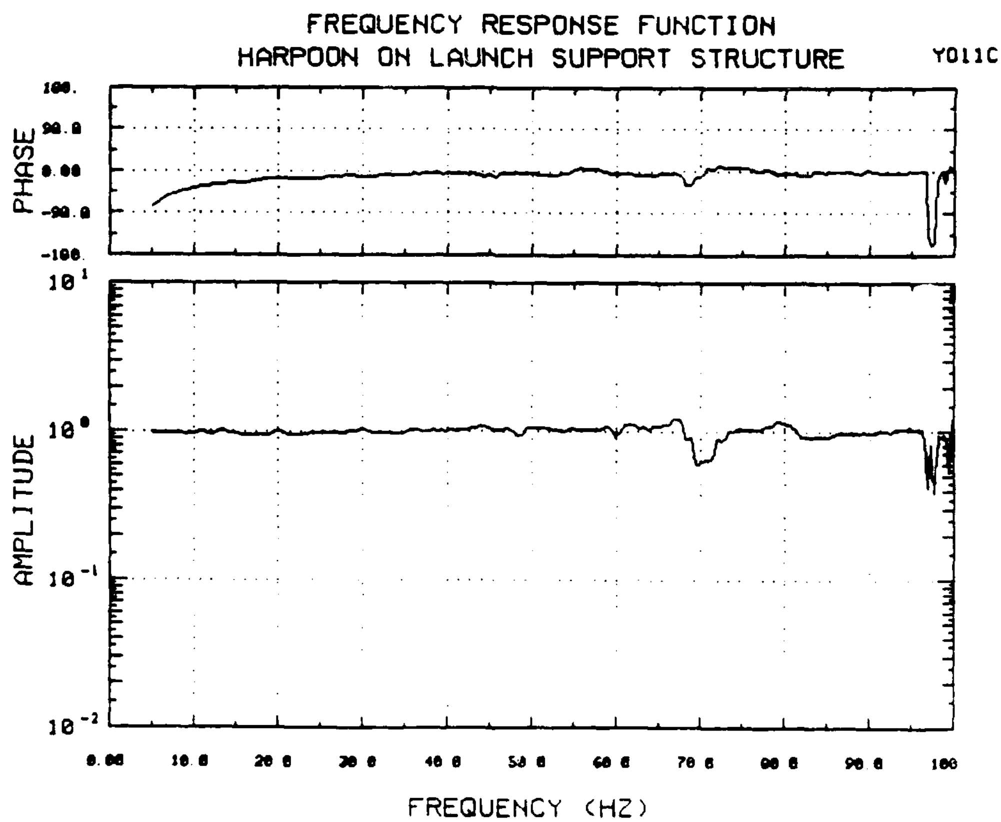

Figure 10.12 Y-Axis Response at Forward Right Foot Due to Y-Axis Input, Production Pads

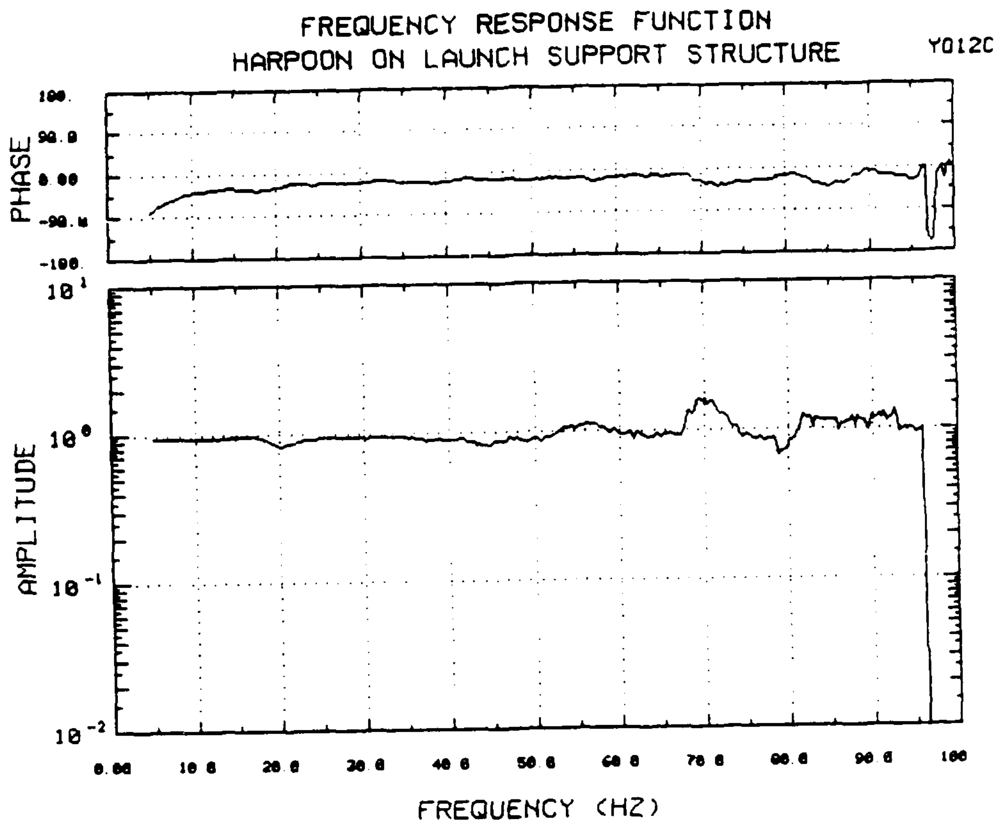

Figure 10.13 Y-Axis Response at Rear Left Foot Due to Y-Axis Input, Production Pads

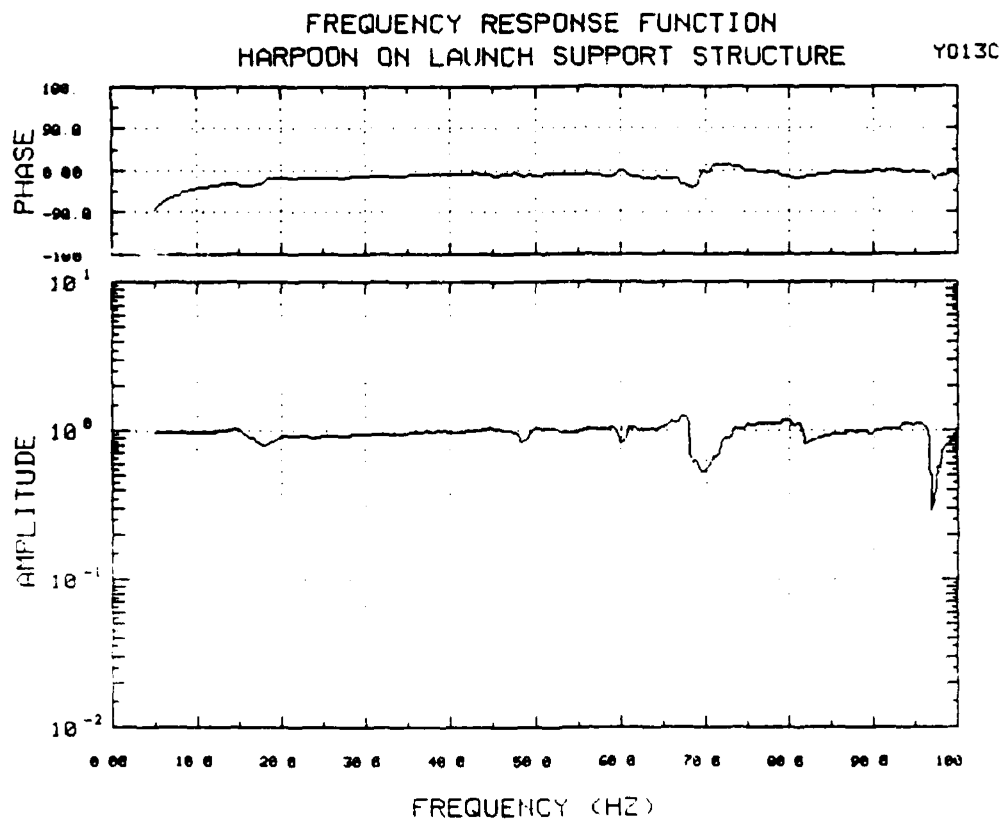

Figure 10.14 Y-Axis Response at Rear Right Foot Due to Y-Axis Input, Production Pads

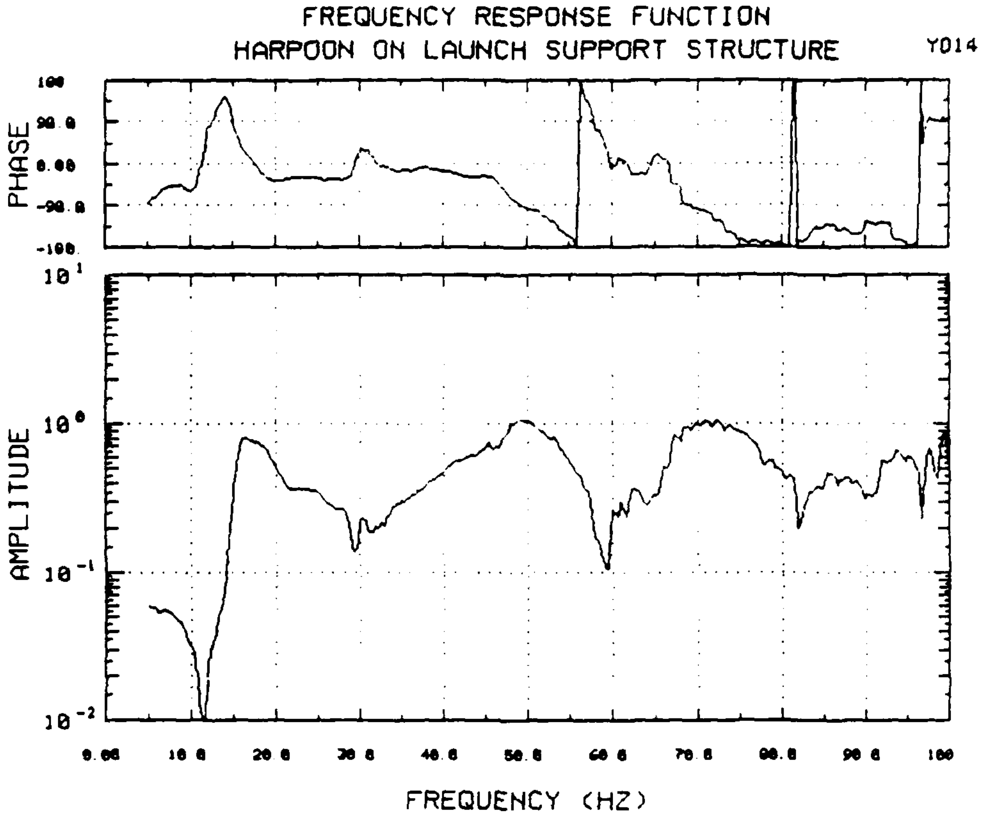

Figure 10.15 Z-Axis Response at Rear Right Foot Due to Y-Axis Input, Production Pads

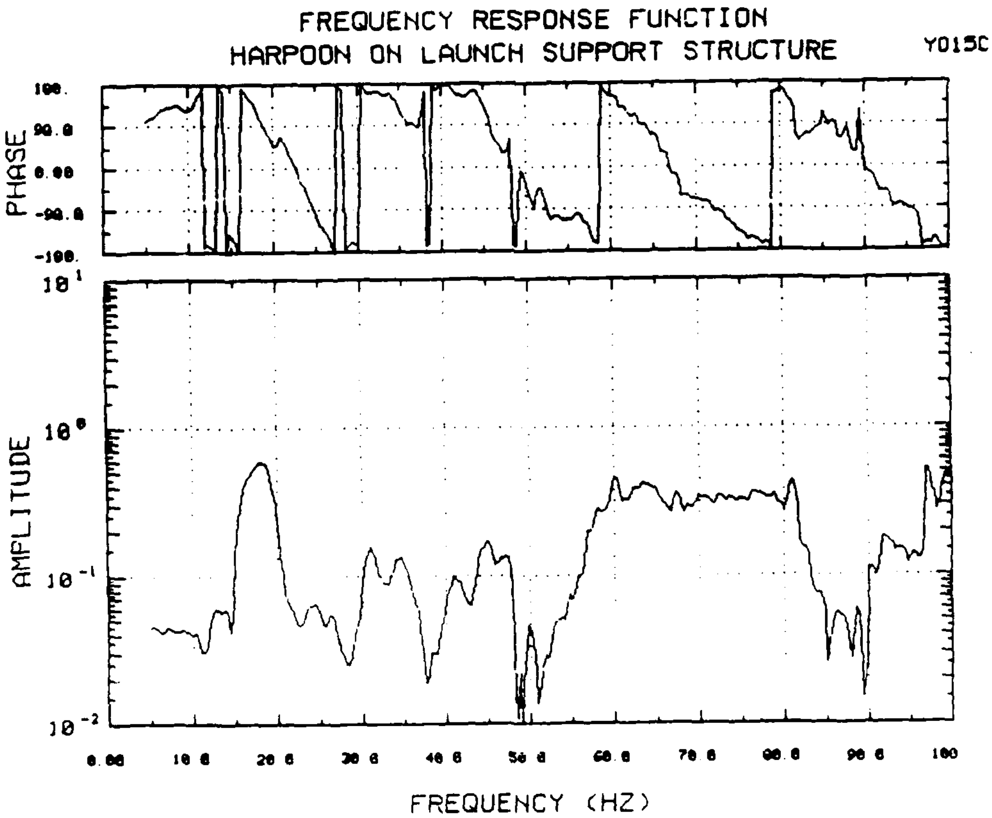

Figure 10.16 X-Axis Response at Rear Right Foot Due to Y-Axis Input, Production Pads

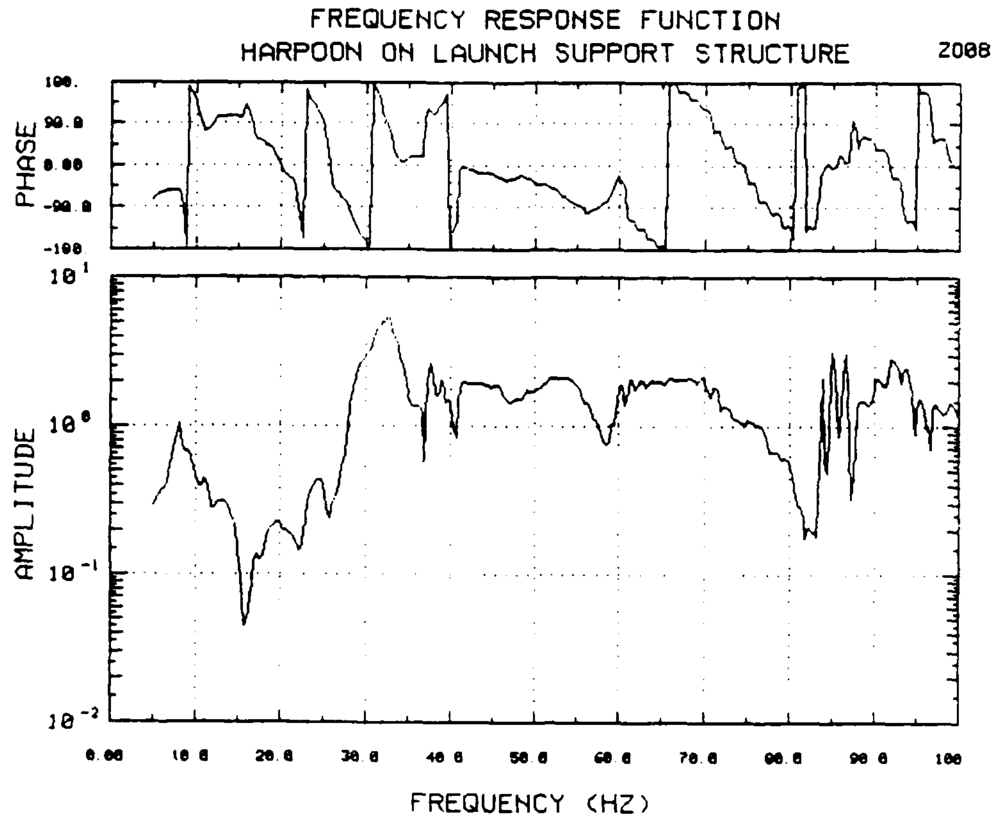

Figure 10.17 Y-Axis Response at Forward Left Foot Due to Z-Axis Input, Production Pads

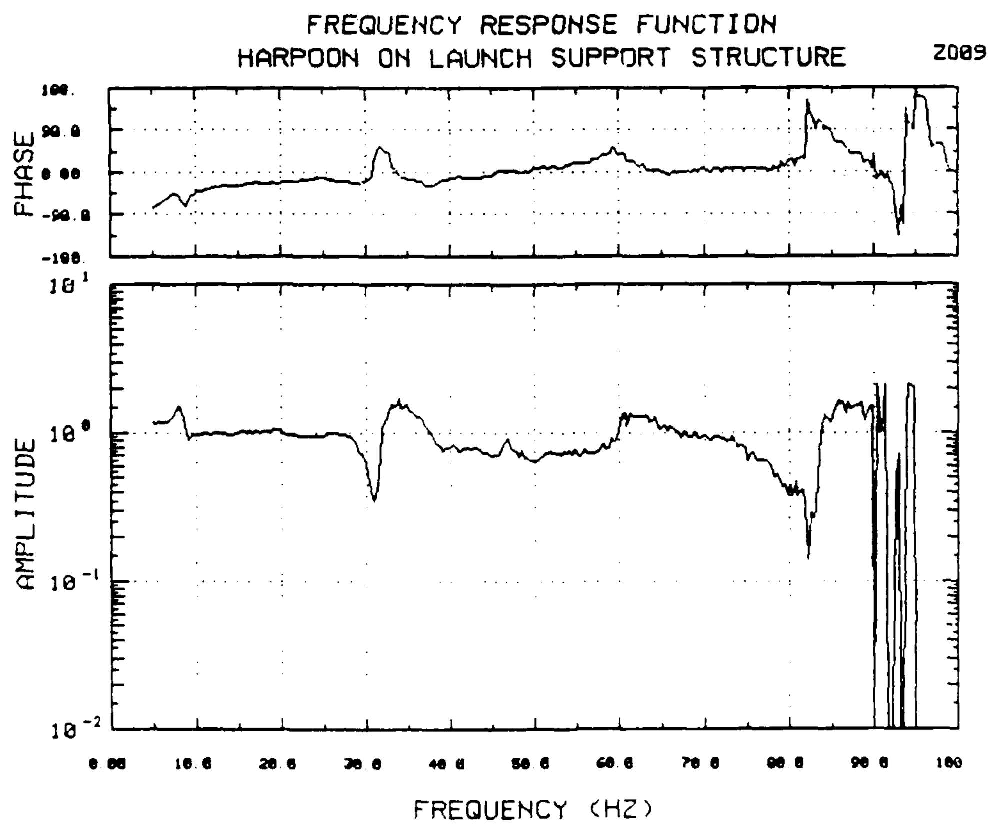

Figure 10.18 Z-Axis Response at Forward Left Foot Due to Z-Axis Input, Production Pads

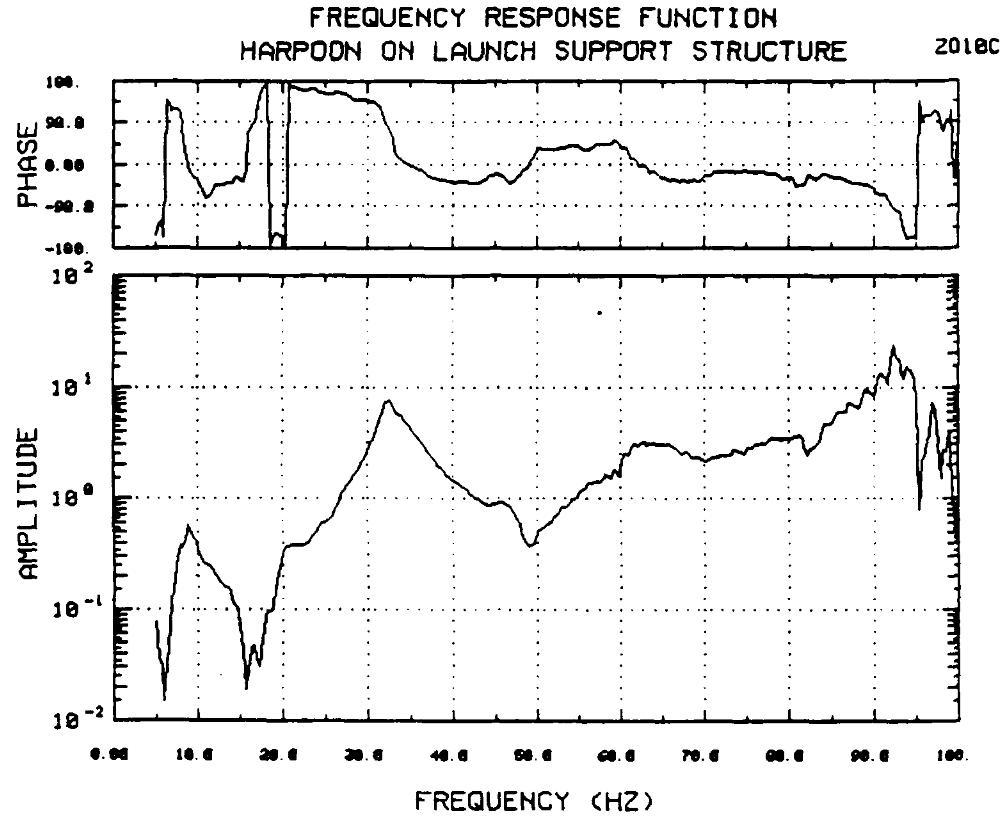

Figure 10.19 X-Axis Response at Forward Left Foot Due to Z-Axis Input, Production Pads

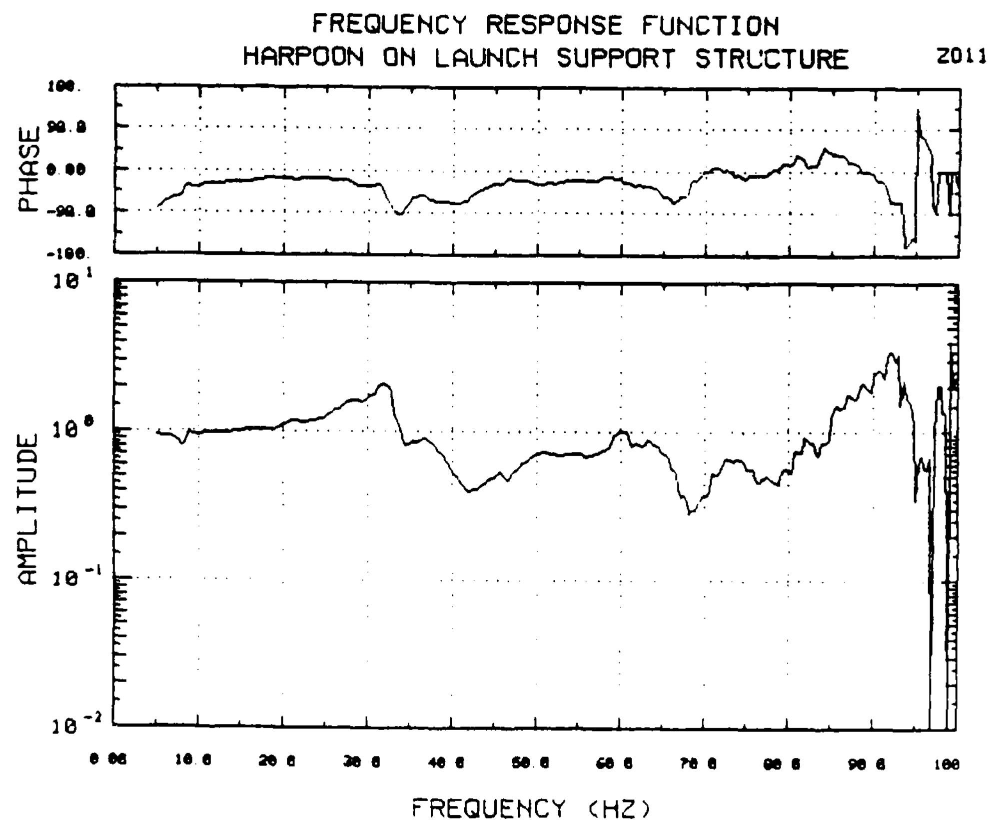

Figure 10.20 Z-Axis Response at Forward Right Foot Due to Z-Axis Input, Production Pads

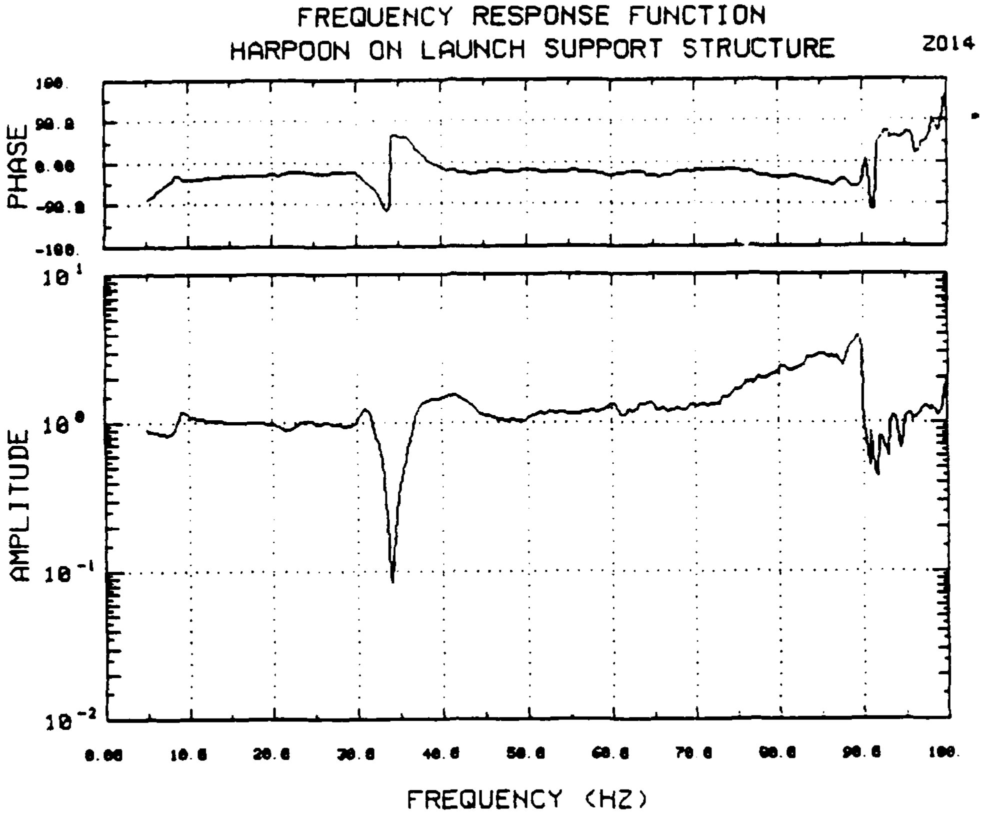

Figure 10.23 Z-Axis Response at Rear Right Foot Due to Z-Axis Input, Production Pads

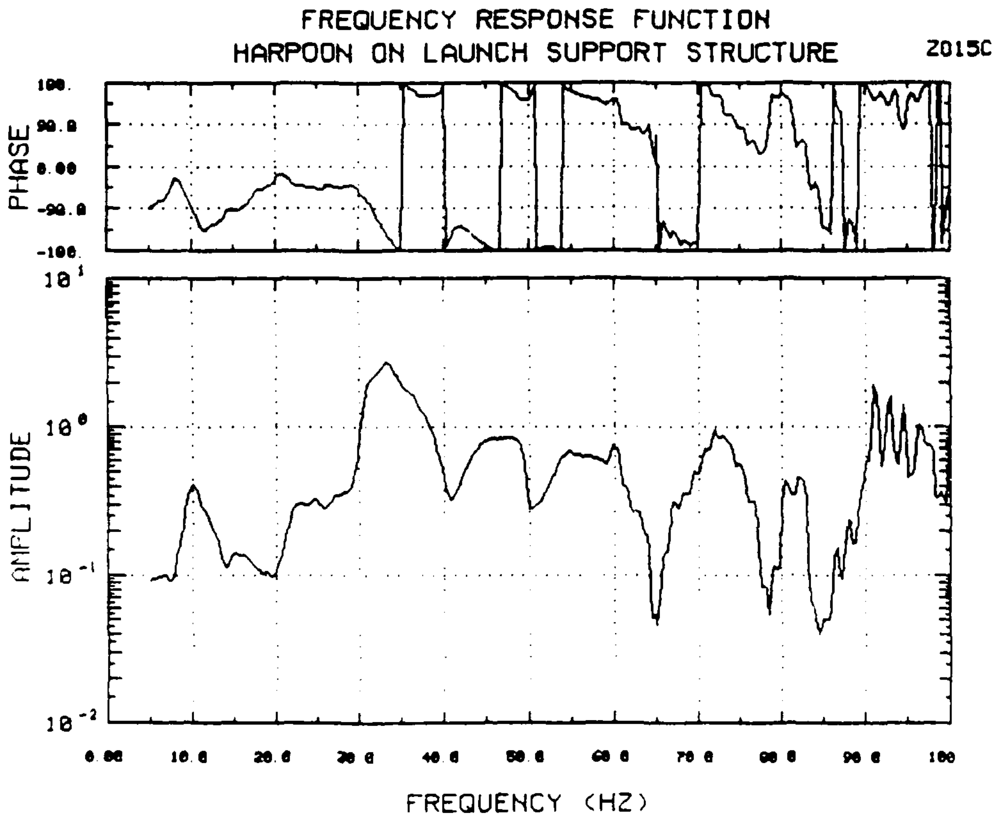

Figure 10.24 X-Axis Response at Rear Right Foot Due to Z-Axis Input, Production Pads

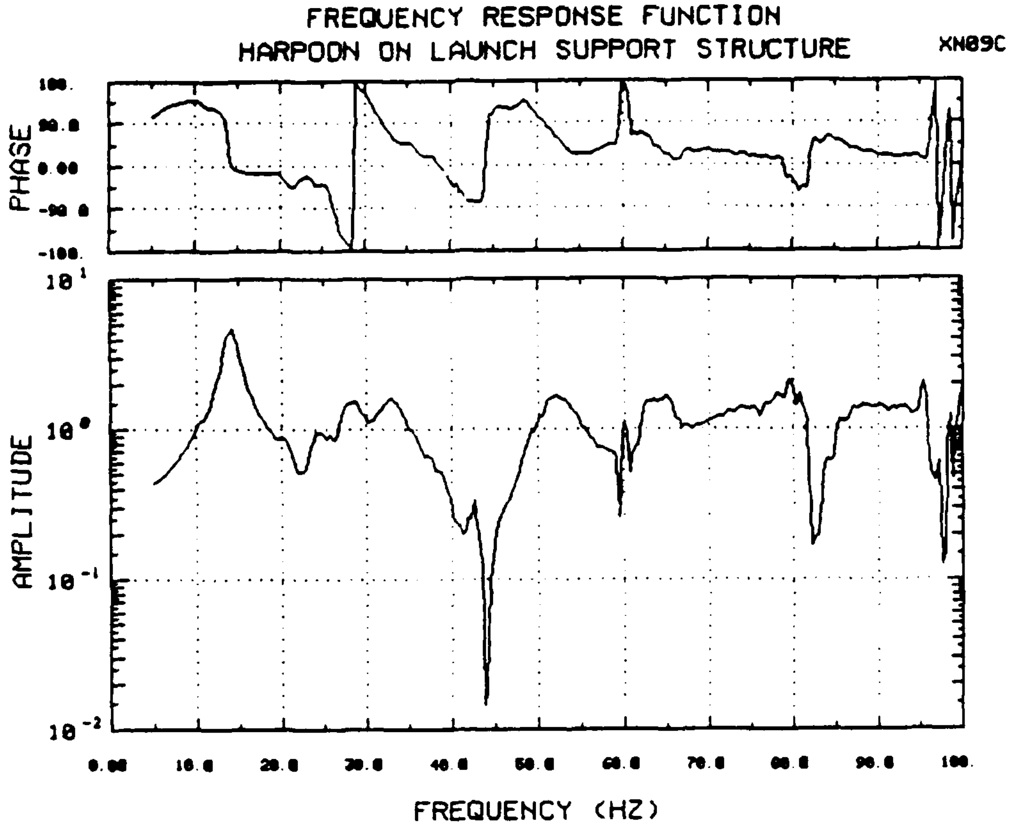

Figure 10.25 Z-Axis Response at Forward Left Foot Due to X-Axis Input, Modified Isolation Pads

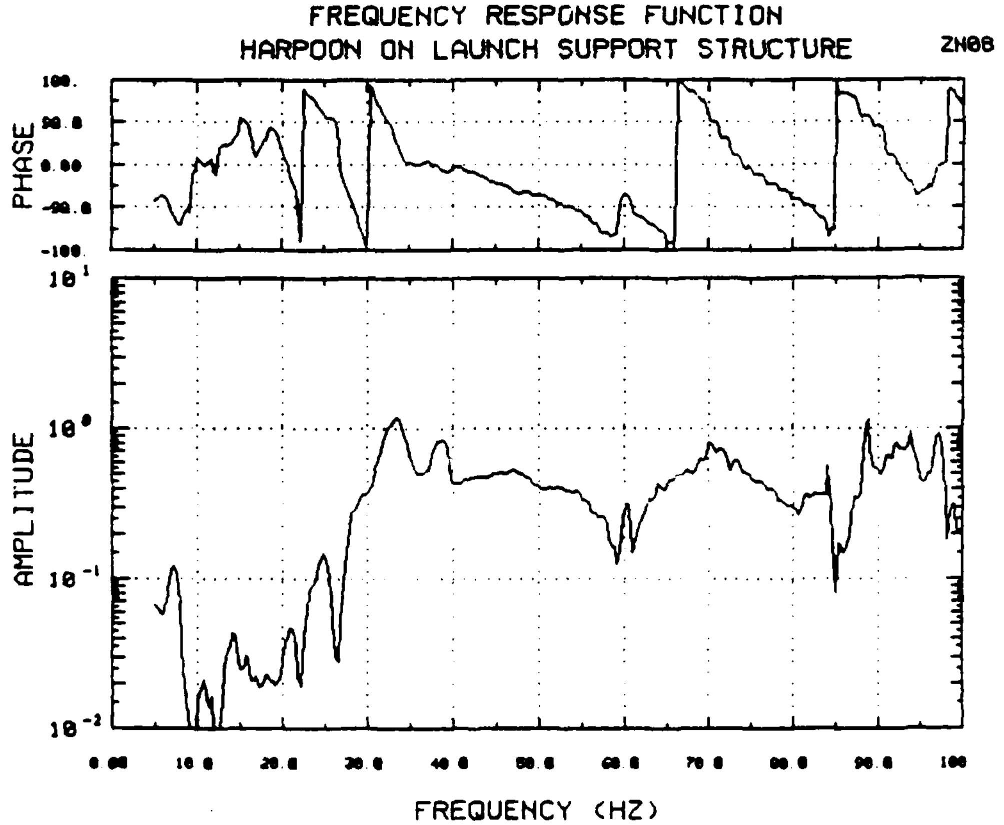

Figure 10.26 Y-Axis Response at Forward Left Foot Due to Z-Axis Input, Modified Isolation Pads

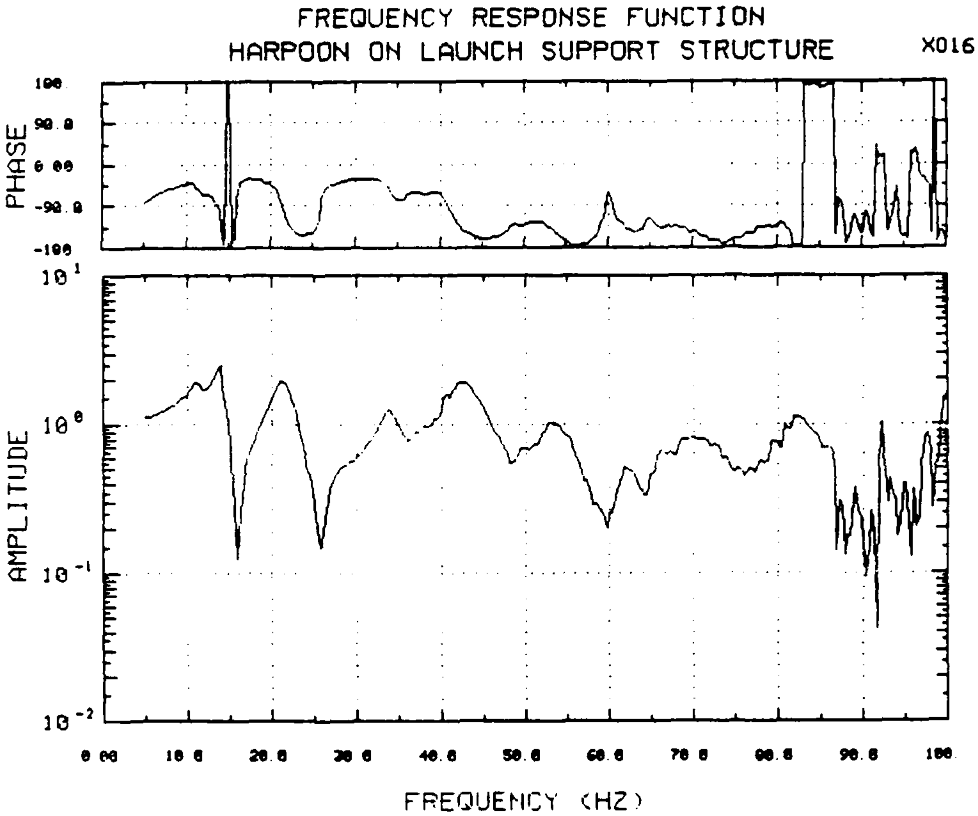

Figure 10.27 X-Axis Transfer Function at Lower Clamp Frame Due to X-Axis Input, Production Pads

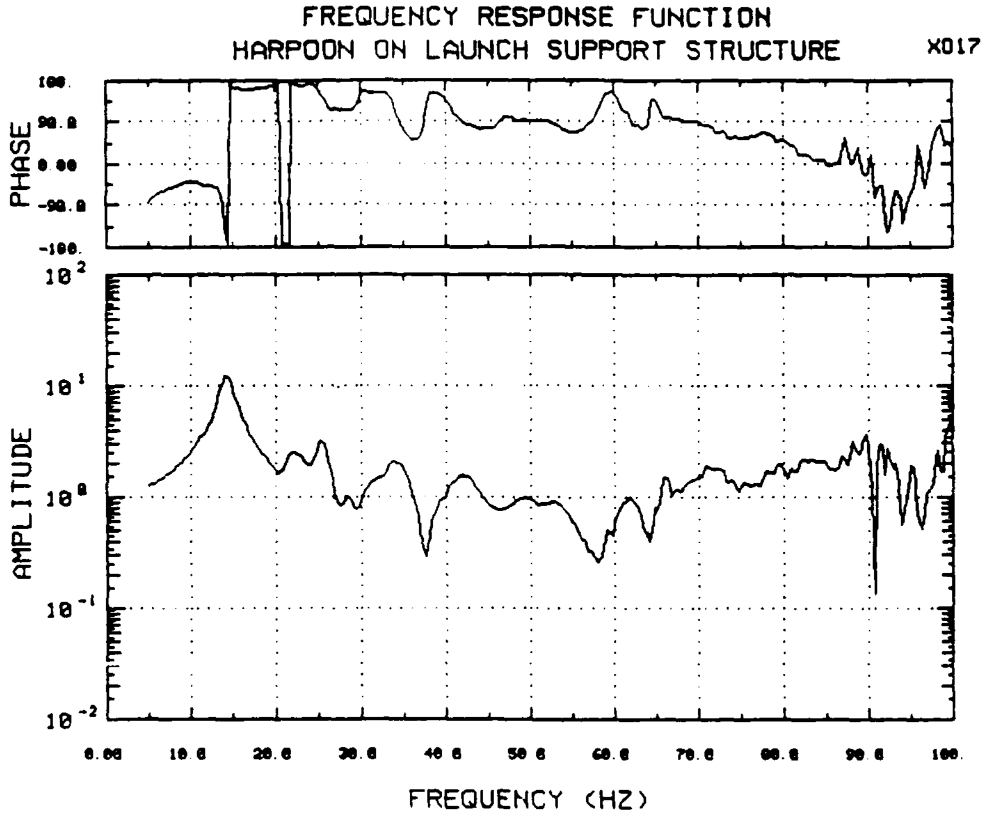

Figure 10.28 X-Axis Transfer Function at Upper Grade B Canister Nose Due to X-Axis Input, Production Pads

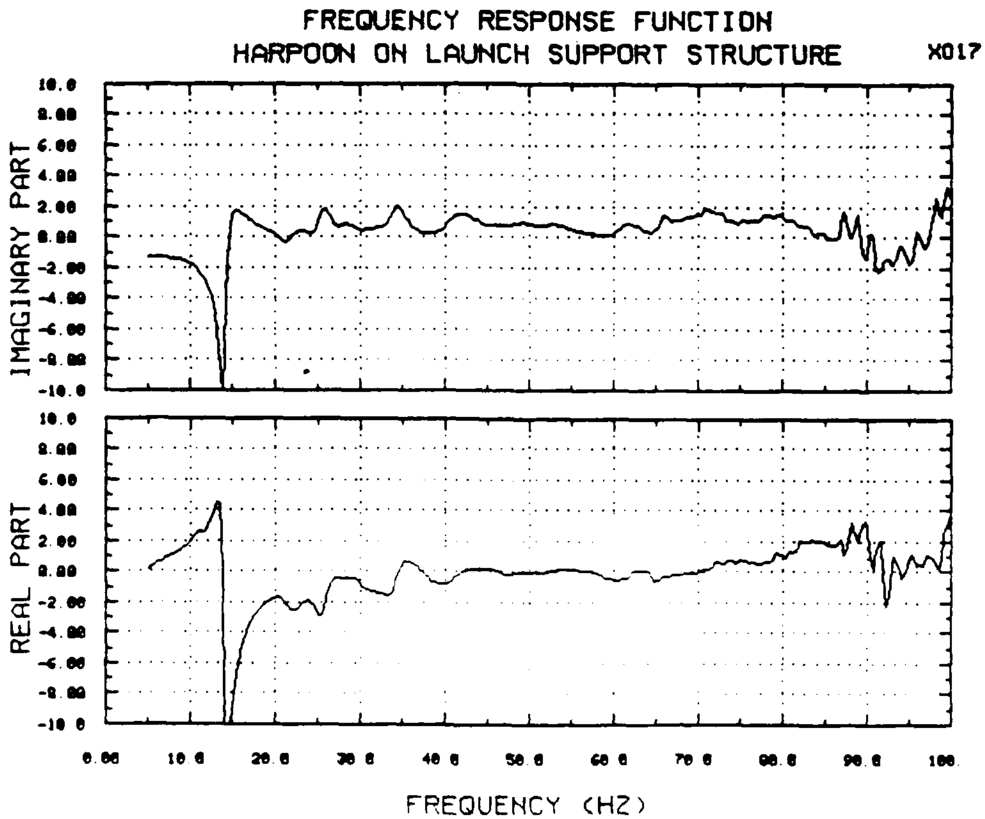

Figure 10.29 X-Axis Real and Imaginary Transfer Function at Upper Grade B Canister Nose Due to X-Axis Input, Production Pads

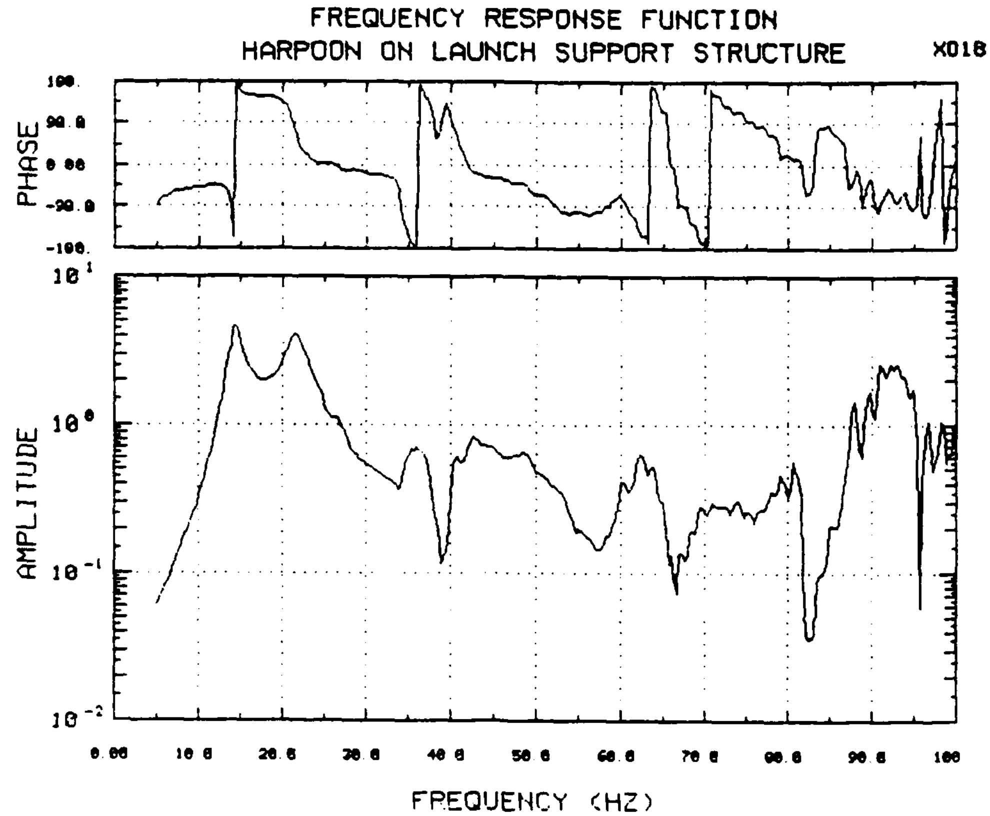

Figure 10.30 Y-Axis Transfer Function at Upper Grade B Canister Clamp Frame Due to X-Axis Input, Production Pads

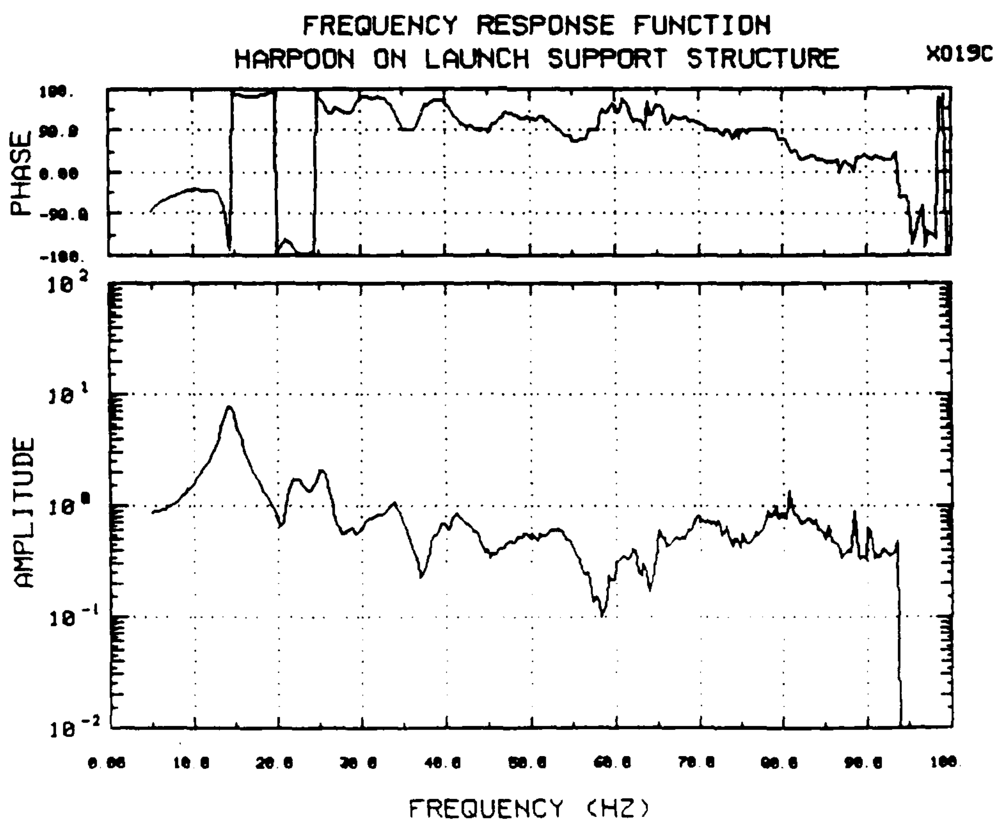

Figure 10.31 X-Axis Transfer Function at Upper Grade B Canister Clamp Frame Due to X-Axis Input, Production Pads

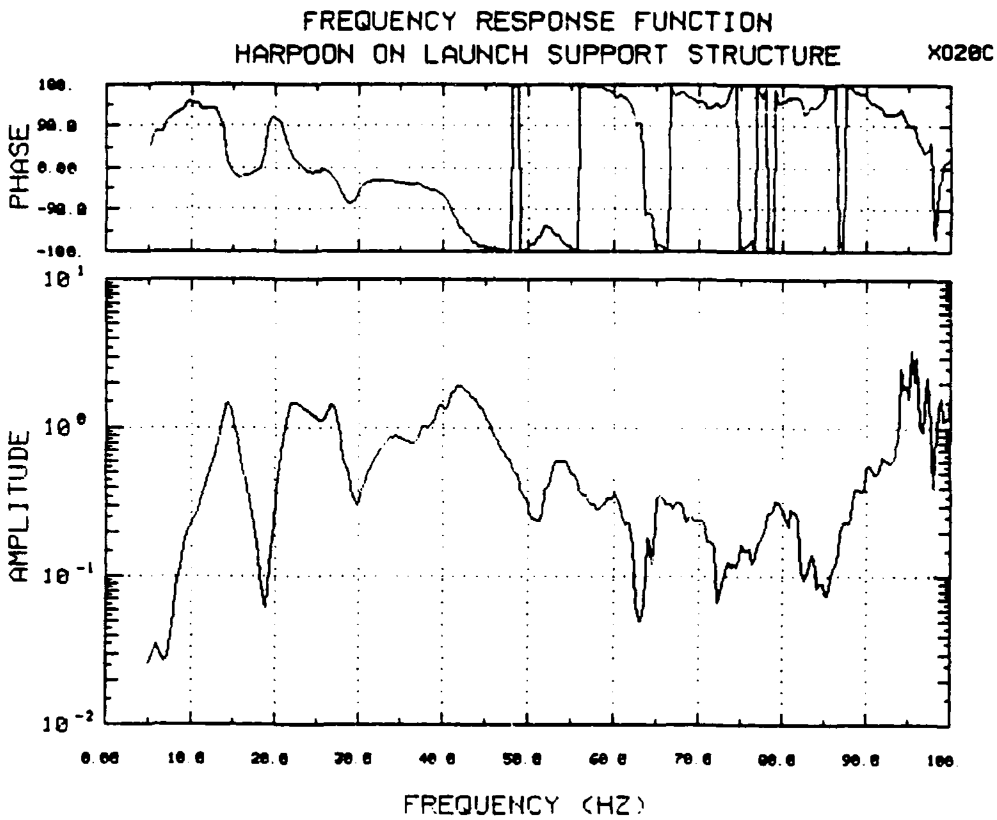

Figure 10.32 .Z-Axis Transfer Function at Upper Grade B Canister Clamp Frame Due to X-Axis Input, Production Pads

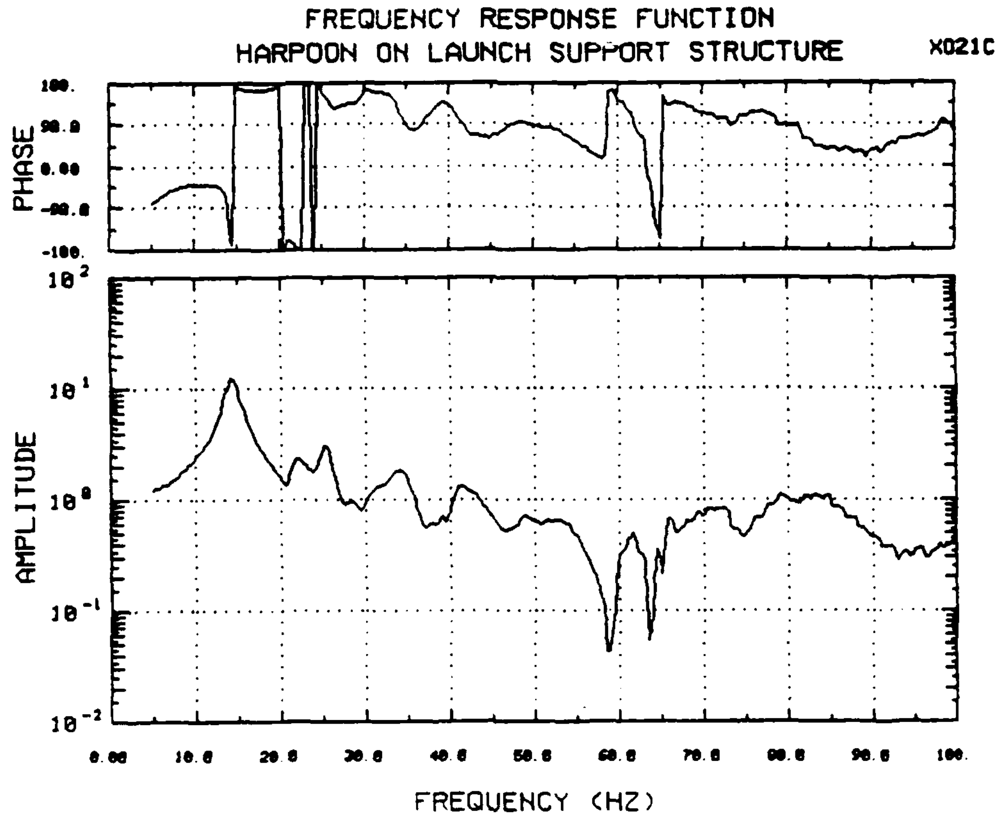

Figure 10.33 X-Axis Transfer Function at Upper Clamp Frame Due tc X-Axis Input, Production Pads

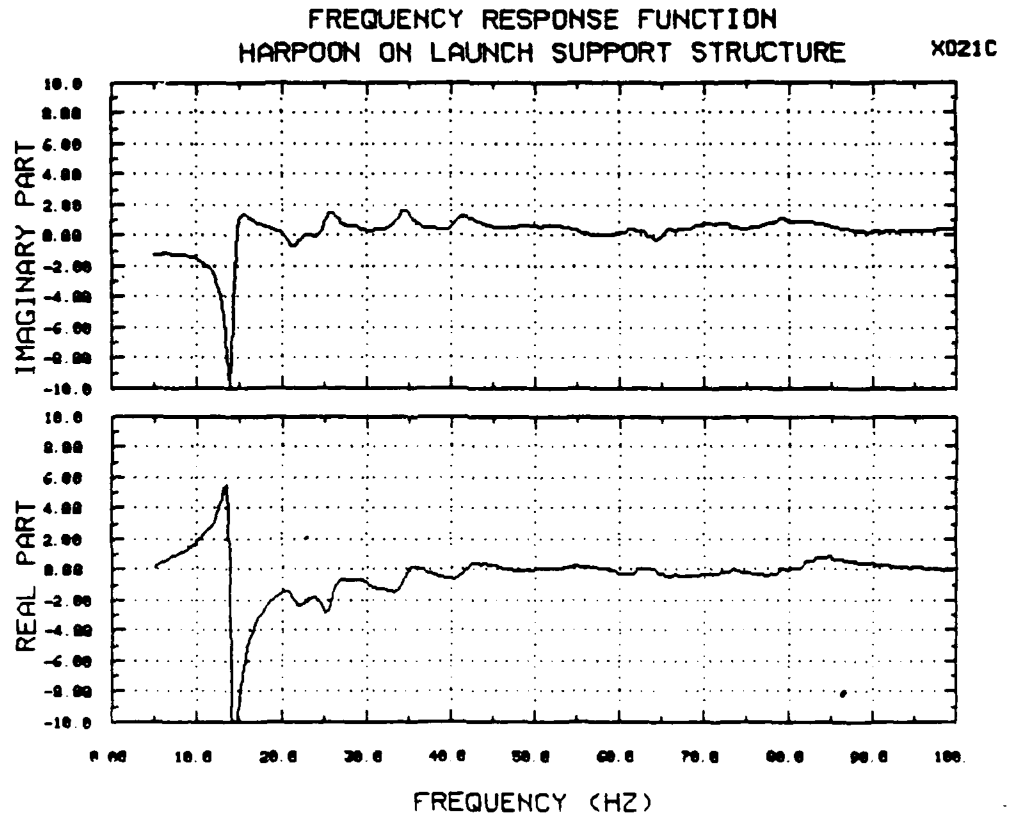

Figure 10.34 X-Axis Real and Imaginary Transfer Function at Upper Clamp Frame Due to X-Axis Input, Production Pads

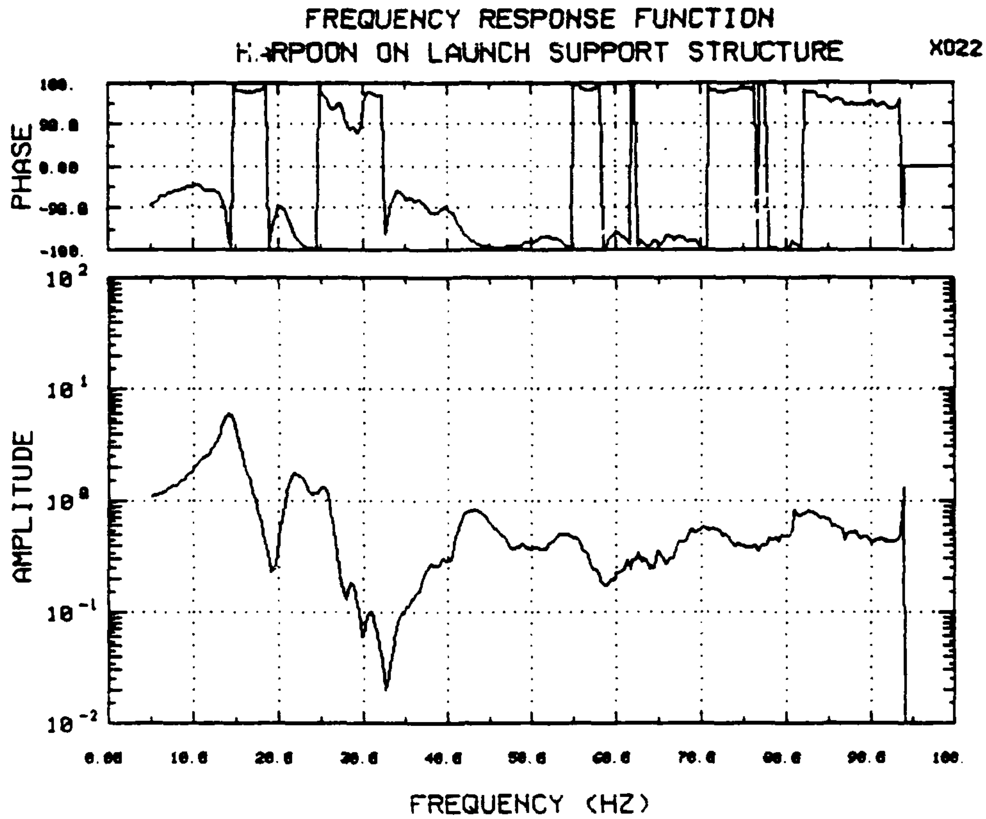

Figure 10.35 X-Axis Transfer Function at Lower Grade B Canister Clamp Frame Due to X-Axis Input, Production Pads

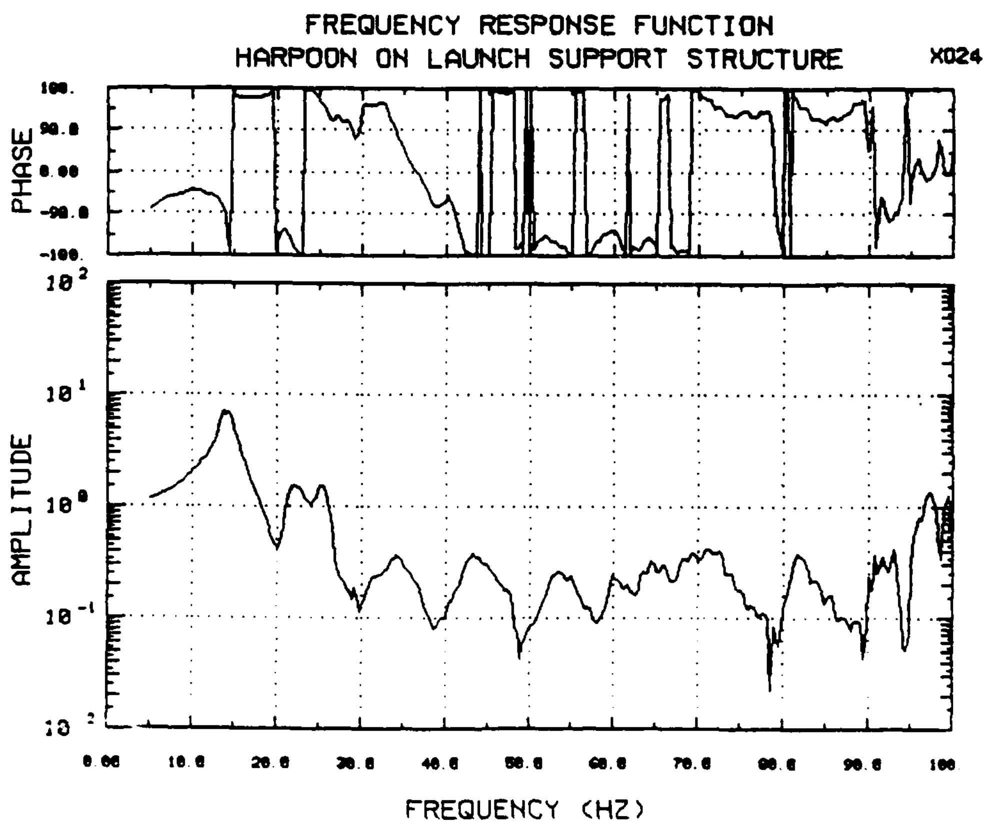

Figure 10.36 .X-Axis Transfer Function at Middle Clamp Frame Due to X-Axis Input, Production Pads

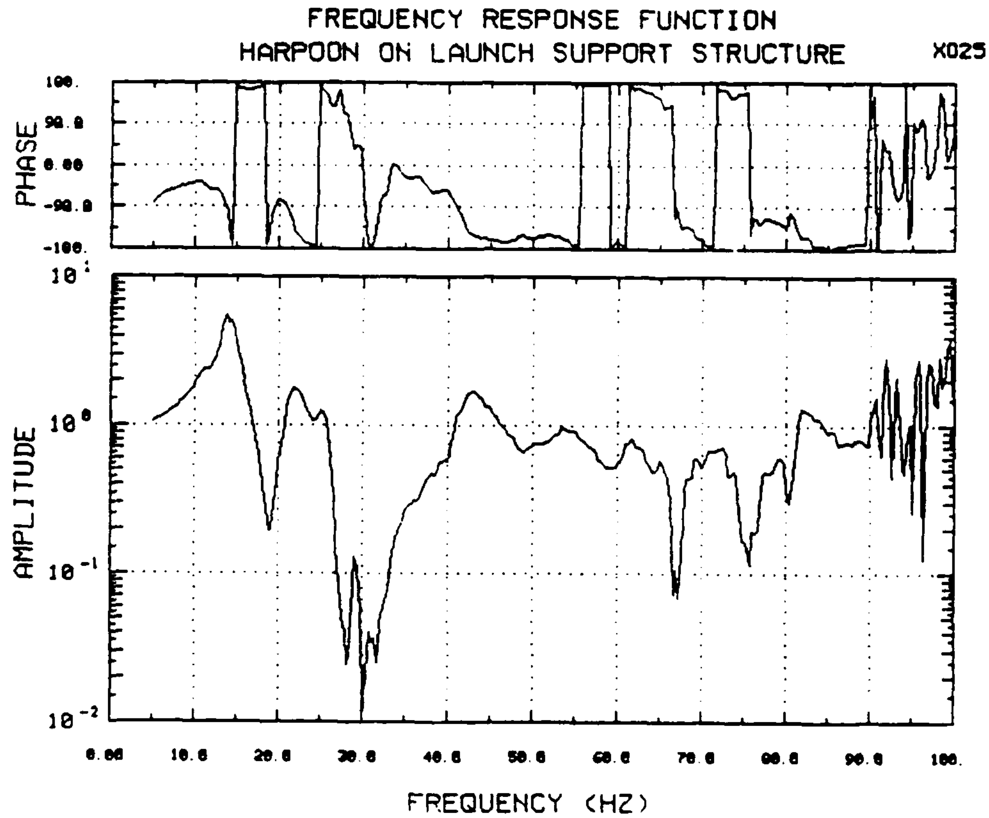

Figure 10.37 X-Axis Transfer Function at Lower Grade B Canister Nose Due to X-Axis Input, Production Pads

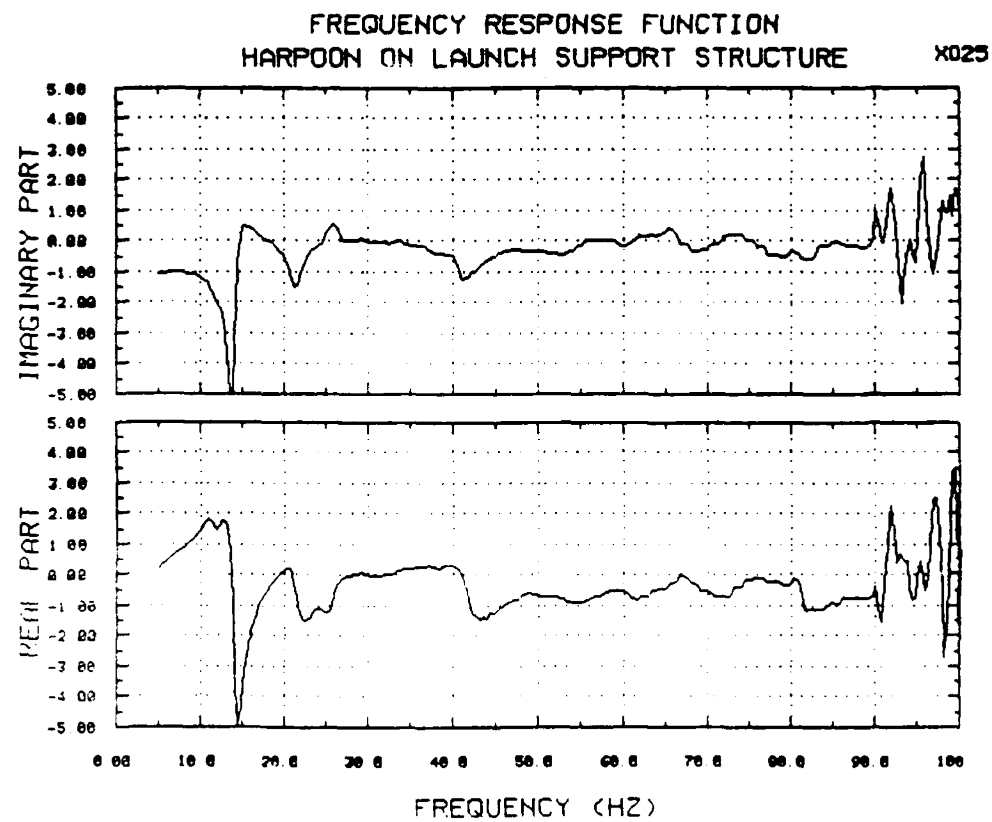

Figure 10.38 X-Axis Real and Imaginary Transfer Function at Lower Grade B Canister Nose Due to X-Axis Input, Production Pads

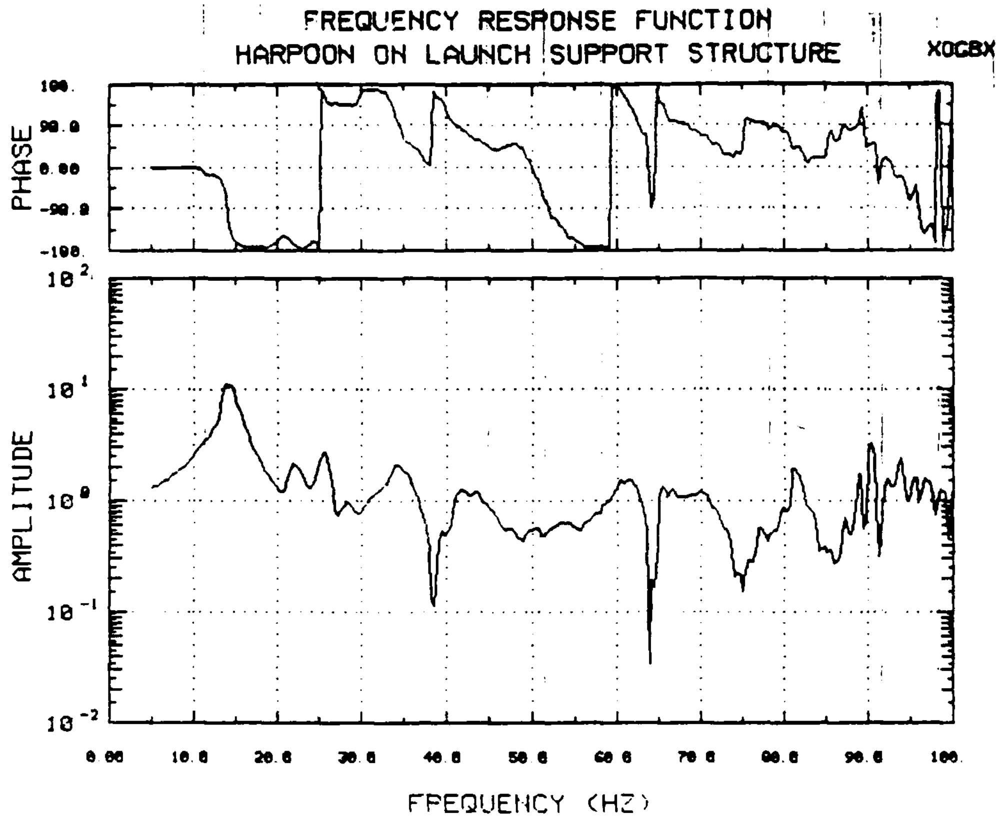

Figure 10.39 X-Axis Transfer Function at Lower Missile Due to X-Axis Input, Production Pads

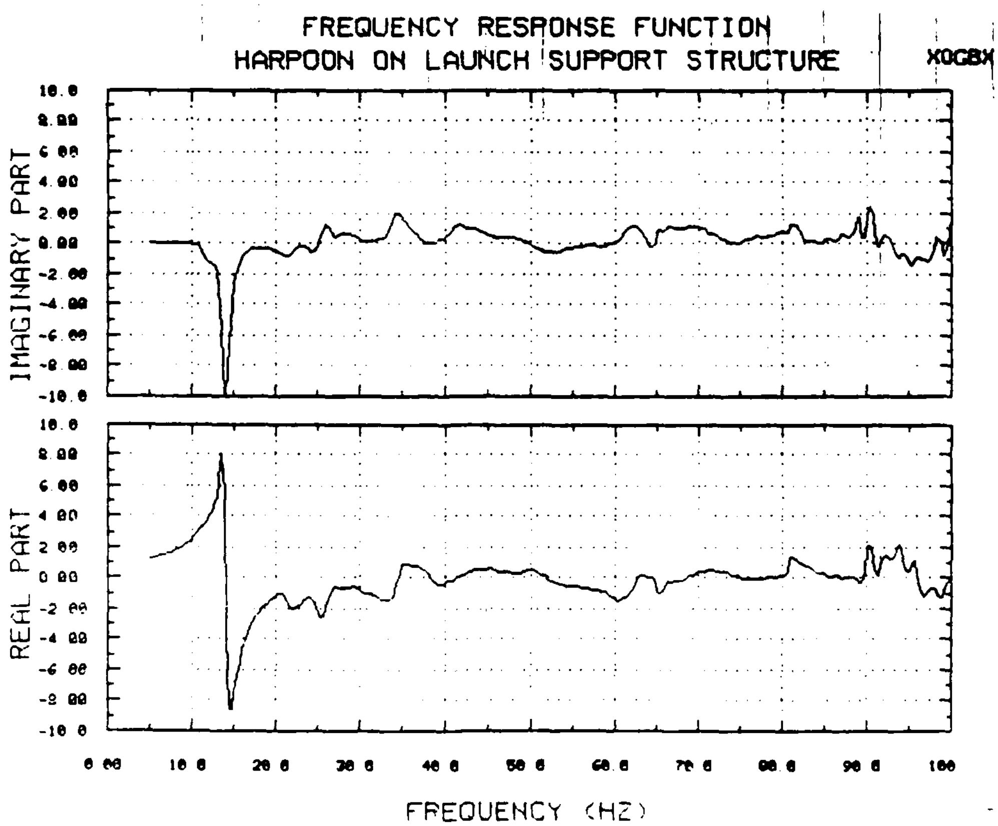

Figure 10.40 X-Axis Real and Imaginary Transfer Function at Lower Missile Due to X-Axis Input, Production Pads

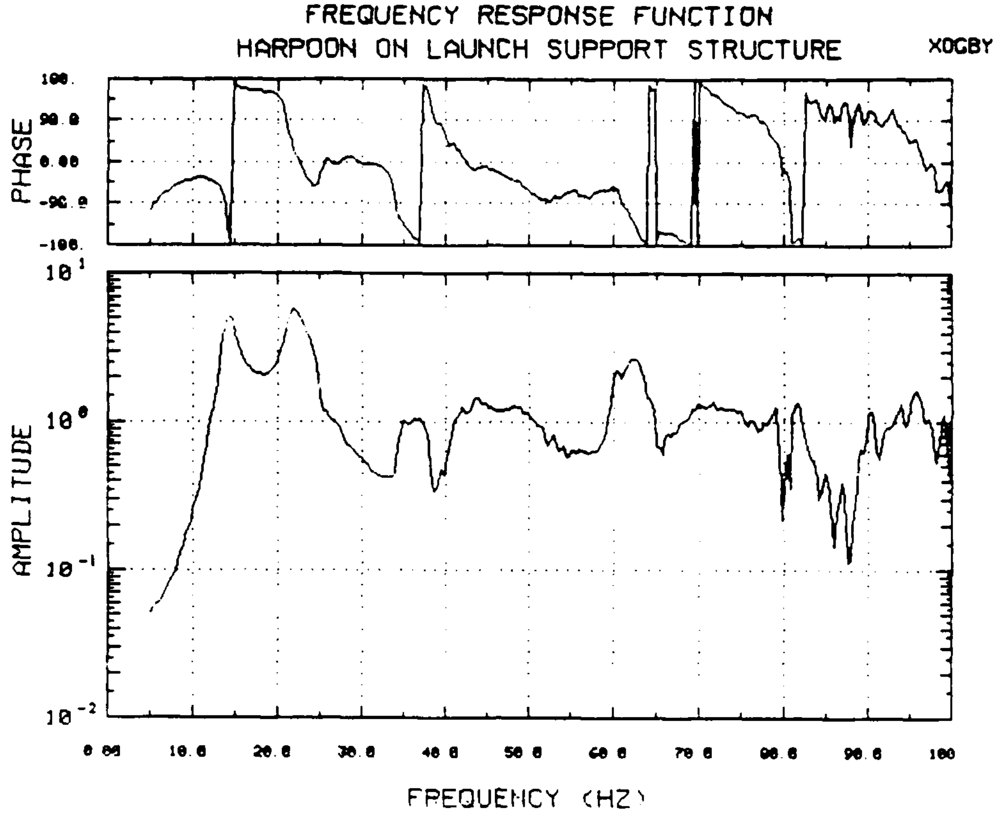

Figure 10.41 .Y-Axis Transfer Function at Lower Missile Due to X-Axis Input, Production Pads

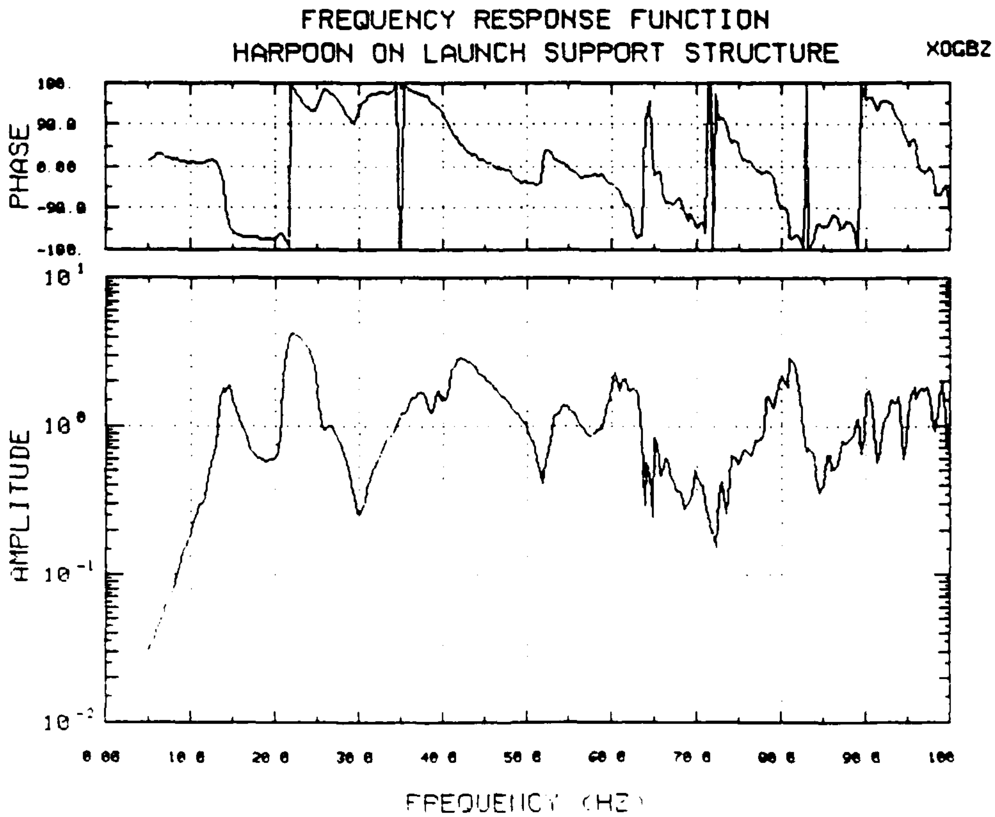

Figure 10.42 Z-Axis Transfer Function at Lower Missile Due to X-Axis Input, Production Pads

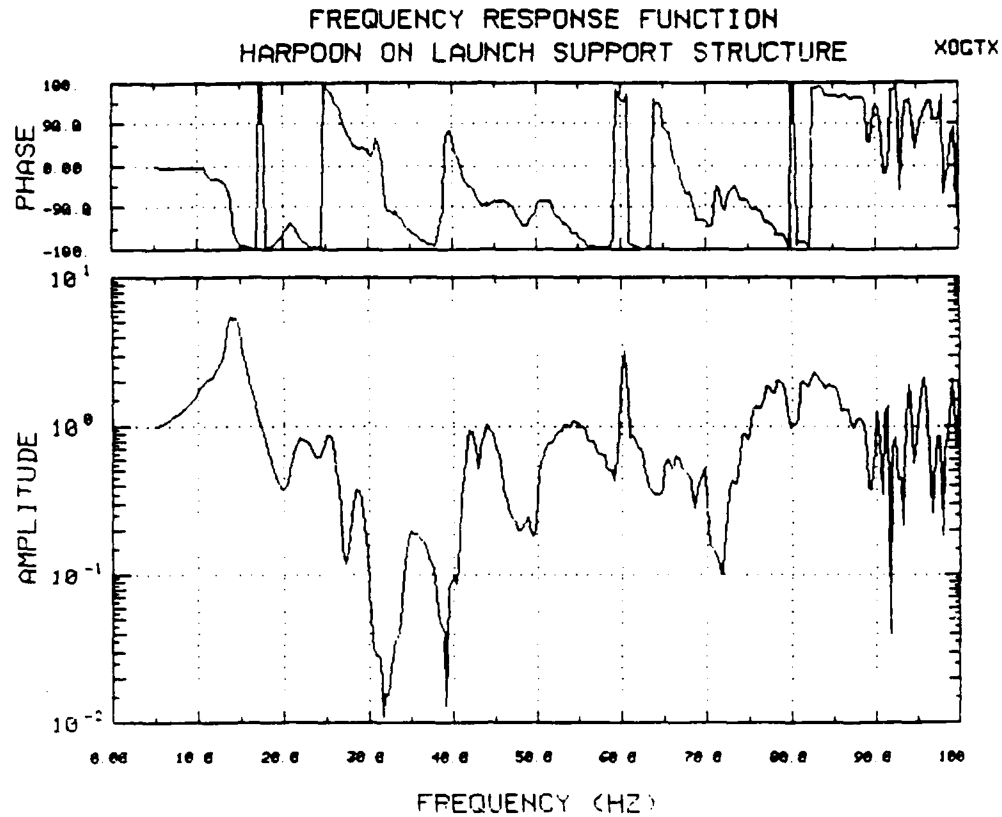

Figure 10.43 X-Axis Transfer Function at Upper Missile Due to X-Axis Input, Production Pads

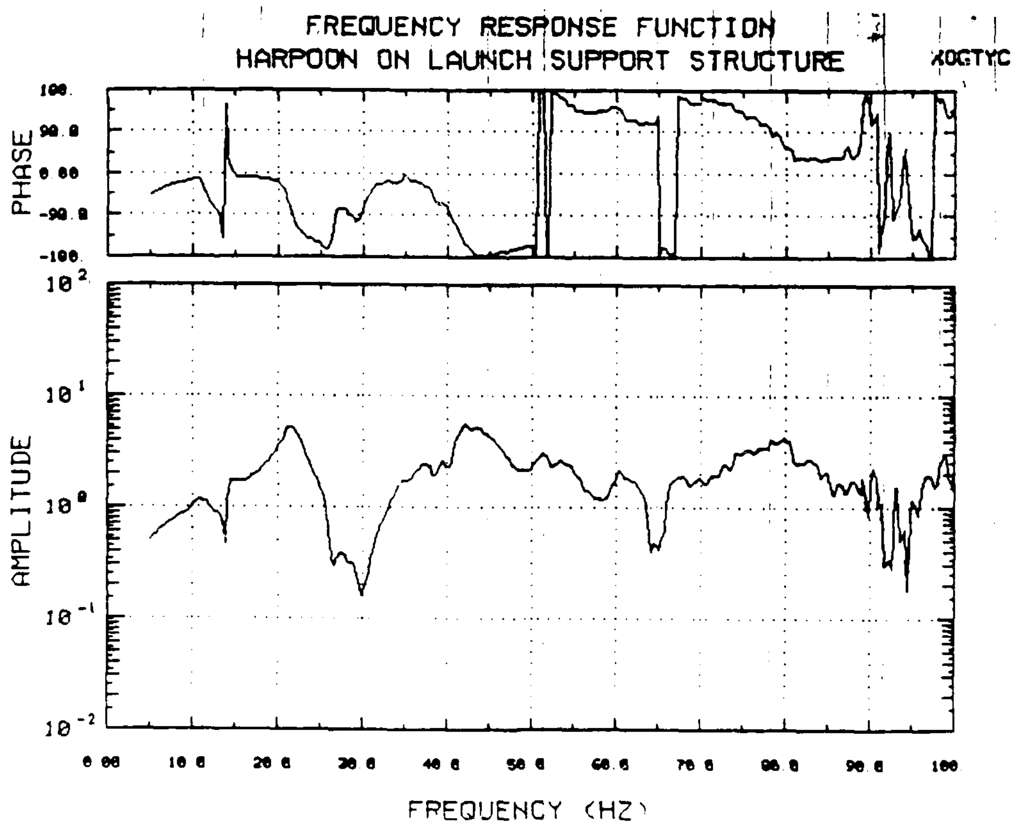

Figure 10.44 .Y-Axis Transfer Function at Upper Missile Due to X-Axis Input, Production Pads

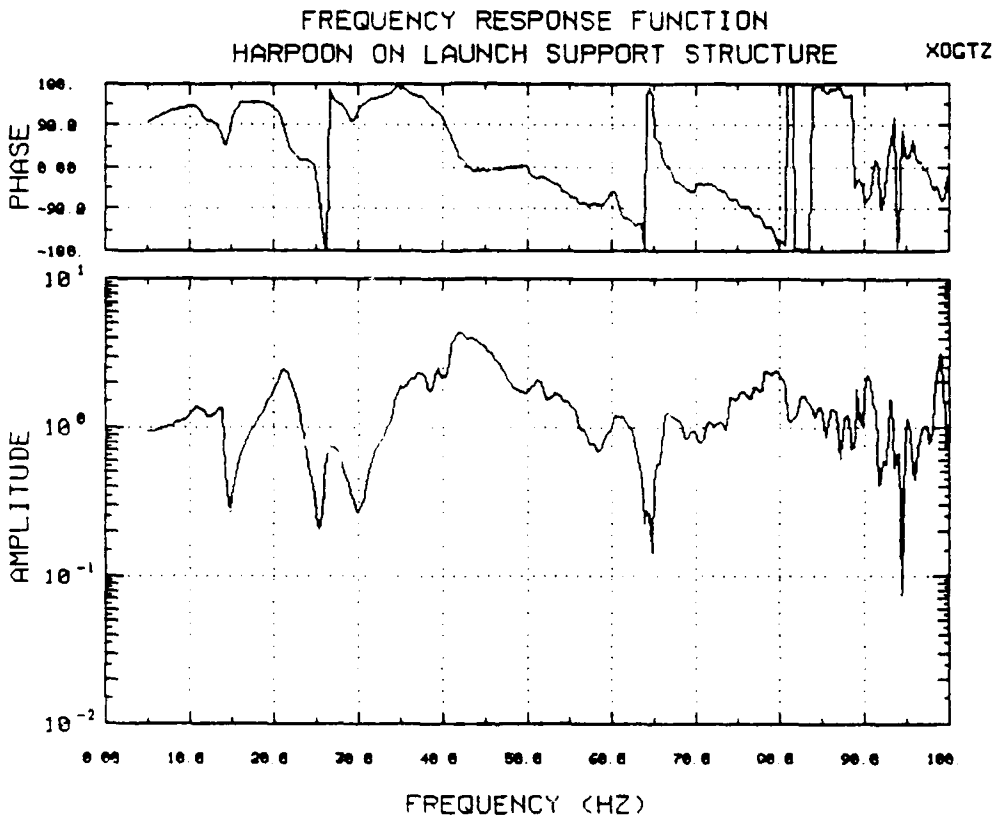

Figure 10.45 .Z-Axis Transfer Function at Upper Missile Due to X-Axis Input, Production Pads

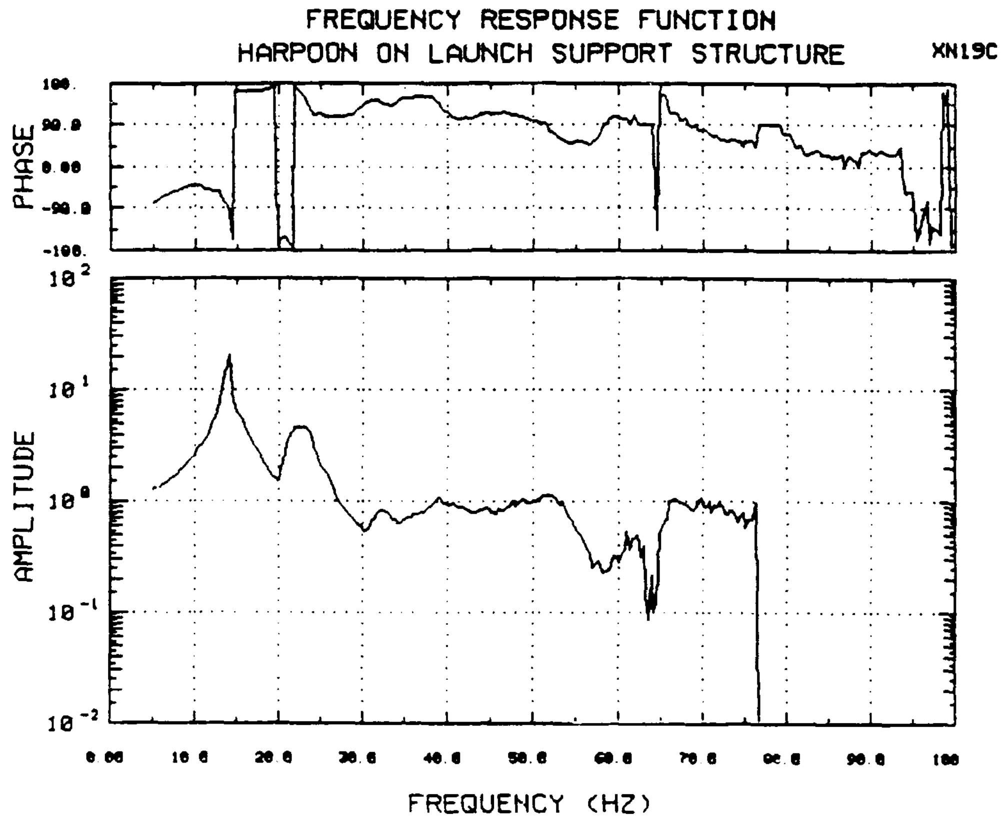

Figure 10.46 X-Axis Transfer Function at Upper Grade B Canister Clamp Frame Due to X-Axis Input, Modified Isolation Pads

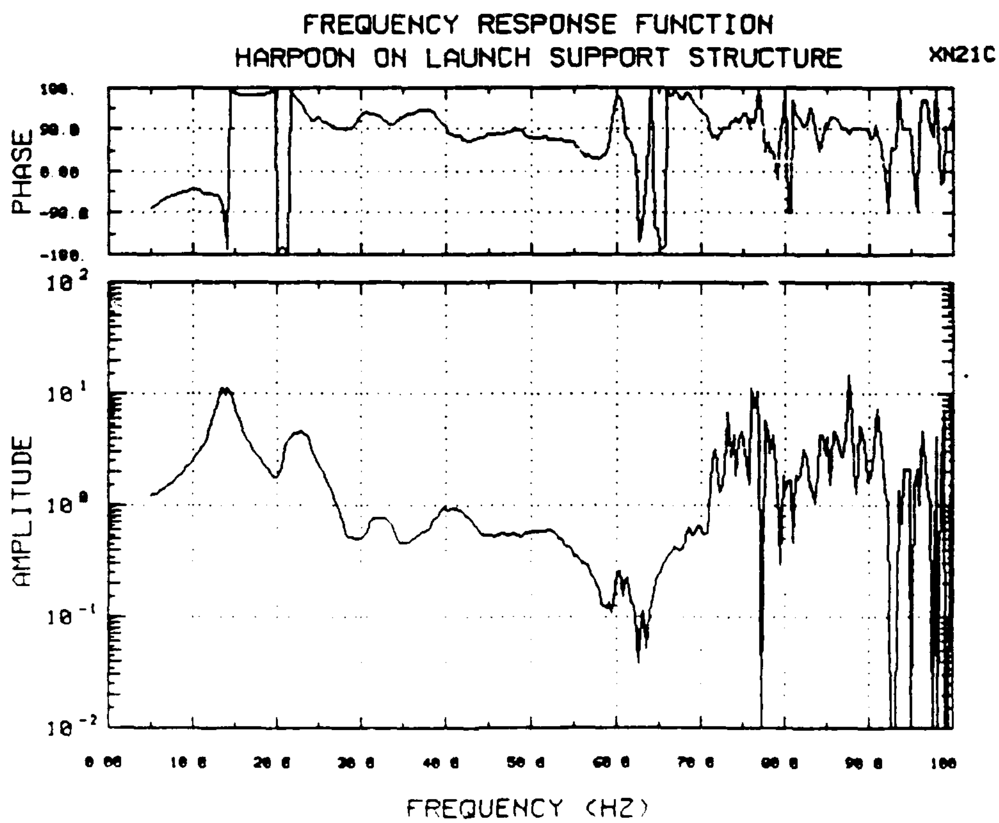

Figure 10.47 X-Axis Transfer Function at Upper Clamp Frame Due to X-Axis Input, Modified Isolation Pads

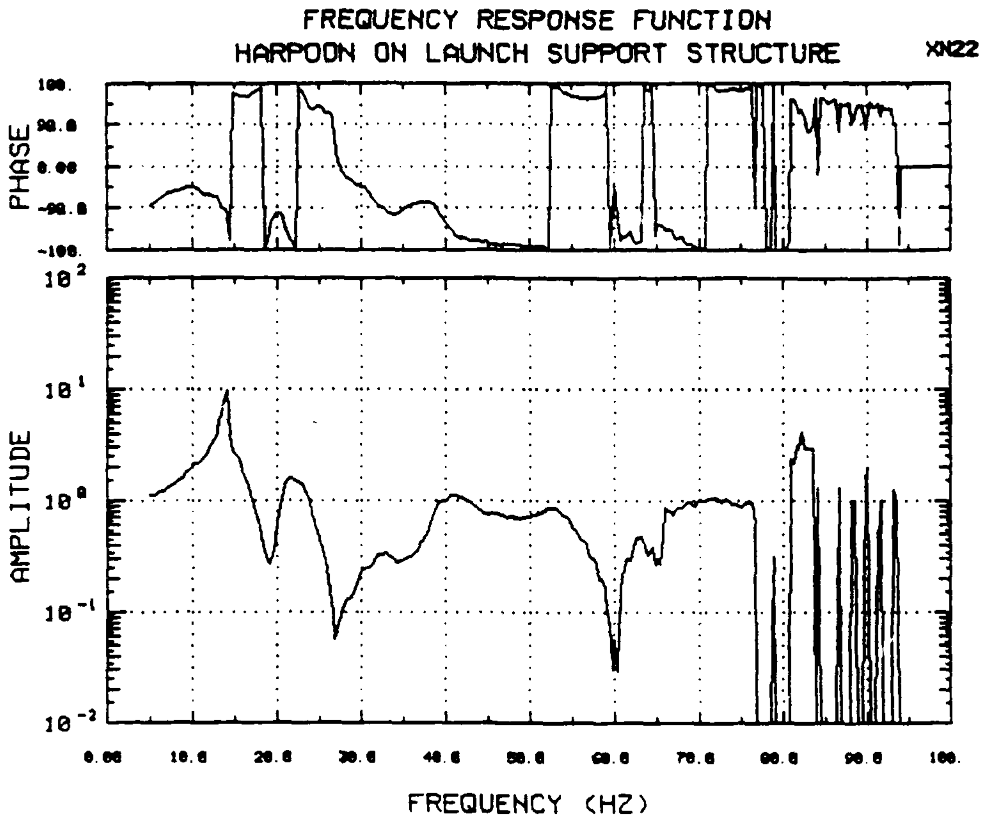

Figure 10.48 X-Axis Transfer Function at Lower Grade B Canister Clamp Frame Due to X-Axis Input, Modified Isolation Pads

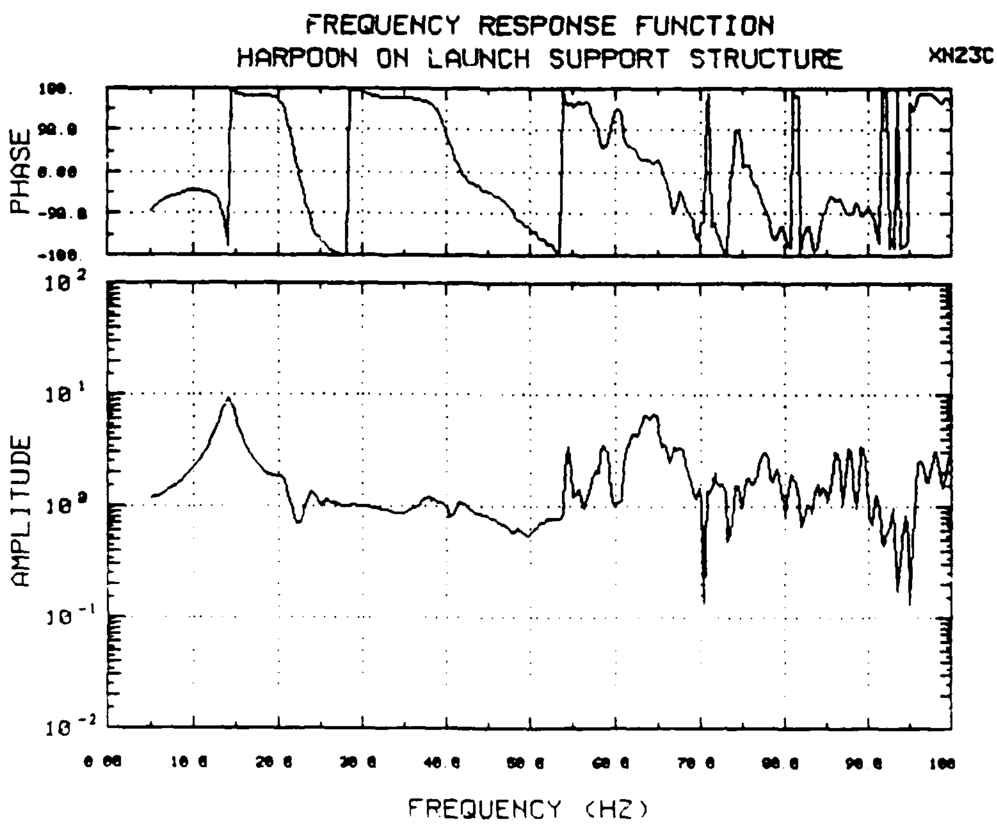

Figure 10.49 X-Axis Transfer Function at Upper Clamp Frame, Trainer Side, Due to X-Axis Input, Modified Isolation Pads

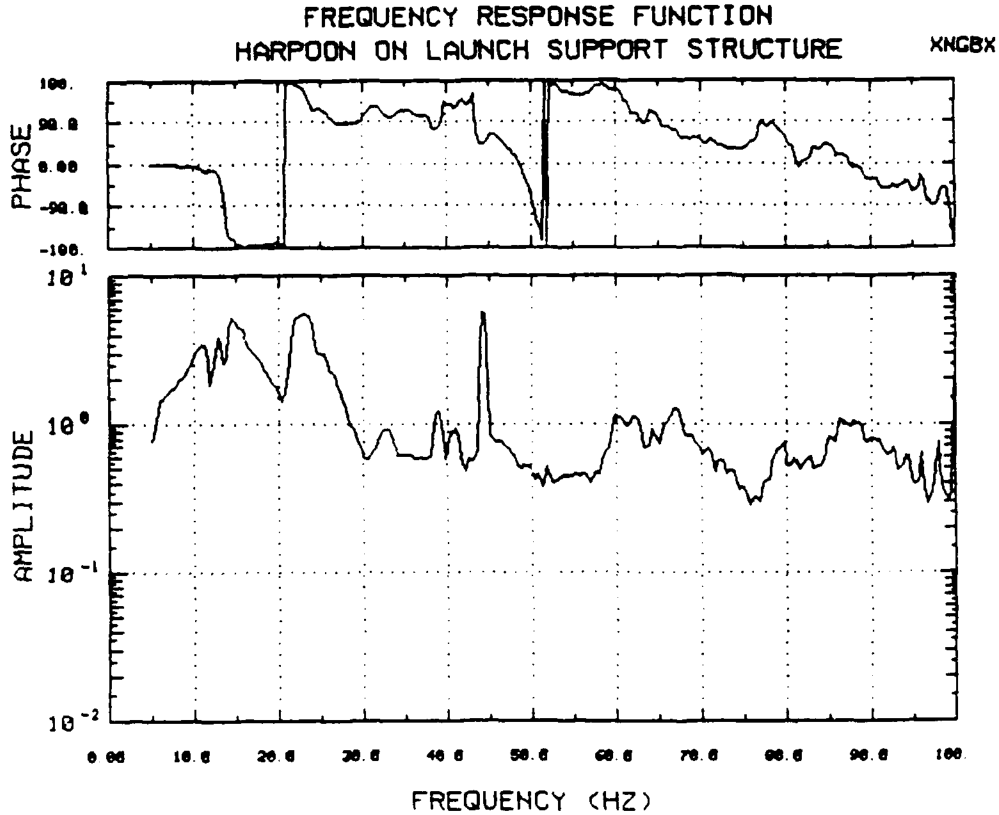

Figure 10.50 X-Axis Transfer Function at Lower Missile Due to X-Axis Input, Modified Isolation Pads

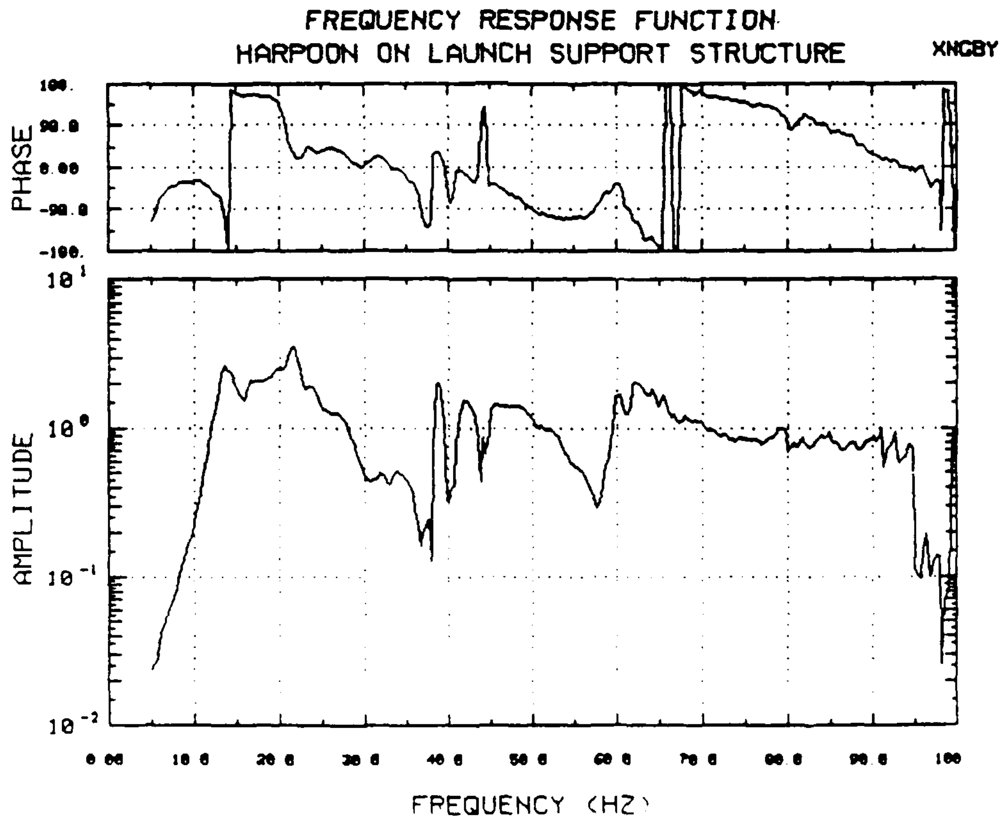

Figure 10.51 .Y-Axis Transfer Function at Lower Missile Due to X-Axis Input, Modified Isolation Pads

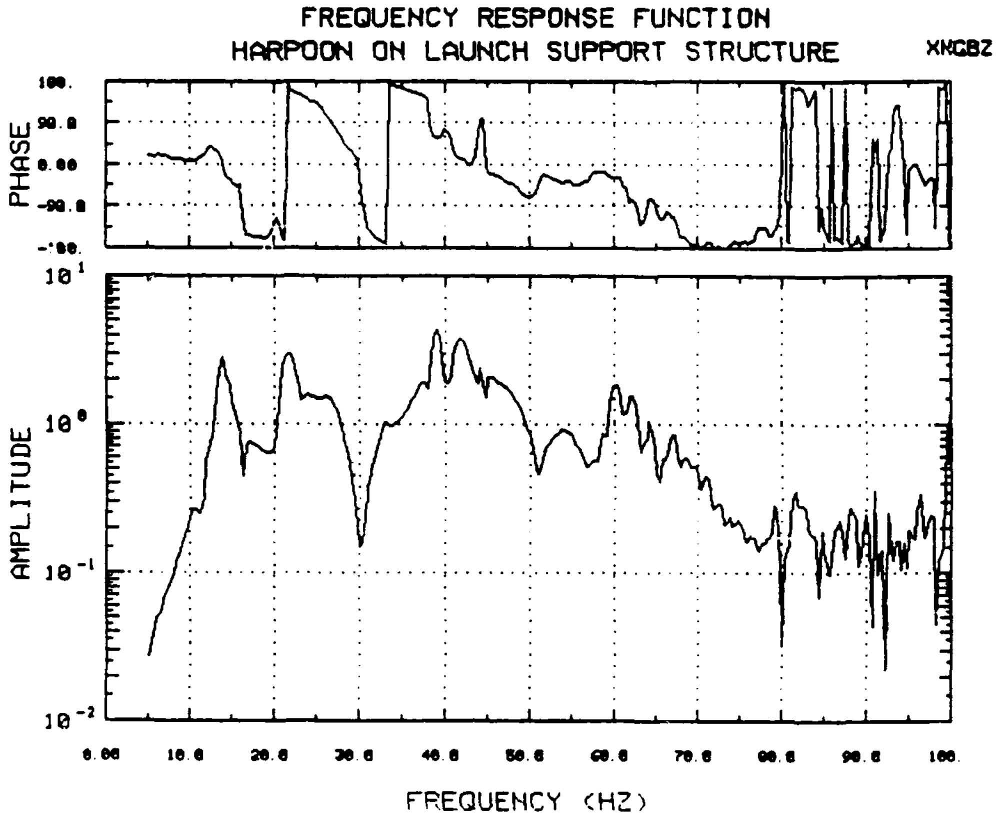

Figure 10.52 Z-Axis Transfer Function at Lower Missile Due to X-Axis Input, Modified Isolation Pads

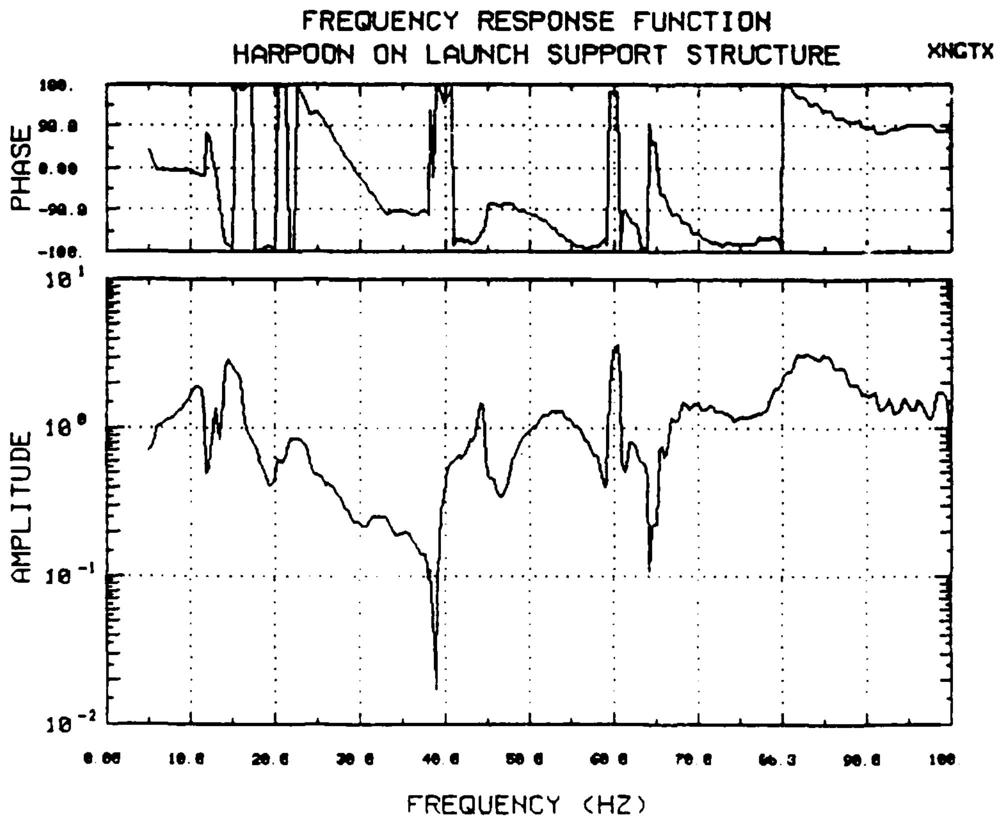

Figure 10.53 X-Axis Transfer Function at Upper Missile Due to X-Axis Input, Modified Isolation Pads

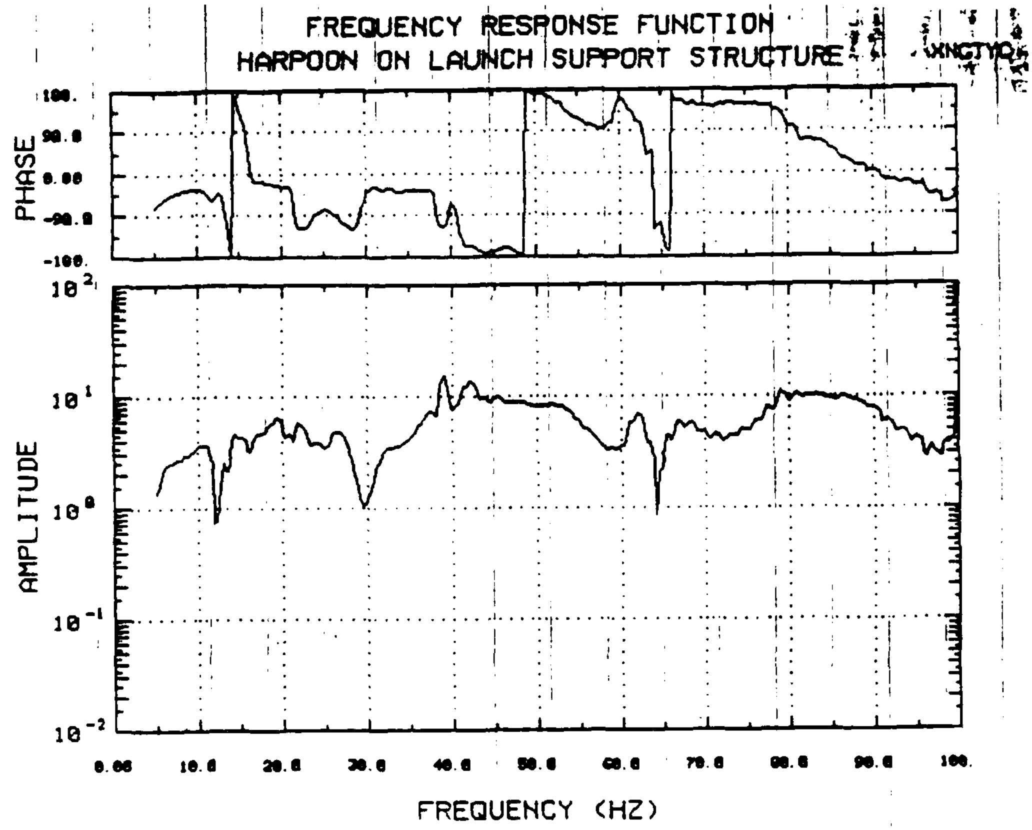

Figure 10.54 Y-Axis Transfer Function at Upper Missile Due to X-Axis Input, Modified Isolation Pads

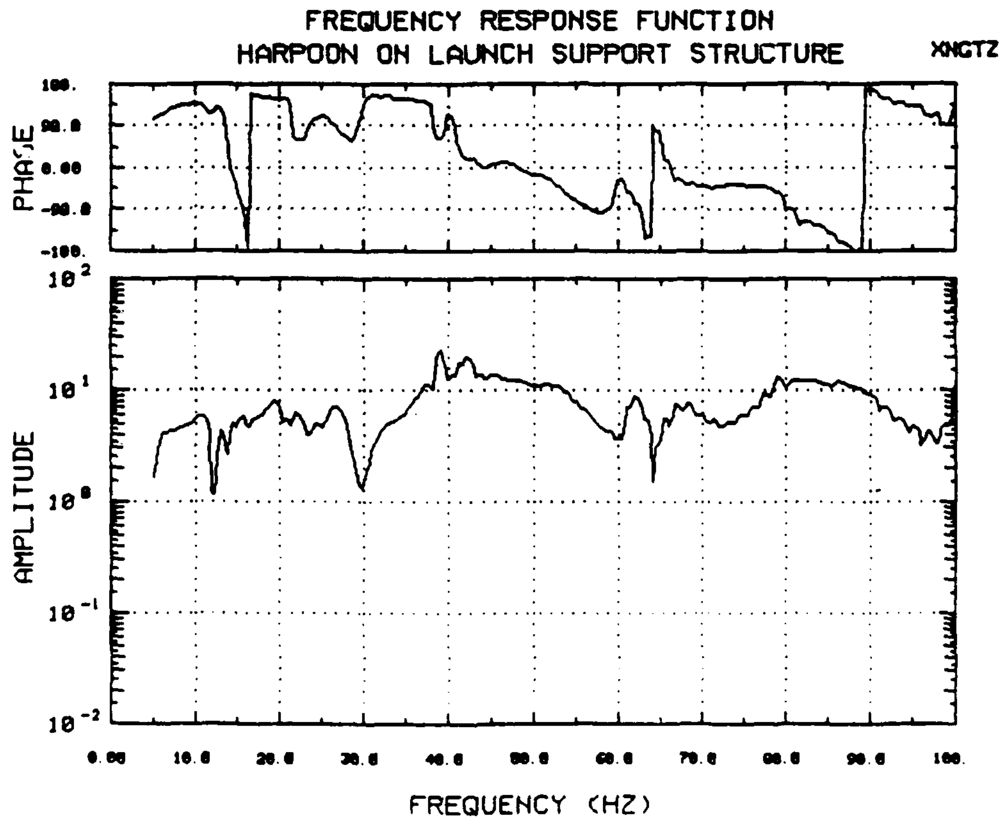

Figure 10.55 Z-Axis Transfer Function at Upper Missile Due to X-Axis Input, Modified Isolation Pads

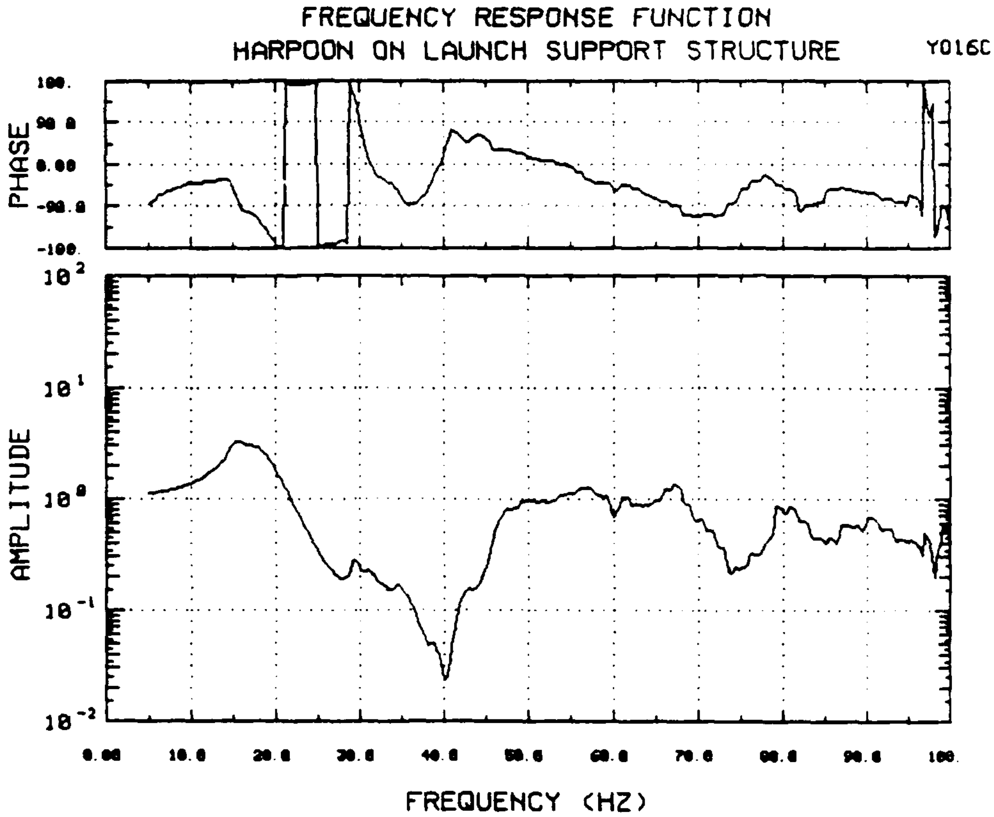

Figure 10.56 Y-Axis Transfer Function at Lower Clamp Frame Due to Y-Axis Input, Production Pads

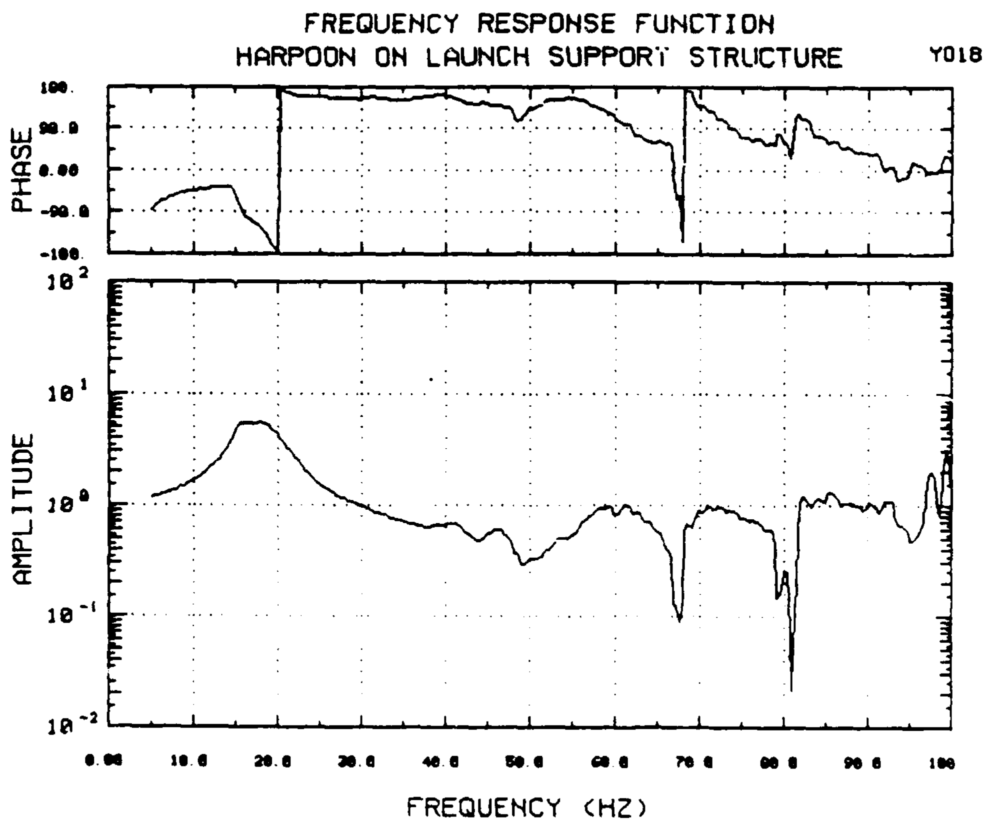

Figure 10.57 Y-Axis Transfer Function at Upper Grade B Canister Clamp Frame Due to Y-Axis Input, Production Pads

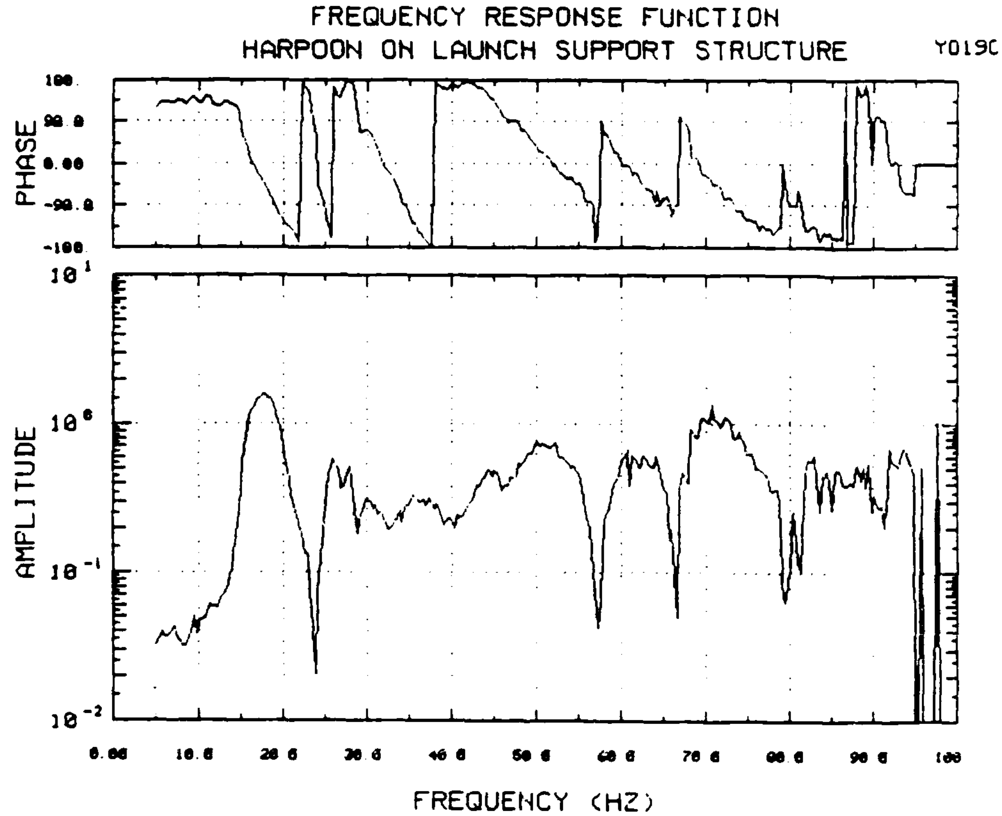

Figure 10.58 X-Axis Transfer Function at Upper Grade B Canister Clamp Frame Due to Y-Axis Input, Production Pads

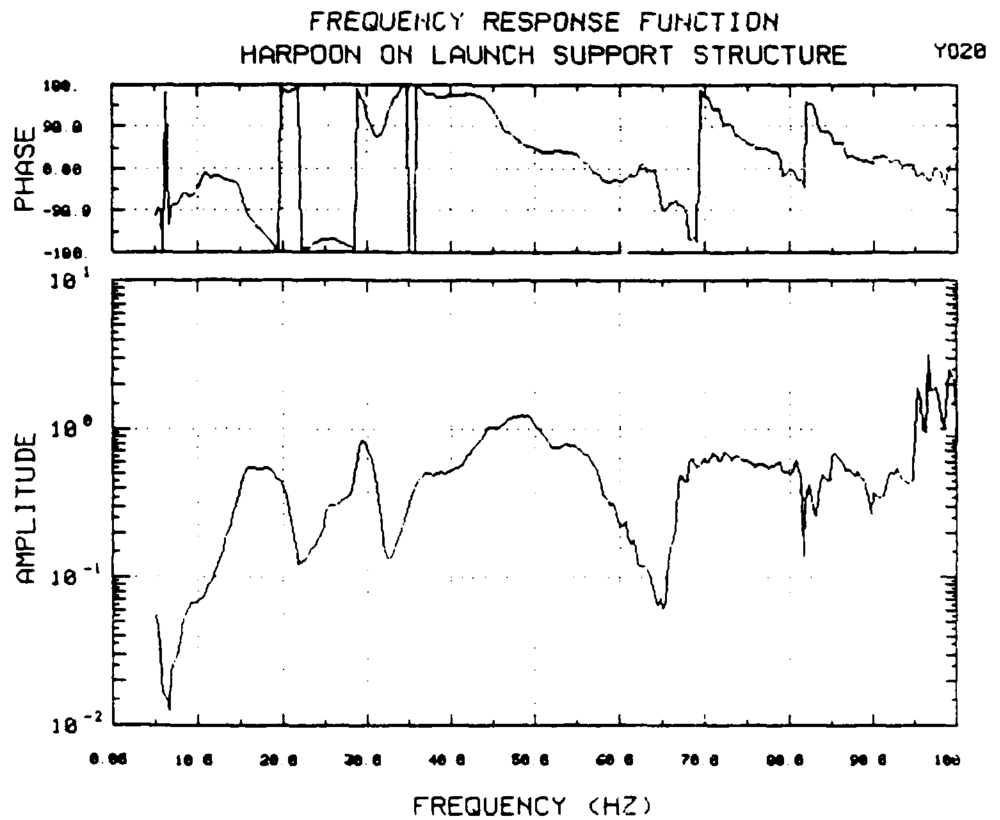

Figure 10.59 Z-Axis Transfer Function at Upper Grade B Canister Clamp Frame Due to Z-Axis Input, Production Pads

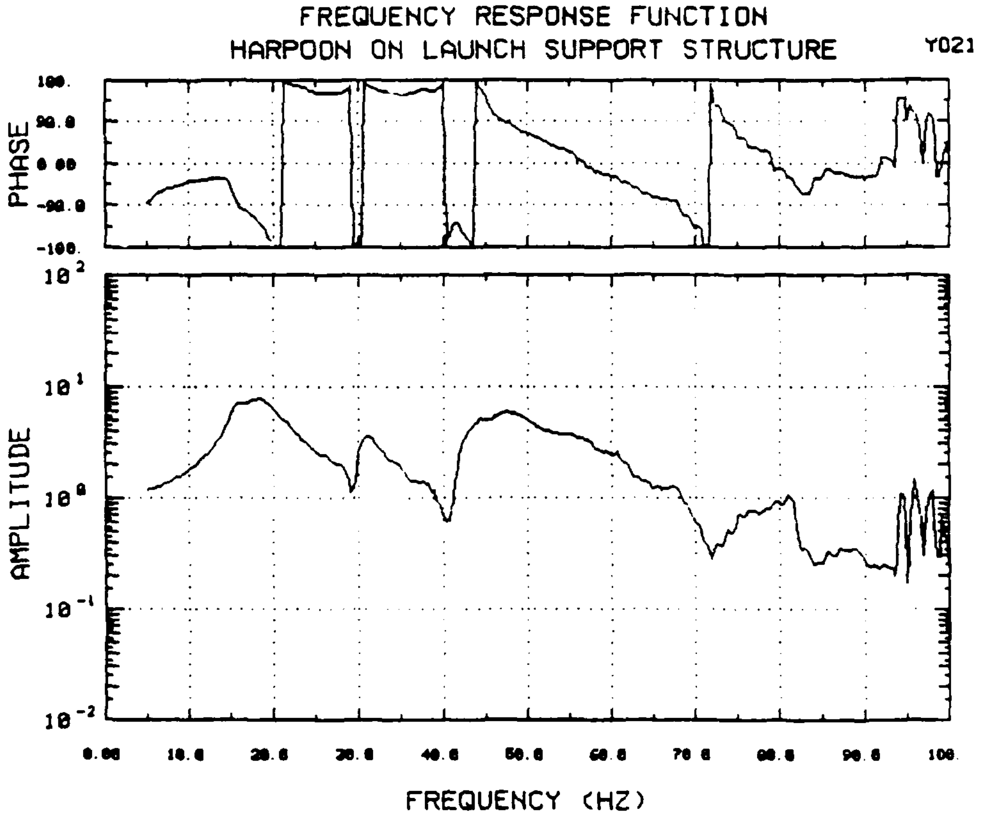

Figure 10.60 Y-Axis Transfer Function at Upper Clamp Frame Due to Y-Axis Input, Production Pads

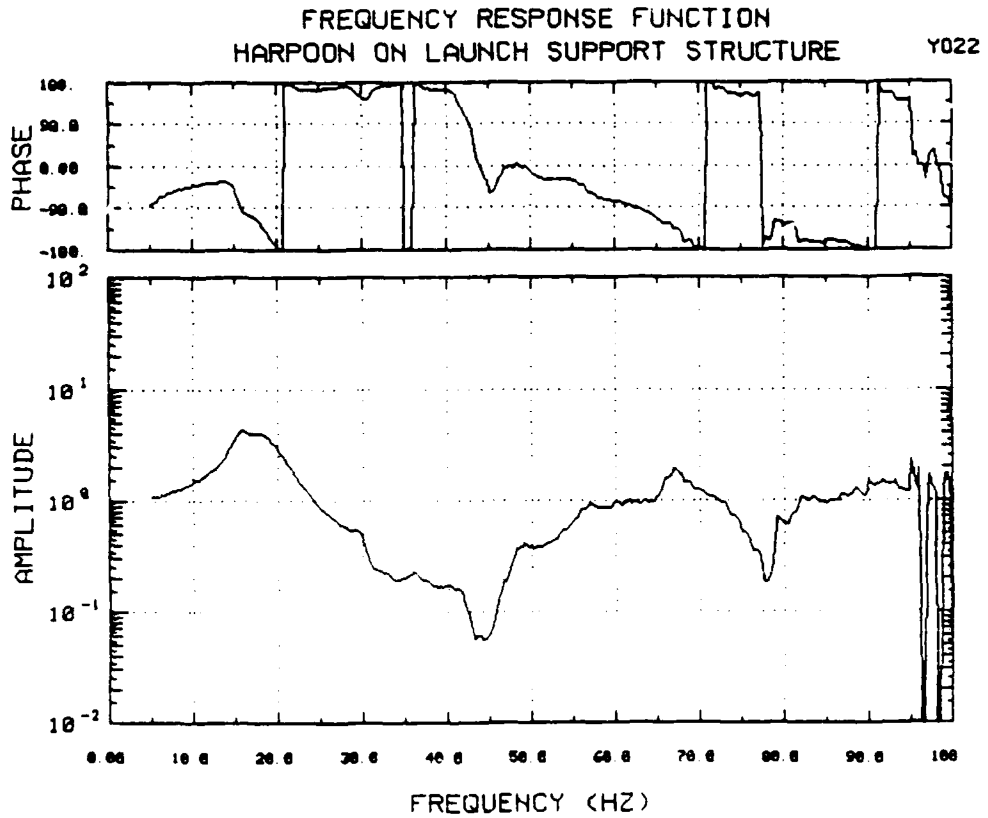

Figure 10.61 Y-Axis Transfer Function at Lower Grade B Canister Clamp Frame Due to Y-Axis Input, Production Pads

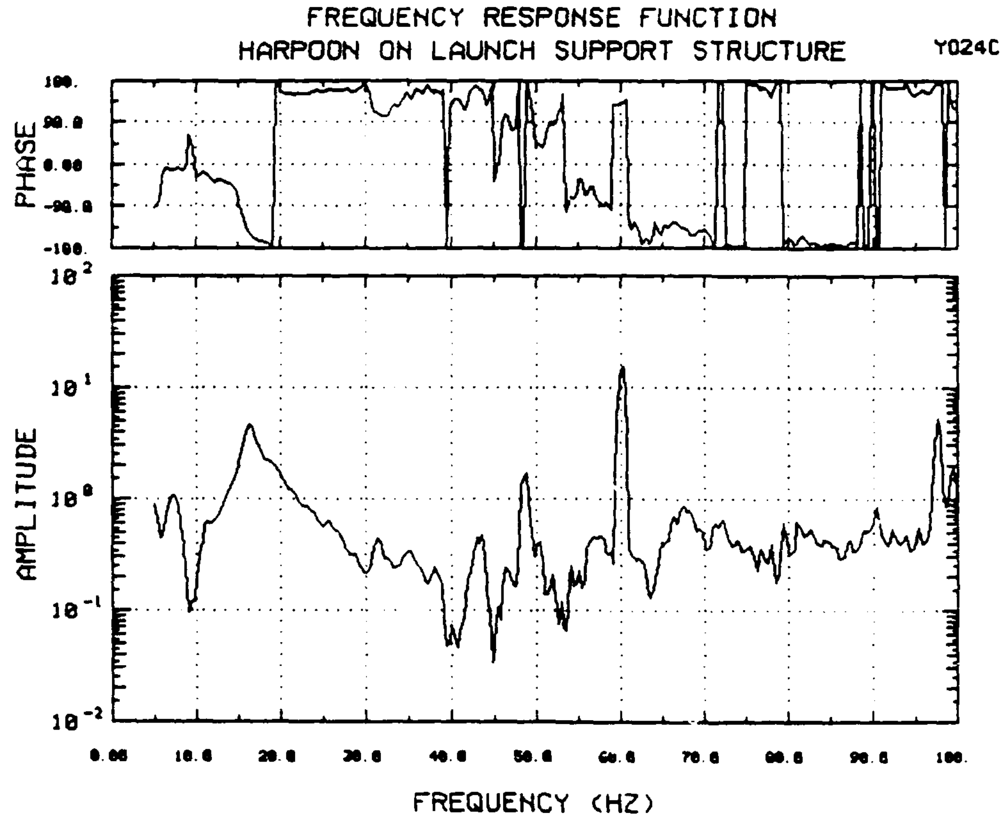

Figure 10.62 .Y-Axis Transfer Function at Middle Clamp Frame Due to Y-Axis Input, Production Pads

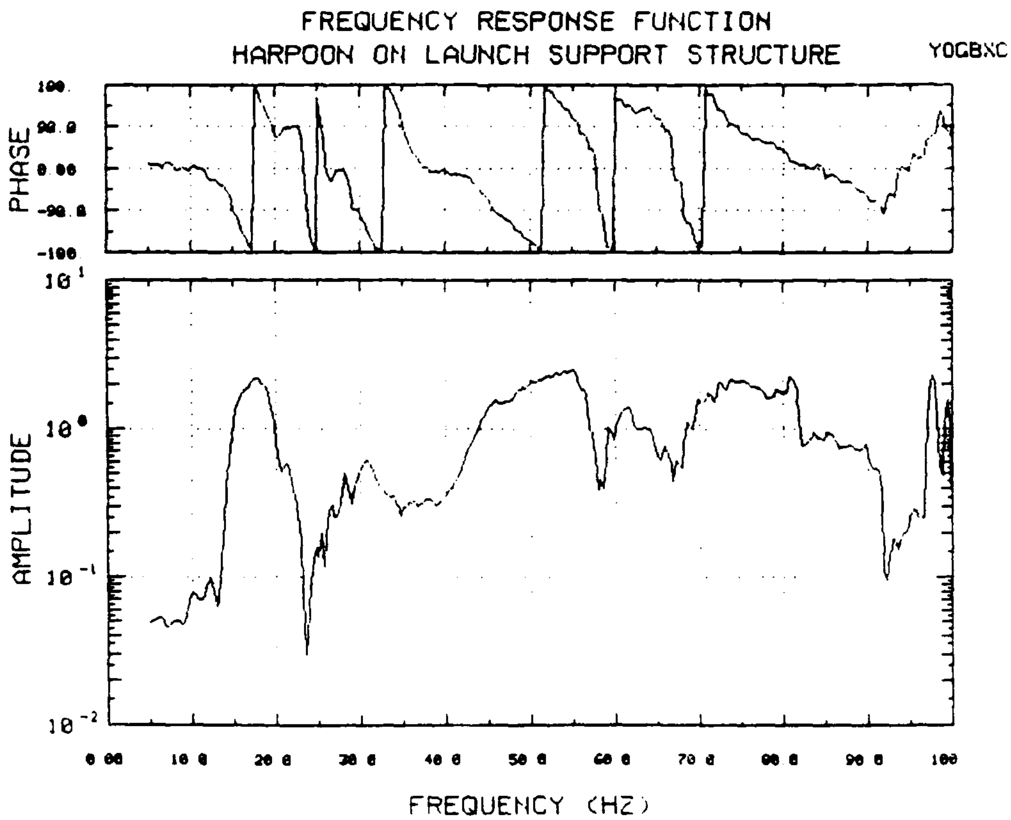

Figure 10.63 X-Axis Transfer Function at Lower Missile Due to Y-Axis Input, Production Pads

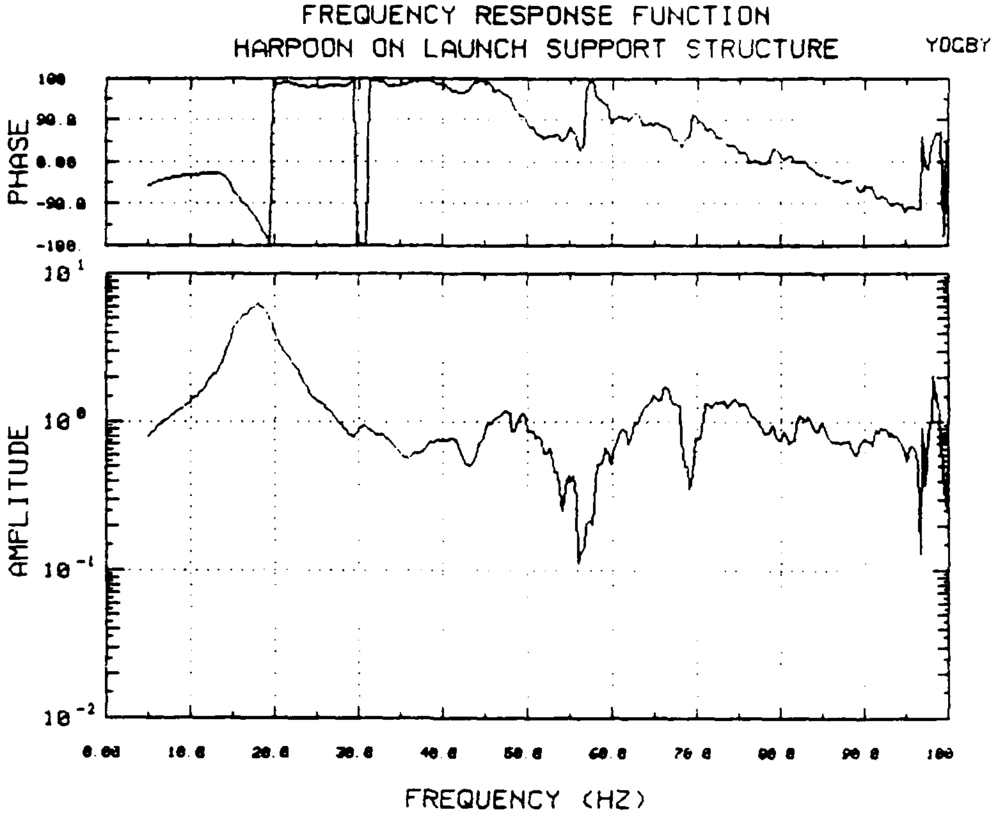

Figure 10.64 Y-Axis Transfer Function at Lower Missile Due to Y-Axis Input, Production Pads

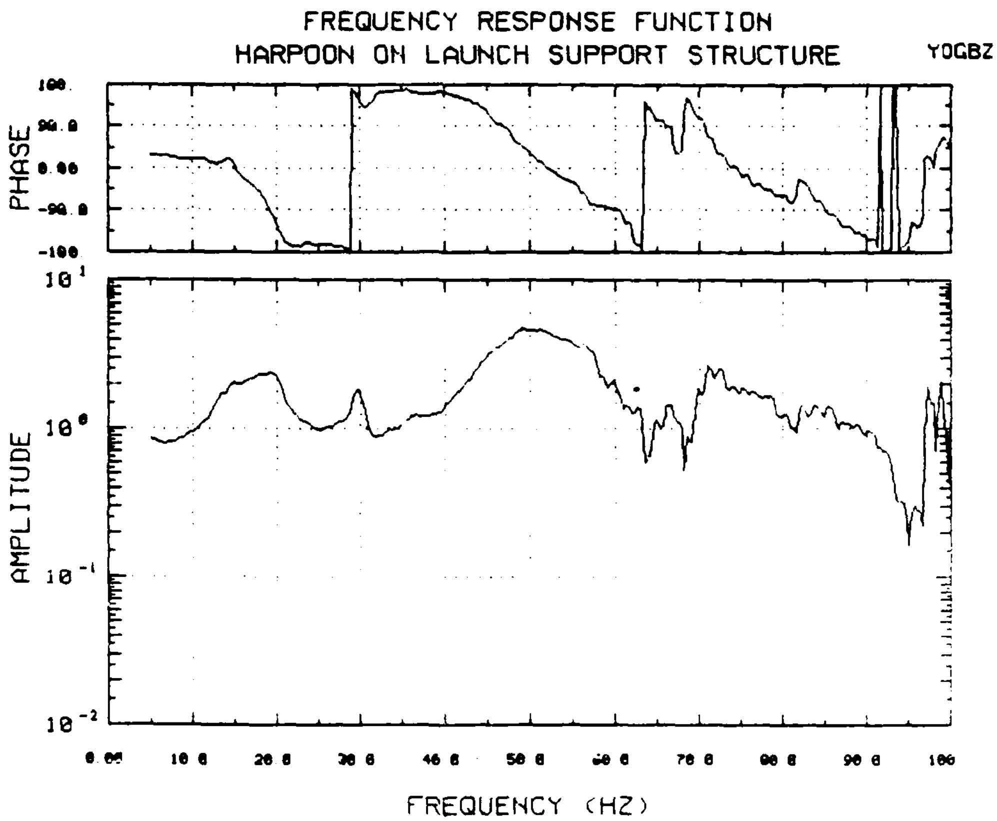

Figure 10.65 Z-Axis Transfer Function at Lower Missile Due to Y-Axis Input, Production Pads

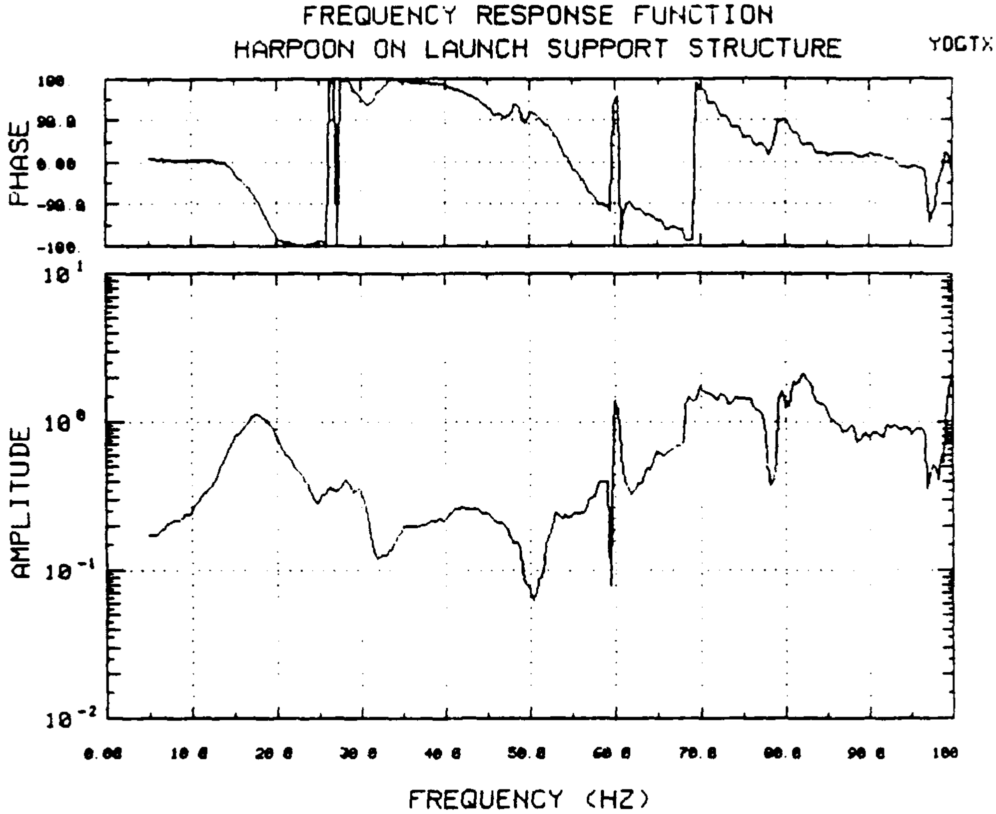

Figure 10.66 X-Axis Transfer Function at Upper Missile Due to Y-Axis Input, Production Pads

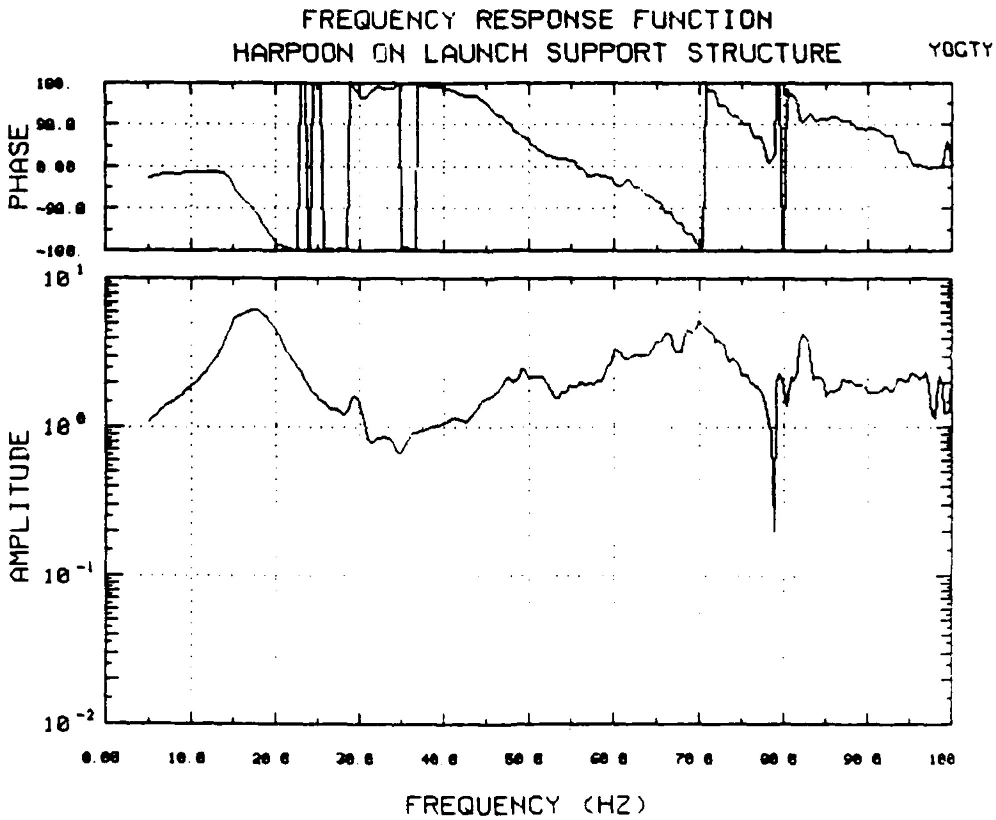

Figure 10.67 Y-Axis Transfer Function at Upper Missile Due to Y-Axis Input, Production Pads

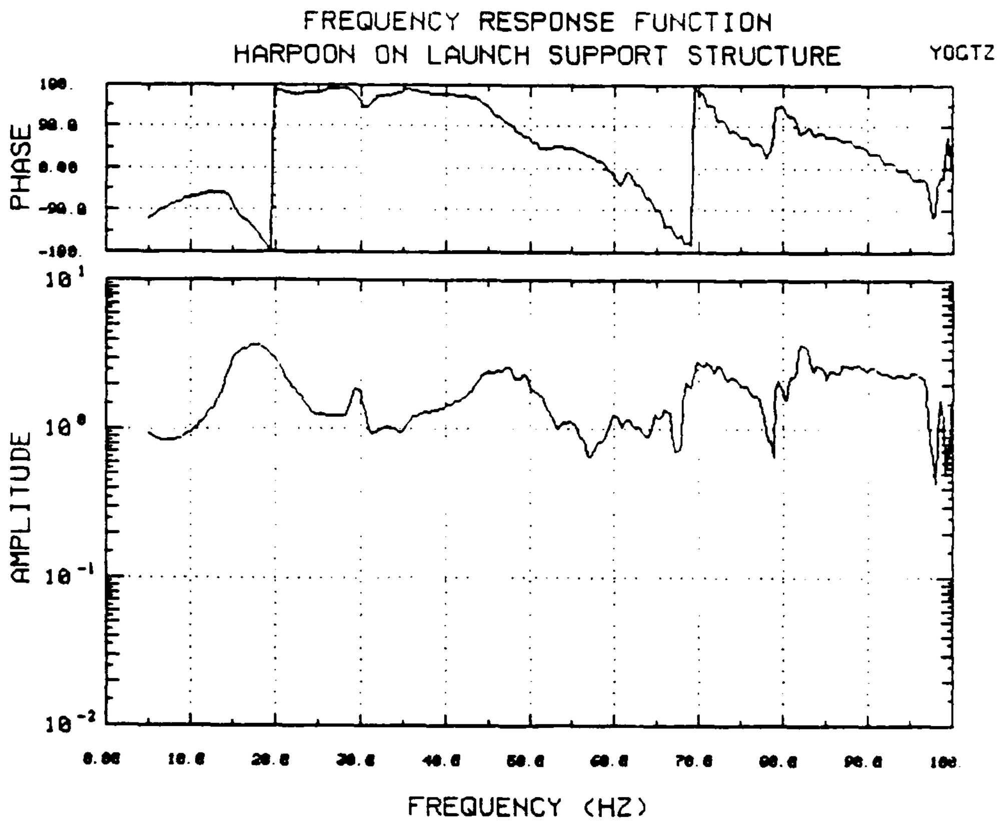

Figure 10.68 Z-Axis Transfer Function at Upper Missile Due to Y-Axis Input, Production Pads

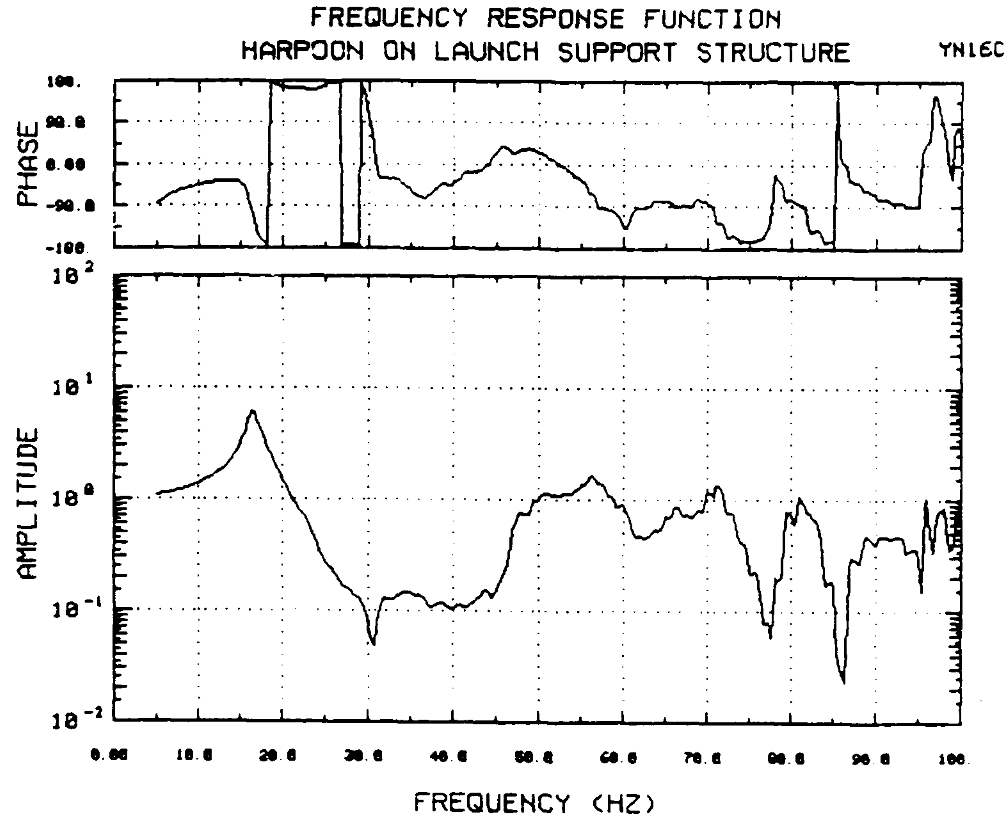

Figure 10.69 Y-Axis Transfer Function at Lower Clamp Frame Due to Y-Axis Input, Modified Isolation Pads

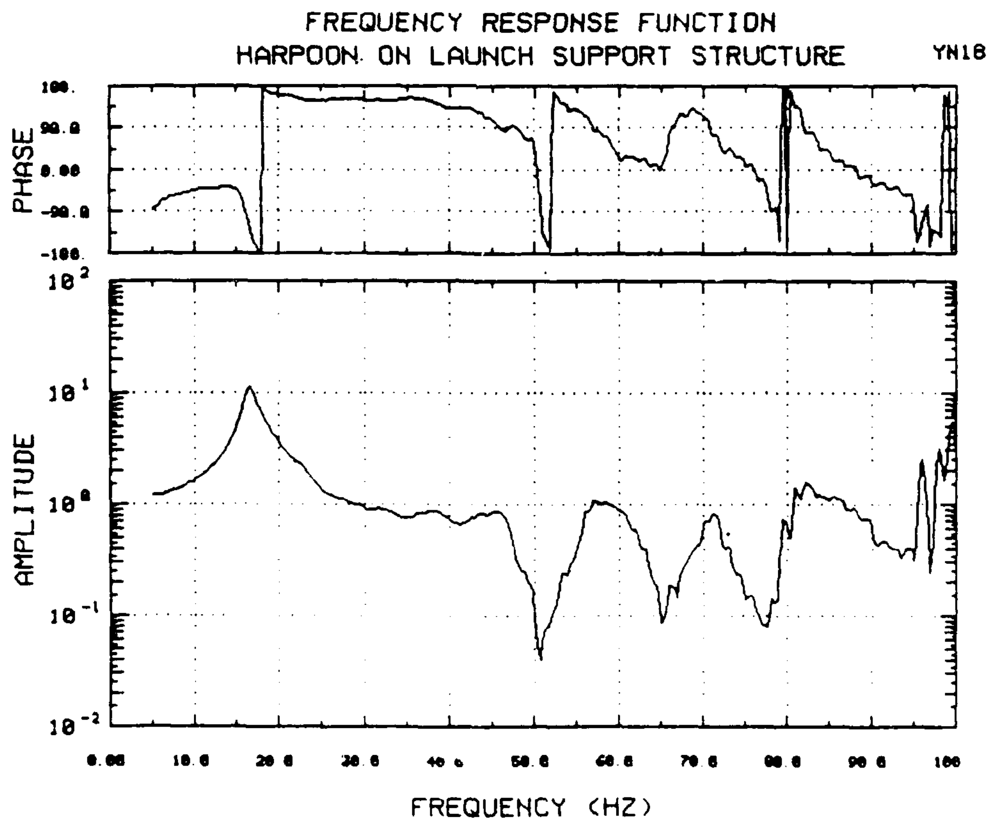

Figure 10.70 Y-Axis Transfer Function at Upper Grade B Canister Clamp Frame Due to Y-Axis Input, Modified Isolation Pads

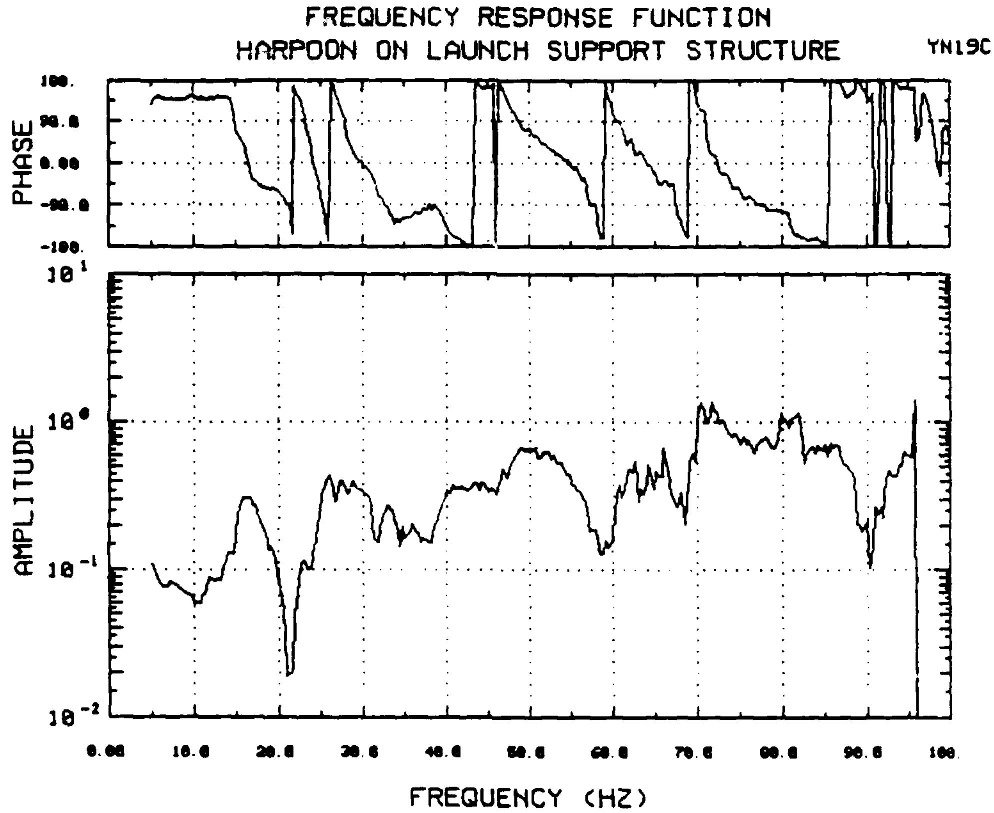

Figure 10.71 X-Axis Transfer Function at Upper Grade B Canister Clamp Frame Due to Y-Axis Input, Modified Isolation Pads

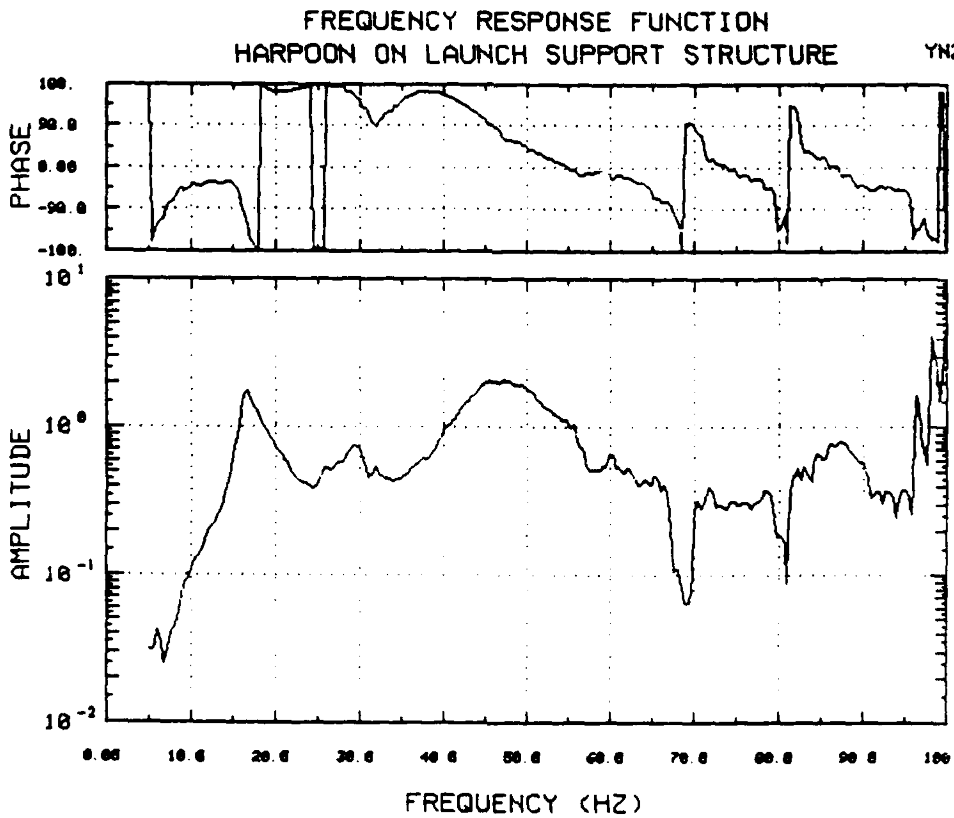

Figure 10.72 Z-Axis Transfer Function at Upper Grade B Canister Clamp Frame Due to Y-Axis Input, Modified Isolation Pads

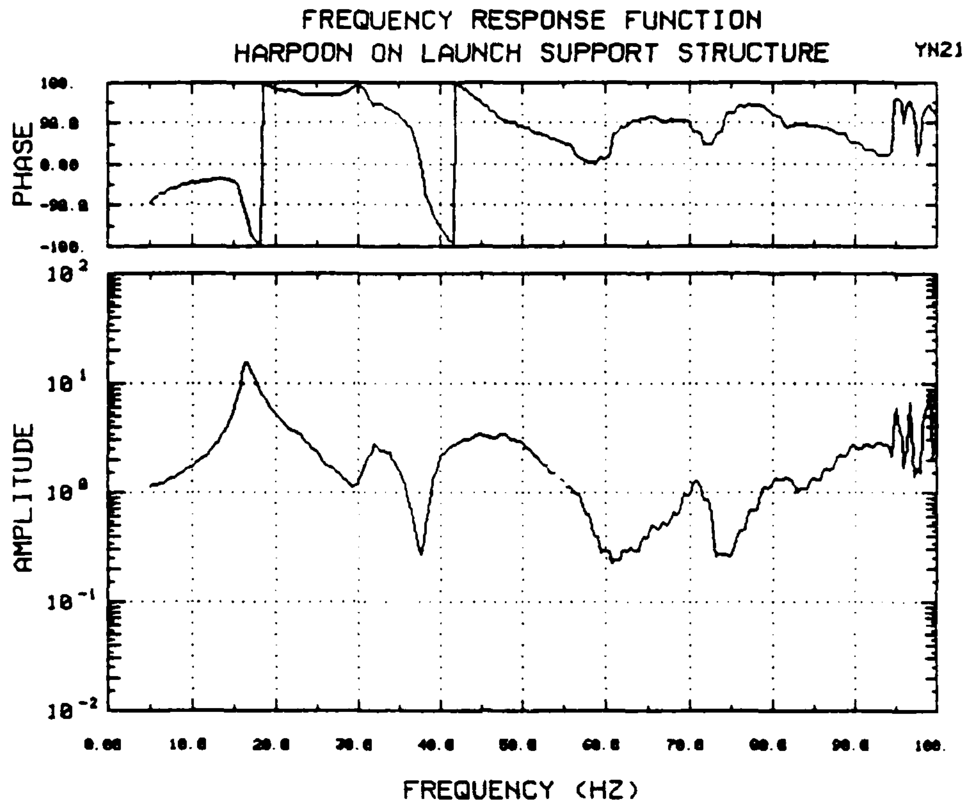

Figure 10.73 Y-Axis Transfer Function at Upper Clamp Frame Due to Y-Axis Input, Modified Isolation Pads

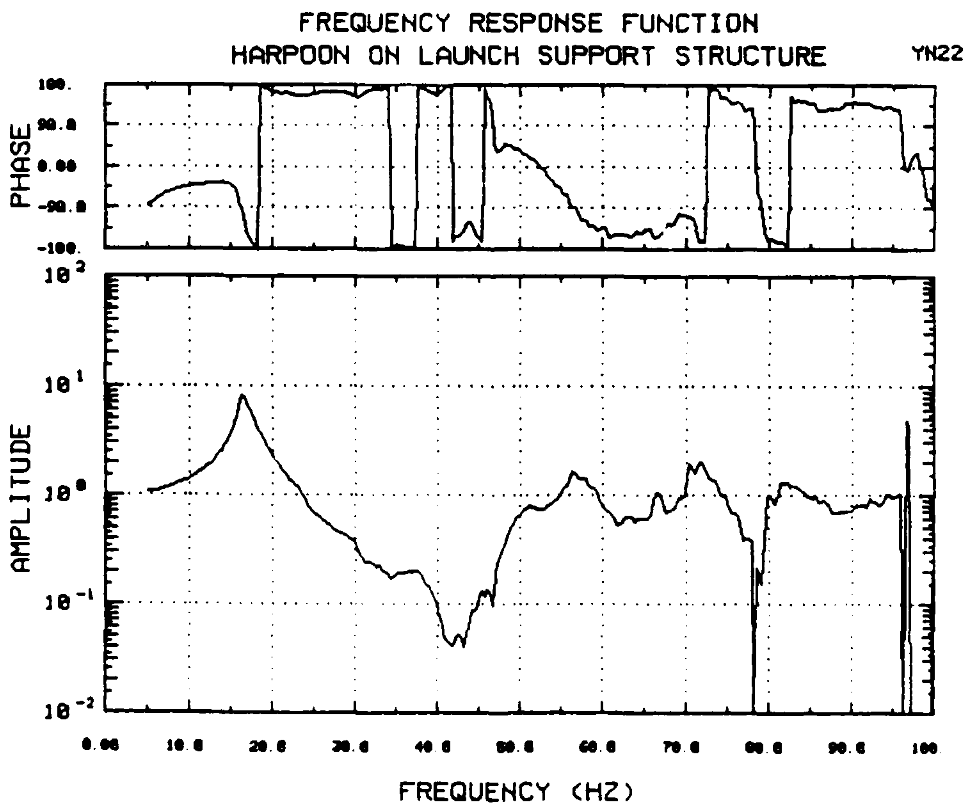

Figure 10.74 Y-Axis Transfer Function at Lower Grade B Canister Clamp Frame Due to Y-Axis Input, Modified Isolation Pads

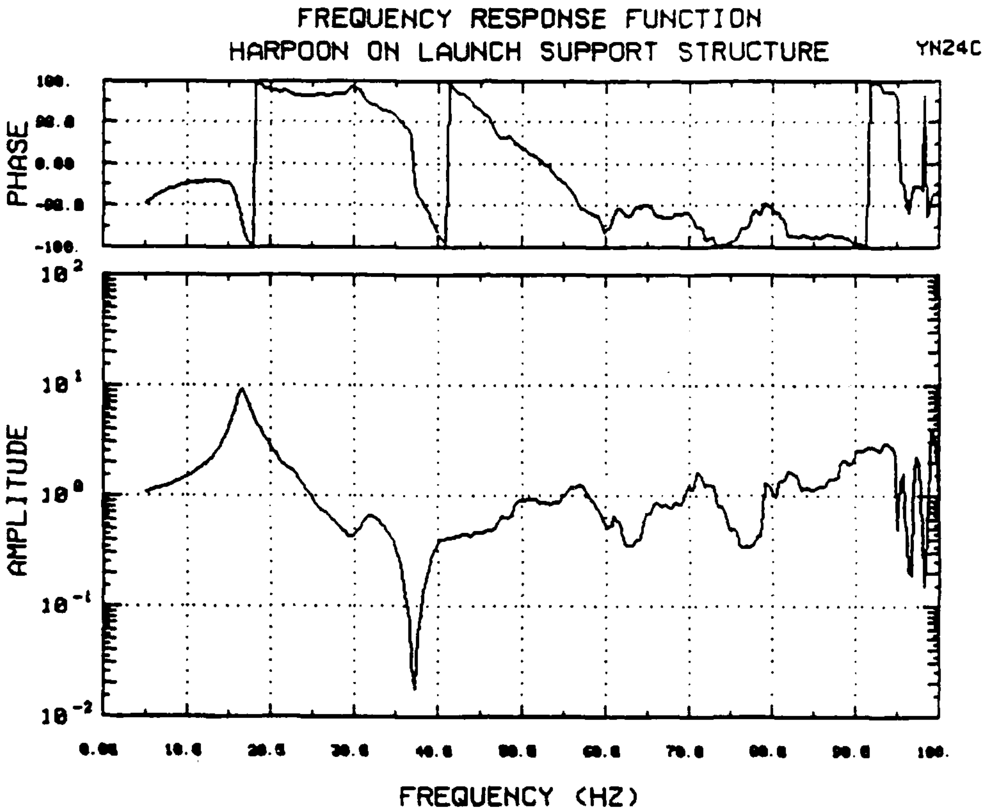

Figure 10.75 Y-Axis Transfer Function at Middle Clamp Frame Due to Y-Axis Input, Modified Isolation Pads

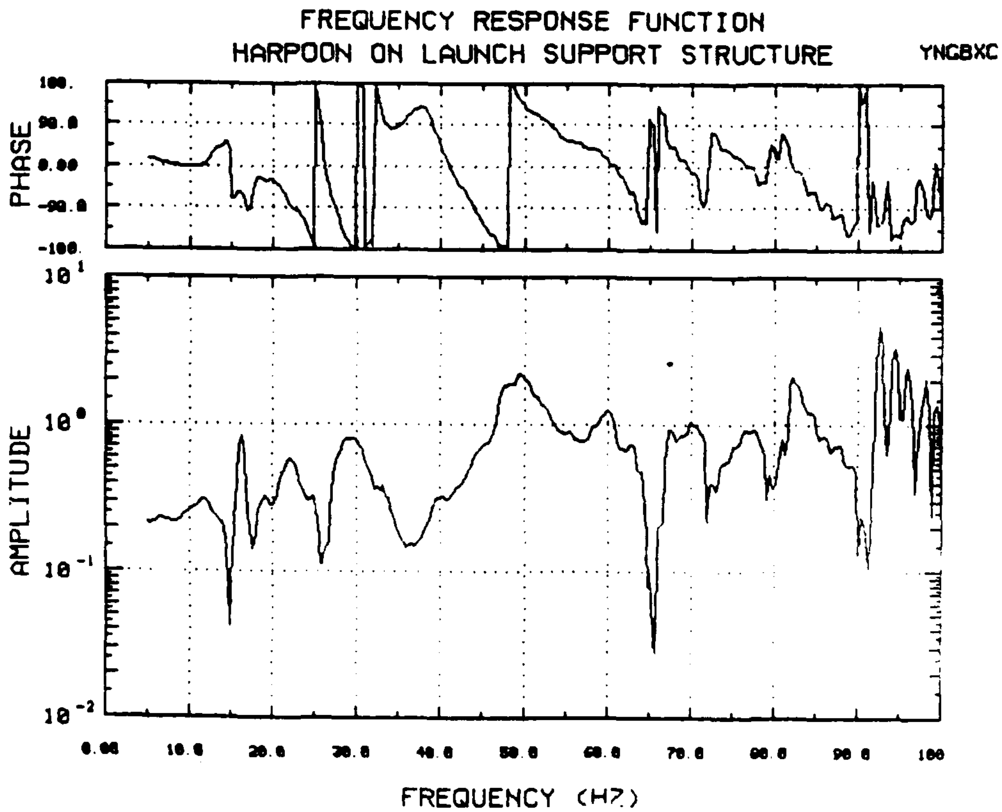

Figure 10.76 X-Axis Transfer Function at Lower Missile Due to Y-Axis Input, Modified Isolation Pads

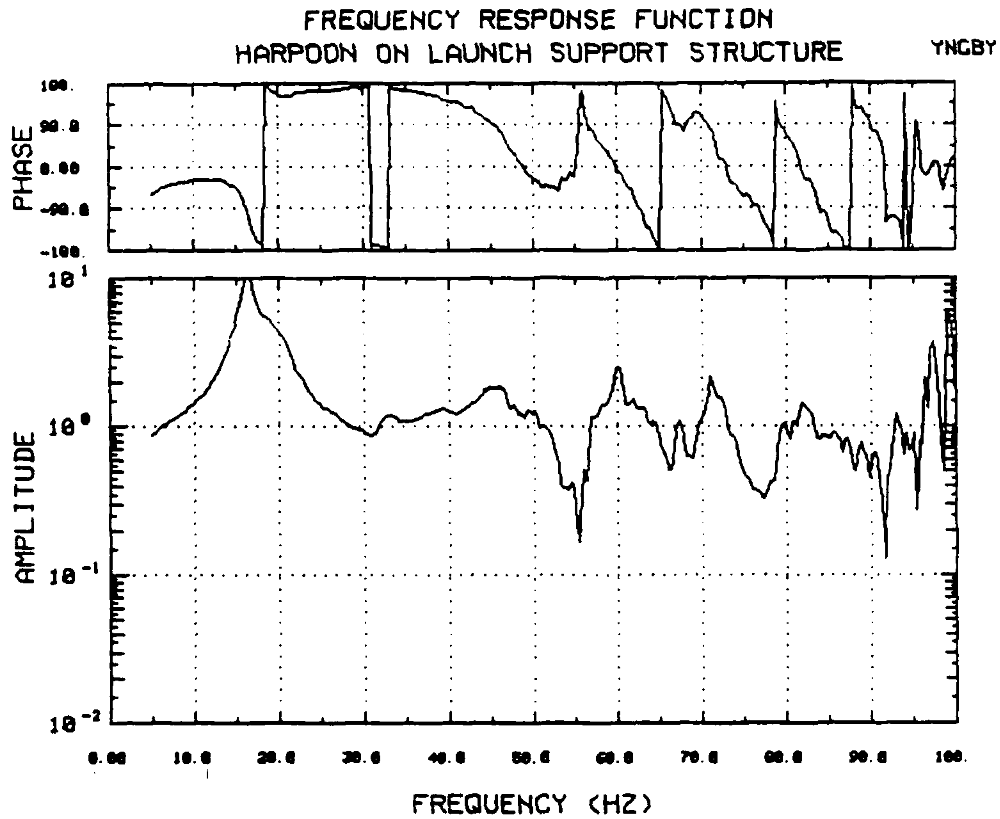

Figure 10.77 Y-Axis Transfer Function at Lower Missile Due to Y-Axis Input, Modified Isolation Pads

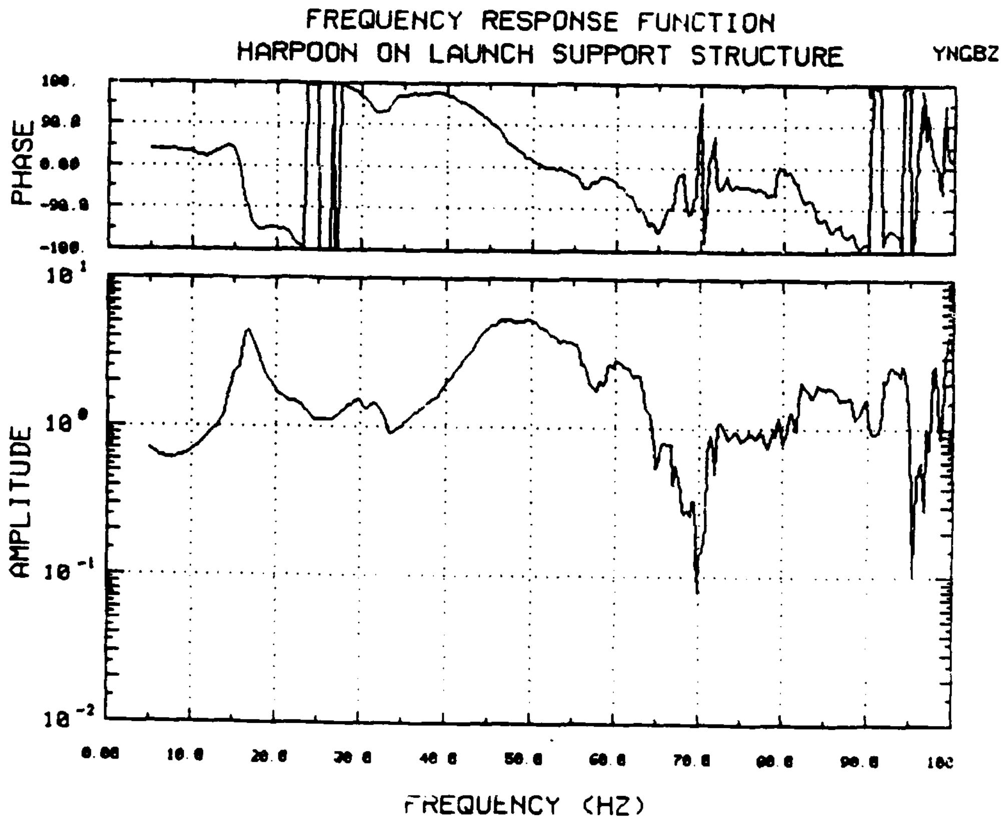

Figure 10.78 Z-Axis Transfer Function at Lower Missile Due to Y-Axis Input, Modified Isolation Pads

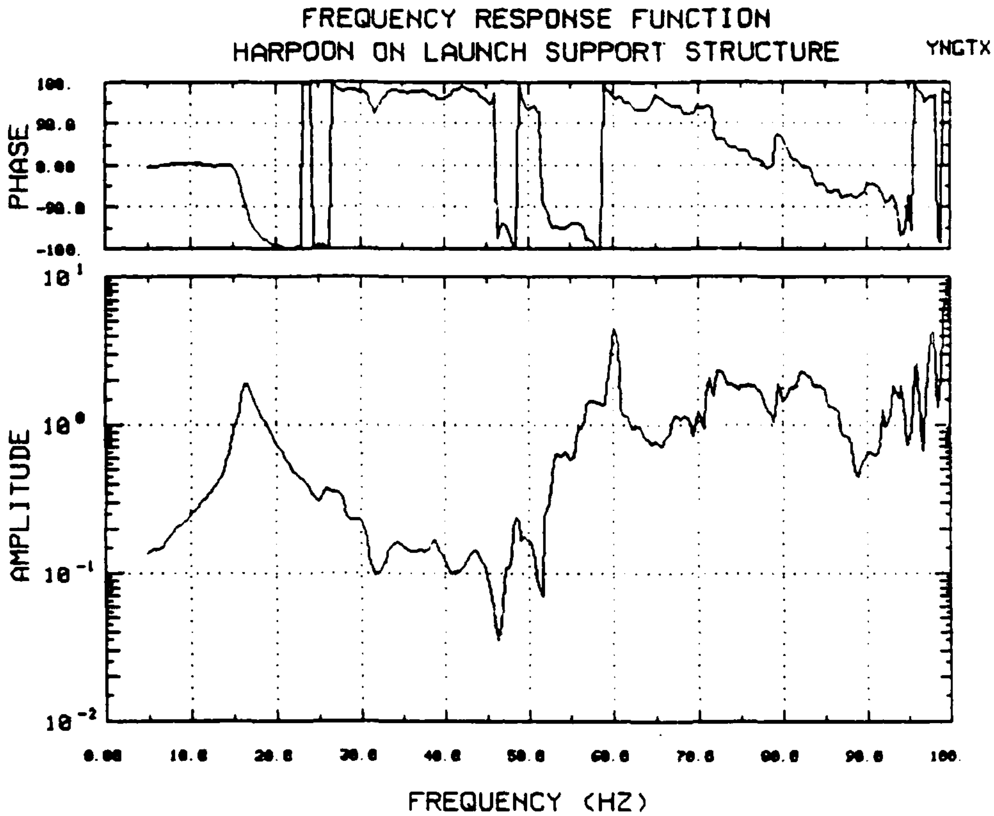

Figure 10.79 X-Axis Transfer Function at Upper Missile Due to Y-Axis Input, Modified Isolation Pads

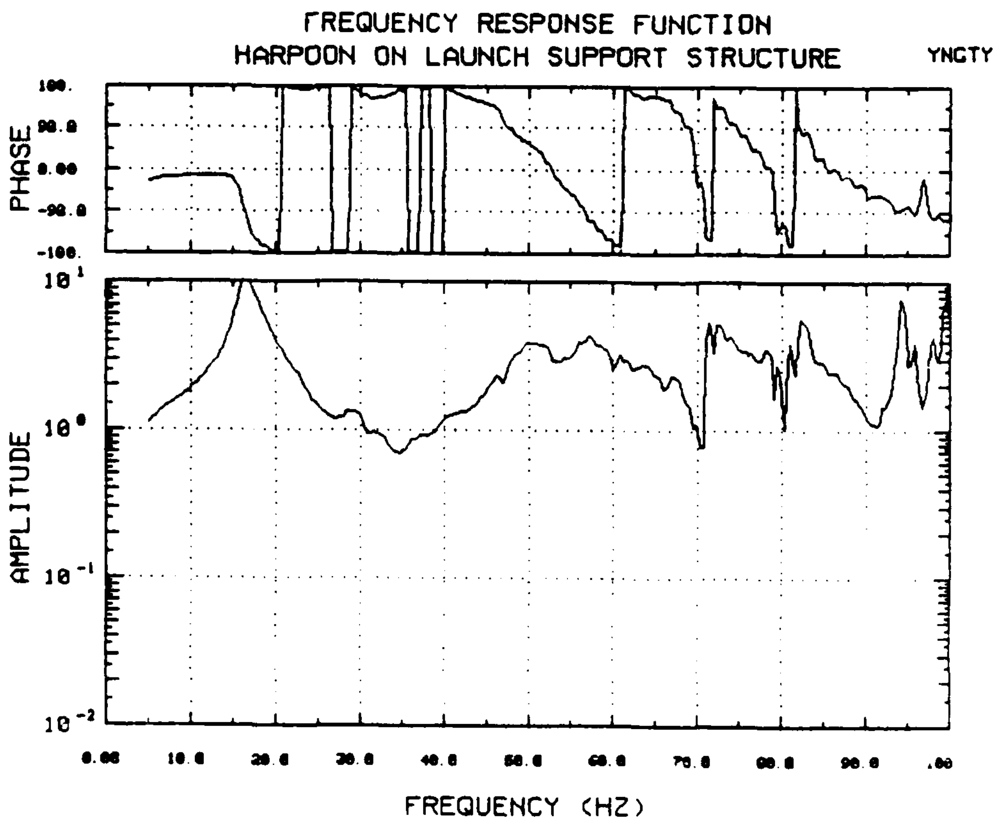

Figure 10.80 Y-Axis Transfer Function at Upper Missile Due to Y-Axis Input, Modified Isolation Pads

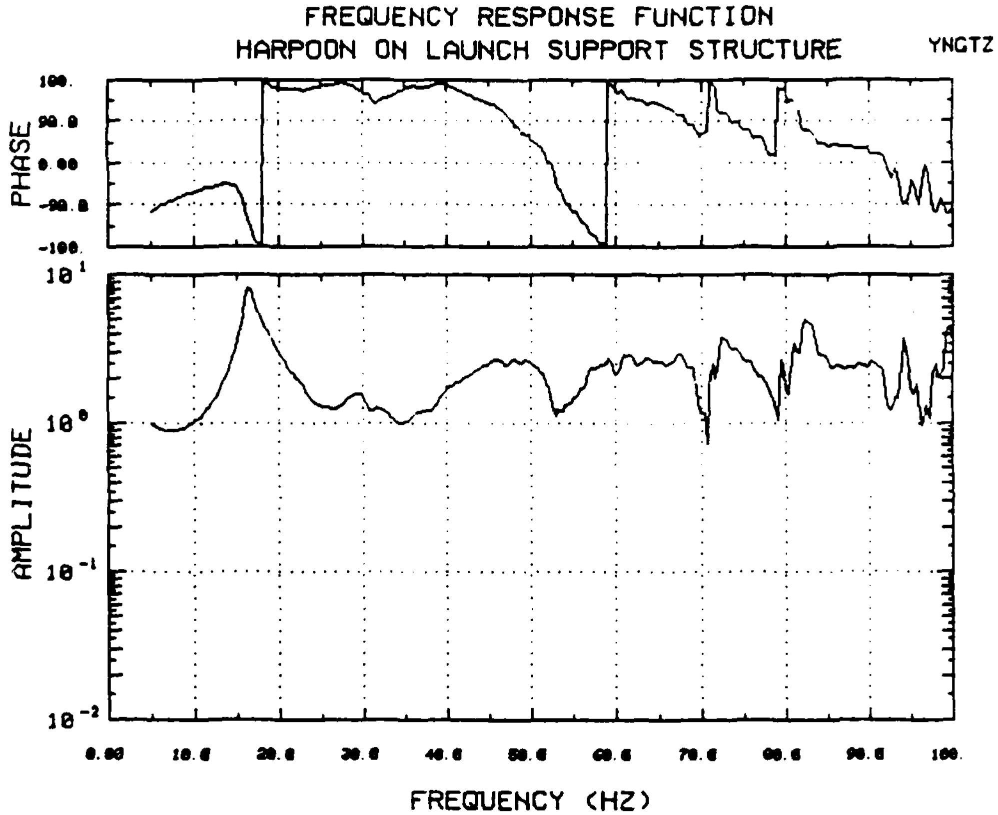

Figure 10.81 Z-Axis Transfer Function at Upper Missile Due to Y-Axis Input, Modified Isolation Pads

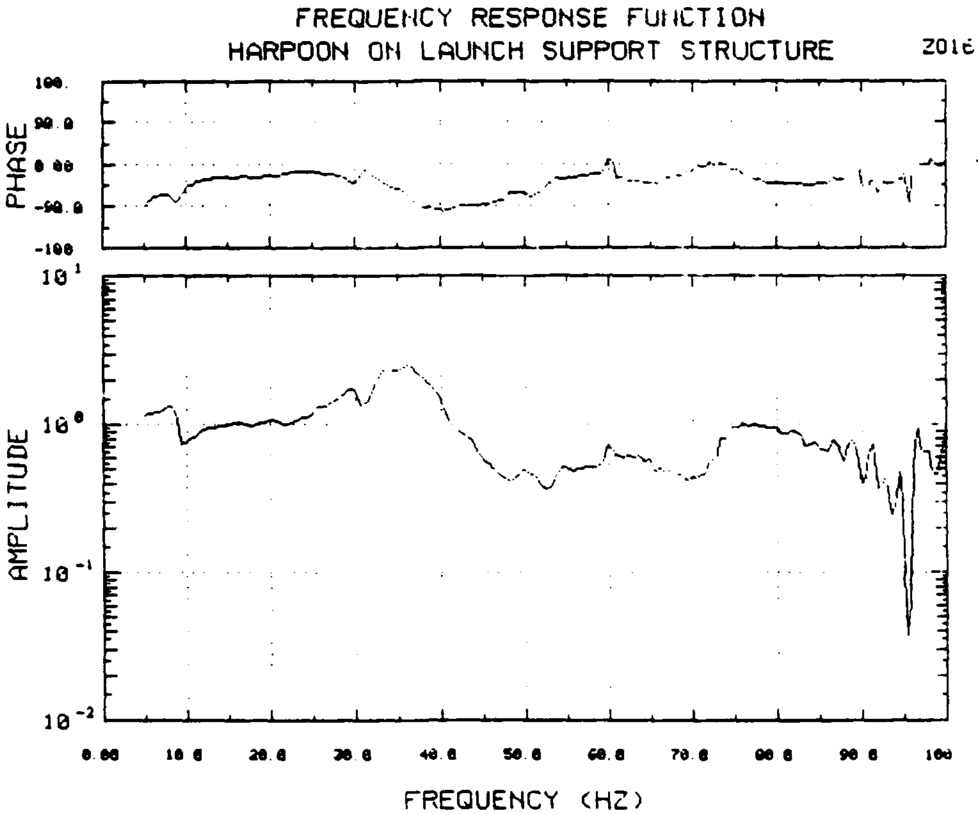

Figure 10.82 Z-Axis Transfer Function at Lower Clamp Frame Due to Z-Axis Input, Production Pads

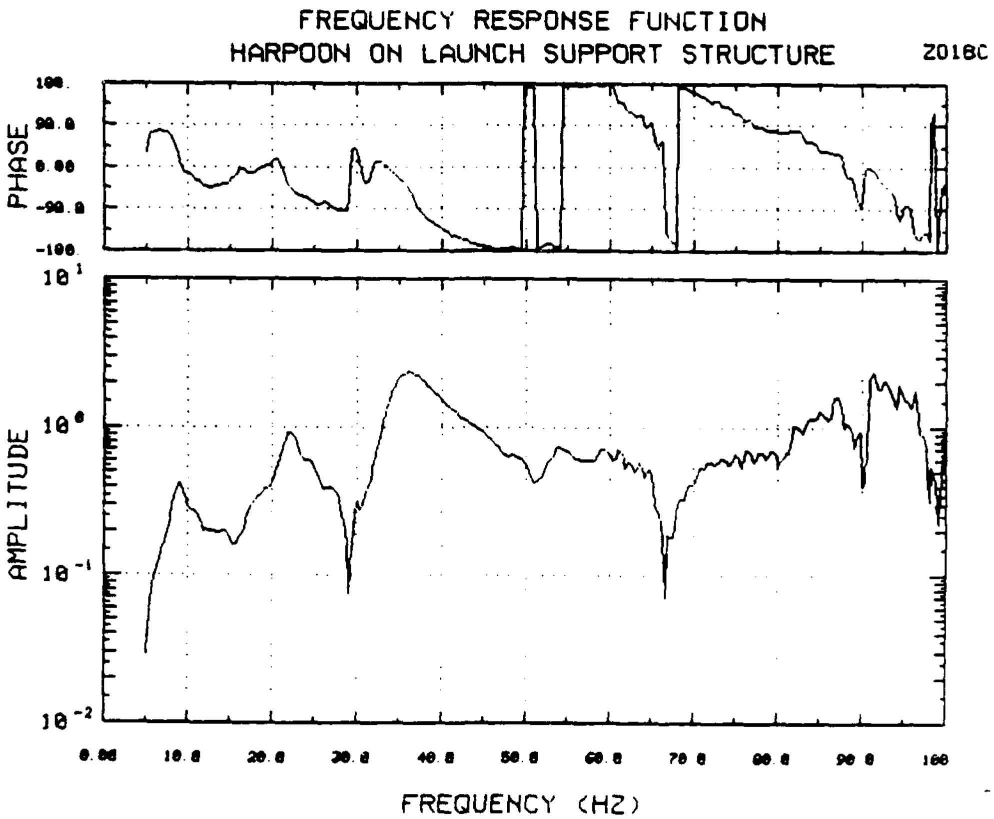

Figure 10.83 Y-Axis Transfer Function at Upper Grade B Canister Clamp Frame Due to Z-Axis Input, Production Pads

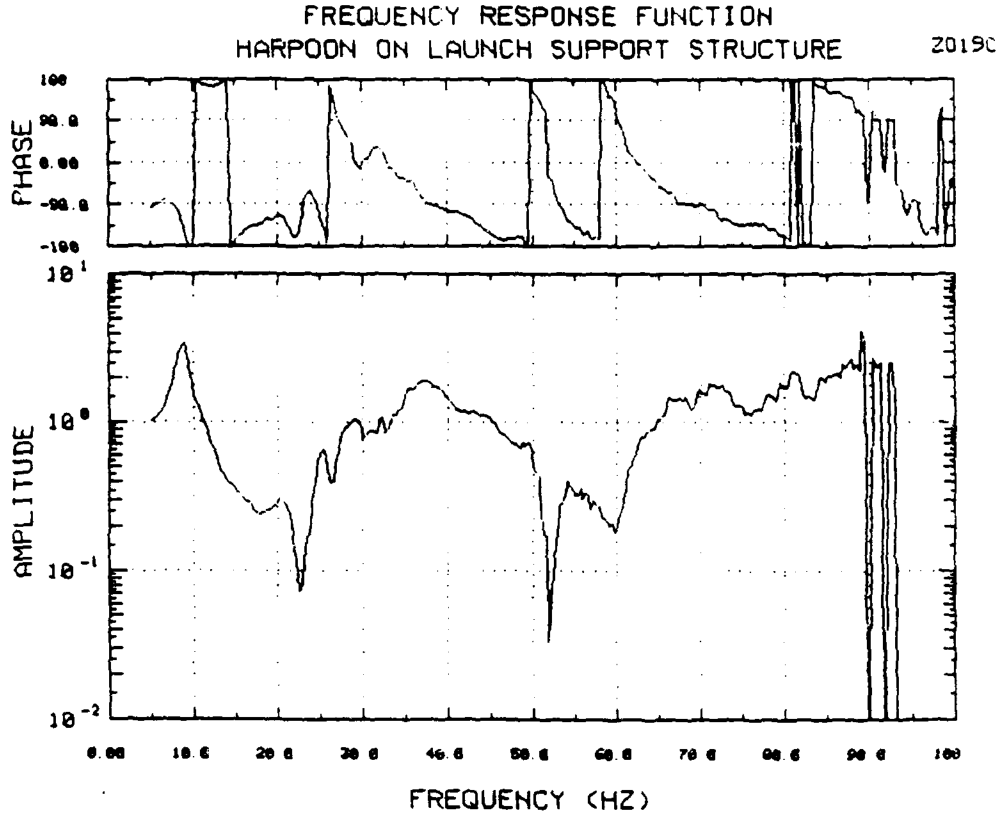

Figure 10.84 X-Axis Transfer Function at Upper Grade B Canister Clamp Frame Due to Z-Axis Input, Production Pads

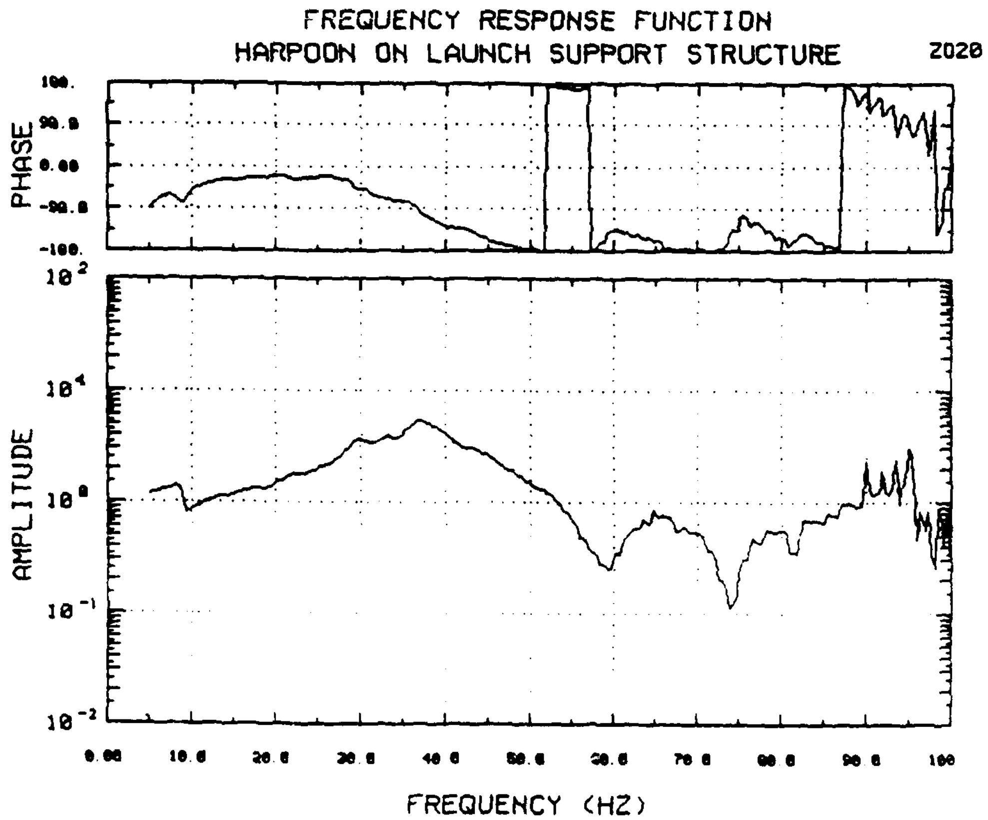

Figure 10.85 Z-Axis Transfer Function at Upper Grade B Canister Clamp Frame Due to Z-Axis Input, Production Pads

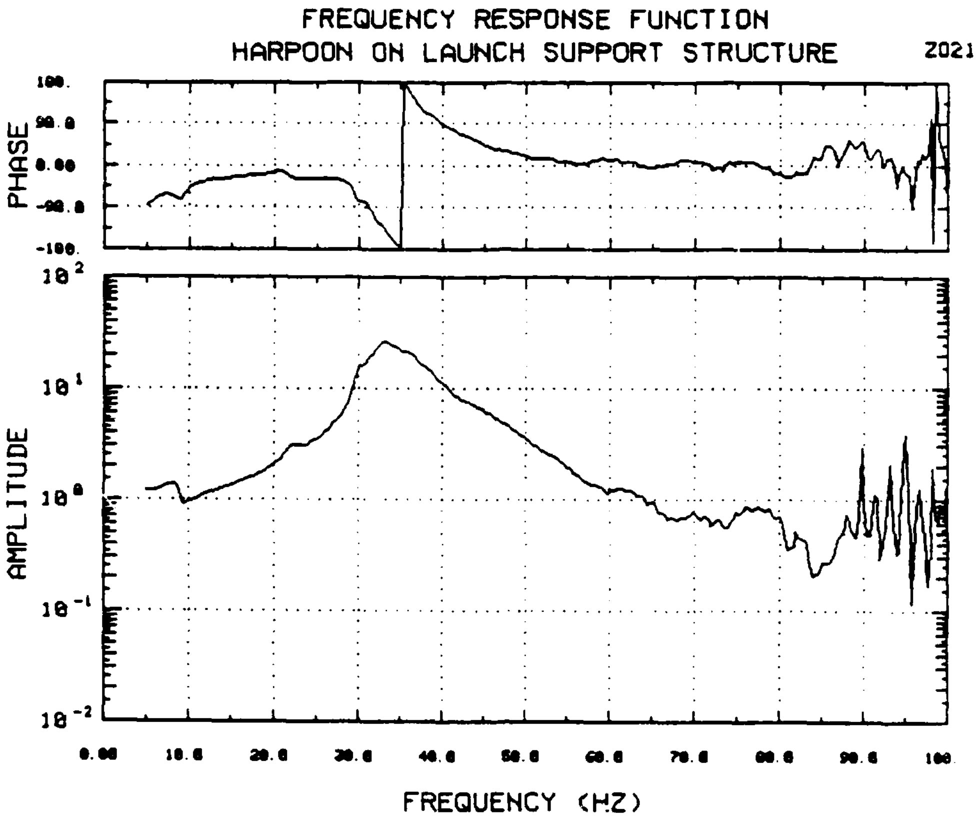

Figure 10.86 Z-Axis Transfer Function at Upper Clamp Frame Due to Z-Axis Input, Production Pads

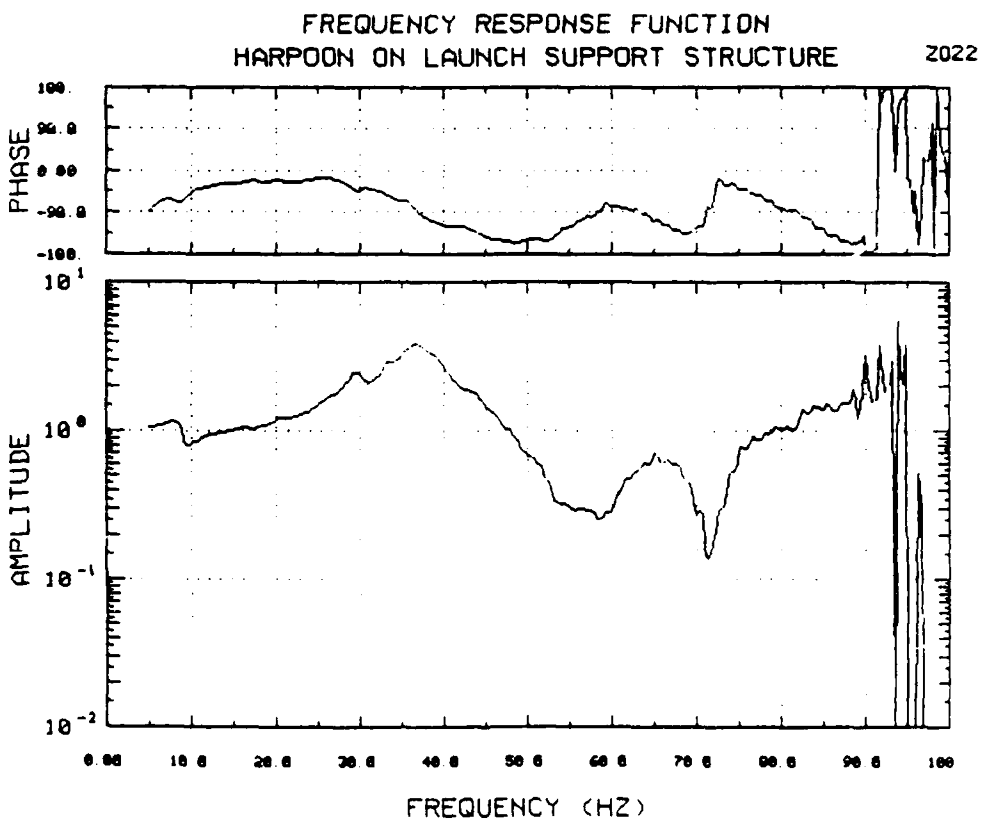

Figure 10.87 Z-Axis Transfer Function at Lower Grade B Canister Clamp Frame Due to Z-Axis Input, Production Pads

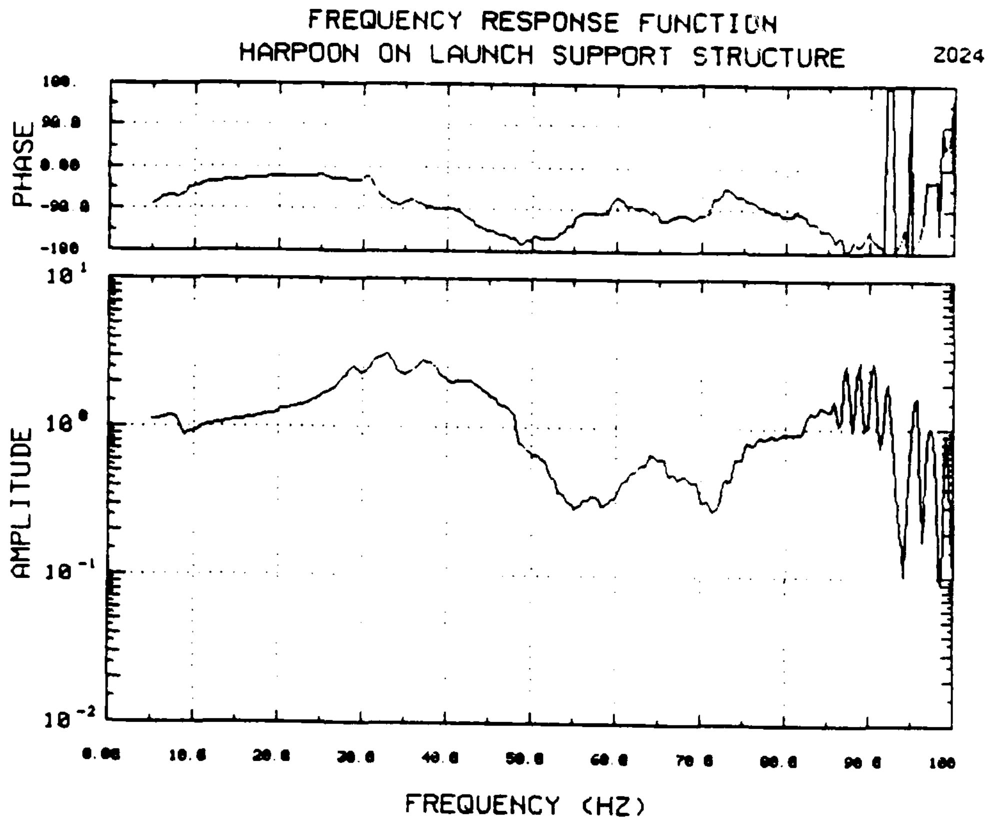

Figure 10.88 Z-Axis Transfer Function at Middle Clamp Frame Due to Z-Axis Input, Production Pads

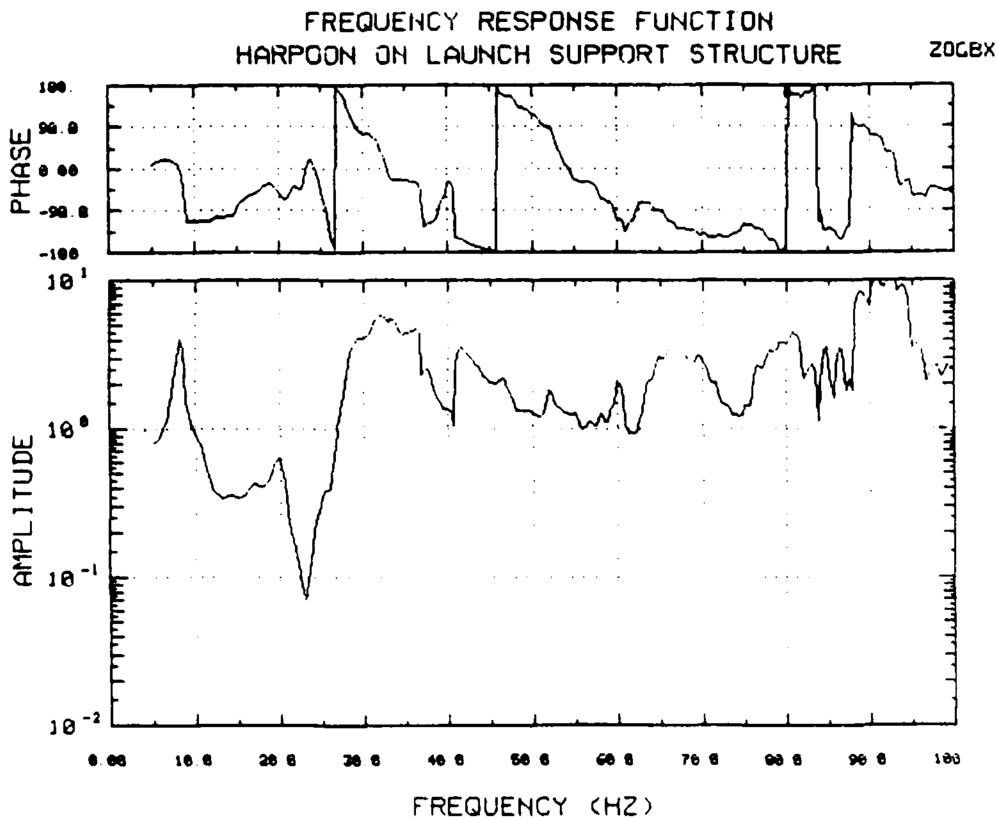

Figure 10.89 X-Axis Transfer Function at Lower Missile Due to Z-Axis Input, Production Pads

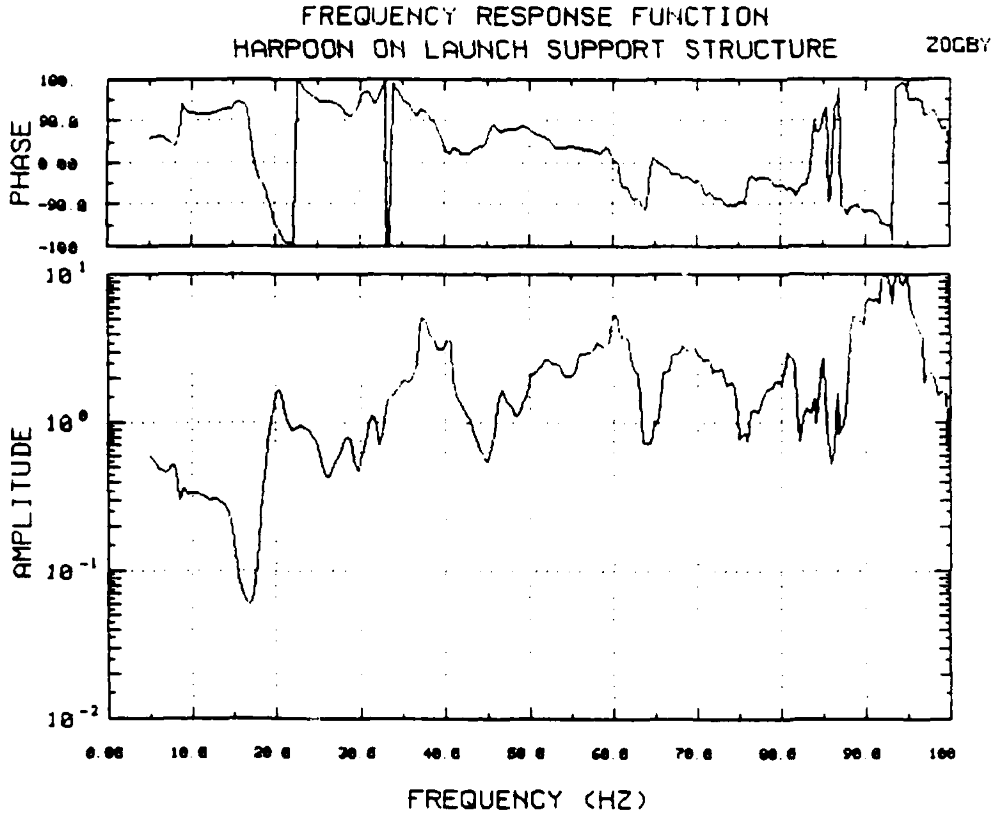

Figure 10.90 Y-Axis Transfer Function at Lower Missile Due to Z-Axis Input, Production Pads

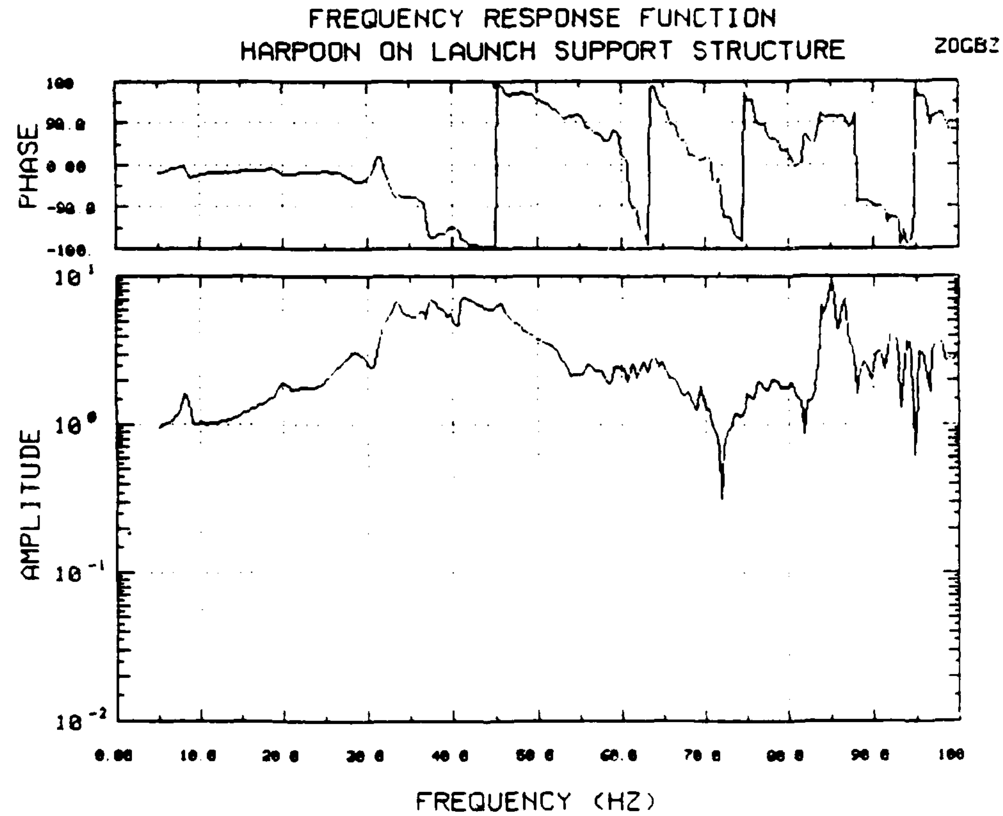

Figure 10.91 Z-Axis Transfer Function at Lower Missile Due to Z-Axis Input, Production Pads

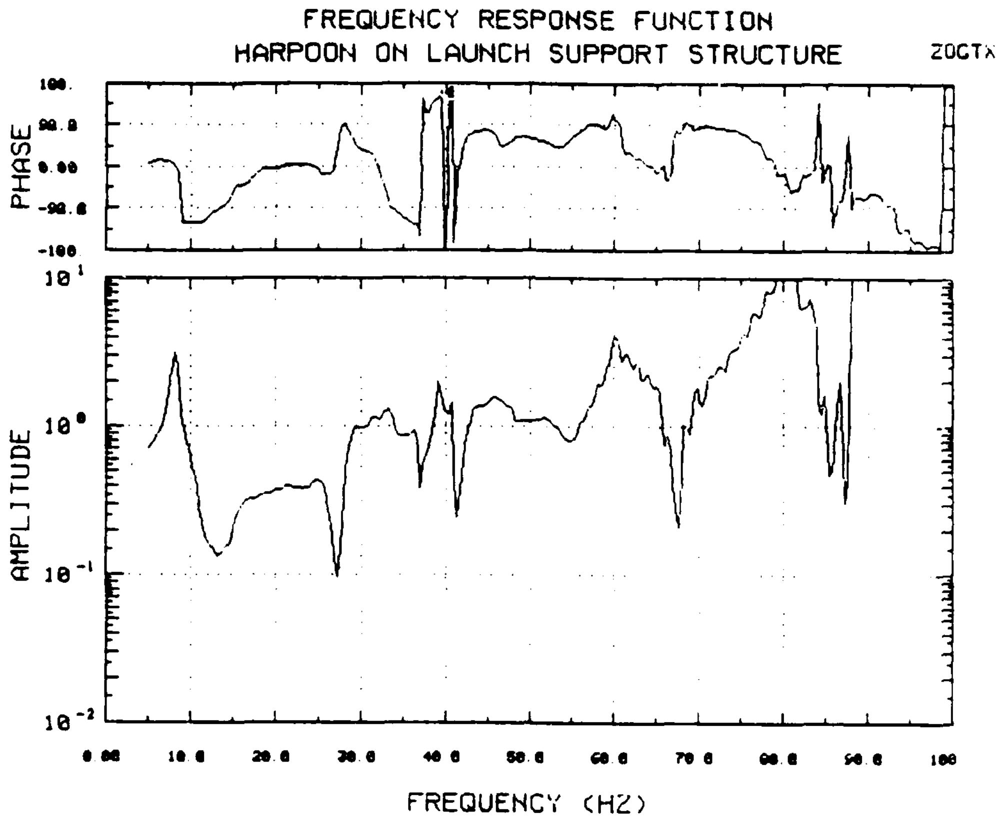

Figure 10.92 X-Axis Transfer Function at Upper Missile Due to Z-Axis Input, Production Pads

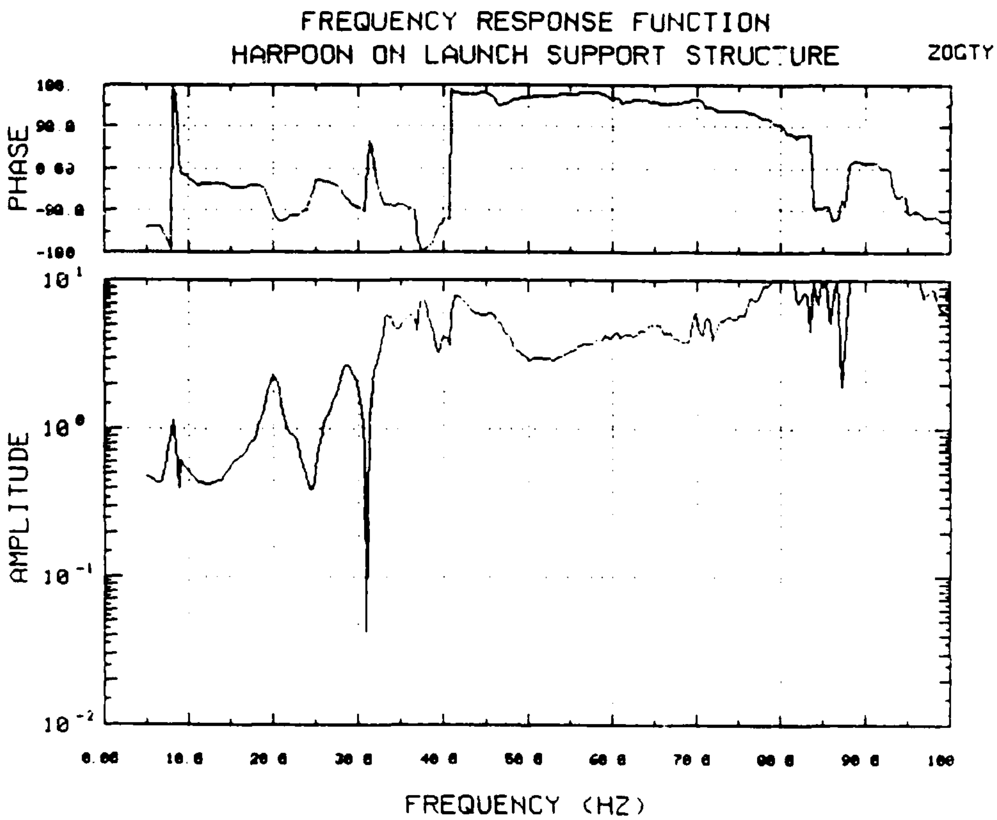

Figure 10.93 Y-Axis Transfer Function at Upper Missile Due to Z-Axis Input, Production Pads

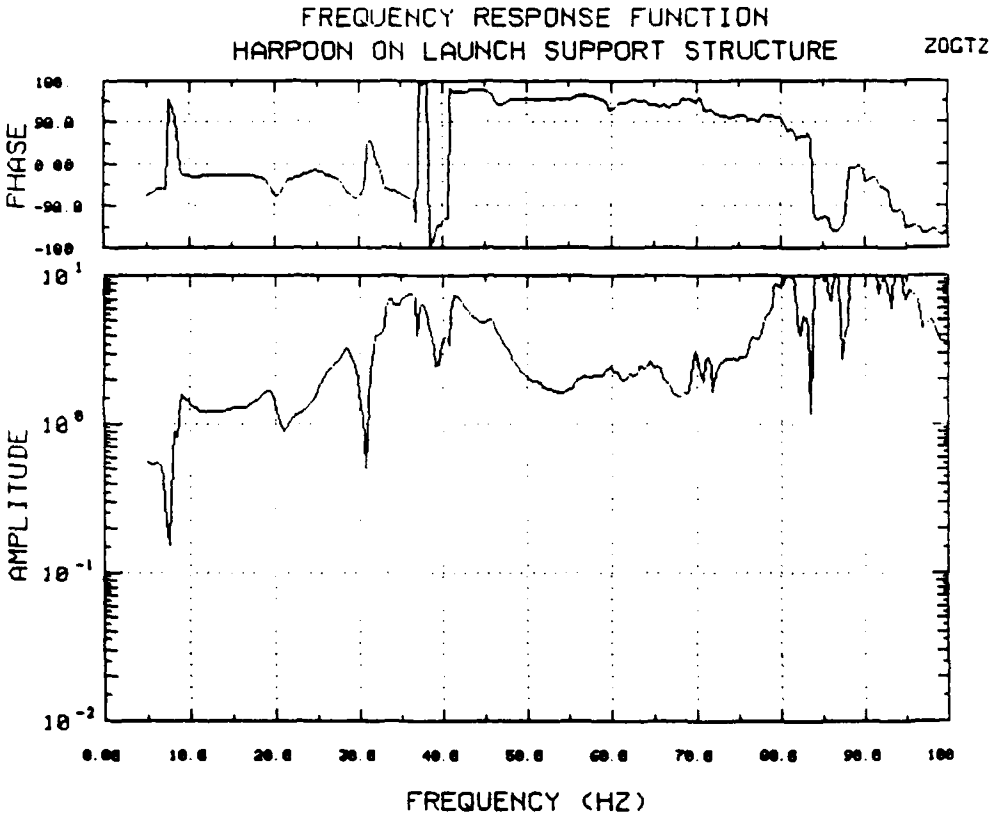

Figure 10.94 Z-Axis Transfer Function at Upper Missile Due to Z-Axis Input, Production Pads

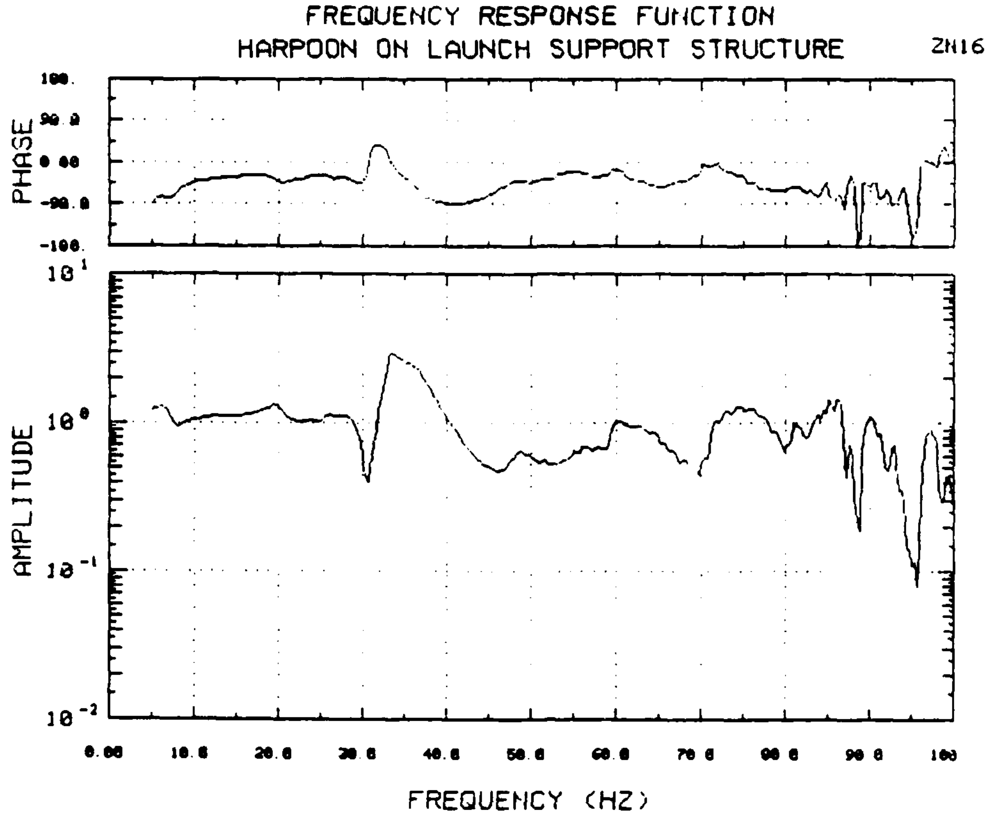

Figure 10.95 Z-Axis Transfer Function at Lower Clamp Frame Due to Z-Axis Input, Modified Isolation Pads

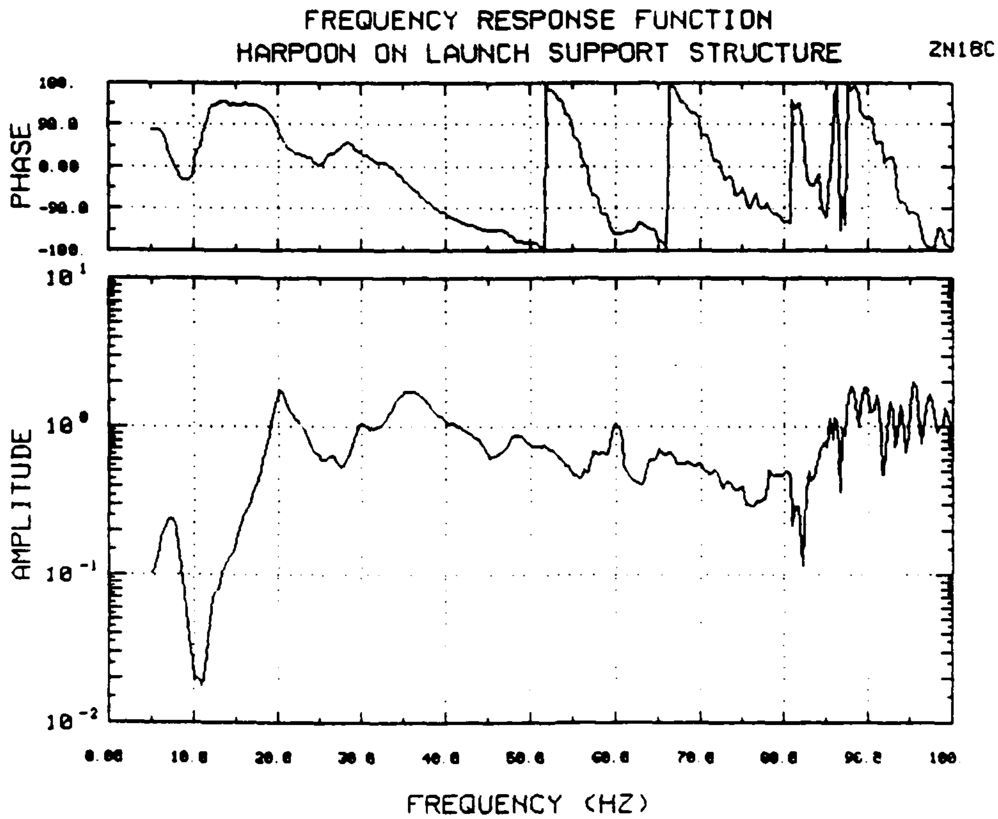

Figure 10.96 Y-Axis Transfer Function at Upper Grade B Canister Clamp Frame Due to Z-Axis Input, Modified Isolation Pads

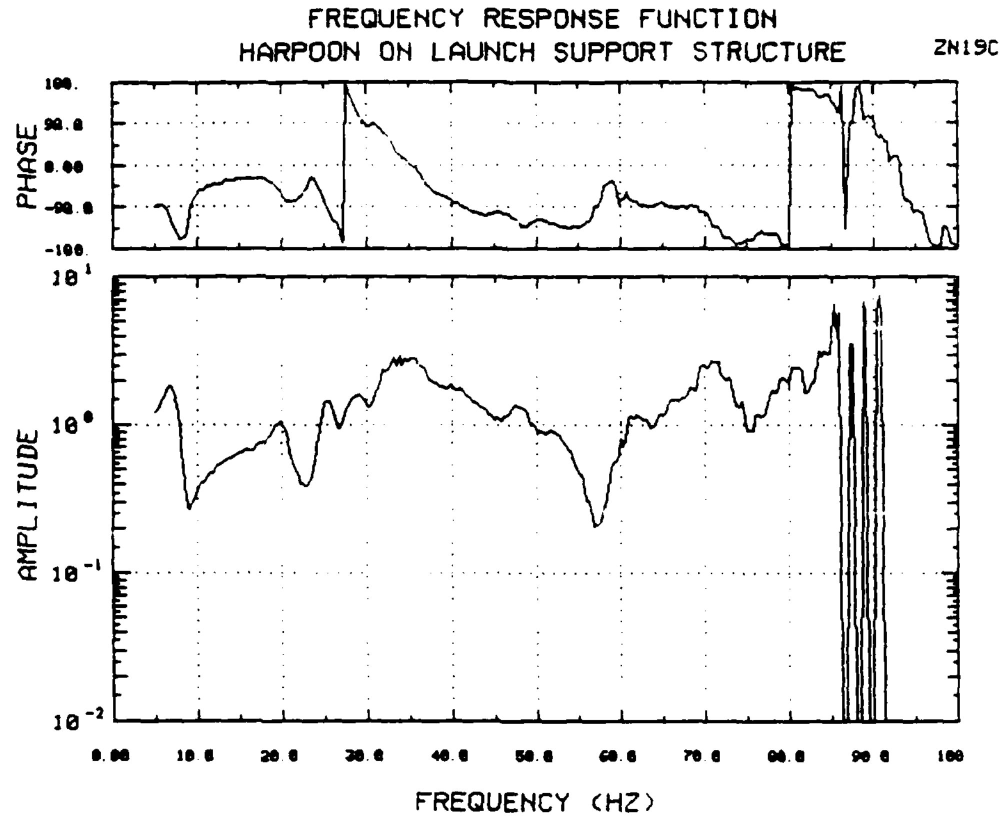

Figure 10.97 X-Axis Transfer Function at Upper Grade B Canister Clamp Frame Due to Z-Axis Input, Modified Isolation Pads

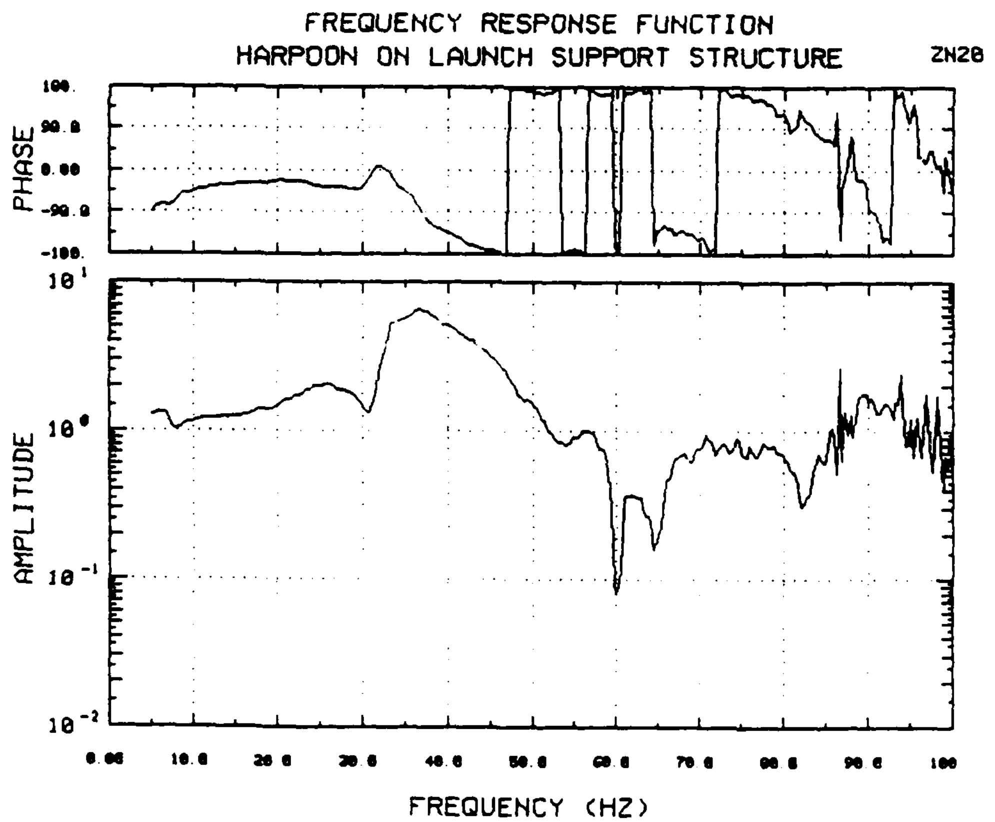

Figure 10.98 Z-Axis Transfer Function at Upper Grade B Canister Clamp Frame Due to Z-Axis Input, Modified Isolation Pads

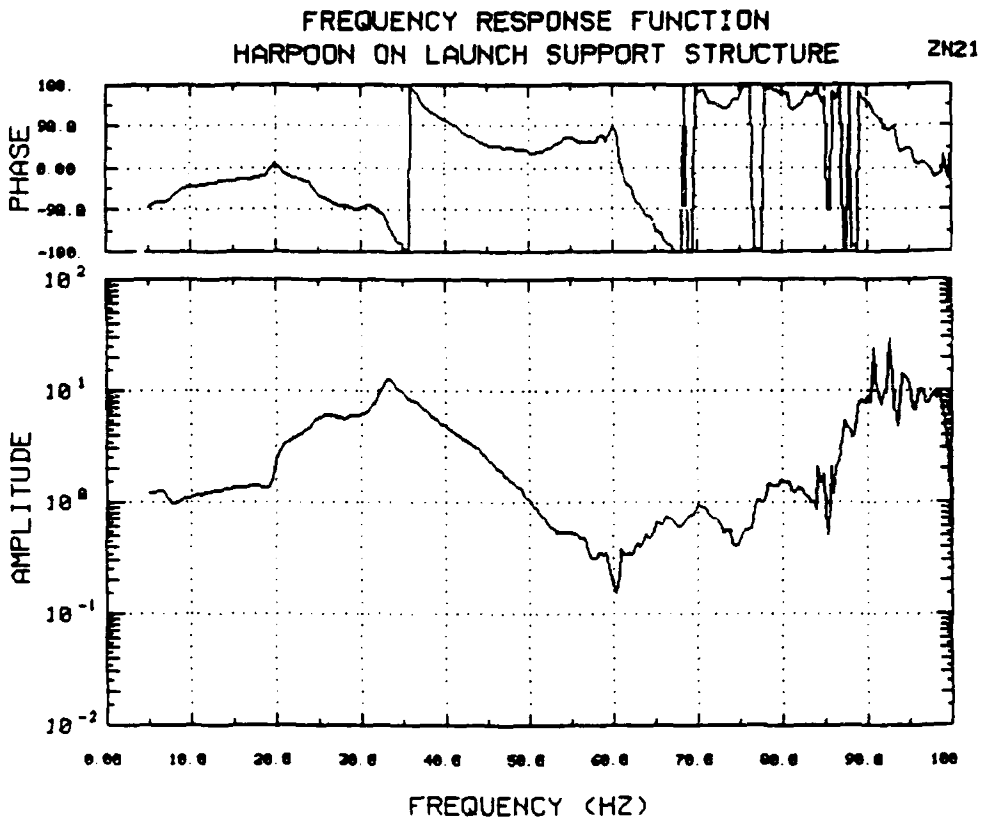

Figure 10.99 Z-Axis Transfer Function at Upper Clamp Frame Due to Z-Axis Input, Modified Isolation Pads

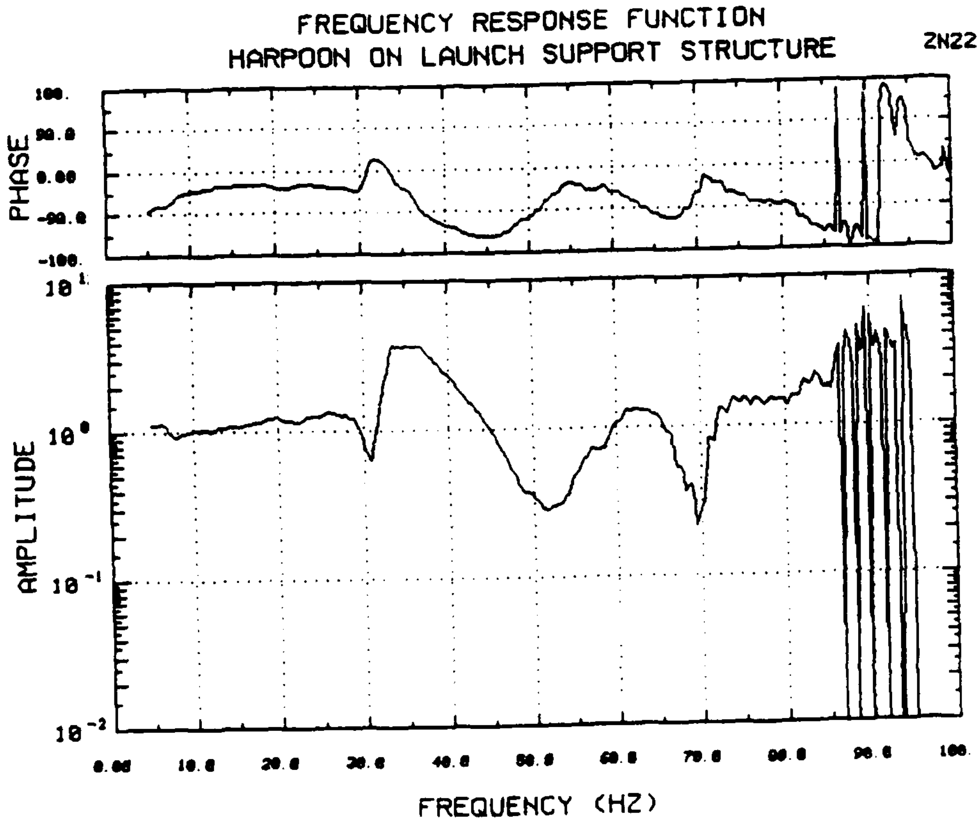

Figure 10.100 Z-Axis Transfer Function at Lower Grade B Canister Clamp Frame Due to Z-Axis Input, Modified Isolation Pads

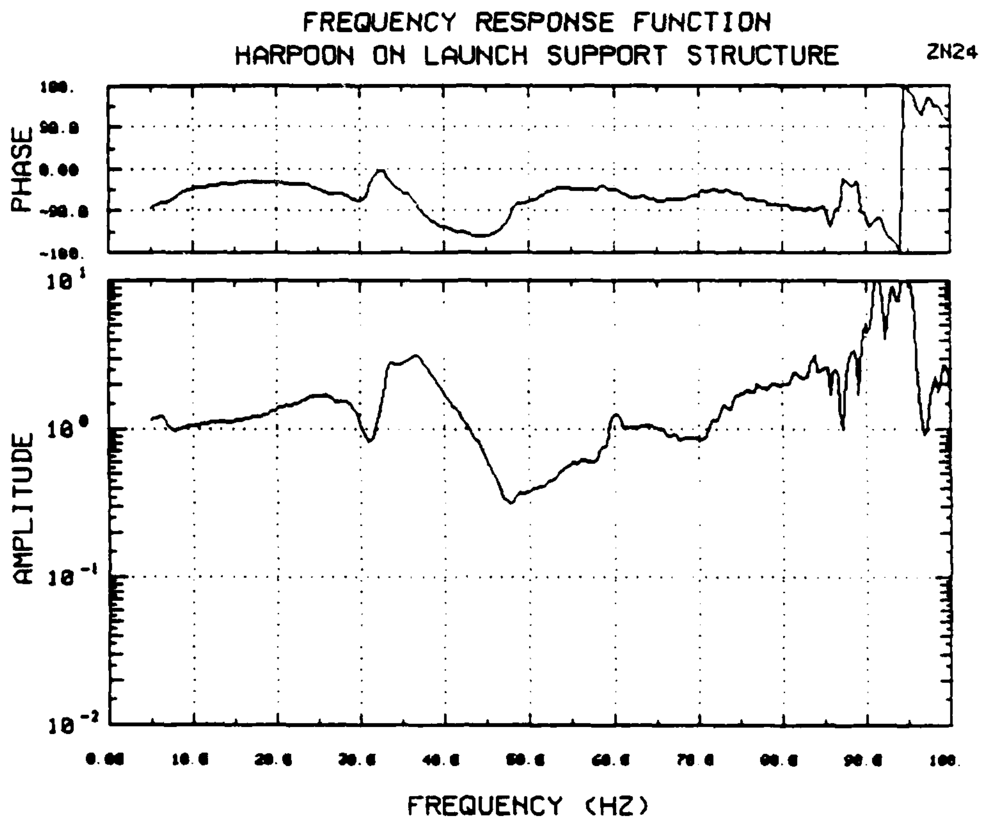

Figure 10.101 Z-Axis Transfer Function at Middle Clamp Frame Due to Z-Axis Input, Modified Isolation Pads

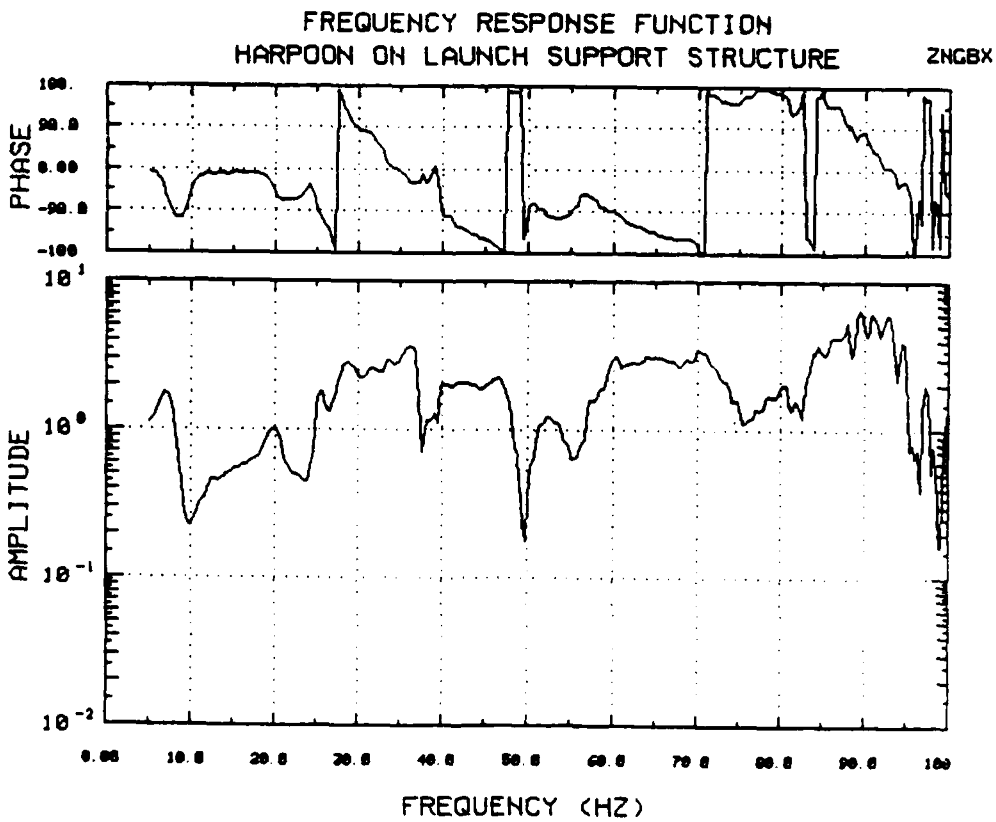

Figure 10.102 X-Axis Transfer Function at Lower Missile Due to Z-Axis Input, Modified Isolation Pads

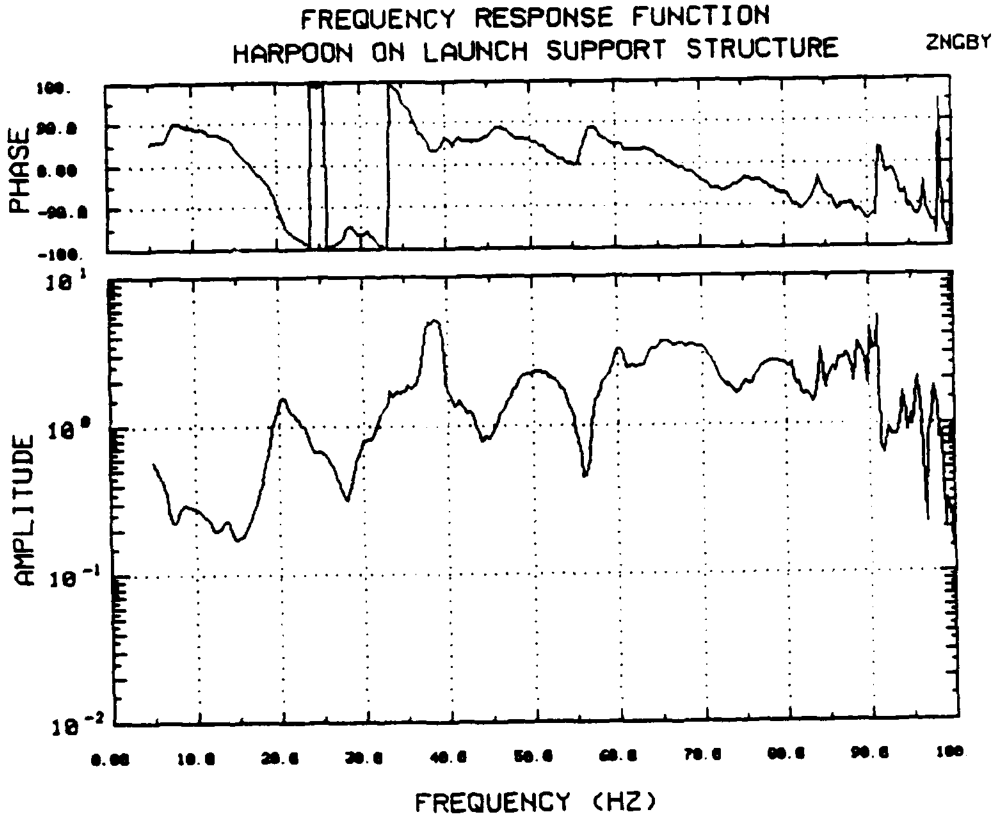

Figure 10.103 Y-Axis Transfer Function at Lower Missile Due to Z-Axis Input, Modified Isolation Pads

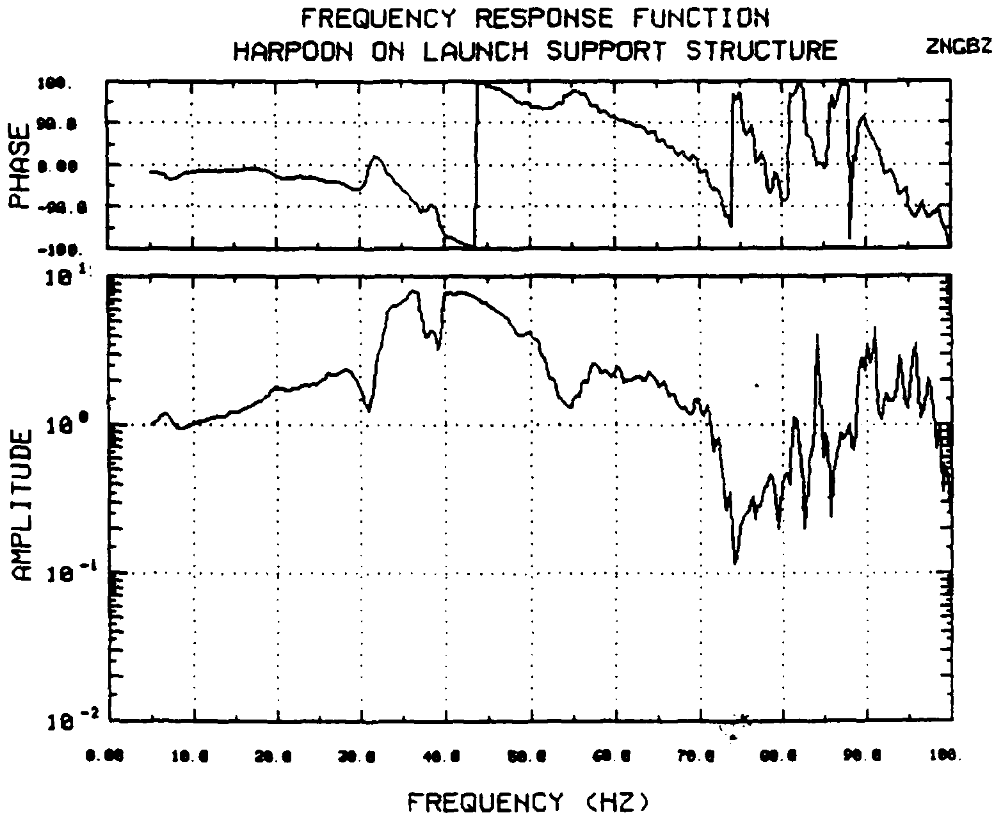

Figure 10.104 Z-Axis Transfer Function at Lower Missile Due to Z-Axis Input, Modified Isolation Pads

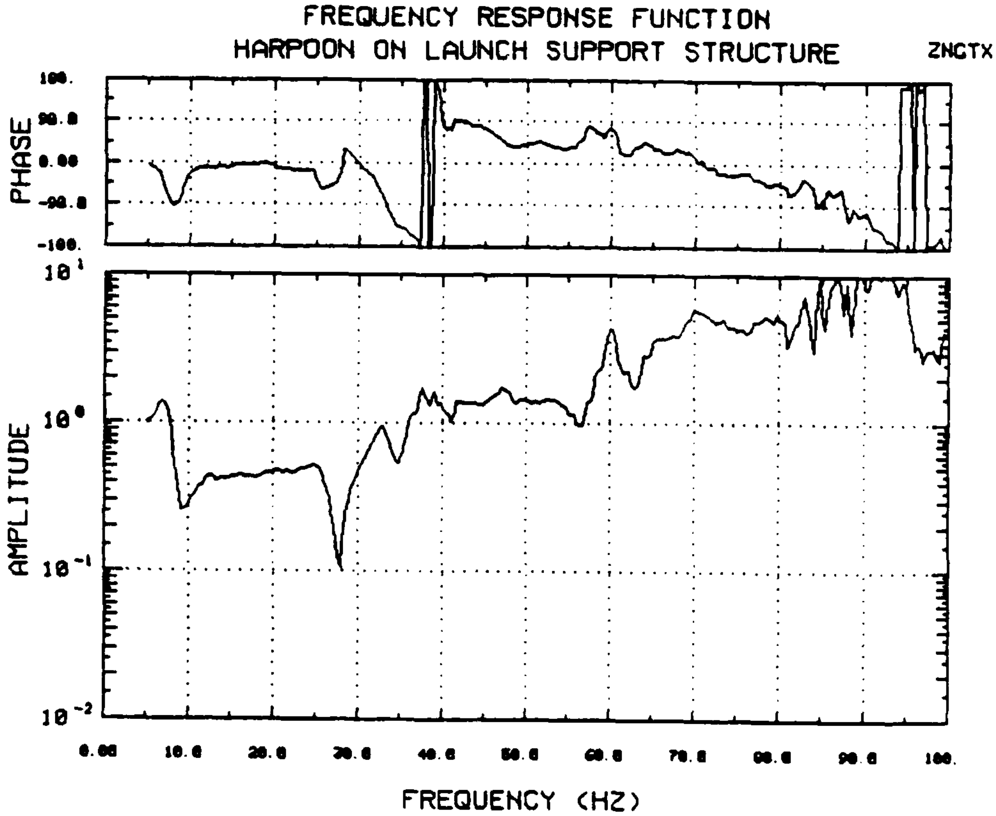

Figure 10.105 X-Axis Transfer Function at Upper Missile Due to Z-Axis Input, Modified Isolation Pads

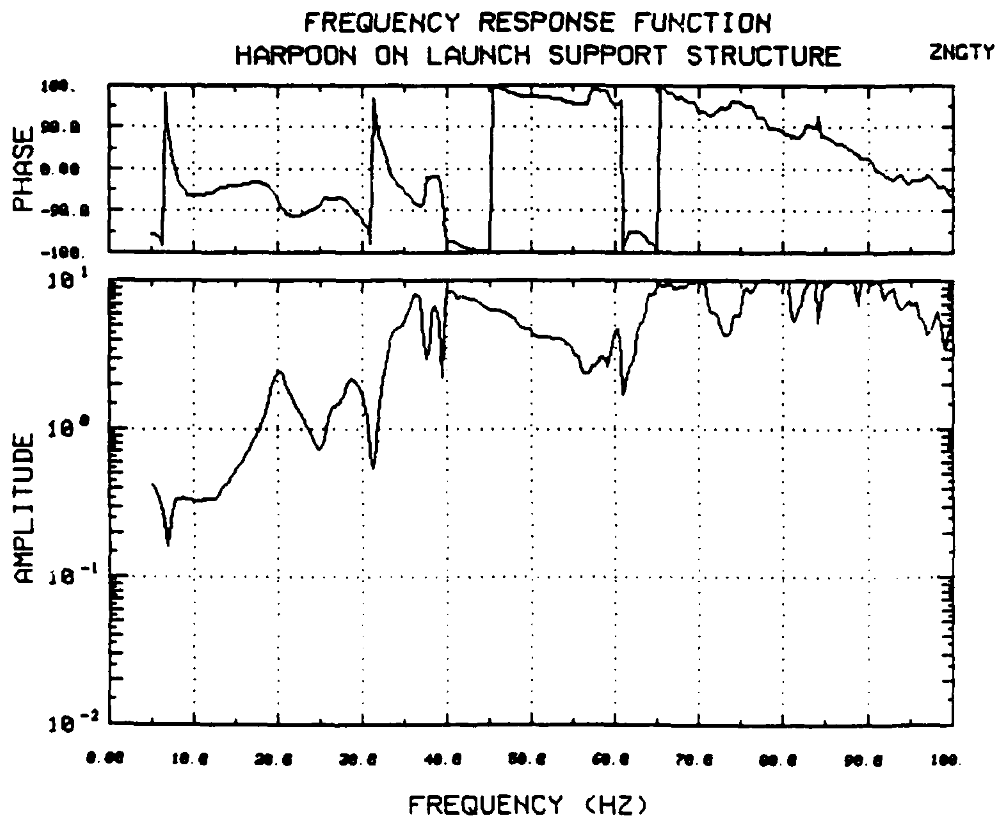

Figure 10.106 Y-Axis Transfer Function at Upper Missile Due to Z-Axis Input, Modified Isolation Pads

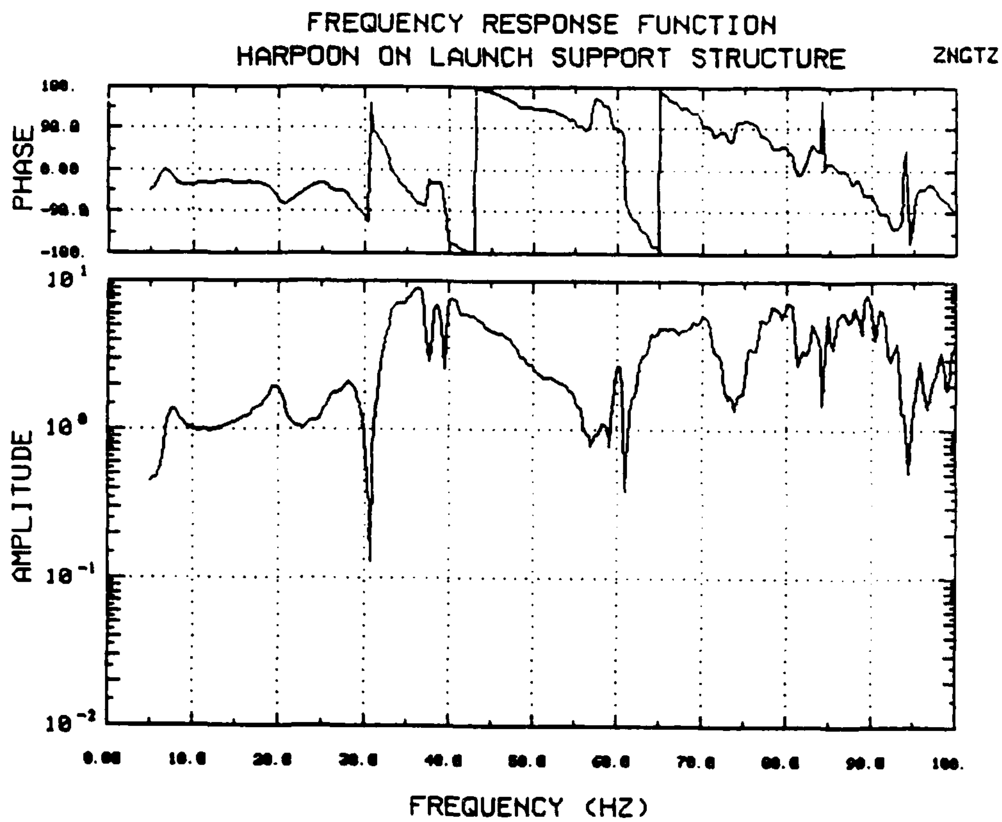

Figure 10.107 Z-Axis Transfer Function at Upper Missile Due to Z-Axis Input, Modified Isolation Pads

SECTION 11.0

MODE SHAPES

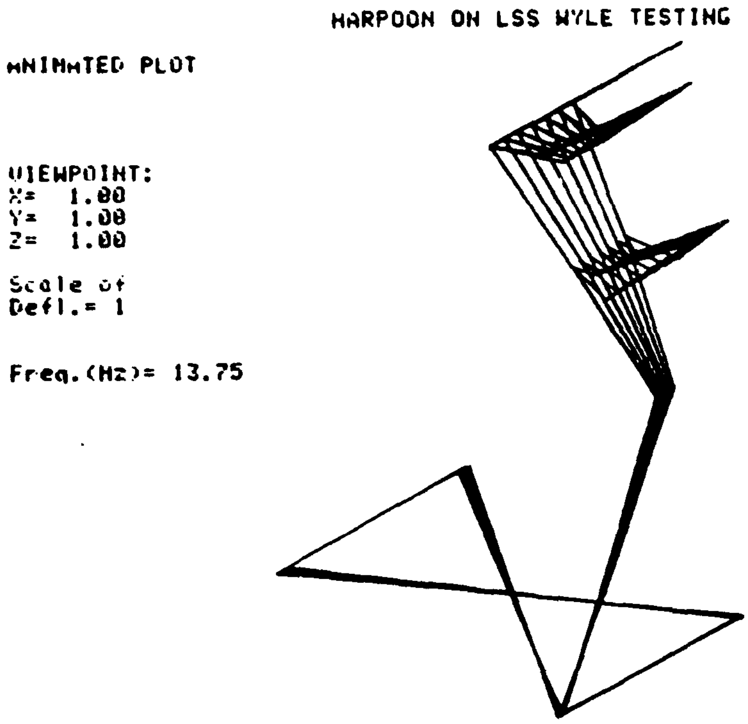

Figure 11.1 X-Axis Input Mode Shape, 13.75 Hz, Production Pads

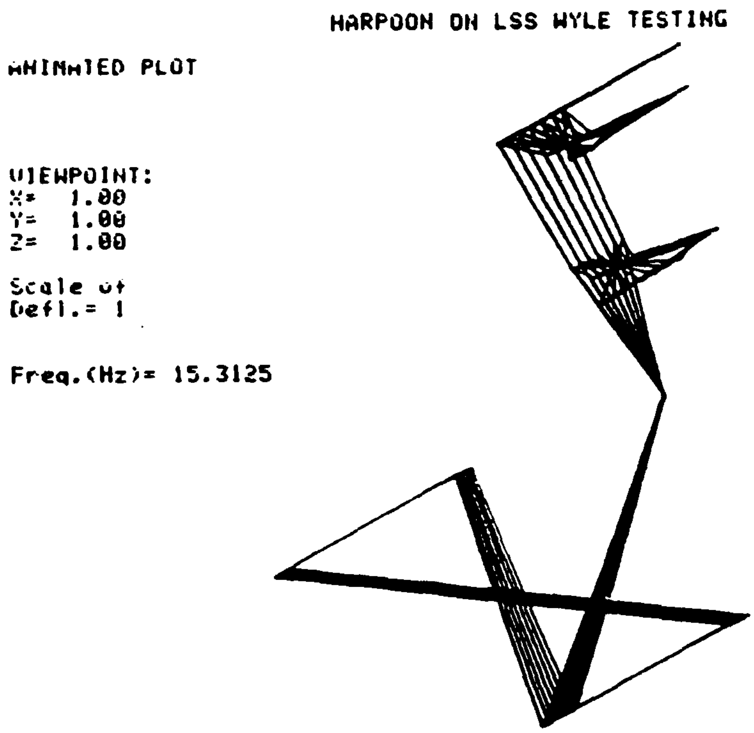

Figure 11.2 X-Axis Input Mode Shape, 15.31 Hz, Production Pads

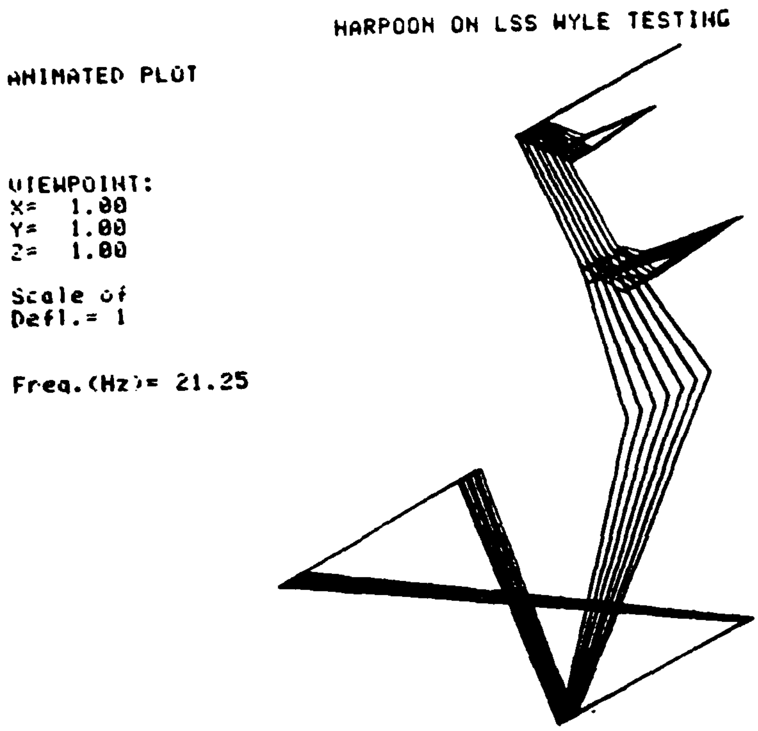

Figure 11.3 X-Axis Input Mode Shape, 21.25 Hz, Production Pads

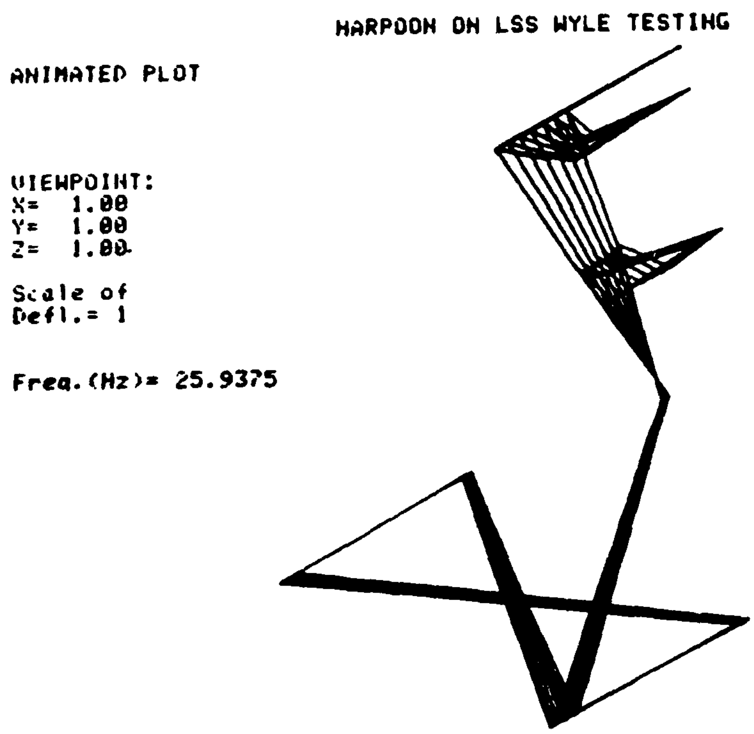

Figure 11.4 X-Axis Input Mode Shape, 25.94 Hz, Production Pads

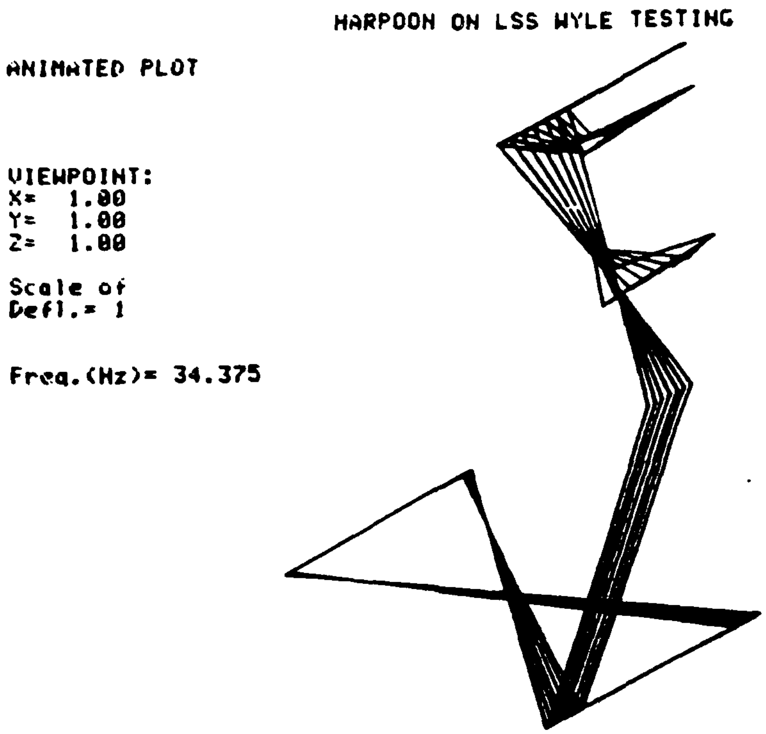

Figure 11.5 X-Axis Input Mode Shape, 34.38 Hz, Production Pads

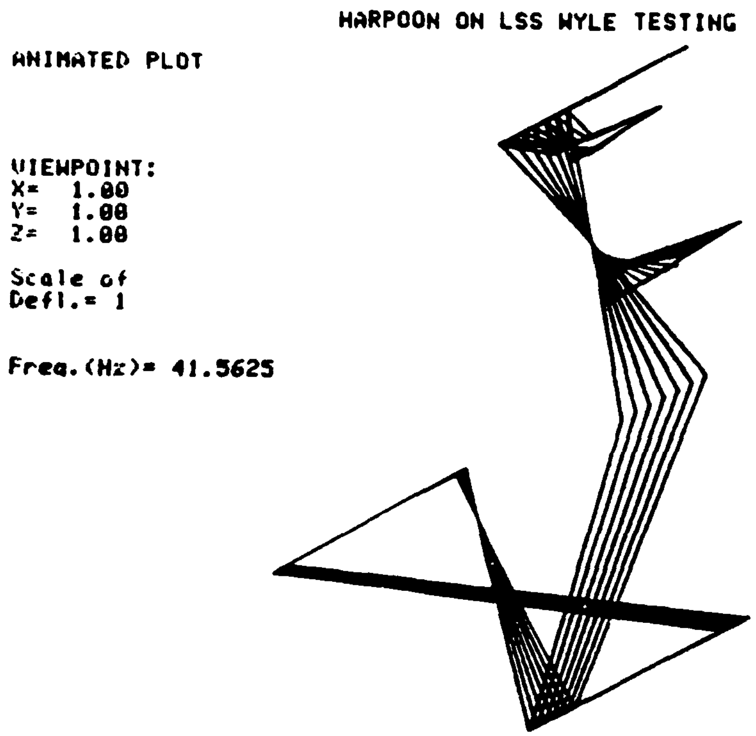

Figure 11.6 X-Axis Input Mode Shape, 41.56 Hz, Production Pads

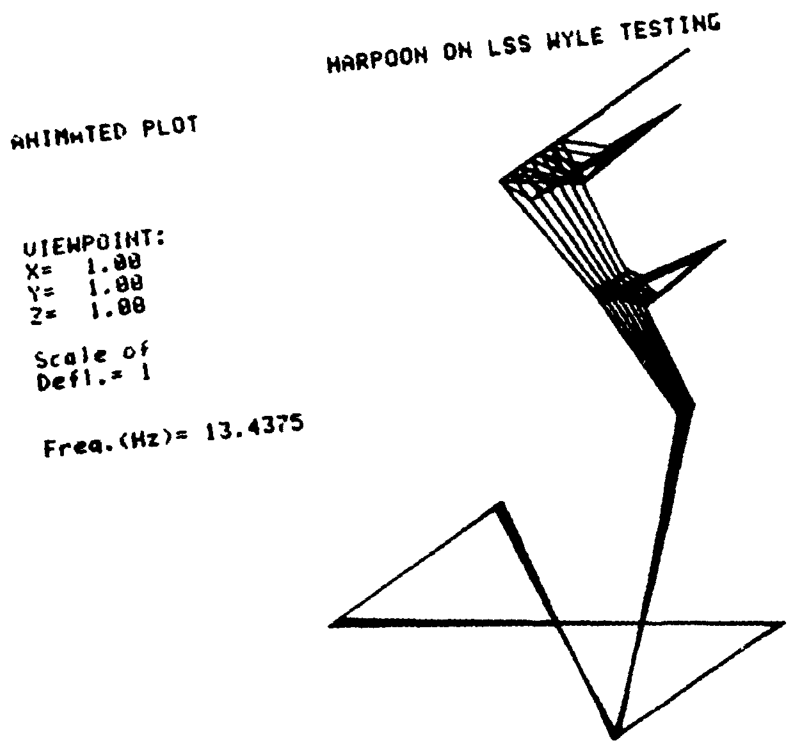

Figure 11.7 X-Axis Input Mode Shape, 13.44 Hz, Modified Isolation Pads

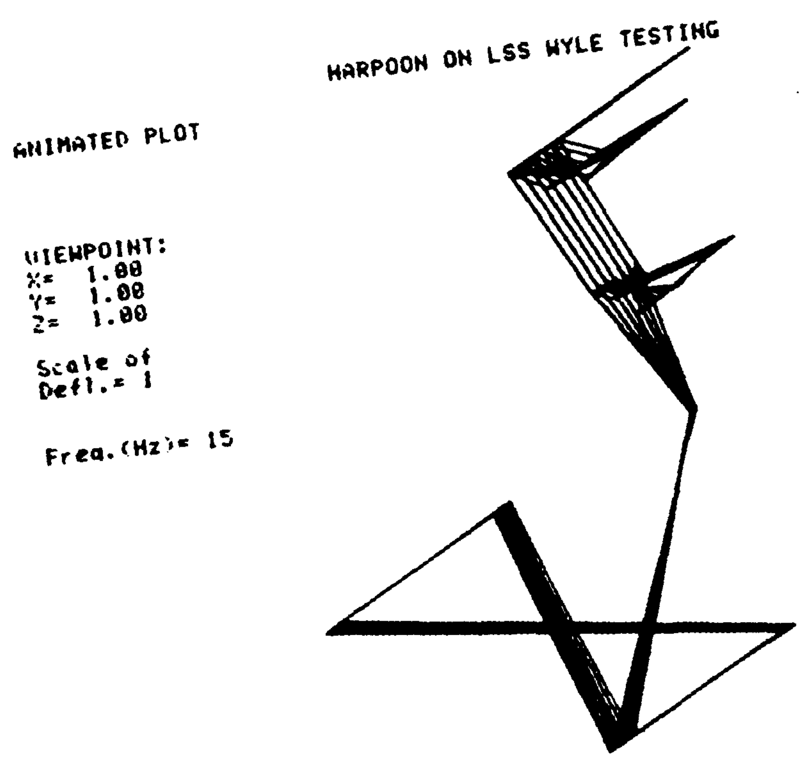

Figure 11.8 X-Axis Input Mode Shape, 15.00 Hz, Modified Isolation Pads

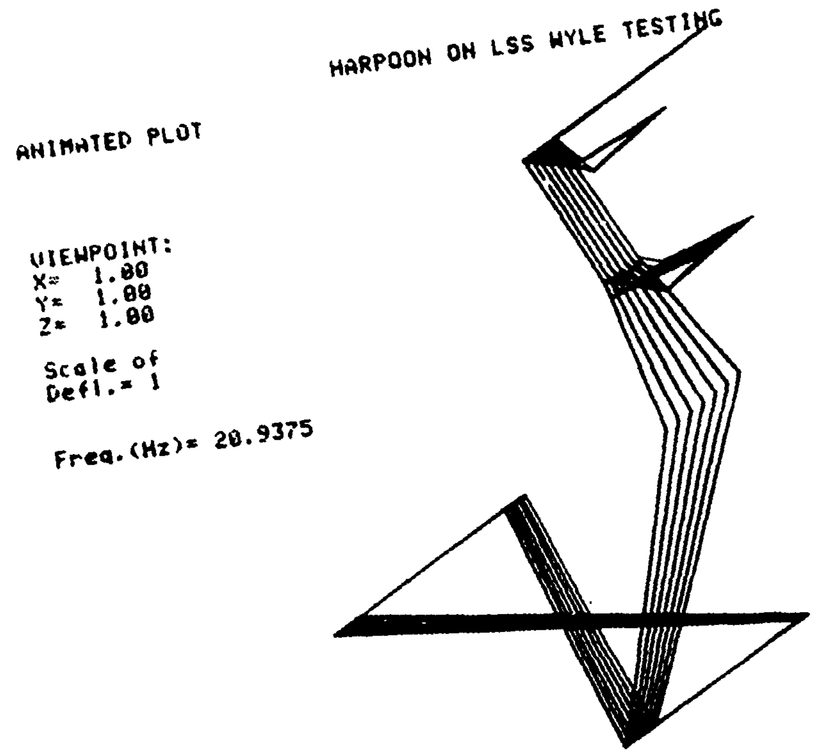

Figure 11.9 X-Axis Input Mode Shape, 20.94 Hz, Modified Isolation Pads

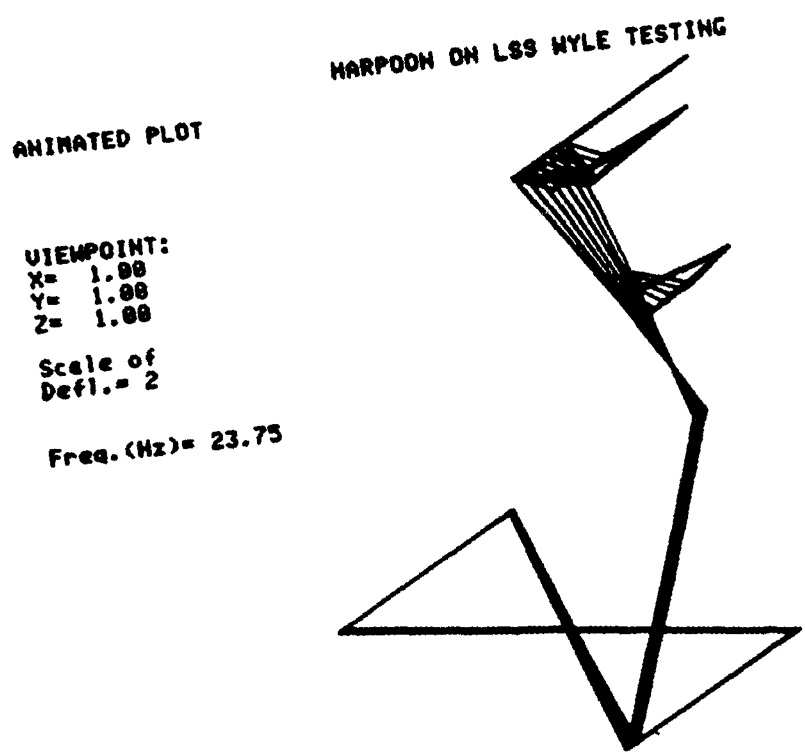

Figure 11.10 X-Axis Input Mode Shape, 23.75 Hz, Modified Isolation Pads

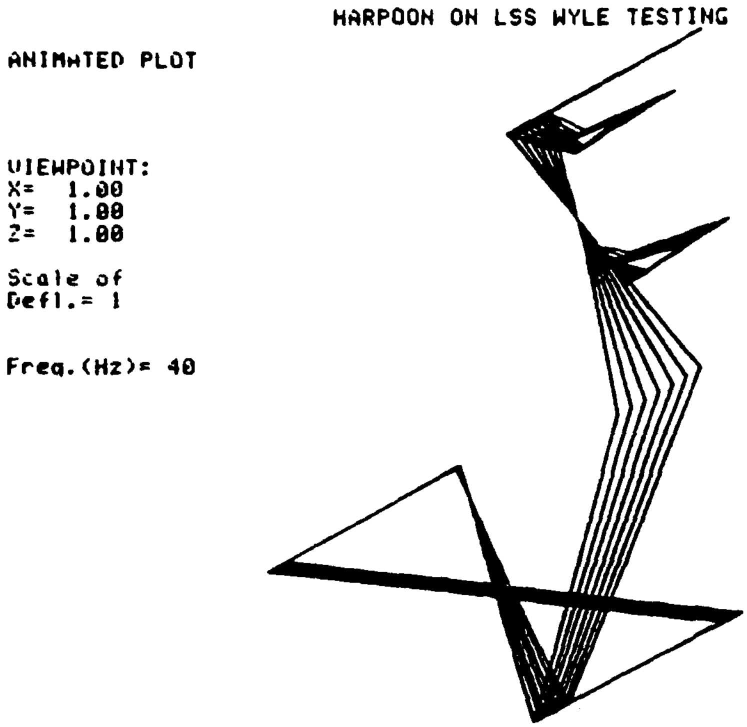

Figure 11.11 X-Axis Input Mode Shape, 40.00 Hz, Modified Isolation Pads

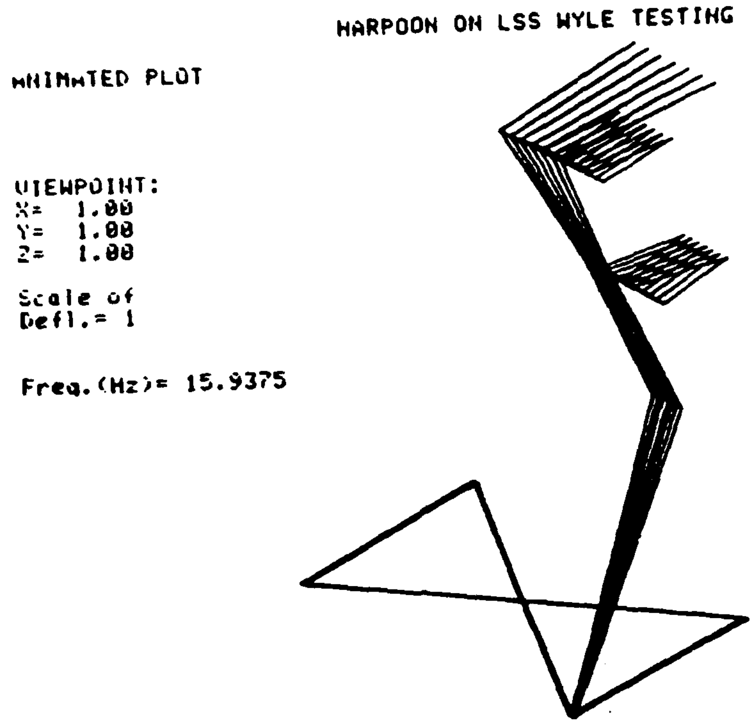

Figure 11.12 Y-Axis Input Mode Shape, 15.94 Hz, Production Pads

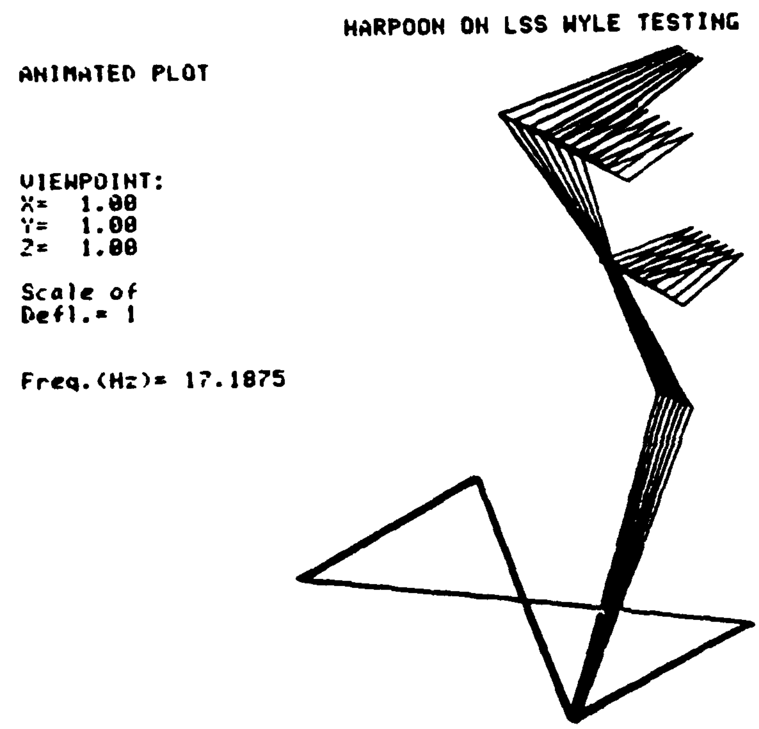

Figure 11.13 Y-Axis Input Mode Shape, 17.19 Hz, Production Pads

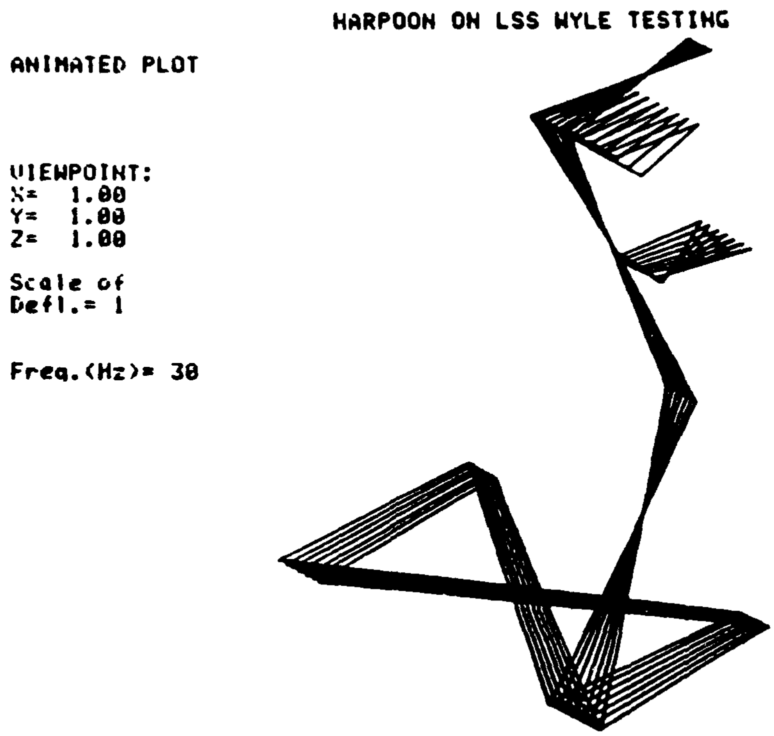

Figure 11.14 Y-Axis Input Mode Shape, 30.00 Hz, Production Pads

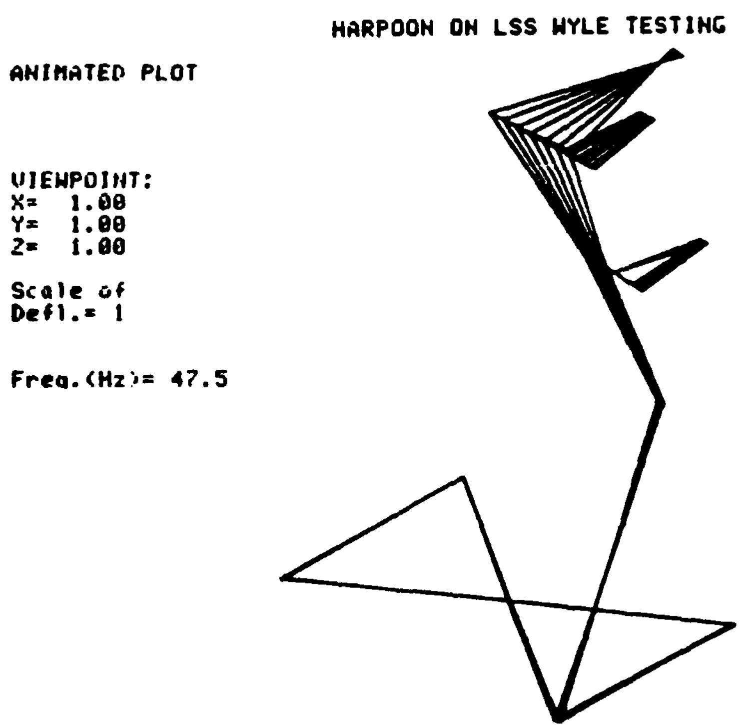

Figure 11.15 Y-Axis Input Mode Shape, 47.50 Hz, Production Pads

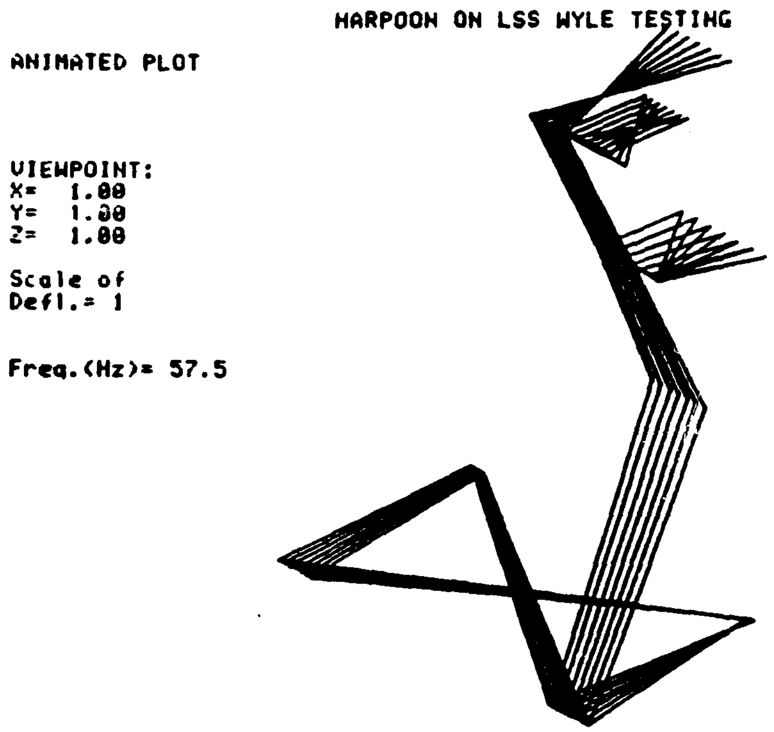

Figure 11.16 Y-Axis Input Mode Shape, 57.50 Hz, Production Pads

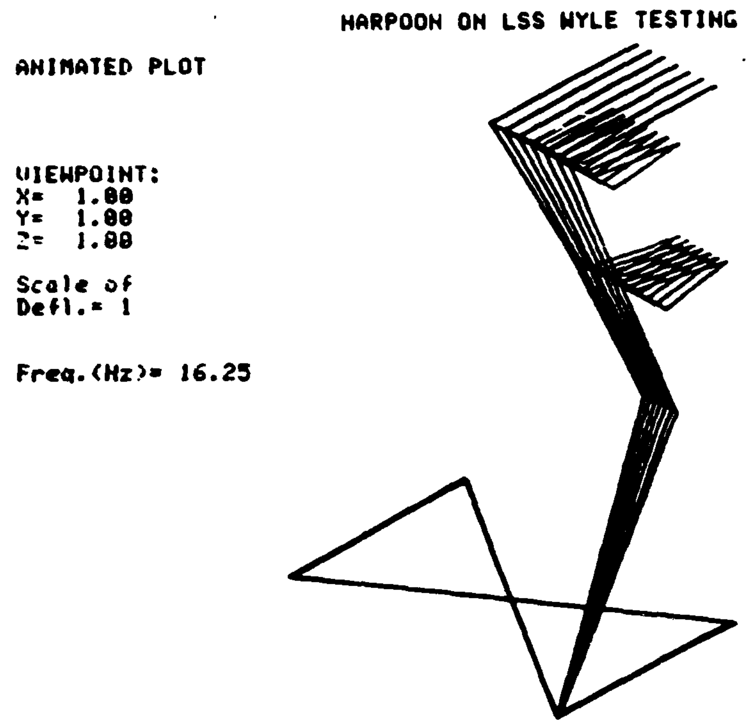

Figure 11.17 Y-Axis Input Mode Shape, 16.25 Hz, Modified Isolation Pads

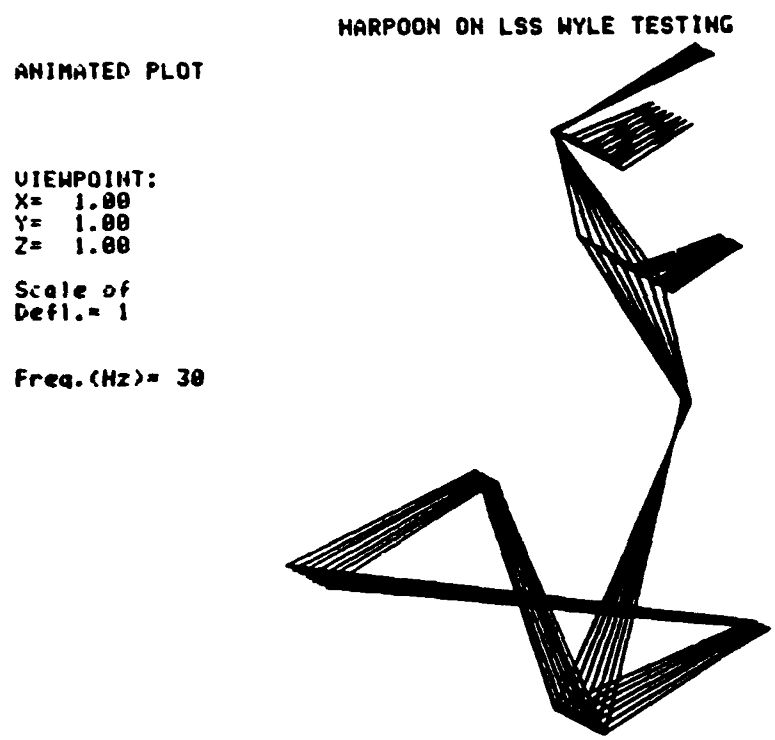

Figure 11.18 Y-Axis Input Mode Shape, 30.00 Hz, Modified Isolation Pads

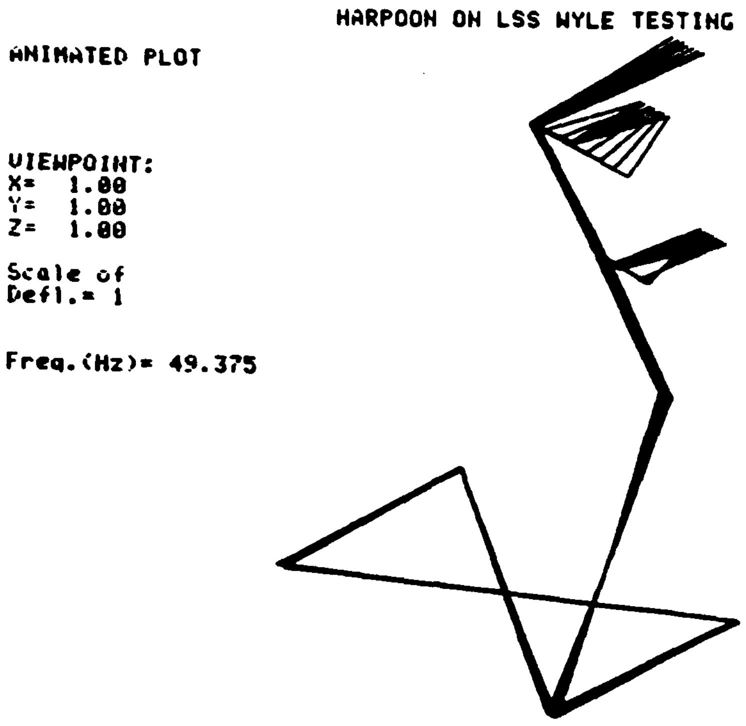

Figure 11.19 Y-Axis Input Mode Shape, 49.38 Hz, Modified Isolation Pads

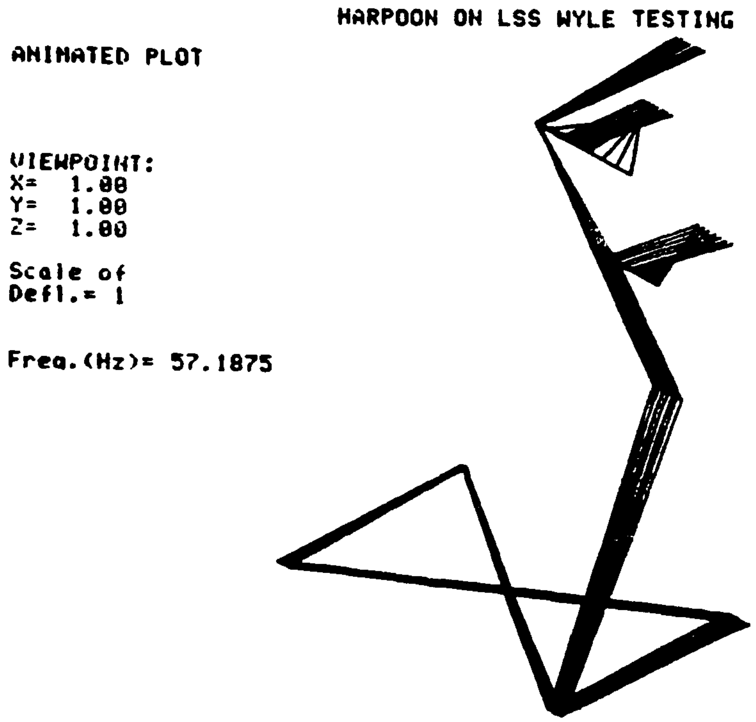

Figure 11.20 Y-Axis Input Mode Shape, 57.19 Hz, Modified Isolation Pads

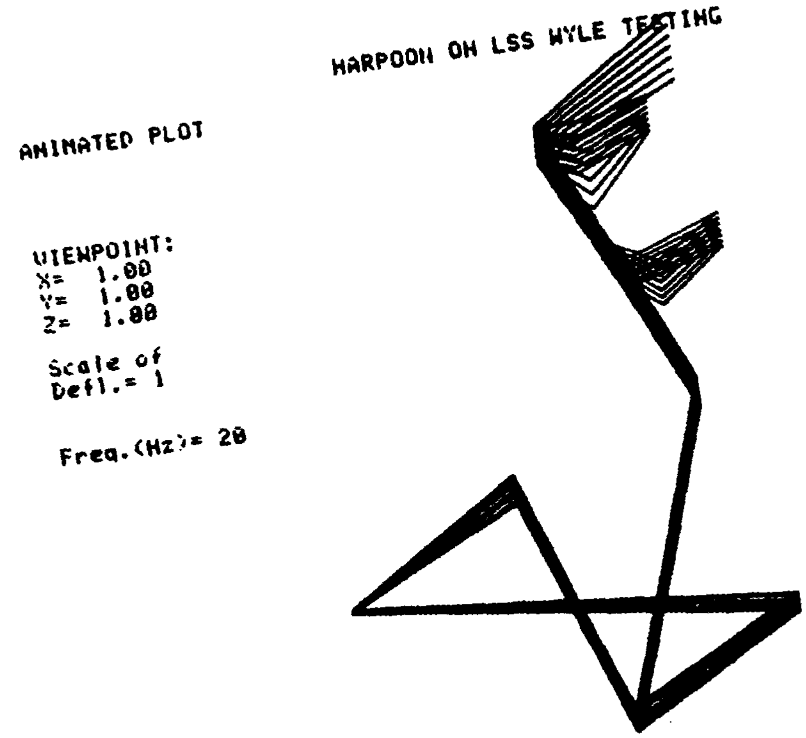

Figure 11.21 Z-Axis Input Mode Shape, 20.00 Hz, Production Pads

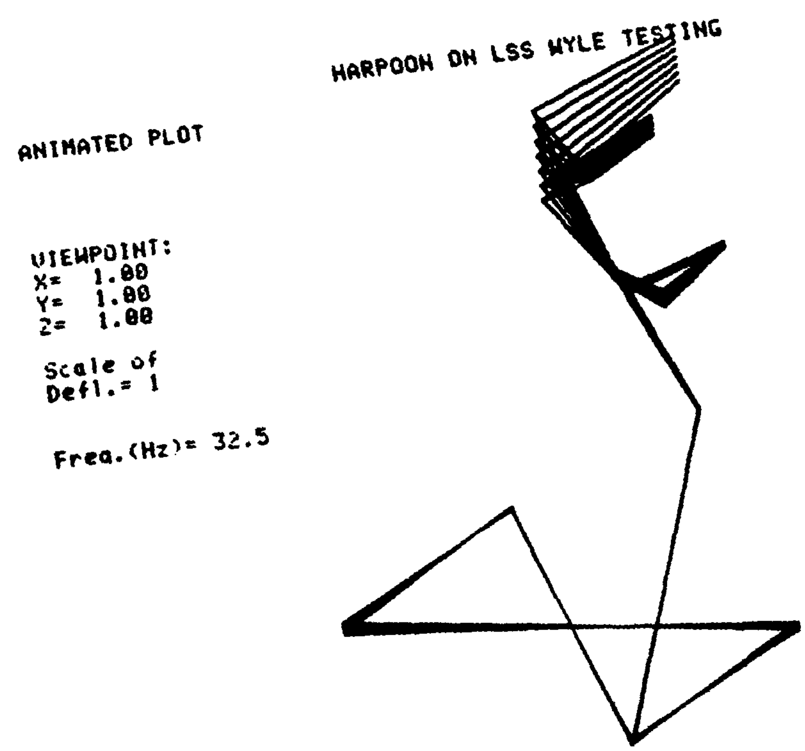

Figure 11.22 Z-Axis Input Mode Shape, 32.50 Hz, Production Pads

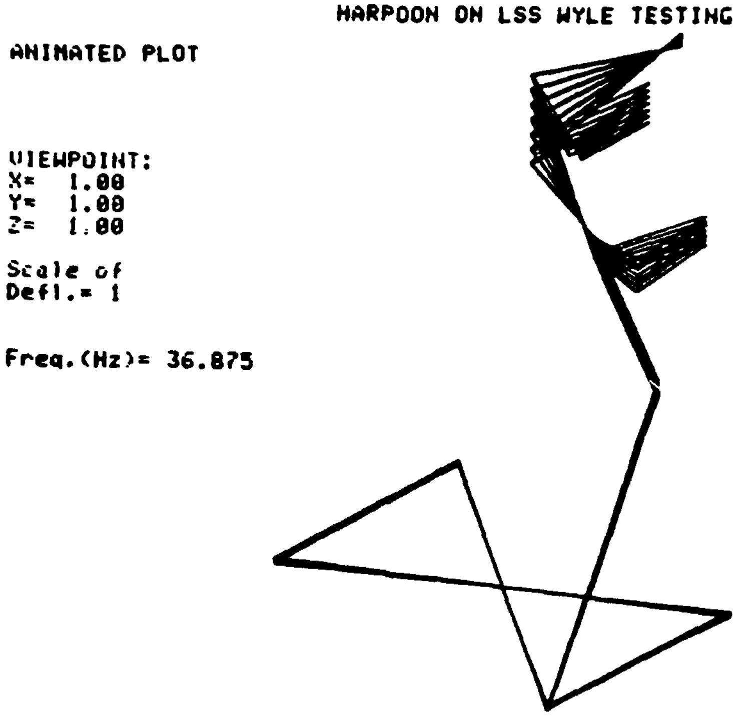

Figure 11.23 Z-Axis Input Mode Shape, 36.88 Hz, Production Pads

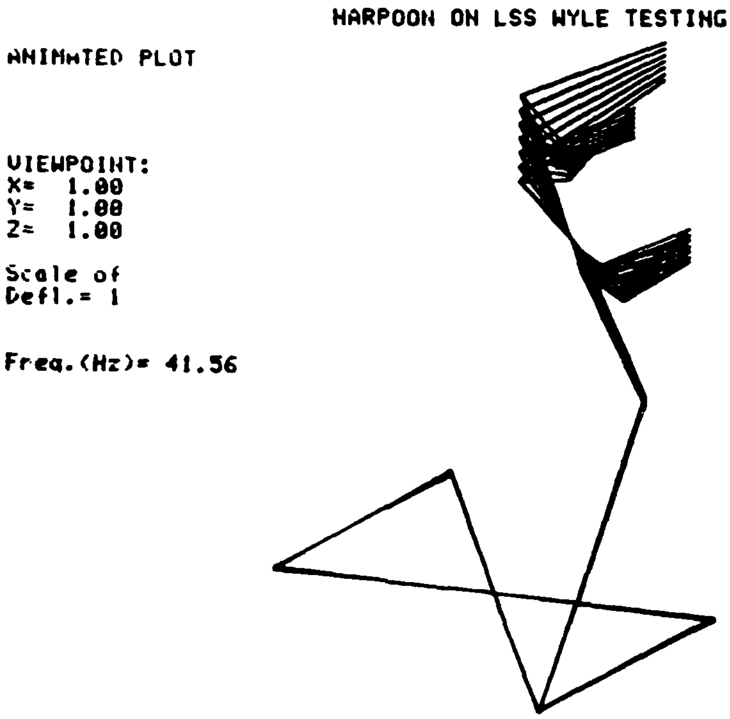

Figure 11.24 Z-Axis Input Mode Shape, 41.56 Hz, Production Pads

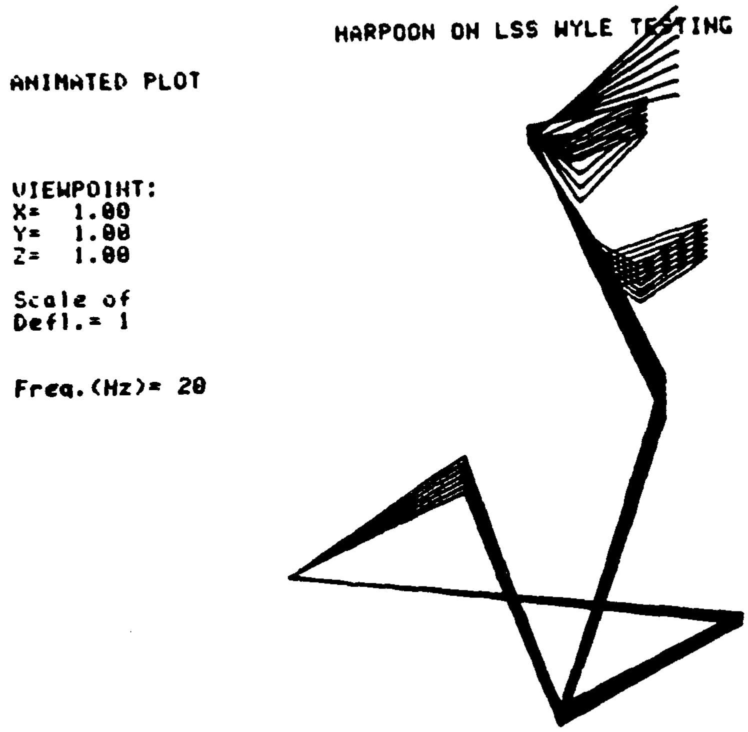

Figure 11.25 Z-Axis Input Mode Shape, 20.00 Hz, Modified Isolation Pads

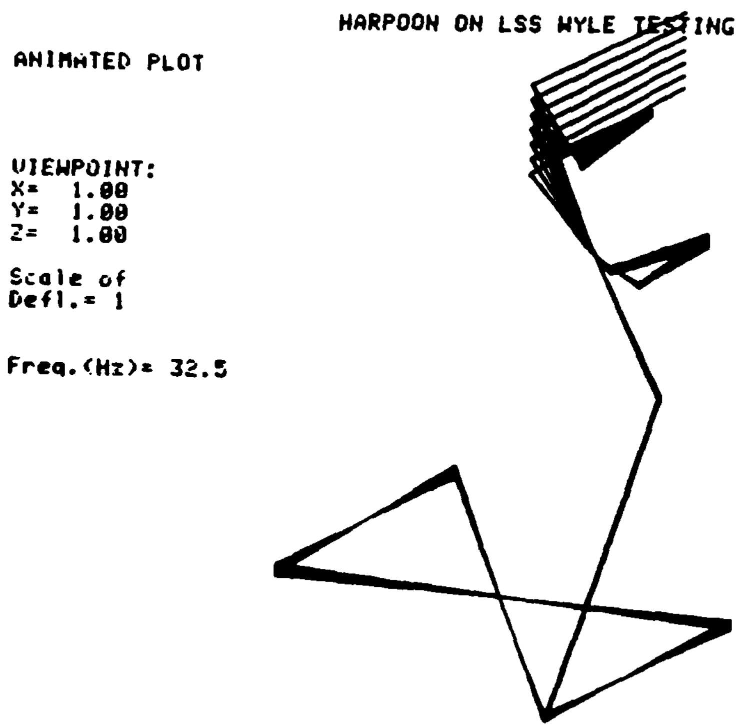

Figure 11.26 Z-Axis Input Mode Shape, 32.50 Hz, Modified Isolation Pads

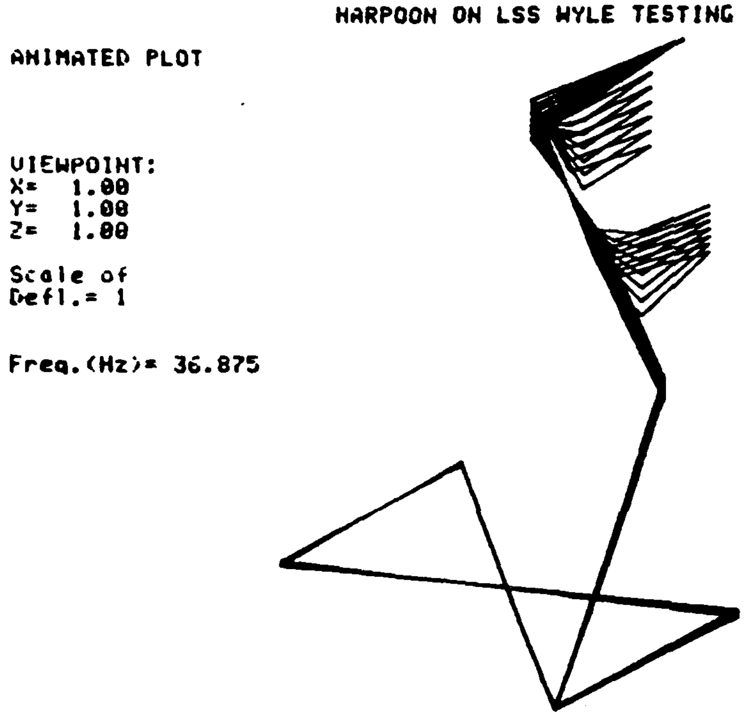

Figure 11.27 Z-Axis Input Mode Shape, 36.88 Hz, Modified Isolation Pads

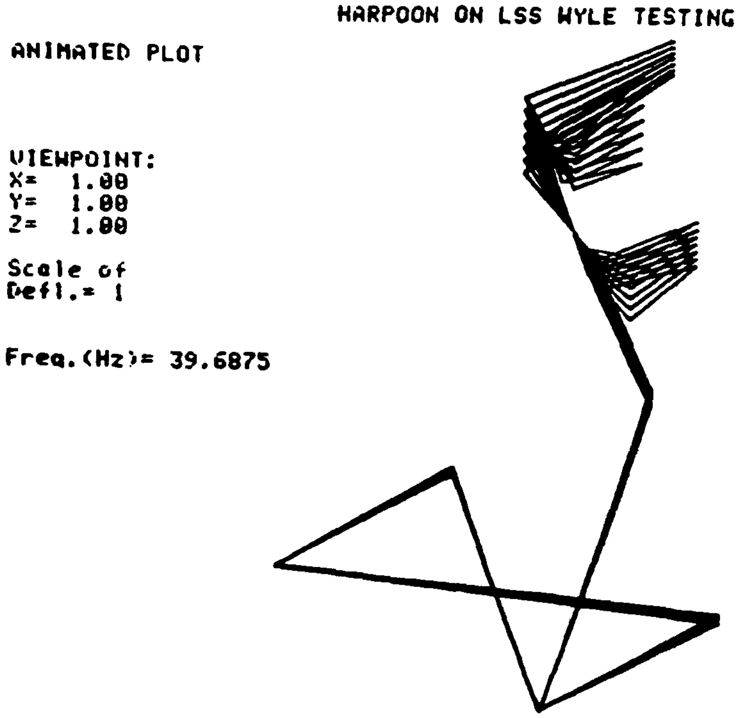

Figure 11.28 Z-Axis Input Mode Shape, 39.69 Hz, Modified Isolation Pads